

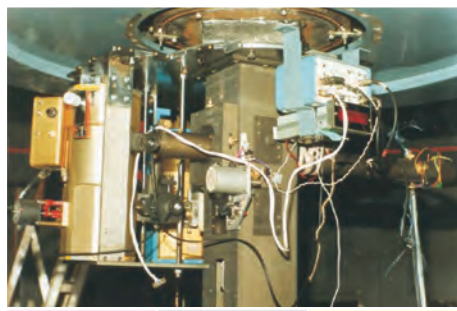
वार्षिक प्रतिवेदन
Annual Report

2012-2013



भौतिक अनुसंधान प्रयोगशाला, अहमदाबाद
Physical Research Laboratory, Ahmedabad

पी.आर.एल. में सुविधाएं
Facilities at PRL



वार्षिक प्रतिवेदन
Annual Report
2012 - 2013



भौतिक अनुसंधान प्रयोगशाला, अहमदाबाद
Physical Research Laboratory, Ahmedabad

Front Cover: Synoptic View of 1.2m Astronomical Observatory, Gurushikhar, Mt. Abu.

Inside front cover: Facilities at PRL.

Inside back cover: Events at PRL.

Back cover: Centre top Panel: New Instrumentation laboratory, Thaltej Campus, PRL, Ahmedabad.

Centre left panel: Full disk image of the Sun obtained by TSFT/PRL on 07 March, 2013.

Centre right panel: Images of high resolution of solar chromosphere showing active region, filaments and prominences during the observing cadence from 06-08 March, 2013.

Centre Bottom Panel: Synoptic View of Udaipur Solar Observatory located in Fateh Sagar Lake, Udaipur.

Compiled & Layout by:
Office of the Dean, PRL.

Published by:
Physical Research Laboratory, Ahmedabad.

Printed by:
Print Vision Private Limited, Ahmedabad.

Council of Management

Chairman

Professor U.R. Rao
ISRO Headquarters
Government of India, Bangalore

Nominee, Government of India

Members

Dr. K. Radhakrishnan
Secretary, Department of Space and Chairman, ISRO
Government of India, Bangalore

Nominee, Government of India

Shri A Vijay Anand
Joint Secretary, Department of Space,
Government of India, Bangalore

Nominee, Government of India

Shri Sanjay S. Lalbhai
Ahmedabad Education Society
Ahmedabad

Nominee, Ahmedabad Education Society

Shri Kartikeya V. Sarabhai
Chidambaram,
Usmanpura, Ahmedabad

Nominee, Karmakshetra Educational
Foundation

The Principal Secretary,
Department of Education,
(Higher & Technical Education)
Government of Gujarat, Gandhinagar

Nominee, Government of Gujarat

Professor J.N.Goswami,
Director,
Physical Research Laboratory, Ahmedabad

(Ex-Officio)

Member-Secretary

Shri Y.M.Trivedi,
Registrar
Physical Research Laboratory, Ahmedabad

(Ex-Officio)

Contents

Director's Foreword	1
Science Highlights	3
Awards and Honours	8
Human Resource Development	11
Theses Submitted	12
Colloquia/Public Lectures by Visitors	13
Conference/Symposia/Workshops held by PRL	15
Invited Talks at Conference/Symposia / Workshops	16
Lectures at Universities/Institutions	23
Science	
<i>Astronomy and Astrophysics</i>	27
<i>Solar Physics</i>	40
<i>Planetary Sciences and PLANEX Program</i>	49
<i>Space, Atmospheric, Molecular and Laser Physics</i>	60
<i>Geosciences</i>	74
<i>Theoretical and Computational Physics</i>	94
Publications	
<i>Publications in Journals</i>	103
<i>Publications in Proceedings of Conference/Symposia/Workshops</i>	110
<i>Books Edited/Review Articles</i>	113
Promotion of Basic Sciences and Official Language	114
Facilities and Services	117
Honorary Fellows	121
Honorary Faculty	122
Academic Faculty	123
Technical Faculty	127
Statement of Audited Accounts	128

Director's Foreword

The acceptance of all the major scientific programs proposed by PRL for the 12th five year plan by the Department of Space has now paved the way for further strengthening and expanding scientific activities at PRL in the coming years. Several new research domains that will be explored are formation of molecules in cold astrophysical environment, studies on photon entanglement and role of volatile hydrocarbons in the troposphere. Two new experimental facilities, a 2.5m Telescope for astronomical studies and an Accelerator Mass Spectrometer for studies in planetary geosciences and paleoclimate will be set up during the plan period. High end computing facilities for analytical and modelling studies will also be in place. All these new additions will provide both challenges and opportunities to PRL scientists to carry out research in frontier areas in multiple disciplines. An Infrastructure Facility for housing the newly acquired major instruments is nearing completion and will be ready for use during 2013.

Significant results have been obtained from studies carried out in different fields of research conducted at PRL during the last year. Systematic study of circumstellar environments led to a classification system for the novae in infrared, a new resource addition in this field. First results from exoplanet search using the Echelle Spectrograph developed at PRL was discussed extensively in a meeting of global experts held at PRL. Installation of the Multi-Application-Solar-Telescope (MAST) at the Udaipur lake site is nearing completion; routine observations are expected after the monsoon season. Studies of rare mineral phases in lunar rocks confirm the presence of water in the lunar interior leading to estimation of water content in the lunar mantle. Upper atmospheric processes are shown to be significantly affected by forcing due to dynamics

of the lower atmosphere. Laboratory experiments showed importance of size-segregated aerosol chemical composition in the sub-micron range on the radiative properties of aerosols. Multi-photon ionization using fundamental and frequency tripled wavelength exhibited remarkable difference in the ion spectra that could be explained considering electron re-collision mechanism. Striking differences seen in the intensity correlation in the scattering of a Gaussian beam and an optical vortex matched exact analytical results. A significant reduction in nitrogen uptake by plankton and hence productivity with decrease in salinity was found in a mesocosm experiment conducted in the Arabian Sea. Neodymium isotope composition in the Arabian Sea water column showed negligible riverine contribution to the surface water and highlight the significant dust deposition over this Sea. A novel way of looking for new physics with polarized beam in the electro-positron collider is proposed. Studies of complex network suggest a universal relation between the critical coupling strength and the largest non-zero eigenvalue of the coupling matrix. Several payloads for Chandrayaan-2 mission as well as Aditya mission are currently under development. Work is also in progress for development of other payloads for future planetary, Space and Astronomy missions.

The combined strength of academic and engineering Faculty remained nearly at the same level with a couple of superannuation and induction of several new faculty members. The number of research scholars and post-doctoral fellows also remained steady, while the number of project associates has increased due to various experimental projects taken up by faculty members that are funded by the Department of Earth Sciences and the Department of Science and Technology.

The eighth UN CSSTEAP course on Space Sciences for the Asia-Pacific region conducted by PRL started in mid-2012 with fourteen participants from seven countries and is scheduled for completion by end of April, 2013. PRL continued its effort for increased academic interactions with universities during the year and initiated bilateral relation with Sardar Patel University, Vallabh Vidyanagar, and Pondicherry University, Pondicherry. PRL also offers short-term Associateship to university faculty to visit PRL and carry out collaborative research with PRL faculty members.

On the academic front, PRL has maintained a high level of excellence with more than two hundred scientific publications, with a significant number in high impact journals, and seven invited review articles. Eleven research scholars have submitted their thesis during the year. Collectively, PRL Faculty members have been invited to give more than two hundred invited lectures at a large number of Conference, Symposium and Workshop and also at Universities and Academic Institutions. PRL also hosted more than twenty faculty members from both within the country and abroad for scientific interactions during the year and organized half a dozen conferences and symposia in its campus and also co-hosted a couple of meetings held in other academic institutions.

Research done at PRL has received both national and international recognitions as reflected by the honours and acclamation received by PRL faculty members from different academic forum and organizations. These include J. C. Bose Fellowship of DST, Fellowship and young scientist award from Science Academies, Member, Scientific Advisory Committee of International forum, Indian Science Congress Gold medal, Life time Achievement award, Member, Editorial Board of International Journals, Member, Indo-Japan Council, Chair, Research Advisory Committee, CSIR, Astronautical Society Award in Space Sciences and membership of Council and Advisory Committees of several academic institutions as well as government departments such as DST, CSIR and MOES. A PRL PhD scholar received the Best Thesis award of the year from Astronomical Society of India and a few others received awards in several scientific meetings.

PRL is expanding its HRD activities by inducting more number of college and university students from all over India for its summer programme and also through its association with similar programme conducted by the Science Academies. More than fifty graduate and a few undergraduate students have participated this year in the PRL summer programme. PRL also provides opportunity to graduate engineering students from local colleges to carry out long-term project work.

PRL is entrusted to conduct the PLANEX and RESPOND programmes of the Dept. of Space and currently more than

fifty research groups at various universities and research institutions are receiving funds and advice through these projects to carry out scientific investigations in the fields of Astronomy, Planetary and Space Sciences. Thanks to the PLANEX programme, several universities have now introduced Planetary Science course at graduate level and more than fifteen research groups at various universities and institutes are currently pursuing research in the field of planetary sciences.

“ Science Day” celebration at PRL has now become a major event for high school students in the state of Gujarat. The preliminary selection of school students for participation in the event at PRL takes place in close to a dozen regional centres in the state. PRL offers scholarships and incentives to students who fare well in various events conducted at PRL on the science day. The celebration during the current year also included a special event arranged for the accompanying teachers that was very well received.

Significant steps are being taken to ensure use of Hindi in more areas of administration and official communications. The Hindi version of PRL web site is operational at present. Work done at PRL in implementation of Hindi in various domains has also been recognized by the Town Official Language Committee.

The smooth implementation of the 12th Five year plan will be a major agenda for PRL in the next couple of years. The exemplary support received from DOS has to be matched by unstinted devotion from all members of “Team PRL” and collective effort and coordination between academic and administrative personnel to ensure timely acquisition and establishing of new facilities and infrastructures and delivering science output at the highest level. PRL has been able to perform reasonably well so far, thanks to the untiring effort put in by all members of the PRL family, and we need to continue our efforts and give our best to achieve our cherished scientific goals.

I am grateful to all the members of the PRL Council for their encouragement during preparation of the PLAN document and their continued support and invaluable advice on various academic and administrative matters. In particular, I am indebted to Chairman, PRL Council, and Chairman, ISRO, for their sage and timely advice that resulted in a year of steady progress and improvement in both academic and administrative spheres of the laboratory.

J.N. Goswami

Director

SCIENCE HIGHLIGHTS

Astronomy and Astrophysics

- A search for the aluminium monoxide (AlO) molecule in circumstellar environments detected infrared bands of AlO in 13 out of the 17 preselected sources showing that AlO is fairly prevalent in Asymptotic giant branch (AGB) stars with cool and dusty O-rich shells. A classification system for the early post-outburst optical spectra of novae in the infrared was made based on observations covering the entire sample of novae studied from Mt Abu during the last several years. While an optical classification scheme already existed, the IR classification scheme is a new resource addition in the field of novae research.
 - Polarimetric studies of a recently detected flaring gamma-ray source, the exact nature of which is uncertain, have helped to classify it as a low frequency peak Blazar based on its high and variable polarization (9% to 21%). It was shown that Lyman beta fluorescence is indeed the key mechanism for enhancing the strength of certain important oxygen lines seen in the spectra of Be stars.
 - Galactic X-ray binaries are among the brightest X-ray sources in the sky and are known to be variable over time scales ranging from milli-seconds to years. However, over the intermediate time scale of few minutes to hours, these sources, particularly the black hole binaries, are not known to vary significantly.
- GRS1915+105 was the only blackhole binary exhibiting strong heartbeat type systematic and large amplitude variability over the intermediate time scale. Using an innovative method of phased resolved spectroscopy, it has been shown that the high mass accretion rate is responsible for the observed heartbeat type variability.
- Previous studies suggested that the solar radiation reaching the Martian surface could be lethal to any living organism there. Based on the measured X-ray spectra of the ten strongest solar flares in solar cycle 23, it is shown that the radiation exposure on the Martian surface during such flares or even the total integrated dose over a period of one month is not lethal for living organisms.
 - Regular science observations with PARAS, the PRL Advanced Radial-velocity All-Sky Search Echelle spectrograph that was designed and built at PRL, started in April 2012. The spectrograph, maintained under very stable conditions of pressure and temperature, can detect and characterize exo-planets by measuring their radial velocities. This spectrograph can detect radial velocities down to 1.5 m s^{-1} .
 - Polarimetric studies of celestial X-ray sources is a completely unexplored field at present. A program to design and develop a laboratory prototype of a hard X-ray polarimeter that can be used as a focal plane detector for hard X-ray optics has been initiated. Detailed numerical simulations to estimate

the sensitivity of such a detector was done and experimental activity to fabricate the first prototype version has been initiated.

- The variability of iron emission lines in the high mass X-ray binary pulsar Centaurus X-3 was investigated during eclipse, eclipse-egress and out-of-eclipse phases. Iron emission lines at 6.4 KeV, 6.7 KeV and 6.97 KeV are found to be very strong irrespective of different binary phases of the pulsar. Based on the results obtained, the most probable emitting region of 6.4 KeV fluorescent line is identified to be close to the neutron star, whereas the other two lines are produced in a region that is far from the neutron star, probably in the highly photo-ionized wind of the companion star or in the accretion disk corona.
- Broad-band timing and spectral properties of the transient Be/X-ray binary pulsar EXO 2030+375 were investigated. Pulsations with a period of 41.41 s and strong energy-dependent pulse profiles were clearly detected up to 100 KeV. Narrow dips are seen in the pulse profiles up to ~ 70 KeV, which were not seen before. The spectral fitting did not require any cyclotron feature in the spectrum at ~ 36 KeV that was reported earlier.

Solar Physics

- The magnetic helicity injection by photospheric shear motion for two recent solar active regions, NOAA 11158 and 11166, during their six-day evolution period have been estimated to be $14.16 \times 10^{42} \text{ Mx}^2$ and $9.5 \times 10^{42} \text{ Mx}^2$, respectively. This study suggests that flux motions and spatial distribution of helicity injection are important for understanding the complex nature of the magnetic flux system of the active regions, as well as identifying the favourable conditions for eruptive events.
- From the location, timing, strength, and spectrum of hard X-ray (HXR) emission during a prominence eruption, we could conclude that the prominence eruption is driven by a few distinct episodes of magnetic reconnection occurring in the current sheet below the erupting prominence.
- Analysis of flare associated line profile changes, observed in the solar active region NOAA 11158 during an X2.2 class flare, showed that the distortions in the line profiles are compatible with the changes in the global atmospheric parameters of the line profiles at the flare kernels.
- A 3-D reconstruction of the Coronal Mass Ejections (CME) image in the inner heliosphere has been made based on continuous tracking in imaging observations by coronagraph COR2 and heliospheric imager H1 on board STEREO. This analysis reveals that kinematics of CMEs estimated by exploiting wide angle imaging observations of STEREO combined with modelling improve the prediction of arrival time of CMEs with errors in the range of 3 to 9 hours.
- Remote sensing and in-situ observations of two CMEs associated with eruptive filaments on 5 January 2005 showed that these eruptions caused two distinct but slow Interplanetary Coronal Mass Ejections (ICMEs) travelling at different velocities that interacted in the interplanetary medium and resulted in complex magnetic structures. These structures, coupled with Earth's space and terrestrial environment, triggered a series of substorms in the main phase of a moderate geomagnetic storm.

Planetary Science and Planex Program

- Analysis of volatile (water, chlorine, fluorine and hydroxyl) content in late-crystallizing apatite grains present in the lunar sample 15555, a low-Ti olivine mare basalt, using Nano-SIMS, revealed presence of water and other volatiles with concentration of water in the range of 2000-8000 ppm. A minimum value of water content in the parent melt is estimated to be $\sim 100\text{--}380$ ppm. The abundance of water and other volatiles appears to vary in different water-bearing reservoirs in the lunar mantle.
- Tissint meteorite is the fifth Martian meteorite to be collected soon after its observed fall. Studies of noble gas suggest an exposure age of 1 ± 0.1 million years in space before its fall. The minimum pre-atmospheric size of Tissint is determined to be 22 cm. Seven Martian meteorites of "Tissint" type have similar exposure age and may have been ejected in a single event from Mars. Signature of both Martian atmospheric and Martian interior components can be discerned in the nitrogen and noble gas isotope data.
- The isotopic and elemental ratios of trapped He, Ne and Ar in Washington County meteorite (WCM), an ungrouped iron meteorite, conclusively prove the presence of solar wind component both in the surface and the interior of the meteorite. The solar wind gases are likely to have been acquired during formation of parent body and not lost subsequently.
- A Cerium-doped Lanthanum bromide gamma ray spectrometer (GRS) is under development for a possible future planetary mission. Front-end electronics, FPGA based processing electronics and Lab-View based data acquisition software for GRS have been developed in-house. The energy resolution at 1.274MeV (^{22}Na line) with the present GRS configuration is estimated to be $\sim 3\%$.
- The spatial distribution of spinel-rich rocks in the Orientale basin on moon, inferred from Chandrayaan-1

M³ data, suggests scarcity of spinel in non-mare units, particularly Inner Rook Ring, and indicates the absence of deep-seated extensive spinel-rich layer in the primordial lunar crust. The co-existence of spinel-anorthosite exposures and presence of pyroxenes in adjoining areas at several locations of this basin suggests that spinel was present alongside pyroxene and anorthosite at a comparatively lesser depth. This is likely if the spinels were product of melt-wall rock reaction from an earlier epoch of pre-Orientele magmatism.

Space, Atmospheric, Molecular and Laser Physics

- The upper atmosphere has traditionally been considered to be affected by solar influences alone. However, based on systematic and continuous measurements of daytime optical emissions (OI 557.7 nm, OI 630.0 nm, and OI 777.4 nm) as well as radio and magnetic measurements, spanning over a period of two years, it has been shown that the upper atmosphere is significantly influenced by forcings from the dynamics of lower atmospheric regions. This influence of lower atmosphere was stronger in the year 2011 (when solar activity was quite low) as compared with that of 2012 (when the solar activity was relatively high), and was absent when the solar activity was highest during 2001.
- Recent rocket borne measurements revealed the absence of the E region streaming plasma waves of (0.5 m -15 m scale sizes) in contrast to all the earlier rocket observations conducted during noontime from Thumba (8.47°N, 76.6°E). Radar observations over several years revealed a systematic transition from appearance to non-appearance of streaming waves at a particular scale size. Systematic ground-based magnetometer measurements from Thumba revealed a movement of the magnetic dip equator towards south by about 2° during 1985-2010. Based on thin-shell model, it is shown that the generation of streaming waves ceases to exist when the value of the magnetic dip angle is close to 1.5°.
- Single particle aerosols and their chemical composition in the sub-micron and micron size ranges have been measured using an aerosol time-of-flight mass spectrometer in real time. In the sub-micron size range aerosol species such as dust, sea salt, elemental carbon, and organic carbon are dominant and they are mixed in the atmosphere. The size segregated aerosol chemical composition can change the radiative properties of aerosols. Aerosol single scattering albedo is found to be higher when size segregated aerosol chemical composition is used, as compared to the single scattering albedo obtained assuming external mixing (no physical or chemical interactions among different aerosol species). Thus, these results will enable a more accurate evaluation of aerosol radiative forcing.
- Simultaneous measurements of concentration of O₃, CO, NO_x, CH₄ and light non-methane Hydro carbons were made over the Bay of Bengal (BoB) during 28 October - 17 November, 2010 to study the role of chemistry and dynamics. Higher levels of O₃ and some of its precursors were observed when the winds were from the surrounding land masses. Estimated south to north latitudinal gradients in O₃ and CO were significantly higher than those observed during earlier campaigns. Diurnal variations in surface O₃ show daytime increase in the northern BoB and decrease during noon hours over the cleaner southern BoB. These features have been captured using a photochemical box model.
- A new calibration free algorithm was developed for retrieval of elemental concentrations using Laser Induced Breakdown Spectroscopy. It needs only one trial parameter to estimate all other concentration. Estimation of the composition of a brass sample agree within 1% with Electron Probe Micro Analyzer measurements.
- When sufficient energy is deposited in a molecule, changes occur in its electronic configuration and in the arrangement of its constituent nuclei. By studying how the energy is shared between the electrons and ions ejected in the ionisation process, we can understand these changes. An instrument which performs a correlated analysis of the energy of the ejected electrons and the momenta of fragment ions in such break-ups has been developed. It is shown, that photo-double-ionisation of the OCS molecule followed by its breaking into three fragments occurs mostly via bending of the molecule followed by step-by-step breaking of the two bonds. In another study the fragmentation of doubly charged N₂ and CO, which are isoelectronic diatomic molecules, is analysed theoretically and experimentally. It is shown, that excitation to purely repulsive potential energy configurations, to quasi-bound configurations, as well as autoionisation, can lead to fragmentation into atomic ions. However, the proportion of the contribution of the three pathways differs in the two species, which is attributable to the difference in the symmetries of the molecules.
- Multi-photon ionisation of xenon clusters created by nozzle expansion has been investigated by time-of-flight mass spectrometry. Multi-photon ionization using fundamental (1064 nm) and frequency tripled (355 nm) wavelengths were used to ionize the clusters for detection exhibited remarkable difference in the ion spectra. Under 355 nm radiation, Xe clusters up to Xe⁸⁰⁺ were observed, whereas multiply ionized Xe (up to Xe⁵⁺) were observed during 1064 nm ionization. The observed higher charge states in the spectra were explained by invoking the electron re-collision mechanism, where electrons are energised by the photon field of the laser at large wavelength.

- A simple, effective method to determine the topological charge of an optical vortex has been demonstrated by using a spherical convex lens. By tilting the lens and recording the intensity distribution at a predicted position past the lens, both sign and magnitude of the topological charge could be measured. The results validated prediction from analytical treatment of the process.
- Striking differences in the intensity correlations were observed in the scattering of a Gaussian beam (GB) and an optical vortex (OV) on a rotating ground glass plate. For short time delays, intensity correlations of OV follow the same pattern as the scattered GB, with vortices decay rate depending on the order of the vortex. For longer time delays, the OV intensity correlations were modulated, and the strength of modulation was dependent on the order of vortex. This seemingly counterintuitive observation was supported by exact analytical results.

Geo-Sciences

- Preliminary mesocosm experiments with the planktons in the Arabian Sea have revealed a significant reduction of the nitrogen uptake and hence productivity by them when the salinity decreases, as expected in the future due to stratification of the oceans by the strengthened hydrological cycle.
- A significant dry period has been discovered in the past at around 2.1 ka, based on oxygen isotope studies of soils of Gujarat and speleothems of Andamans. Carbon isotopic studies show that the turnover time of soil carbon is longer when it is associated with clays.
- Direct measurement of the isotopic composition of water vapour over the oceans reveals that it is controlled by atmospheric temperature rather than sea surface temperature and large scale convection is associated with monsoon rain events in Kerala, when oxygen gets highly depleted.
- The concentration and isotopic composition (ϵ Nd) of dissolved Nd in the water column of the Arabian Sea indicate a negligible riverine contribution to the Arabian Sea surface waters and reaffirm the supply of surface waters from the Bay of Bengal to the Arabian Sea during winter monsoon. This study highlights the significant dust deposition over the Arabian Sea resulting in considerable amount of dissolved Nd in its surface water. The dust deposition flux over this oceanic basin is estimated to be $8 \pm 2 \text{ g.m.}^{-2}\text{y}^{-1}$ contributing ~ 40 million gram Nd annually to the Arabian Sea, about two order magnitudes higher compared to its riverine supply.
- A study carried out in the Narmada and the Tapi rivers and estuaries indicates fractionation of Mo isotopes both in rivers and estuaries through particle adsorption and desorption in rivers and estuaries, respectively. Mo isotopes display non-conservative behaviour in these estuaries resulting from significant input of lighter Mo isotope, either from particle release or its supply from submarine groundwater discharge in estuary. This study underscores the need to characterize Mo isotope composition of global rivers and estuaries before using it as a proxy of paleo-redox condition.

Theoretical and Computational Physics

- We studied the question of vacuum stability of the Higgs potential and the constraints on new physics, in particular, the neutrino see-saw models from the Higgs vacuum stability criterion. The issue of vacuum stability and large radiative correction to the Higgs mass are also addressed by extending the symmetry of the standard model with Supersymmetry. This, however, poses a new problem in that the mass of the Higgs predicted in Supersymmetry is close to the Z-boson mass and much lower than the observed 125 GeV boson seen at the LHC. Extensions of the minimal supersymmetric standard model which would solve the Higgs mass problem have been explored. Models of supersymmetric dark matter which are consistent with the observation of the relic density, direct detection experiments and possible signals in cosmic rays have also been studied.
- Grand Unified models of the strong and electroweak interactions have been constructed which would explain the observed neutrino masses and mixings. A $\mu - \tau$ symmetry is proposed for the fermion masses to explain the observed neutrino masses. These models stand aside other similar models due to their testability in the future neutrinoless double-beta decay experiments. The consequences for neutrinoless double beta decay have also been studied in the context of TeV scale left-right symmetric extensions of the Standard Model. Such models and TeV scale see-saw models of neutrino mass were studied with testable predictions at the LHC.
- A Model of neutrino decay and oscillation into sterile species have been constructed which would explain why the Bahcall-Waxman prediction for neutrino flux from Gamma Ray Bursts was not observed in the IceCube experiment.
- An experiment using liquid argon based detector is proposed which would determine the hierarchy of neutrino masses and the octant of the 2-3 mixing angle using atmospheric neutrinos as well as collimated neutrinos from colliders.
- The experimental result that neutrinos could travel faster than light was shown to be inconsistent with the other known physics like pion and kaon decay rates. The methodology of calculating the decay rates

of light mesons when Lorentz invariance is violated has subsequently been generalized to discriminate the Lorentz invariance violation from the violation of equivalence principle.

- Tests of properties of the top quark at the LHC and at future electron-positron colliders have been suggested. A general analysis of the top spin has been done and a novel way of looking for new physics with polarized beams at an electron-positron collider have been proposed. On the other hand, at hadron colliders, looking for anomalous couplings of the top quark with gluons through decay-lepton asymmetries would provide useful information about new physics beyond the standard model.
- The bulk and shear viscosities of quark gluon plasma and dense hadron gas were computed which could be tested in heavy ion collision experiments like RHIC and FAIR. The kinetics of chiral phase transitions was studied with emphasis on the inertial term in the Langevin equation. The thermal conductivity of quark matter was also computed with testable predictions in heavy ion collision experiments.
- Quantum phase transitions (QPT) - that is phase transitions that occur at zero temperature as a function of a coupling constant - have become very important as the concept of QPT can be used in mesoscopic systems. These are studied in nuclei employing interacting boson models. Recent data on low lying Sulfur isotopes have been interpreted by doing a large shell model calculation. A relativistic coupled clustered theory was developed for the purpose of computing the electric dipole polarizabilities of Ne, Ar, Xe and Rn.
- Nuclear charge radii of a number of Ra isotopes has been computed which would be useful in measurements of atomic parity violation in Ra. The computed nuclear octupole moment of ^{137}Ba differ significantly from earlier calculations that was reported in literature. The octupole moment of ^{173}Yb was computed from the measurement of hyperfine transitions and the hyperfine coefficients resulting from these calculations are improved by two order of magnitude in accuracy over the earlier calculations.
- Kelvin-Helmholtz (K-H) instability in dusty plasma was studied and new instabilities in the strongly coupled regime were determined. It was observed that in addition to the conventional nonlocal KH instability, there exists a local instability in the strong coupling case. The interplay of the KH mode with this local instability shows up in the simulations as an interesting phenomenon of recurrence in the nonlinear regime.
- Complex networks were studied and the issue of amplitude death by environmental coupling was investigated. The results suggest an universal relation between the critical coupling strength and the largest non-zero eigenvalue of the coupling matrix.
- There exist extreme events such as the traffic jams, floods, power black-outs that take place on network. Such extreme event fluctuations in random walk systems were studied using the model of complex networks. It was found that the nodes with larger value of strength, on an average, display lower probability for the occurrence of extreme events compared to the nodes with lower value of strength.
- The synchronization of time-varying networks was studied and stability conditions were derived. Relations between critical coupling constants for synchronization and switching times for time-varying and time average networks were found.
- The optical conductivity of the cuprate CN-COC was studied using the Yang-Rice-Zhang (YRZ) renormalised mean field theory. The analysis shows that YRZ phenomenological model although quite successful in photoemission spectroscopy needs further improvements in addressing the charge transport in CuO_2 planes.

Awards and honours

Faculty Members

U. R. Rao

1. Inducted into the highly prestigious “Satellite Hall of Fame” – 2013.

J. N. Goswami

2. Member, Scientific Advisory Committee, COSPAR – 2013.
3. Member, Indo-Japan Science Council – 2013.
4. Chairman, Earth and Environmental Science Research Committee, CSIR.

N. Bhandari

5. ISRO Outstanding Achievement Award.

A. K. Singhvi

6. Birbal Sahni Centenary Gold Medal of the Indian Science Congress – 2013.
7. Chair, Program Advisory and Monitoring Committee for Geosciences, Ministry of Earth Sciences, Government of India.

V. K. B. Kota

8. Life Time Achievement Award, Organizing committee of the International Conference on “Recent Trends in Nuclear Physics-2012”, Barotiwala (H.P.), November 19-21 (2012) and the Chitkara University, for valuable contribution to the nuclear physics research in India.
9. Member, Programme Advisory Committee, DST, on Plasma, High Energy, Nuclear Physics, Astronomy & Astrophysics and Non-linear Dynamics, 2012-2015.

P. Venkatakrishnan

10. Member, editorial Board of Solar Physics, 2013-16
11. Chaired a session, Indo-UK Workshop on Coronal Physics, IIA, Bangalore, January 21, 2013

R. Ramesh

12. Professor Sir Albert Charles Seward Memorial Lecture Award, BSIP, Lucknow, 2012.

M. M. Sarin

13. Member, Scientific Advisory Committee, Space Physics Laboratory, Trivandrum.
14. Member, Project Appraisal and Monitoring Committee on Atmospheric Sciences, Ministry of Earth Sciences, New Delhi.

15. Chairman, Project Monitoring Committee, MAPAN, Project on Air Quality Monitoring Stations, Ministry of Earth Sciences, New Delhi.

S. K. Gupta

16. NGRI-AHI Indian National Hydrology Lecture Award - 2012, CSIR-NGRI-AHI, Hyderabad.

N. M. Ashok

17. Astronautical Society of India award for "Space Sciences and Applications", 2011.

A. Ambastha

18. Member, Editorial Board, Journal of Astrophysics and Astronomy, Indian Academy of Sciences, Bangalore (January 2013-December 2015)
19. Chaired the session: "The Sun and Solar System", 30th Meeting of the Astronomical Society of India, Trivandrum, February 20, 2013.

S. Lal

20. J. C. Bose National Fellowship of the DST, 2012.
21. Member, Scientific Advisory Committee (SAC) of the National Atmospheric Research Laboratory, Gadanki.

S. A. Haider

22. Fellow, Indian National Science Academy (INSA)
23. Guest Editor, Special Issue on Advances in Planetary Atmospheres and Exploration in Planetary and Space Science.

T. Chandrasekhar

24. Member, Expert Committee of MoES regarding future of Indian Centre of Space Research, Kolkatta.
25. Member, Board of Studies, Physical Sciences, Indian Institute of Space Science and Technology, Thiruvananthapuram
26. Member, Board of Studies, Space Science, Centre for Space Science and Technology Education in Asia and the Pacific.

R. Sekar

27. Member, Research Advisory Committee, Indian Institute of Geomagnetism, Mumbai.

R. Jain

28. Convener, Planetary Session "Exploring Habitability in the Solar System and Beyond", AOGS-AGU Joint Assembly, Resorts World Convention Centre, Singapore, September, 2012.
29. "Lifetime Achievement Award", Government Autonomous P. G. College Satna, Govt. of Madhya Pradesh, 2013.

D. Pallamraju

30. Vice-Chair, Commission on Earth's Upper Atmosphere and Ionosphere, COSPAR, 2012 – 2016.
31. Main Convener, "General Session on Ionosphere and Atmosphere", 9th annual Asia Oceania Geosciences Society (AOGS) Meeting, Singapore, August 2012.
32. Member, Scientific Organizing Committee, 2012 ISWI & MAGDAS School on Space Science, 17–26 September, LAPAN, Bandung, West Java, Indonesia.
33. Member, Scientific Organizing Committee, International Symposium on Solar Terrestrial Physics, 4–9 November, 2012, IISER, Pune, India.

S. K. Singh

34. Member, International GEOTRACES Data Management Committee.

N. Srivastava

35. LPI Career Development Award, USA, 2013.

R. D. Deshpande

36. Expert, Isotope Hydrology, International Atomic Energy Agency (IAEA), Vienna, to conduct a Single Faculty Training Programme for two weeks, Thailand Institute of Nuclear Technology, Bangkok, Thailand.
37. Member, Expert Committee for Earth and Atmospheric Sciences, Fast Track Young Scientist Scheme of DST-SERB.
38. Member, Research Advisory Group, National Institute of Hydrology, Roorkee.
39. Member, Advisory Committee, International Symposium on Integrated Water Resources Management, Centre for Water Resources Development and Management, Kozhikode, India and McMaster University, Canada.

Nandita Srivastava

40. Chaired the Space weather session, 39th COSPAR General Assembly, Mysore, 14-22 July, 2012

41. Chaired the tutorial session, ISSTP 2012, Pune, 5-9 November, 2012
42. Convener, session on "New and ongoing initiatives in ground-based solar observations", European Geophysical Union Meeting, Vienna, 7-12 April, 2013

B. K. Sahoo

43. Indian National Science Academy Medal for Young Scientists, 2012.

Students

S. Tiwari

44. Justice Oak Award for best thesis conferred by Astronomical Society of India, February, 2013.

S. K. Bisoi

45. Best poster award for a paper "Asymmetry in periodicity of the photospheric magnetic field of the Sun: A probe to the unusual solar minimum prior to the solar cycle 24", IAU Symposium: 294, Solar and Astrophysical Dynamos and Magnetic Activity, Beijing, China, August, 2012.

T. Basak

46. First prize in an essay competition on the topic "What is the meaning of the discovery of Higgs boson? If it is the 'Higgs', how would you name it?", Summer School, SLAC Summer Institute, Stanford, California, August 2012.

S. G. Reddy

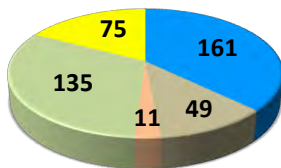
47. 1st place student presentation for a paper entitled, "Determination of Mueller matrix of an optical component with Simon-Mukunda polarization gadget", International conference of Fiber Optics and Photonics, IIT Madras, Chennai, December 10-12, 2012.

Administration

48. PRL has received Second Prize, conferred by Town Official Language Committee (TOLIC), Ahmedabad for excellent contribution towards implementation of Official Language Policy during 2012-2013. A certificate of appreciation has also been given to Shri R. S. Gupta, Hindi Officer-II & OSD.

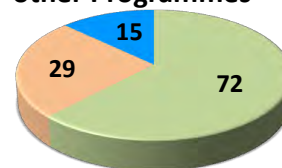
Human Resource Development

Scientific Contributions



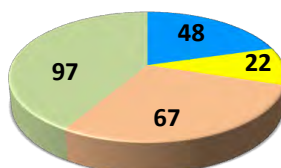
- Publications in Journals
- Publications in Proceedings of Conference / Workshop / Symposia
- Ph.D. Theses
- Invited Talks at Conference / Symposia / Workshop
- Lectures at Universities / Institutions

Doctoral, Post Doctoral and other Programmes



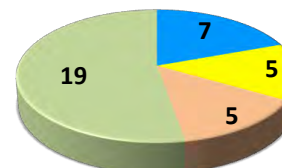
- Research Fellows
- Post - Doctoral Fellows
- Project Associates

Staff Structure



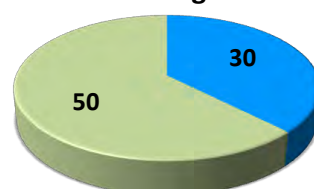
- Administrative
- Auxilliary
- Scientific
- Technical

Staff in Allied Services



- Tradesman Trainees
- Project Engineers
- Library Trainees
- Office + Computer Operator Trainees

Technical Programmes



- Engineering Trainees
- Summer Trainees

Theses Submitted

Vishal H. Joshi

1. "Probing the Secondary Star and Accretion Geometry of Intermediate Polars", Gujarat University, Ahmedabad, April 2012.

Pravin Vaity

2. "Propagation of Engineered Beams through Photorefractive Materials", Mohanlal Sukhadia University, Udaipur, July 2012.

Bikkina Srinivas

3. "Atmospheric Deposition of N, P and Fe to the Northern Indian Ocean", Mohanlal Sukhadia University, Udaipur, July, 2012.

Moumita Das

4. "Theoretical Studies of Cosmological Models in the light of Experimental Observations", Mohanlal Sukhadia University, Udaipur, July, 2012.

Suman Acharya

5. "Study of Synchronization in Coupled Dynamical Systems", Mohanlal Sukhadia University, Udaipur, August, 2012.

Vimal Kishor

6. "Study of dynamical processes on complex networks", Mohanlal Sukhadia University, Udaipur, September, 2012.

Prasant Rajput

7. "Atmospheric Polycyclic Aromatic Hydrocarbons: Identification, Abundances and Spatio-Temporal Variation", Mohanlal Sukhadia University, Udaipur, September, 2012.

Satinder Pal Singh

8. "U, Re, Mo and isotopic studies of Boron in water and sediments of the northern Indian Ocean: Implications to Contemporary and Paleo-Biogeochemical processes, Mohanlal Sukhadia University, Udaipur, October 2012.

Ashish Raj

9. "Near Infrared Spectroscopy and Photometry of Novae, Mohanlal Sukhadia University, Udaipur, November 2012.

Tapas Baug

10. "Lunar Occultation Studies of Late type Stars, Mohanlal Sukhadia University, Udaipur, November 2012.

Neeraj Awasthi

11. "Geochemical and Isotopic studies of sediments from the Andaman Islands and the Andaman Sea, M.S. University, Vadodara, December 2012.

Colloquia/Public Lectures by Visitors

Prof. R. Krishnan

Indian Institute of tropical Meteorology, Pune

Will the South Asian monsoon overturning circulation stabilize any further?

Prof. Satish R. Shetye

National Institute of Oceanography, Goa

Physical process in monsoonal estuaries of India: need for a new research approach

Prof. Arikala Raghurama Rao

Tata Institute of Fundamental & Research, Mumbai

Black holes in the universe: an X-ray view

Prof. Wing-Huen Ip

National Central University, Taiwan

The Mysteries of Saturn's Rings

Prof. Wim Hermsen

Netherlands Institute for Space Research, Netherlands

Research at the Netherlands Institute for Space Research

Prof. Raj Gandhi

Harish Chandra Research Institute, Allahabad

Ultra-High Energy (UHE) Neutrinos: Status and Puzzles

Prof. V. V. S. S. Sharma

National Institute of Oceanography, Vishakhapatnam

Biogeochemistry of Indian estuaries

Prof. Sanjay Puri

Jawaharlal Nehru University, New Delhi

Kinetics of Phase Transitions

Prof. R. Shanker

Banaras Hindu University, Varanasi

Formation, structure and fragmentation dynamics of CO_2^{q+} ($q \leq 3$) ions due to impact of 12 keV electrons

Prof. R. Rajaraman

Jawaharlal Nehru University, New Delhi & Co-Chairman, International Panel on Fissile Materials

Nuclear Energy: Problems and Prospects

Prof. Robert F. Anderson

Lamont-Doherty Earth Observatory and Columbia University, USA

Abrupt climate change and CO_2 : The bipolar seesaw vs. the winds

Prof. Ian. D. Hutcheon

Glenn Seaborg Institute, Lawrence Livermore National Laboratory, USA

Nuclear Forensics: An Emerging and Still Inexact Science

Prof. M. Vijayan

Indian Institute of Science, Bangalore

Form and function of proteins. Historical background and the Indian effort.

Prof. A. Surjalal Sharma

Goddard Planetary Heliophysics Institute, University of Maryland, United States

Multiscale Phenomena of the Earth's Magnetosphere

Prof. E. Masso

Universitat Autònoma de Barcelona(UAB), Spain

The search for new light weakly-interacting particles

Prof. Sunanda Banerjee

Saha Institute of Nuclear Physics, Kolkata

Higgs Boson- Have we seen it?

Prof. Debi. Prasad. Choudhury
California State University, USA
Structure of Sunspot

Dr. Manoj Purvankara
University of Rochester, USA
Infrared Spectroscopy of Protostars with Spitzer & Herschel: Probing the earliest stages of stellar birth

Prof. Girijesh Kumar Mehta
Inter University Accelerator Centre, New Delhi
Charge Particle Nanotechnology [CHARPAN]-The New Frontier

Prof. Milan Sanyal
Saha Institute of Nuclear Physics, Kolkata
Low-dimensional Physics and Ordering in Nano-structured Materials

Prof. Carlos A. Trallero
Kansas State University, USA
Learning about molecules with extreme non-linear optics

Dr. Ashish Mahabal
California Institute of Technology, USA
It's time for time domain Astronomy

Prof. Himanshu S. Mazumdar
Dharamsinh Desai University, Nadiad
Challenges in Autonomous Robotics Research and its Applications

Prof. Deepak Mathur
Tata Institute of Fundamental Research, Mumbai
Ultrafast Science: Adventures on the Interface of Physics, Chemistry and Biology

Prof. M. D. Sastry
Gemological Institute of India, Mumbai
Colourful Story of Diamond: A Journey from Crown Jewel to Quantum Information Processing-Role of Spectroscopy of point defects

Dr. Ashima Anand
Vallabhbhai Patel Chest Institute, University of Delhi, New Delhi
Determining Authorship: Criteria & Ethical Niceties

Conferences/Symposia/Workshops by PRL

Astronomy & Astrophysics

1. "X-ray View of Cosmos", PRL, 23-25, April, 2012.
2. "International Workshop on Radial Velocity: Current and Future trends", PRL, 21-22, January, 2013.

Planetary Sciences & PLANEX Program

3. ISROs STP Course on Planetary Exploration, at PRL, 19-21, December, 2012.
4. 13th PLANEX Workshop on "Impacts on Solar System Objects", CSIR-NGRI, Hyderabad, 6-12, January, 2013.
5. PLANEX Projects PIs Review meeting, PRL, 8-9, March, 2013.

Space, Atmospheric, Molecular and Laser Physics

6. "International Symposium on Atmospheres of Terrestrial Planets: Observations & Modeling", PRL, 23-24, July, 2012.

Geosciences

7. "International Workshop on International Quaternary Union's Dunes Atlas program", PRL, Ahmedabad, with a field excursion in Thar Desert, 25 March-02 April, 2012.
8. "International GEOTRACES Data Management and Scientific Steering Committee Meeting", Goa, 27-31, October, 2012.

Theoretical and Computational Physics

9. "Program on CP Violation in Elementary Particles and Composite Systems", Jointly organized by ICTS, Bangalore, IIA, Bangalore and PRL, Mahabaleshwar, 7-23, February, 2013.

Invited Talks at Conference / Symposia / Workshops

Astronomy & Astrophysics

N. M. Ashok

1. "An infrared view of novae outbursts from Mt. Abu Observatory", 30th meeting of the Astronomical Society of India, Thiruvananthapuram, February 20-23, 2013.
2. "Near-infrared studies of novae and related objects", International Conference on Transients and Timing: A multi-wavelength approach, IUCCA, Pune, March 04-08, 2013.

P. Janardhan

3. "The Solar Wind", First IIST-IUCAA Introductory Workshop on Solar Physics, November 29- December 01, 2012.

R. Jain

4. "Sun-Earth Connection", DST Sponsored workshop on INSPIRE Programme, Hemchandracharya North Gujarat University, Patan, July 28–August 01, 2012.
5. "Sun in Multi-wavelength", IUCAA Resource Centre (IRC), Department of Statistics, Calcutta University, August 25, 2012.

S. Naik

6. "X-ray and near-infrared studies of Be/X-ray binaries", Conference on Neutron Stars: Inside and Outside, Saha Institute of Nuclear Physics, Kolkata, October 18-19, 2012.
7. "Accretion Powered Binary X-ray Pulsars", 2nd IUCAA X-ray Astronomy School, IUCAA, Pune, February 03–March 02, 2013.
8. "X-ray and Infrared Studies of Be/X-ray Binary Pulsars" and "Recent trends in the study of compact objects: Theory and Observation", IIT Guwahati, March 11-13, 2013.

S. Vadawale

9. "Advance Si Detectors for X-ray astronomy" and "Advance concepts in X-ray spectroscopy", 2nd IUCAA X-ray Astronomy School, IUCAA, Pune, February 03–March 02, 2013.
10. "Measuring X-ray polarization with CZTI onboard Astrosat", Meeting on 'Prospects with Astrosat CZT-I', TIFR, Mumbai, September 06-07, 2012.
11. "Orbital Remote Sensing of Planets: Determining surface chemistry with X-ray Fluorescence Spectroscopy", ISRO STP course, Physical Research Laboratory, December 19-21, 2012.

T. Chandrasekhar

12. "Lunar Occultations in the Infrared: Evolution from single element detectors to Sub-arrays", 30th meeting of the Astronomical Society of India (ASI), Thiruvananthapuram, February 20-23, 2013.
13. "Minor bodies of the Solar System", 13th PLANEX Workshop on Impacts on Solar System Objects, NGRI, Hyderabad, January 06-12, 2013.

Solar Physics**A. Ambastha**

14. "Observing the Sun on total eclipses and planetary transits" under sponsorship of Vigyan Prasar, "Orientation workshop on transit of Venus", M.L.Sukhadia University, Udaipur, April 26-28, 2012.
15. "Photospheric Transients and Spectral Line Changes Associated with a Large X2.2 Flare", COSPAR 2012, Mysore, July 20, 2012.
16. "The Sun-Our Daytime Star", "Helioseismology - Probing the Structure and Dynamics of the Solar Interior", and "Solar magnetic Field", IUCAA Workshop on Solar Physics, Ramakrishna Mission Vivekananda University, Belur, Kolkata, February 05-06, 2013.

B. Joshi

17. "Solar Eruptive Phenomena", RKMVU – IUCAA Introductory Workshop on Solar Physics, Ramakrishna Mission Vivekananda University, Belur Math, Howrah, West Bengal, February 05-07, 2013.
18. "RHESSI and TRACE observations of multiple flare activity in AR 10656 and associated filament eruption", 30th meeting of the Astronomical Society of India (ASI), Thiruvananthapuram, February 20 - 22, 2013.
19. "Evidence of magnetic reconnection during the extended X-ray precursor phase of an X-class solar flare", Scientific assembly of the Asia Oceania Geosciences Society (AOGS), Singapore, August 13 - 17, 2012.
20. "Soft X-ray flare index during solar cycles 21-24: evolutionary aspects and hemispherical asymmetry", Scientific assembly of the Asia Oceania Geosciences Society (AOGS), Singapore, August 13 - 17, 2012.
21. "Multi-wavelength investigation of pre-flare activity and magnetic reconnection during the evolutionary phases of a solar eruptive flare", 39th Scientific assembly of the Committee on Space Research (COSPAR), Mysore, July 14 - 22, 2012

B. Kumar

22. "SDO/HMI perspectives of the flare-induced seismicity in the active region NOAA 11158 during an X2.2 class flare", GONG 2012/ SOHO 27/ SDO-5 International

Conference, Palm Cove, Queensland, Australia, November 12-16, 2012.

Nandita Srivastava

23. "On the estimation of true speeds and arrival times of CMEs", E3.1 session, 39th COSPAR General Assembly, Mysore, July 14-22, 2012.
24. "CMEs and ICMEs", ISSTP 2012, Pune, November 05-09, 2012.

P. Venkatakrishnan

25. "Electric Currents in Sunspots", 39th Scientific assembly of the Committee on Space Research (COSPAR), Mysore, July 14 - 22, 2012.
26. "Signatures of sub-photospheric electric currents", 39th Scientific assembly of the Committee on Space Research (COSPAR), Mysore, July 14 - 22, 2012.
27. "Multi-Application Solar Telescope", ISSTP 2012, Pune, November 05-09, 2012.

Planetary Sciences & PLANEX Program**J. N. Goswami**

28. "Micro-analytical Techniques in Planetary and Earth Sciences", National Institute of Oceanography, Goa, May 04, 2012.
29. "The new face of the Moon", Interdisciplinary Talk, COSPAR, Mysore, July 15, 2012.
30. "Exploring the unknown", Inaugural Talk, DST Inspire Program, NIO, Goa, November 19, 2012.
31. "Exploration of the Solar System : The Indian scenario, Plenary Talk", Centenary Indian Science Congress, Kolkata, January 04, 2013.
32. "Planetary Geosciences: Achievements and Future Trends", Earth Sci. Session, Centenary Indian Science Congress, Kolkata, January 05, 2013.
33. "The first ten million years of the Solar System", Inaugural Address, ISMAS-TRICON, Goa, March 03, 2013.

S. V. S. Murty

34. "Evolution of Mars atmosphere: Results from martian meteorites", International symposium on Atmospheres of terrestrial planets: Observations and modeling, PRL, Ahmedabad, July 23-24, 2012.
35. "Isotope Cosmochemistry: Techniques and some important results", XXXI Annual conference Indian Council of Chemists, Saurashtra University, Rajkot, December 26-28, 2012.
36. "What have we learnt about Mars from martian meteorite studies", 100th Indian Science Congress, Kolkata, January 04-08, 2013.

37. "Giant impacts and consequences", 13th PLANEX Workshop on Impacts on solar system objects, CSIR-NGRI, Hyderabad, January 06-12, 2013.
38. "Exploration of Moon and Mars: ISRO Plans", Workshop on 'Current trends in Radial Velocity and Exoplanets', PRL, Ahmedabd, January 21-22, 2013.
39. "Recent results from Moon and Mars missions", International Workshop on 'Chemical evolution and origin of life', IIT, Roorke, March 21-23, 2013.
40. "Evolution of Earth, Moon and Mars", ISRO STP Course on Planetary Exploration, PRL, Ahmedabad, December 19-21, 2012.
41. "ISROs Mars Orbiter Mission", Special lecture, DST-SERC school on Tokamaks and magnetized Plasma Fusion, IPR, Gandhinagar, February 25-March 15, 2013.
50. "Latitudinal/Longitudinal coupling of atmospheres during Space Weather disturbances", International Symposium on Solar Terrestrial Physics, Indian Institute of Science Engineering and Research, Pune, November 04-09, 2012.
51. "Geospace Response to Space Weather", Seminar on high potential areas of physics, St. Xaviers College & INSA, Ahmedabad, January 31, 2013.
52. "Optical investigations of upper atmospheric phenomena", ISRO-CNES Discussion Meet on Future Cooperation, ISRO HQ, Bangalore, February 05, 2013.
53. "Optical manifestations of Space Weather phenomena", Workshop on Remote Sensing of Atmospheres and Space, University of Calcutta, Kolkata, March 07, 2013.
54. "Space Weather interactions on Earth's atmospheres: Science and Applications", Workshop on Remote Sensing of Atmospheres and Space, University of Calcutta, Kolkata, March 07, 2013.

Space, Atmospheric, Molecular and Laser Physics

B. Bapat

42. "Why Study Physics", DST-INSPIRE Camp, Gogate-Jogalekar College, Ratnagiri, October 27, 2012.
43. Lecture series on "Charged Particle Spectrometry", DST-SERC School on Atomic and Molecular Physics, TIFR, Mumbai, February 17-20, 2013.
44. "Association of atoms and formation of exotic molecular ions by electron impact on molecules", National Conference on 'Electron Collision Processes in Atomic and Molecular Physics', RP&VPTP College, Vallabh Vidyanagar, March 07-09, 2013.

D. Pallamraju

45. "Investigations on the energetics of high-latitude upper atmosphere using combined radar & optical probing measurements", 39th COSPAR Scientific Assembly, Mysore, July 14-22, 2012.
46. "Investigations on upper atmospheric interactions carried out under the CAWSES-India Program", 39th COSPAR Scientific Assembly, Mysore, July 14-22, 2012.
47. "Geospace response to space weather using ground-based optical and radio measurements", Panel of Space Situational Awareness, Space Weather and Space Debris Research, 39th COSPAR Scientific Assembly, Mysore, July 14-22, 2012.
48. "Investigations of upper atmospheric phenomena using ground and balloon-borne platforms", Workshop on Space Science Education and Technology, Indian Institute of Space Technology, Trivandrum, July 25-26, 2012.
49. "Earths atmosphere and its interactions with the Solar and Interplanetary phenomena", DST – INSPIRE Program, Kasturba Walchand College, Sangli, Maharashtra, August 01-05, 2012.

H. Chandra

55. Lectures on "Space Science", CSSTE-AP 8th Course on Space and Atmospheric Sciences, Physical Research Laboratory, Ahmedabad, 2012 - 2013.(46 lectures)

L. Sahu

56. "Change in oceanic emissions of light alkenes due to monsoon circulations over northern Indian Ocean", Second International Symposium: Effect of Climate Change on the World's Oceans, Yeosu, South Korea, May 15-19, 2012.
57. "Earth's Atmosphere: Green House Gases (GHGs), Aerosols and Climate Change", Three-Days Seminar on Current Trends in Science, Rajasthan English Hr. Sec. School, Ahmedabad, December 21-23, 2012.
58. "Black carbon and climate in India", Challenges and opportunities in Air Pollution and Climate Change-2 (CHOP-C2) "Germany-India-2013", Sree Ramachandra University, Porur, Chennai, India, January 23-25, 2013.
59. "Volatile Organic Compounds (VOCs) in India and Surrounding Marine Regions", workshop on Climate and Health Effects of Tropical Aerosols, Indian Institute of Technology Madras, Chennai, March 6-7, 2013.

M. Bagiya

60. "Space Weather", CSSTE-AP 8th Course on Space and Atmospheric Sciences, Physical Research Laboratory, Ahmedabad, 2012-2013.
61. "Airglow and Optical Techniques", CSSTE-AP 8th Course on Space and Atmospheric Sciences, Physical Research Laboratory, Ahmedabad, 2012-2013.

R. P. Singh

62. "Optical Vortices – phase singularities of light", Seminar on Recent Advances in Applied Optics and Optoelectronics, The M.S. University of Baroda, September 22, 2012.
63. "Down-Converted Photons: A Study with Optical vortices", DAE-BRNS Symposium on Atomic, Molecular and Optical Physics, Indian Institute of Science Education and Research-Kolkata (IISER-K), December 14-17, 2012.
64. "Optical vortices: classical & quantum studies", 37th National Symposium of Optical Society of India, Department of Physics, Pondicherry University, Pondicherry, January 23-25, 2013.

R. Sridharan

65. "Space Weather – touching our lives everyday", Workshop on Remote Sensing of Atmospheres and Space, University of Calcutta, Kolkata, March 18, 2013.
66. "Chasing the Moon – the Indian way", Workshop on Remote Sensing of Atmospheres and Space, University of Calcutta, Kolkata, March 19, 2013.

S. Lal

67. "Atmospheric Composition and Climate: Past and Future", National Symposium on Current trends in Atmospheric Research including Communication And Navigation, Vigana Bharathi Institute of Technology, Hyderabad, December 21-22, 2012.
68. "Research Activities at Physical Research Laboratory, Ahmedabad", Seminar on Current trends in Research and Applications of Physical Sciences in Gujarat, Sardar Patel University, Vallabh Vidyanagar, December 29, 2012.
69. "Earth's atmosphere and atmospheric chemistry", CSSTE-AP 8th Course on Space and Atmospheric Sciences, Physical Research Laboratory, Ahmedabad, 2012 - 2013. (5 lectures)

R. Sekar

70. "Recent advances on the low latitude ionospheric irregularities over Indian sector", 39th COSPAR Scientific Assembly, Mysore, July 14-22, 2012.

S. A. Haider

71. "Ionosphere of Mars during quiet and disturbed conditions", 9th Annual Meeting of Asia Oceanic Geosciences Society (AOGS), Singapore, August 13-17, 2012.

S. P. Gupta

72. "Middle atmosphere, thermosphere and measurement techniques", CSSTE-AP 8th Course on Space and Atmospheric Sciences, Physical Research Laboratory, Ahmedabad, August-October 2012. (4 lectures)
73. "Impact of plasma irregularities in the meteor trail on propagation of VHF radio waves", National Symposium on Current Trends in Atmospheric Research Including Communication and Navigation, Vigana Bharathi Institute of Technology, Ghatkesar, Hyderabad, December 21-22, 2012.

S. Ramachandran

74. "Black carbon aerosols over an urban region: Characteristics, mixing and radiative forcing", NOAA Earth System Research Laboratory, Boulder, Colorado, USA, August 21, 2012.
75. "Seasonal variation, mixing and radiative forcing of black carbon aerosols", NOAA Geophysical Fluid Dynamics Laboratory, Princeton University, Princeton, New Jersey, USA, September 20, 2012.
76. "Climate change and variability", CSSTE AP 8th Course on Space and Atmospheric Sciences, Physical Research Laboratory, Ahmedabad, October 25-26, 2012. (2 lectures)
77. "Aerosols: Radiative effects", Seminar on Challenges in Climate Research, Indian Centre for Climate and Societal Impacts Research, Ahmedabad, January 05, 2013.
78. "Aerosols and biogeochemical coupling in climate model", ICTS Program on Advanced Dynamical Core Modeling for Atmospheric and Oceanic Circulations, National Atmospheric Research Laboratory, Gadanki, February 18-23, 2013.

S. Sharma

79. "Space & Atmospheric Sciences Research and Societal Perspectives", DST-INSPIRE Program, Kasturba Walchand College, Sangli, Maharashtra, August 01-05, 2012.

Geosciences**A. K. Singhvi**

80. "Geology, Luminescence, Climate, Tectonics, Biology, Medicine and their mutualism", National Seminar on Future trends in Physics, St Xaviers College, Ahmedabad, January 30, 2013.
81. "Land sea correlations: Pitfalls and Remedies", Fourth International Open Science Meeting of Past Global Changes (PAGES) core project, Goa, February 12, 2013.

M. M. Sarin

82. "Ocean Acidification: Present-day issues", DST-INSPIRE Camp, KSKV-Kachchh University, Bhuj, July 05, 2012.
83. "Ocean Carbon Cycle", DST-INSPIRE Camp, M.S. University, Vadodara, July 25, 2012.
84. "Ocean Carbon Cycle", DST-INSPIRE Camp, NMIMS University, Mumbai, October 03, 2012.
85. "Atmospheric carbonaceous aerosols from the Indo-Gangetic Plain: Sources and impacts", IASTA-2012, BARC, Mumbai, December 11-13, 2012.
86. "Atmospheric nano-particles: Potential role in chemistry-climate interaction", International ETPEMM Conference, Punjabi University, Patiala, December 18-20, 2012.
87. "Carbonaceous aerosols from biomass burning emissions in northern India: Sources and impact", International LCLUC Meeting, Karunya University, Coimbatore, January 09-11, 2013.
88. "Atmospheric deposition of N, P and Fe to northern Indian Ocean: Implications", International GESAMP-Nitrogen Workshop, University of East Anglia, Norwich, UK, February 11-14, 2013.
89. "Atmospheric outflow from the Indo-Gangetic Plain: New insights and implications", Indo-German Meeting, Ministry of Earth Sciences, New Delhi, March 08 2013.
96. "Isotope fingerprinting of hydrological cycle over India", Regional Science Congress on Science for Shaping the future of India, M.S. University of Baroda, Vadodara, September 15-16, 2012.
97. "Isotope applications in water resource management", Dept. of Water Resources Engineering, Chulalongkorn University, Bangkok, Thailand, October 05, 2012.
98. "Isotope applications in meteorology", Hydro and Agro Informatics Institute, Bangkok, Thailand, October 08, 2012.
99. "Results from Delta V Plus IRMS of IWIN National Programme", IRMS User Meet, Mussoorie, October 31–November 01, 2012.
100. "Water, earth and our future", DST-INSPIRE Science Camp, C.C. Patel Community Science Centre, Sardar Patel University Vallabh Vidyanagar, December 22, 2012.

R. D. Deshpande

90. "Water resources research using isotopes", DST-INSPIRE Summer Science Camp, Christ College, Rajkot, May 10, 2012.
91. "Water resources scenario of India and importance of isotope tracer applications", Explorations in Earth, Space and Planetary Sciences, S.P. University, Vallabh Vidyanagar, June 15, 2012.
92. "Water resources scenario of India and importance of isotope applications", DST-INSPIRE Internship Camp, Dept. of Earth and Environmental Science, Kachchh University, Bhuj, July 03, 2012.
93. "New insights from IWIN National Programme", Workshop on National Instrumentation facilities in Earth Sciences: Present status and future needs, DST's Integrated Research on High Priority Areas (IRHPA) Scheme. Department of Earth Sciences, Pondicherry University, Puducherry, July 19-20, 2012.
94. "Oxygen and hydrogen isotope systematics for hydrological applications", Workshop on Isotope Fingerprinting of Waters of India (IWIN) Field Campaign Through NIO-FSI collaboration, National Institute of Oceanography, Dona Paula, Goa, August 06-07, 2012.
95. "Application of isotopes for climate change studies", Keynote address, International Meet on Impact of Climate Change on Water Resources, Karunya University, Coimbatore, August 17-18, 2012.

R. Ramesh

101. "Study of the Earth: Geology, Meteorology and Hydrology", School on Application of Space Science, Kathmandu, Nepal, April, 02-11 2012.(3 lectures)
102. "Basics of Meteorology", Training Workshop for the International Science Olympiad, Goa University, Goa, May 08-12, 2012. (8 lectures)
103. "Applications of isotopes in Oceanography", in the 'Seminar on Explorations in Earth, Space & Planetary Sciences', Sardar Patel University, June 15, 2012.
104. "New results from the Indian Ocean", Thermo-Fisher User workshop, Mussorie, October 31, 2012.
105. "Professor Sir Albert Charles Seward Memorial lecture", Birbal Sahni Institute of Paleobotany, Lucknow, November 14, 2012.
106. "Problems of the Anthropocene", Indian Social Science Congress, KISS, Bhubaneswar, December 28, 2012.
107. "Geochemistry of the Indian Ocean", IGU Golden Jubilee Symposium, NIO, Goa, March 21, 2013.

S. Kumar

108. "Nitrogen cycling in Marine and Freshwater Environments", Third National Research Conference on Climate Change, Indian Institute of Science (IISc), Bangalore, November 03-04, 2012.

Theoretical and Computational Physics**A. C. Das**

109. "Introduction to Solar Physics, Magnetospheric Physics and Space Weather", 8th Post graduate Course in Space and Atmospheric Sciences of CSSTEAP, PRL, Ahmedabad, August 2012-Feb 2013.(25 Lectures)

B. K. Sahoo

110. "Probing Fundamental Physics Through Atoms: A key role by a hpc facility", Keynote address talk, 3rd Conference on Meta Computing, May Fair Hotel, Bhubaneswar, India, December 06-07, 2012.
111. "Precise Estimate of Nuclear Properties from Atomic Studies", 3rd DAE-BRNS symposium on Atomic, Molecular and Optical Physics (AMOP 2012), IISER, Kolkata, India, December 14-17, 2012.

D. Angom

112. "Relativistic effects on space clocks", SAC Lecture Series, Space Application Centre, Ahmedabad, July 09, 2012.
113. "A strange matter: coldest in Universe", INSPIRE programme, Manipur University, August 10, 2012.
114. "Light and duality: Newton vs Huygens", INSPIRE programme, Manipur University, August 11, 2012.
115. "Reconnections between vortex rings in superfluids", International Conference on Complex Processes in Plasmas and Nonlinear Dynamical Systems, Institute of Plasma Research, Gandhinagar, November 08, 2012.
116. "Computational Physics", National Seminar on High Potential Research Areas in Physics, St. Xavier's College, Ahmedabad, January 31, 2013

H. M. Mishra

117. "Hot and dense matter and search for perfect fluid", Conference of "Current Trends in Physics", Kendrapara College, Kendrapara, Odisha, January 16, 2013.
118. "Kinetics of chiral transitions and domain growth in quark matter", 8th International workshop on 'Critical point and onset of deconfinement (CPOD2013)', Napa, California, U.S.A., March 11-15, 2013.

J. Banerji

119. "Ultra-sensitive dual-mode waveguide interferometers", DAE-BRNS Symposium on Atomic, Molecular and Optical Physics, Indian Institute of Science Education and Research-Kolkata (IISER-K), December 14-17, 2012.

N. Mahajan

120. "Scalar 2 point function in de Sitter space", Workshop on 'Field theory and Gravity', Indian Institute of Science Education and Research, Thiruvananthapuram, April 05-06, 2012.

N. Singh

121. "Infrared optical properties of Cuprate superconductors: a Yang-Rice-Zhang ansatz study", Special Session, ICTP school and workshop on innovations in strongly correlated electronic systems, ICTP Trieste, Italy, August 06-17, 2012.

P. Konar

122. "Mass and Spin determination at LHC", HIGGSTOP-2013, Birla Institute of Technology & Science, Goa, February 26, 2013.

R. E. Amritkar

123. "Extreme events on complex networks and network failure", Conference on Dynamics Days, Asia Pacific 7, Academia Sinica, Taipei, Taiwan, August 06-09, 2012.
124. "Amplitude death in coupled dynamical systems", Workshop on 'Critical Phenomena and Complex Systems', Academia Sinica, Taipei, August 14, 2012.
125. "Synchronization of coupled non identical dynamical systems", Workshop on 'Critical Phenomena and Complex Systems', National Formosa University, Huwei, Yunlin, Taiwan, September 01-02, 2012.

R. Rangarajan

126. "A Career as a Physicist" and "Astroparticle Physics", INSPIRE Science Camp, M.S. University, Vadodara, June 30, 2012.
127. "Elementary Particles in Nature and the Search for the Higgs Boson", 66th National Level Science Symposium, Christ College, Rajkot, January 20, 2013.

S. D. Rindani

128. "Top polarization as a tool for studying new physics", 2nd KIAS Phenomenology Workshop, Korea Institute of Advanced Study, Seoul, S. Korea, September 10-14, 2012.

U. Sarkar

129. "Cosmological Consequences of Neutron-Antineutron Oscillation", NNbarX Collaboration meeting, Univ. Tennessee, Knoxville, Tennessee, USA, November 16-17, 2012.

V. K. B. kota

130. "Extended Interacting Boson Models for Exotic Nuclei", International workshop on 'Future Plan with Radioactive ion beam (FPRIB2012)', Saha Institute of Nuclear Physics (Kolkata, India), April 16-18, 2012.

131. "Shell model based spectral distribution and deformed configuration methods for double beta decay", International workshop on 'Towards the resolution of the double beta decay problem', European Centre for Theoretical Studies in Nuclear Physics and Related Areas (ECT*), Trento, Italy, September 03-07, 2012.
132. "Interacting Boson Model Applications To Exotic Nuclear Structure", International Conference on 'Recent Trends In Nuclear Physics-2012', Chitkara University, Barotiwala, Himachal Pradesh, India, November 19-21, 2012.
133. "Random Matrix Theory in Nuclear Structure: Past, Present and Future", DAE Symposium on 'Nuclear Physics', Delhi University, Delhi, India, December 03-07, 2012.
134. "Symmetries to Quantum Chaos and Quantum Phase Transitions", National Conference on 'Nuclear Physics', Sambalpur University, Sambalpur, Orissa, India, March 01-03, 2013.
135. "ETD for Preservation: A case Study", 15th International Symposium on Electronic Theses and Dissertation, Lima, Peru, September 12-14, 2012.

Library

Nishtha Anilkumar

Lectures at Universities / Institutions

Astronomy and Astrophysics

A. K. Singal

1. "Absolute Motion of the Earth in the Universe", Colloquium, Cotton College, Guwahati, February 13, 2013.
2. "Our large peculiar motion in the universe determined from the radio sky brightness anisotropy at 1.4 GHz", Colloquium, IIA, Bangalore, October 31, 2012.
3. "Gyro-orbit size, brightness temperature limit and implausibility of coherent emission by bunching in synchrotron radio sources", Colloquium, IISc, Bangalore, October 30, 2012.
4. "Large peculiar motion in the universe determined from the radio sky brightness anisotropy at 1.4 GHz", IIT, Kanpur, August 08, 2012.
5. "Our large peculiar motion in the universe determined from the radio sky brightness anisotropy at 1.4 GHz", RRI, Bangalore, July 04, 2012.

A. K. Awasthi

6. "Multi-wavelength study of Precursor Phase Emission in Solar Flares", National Astronomical Observatory of China (NAOC), September 07, 2012.

P. Janardhan

7. "Low density solar wind events observed at 1 AU and their space weather consequences", High Altitude Observatory, Boulder, Colorado, USA, May 31, 2012.

R. Jain

8. "Exploring the Dynamic Solar Corona", Colloquium, Variable Energy Cyclotron Centre Calcutta, August 24, 2012.
9. "Influences of the Sun on the Earth's Climate", DST Sponsored workshop on INSPIRE Programme Smt. Kasturba Walchand College, Sangli, Maharashtra, August 01-05, 2012.

S. Ganesh

10. "DST-INSPIRE lecture", Saurashtra University, Rajkot, 26-30, November, 2012.
11. "Windows to the Universe", Three-Days Seminar on Current Trends in Science, Rajasthan English Hr. Sec. School, Ahmedabad, December 21-23, 2012.

S. Vadawale

12. "X-ray Polarimetry – Why and How?", Department of Astronomy & Astrophysics, TIFR, May 31, 2012.

Solar Physics**B. Joshi**

13. "Solar eruptive phenomena: A multi-wavelength perspective", Space Physics Laboratory, Vikram Sarabhai Space Centre, Thiruvananthapuram, February 25, 2013.

P. Venkatakrishnan

14. "Sun: An Introduction", IIST, Thiruvananthapuram, November 28, 2012.
15. "Helioseismology", IIST, Thiruvananthapuram, November 28, 2012.
16. "Solar Magnetic Fields", IIST, Thiruvananthapuram, November 29, 2012.
17. "Overview of Udaipur Solar Observatory", Big Bear Solar Observatory, USA, January 08, 2013.
18. "Overview of Udaipur Solar Observatory", Helio Research, California, USA, January 10, 2013.
19. "Overview of Udaipur Solar Observatory", Stanford University, USA, January 18, 2013.

N. Srivastava

20. "On the estimation of true speeds and arrival times of CMEs", Belgian Institute for Space Aeronomy, BIRA-IASB, Brussels, Belgium, September 06, 2012.

Planetary Sciences & PLANEX Program**J. N. Goswami**

21. "Chandrayaan-1 and Beyond", June 12, 2012, ARIES, Nainital.
22. "India's Planetary Exploration Programme", Prof. Venkata Rao Memorial Talk, Gauhati University, September 03, 2012.
23. "The New Moon", Colloquium at the Physics Dept., Indian Institute of Science, Bangalore, February 15, 2013.
24. "Exploration of the Solar System and Beyond", M. S. University, Vadodara, February 24, 2013.

S. V. S. Murty

25. "Laboratory study of astromaterials" S.N. Bose National Centre for Basic Sciences, Kolkata, July 10-13, 2012.

Space, Atmospheric, Molecular and Laser Physics**A. Pandey**

26. "Molecular systems: A theoretical viewpoint", May 28, 2012.
27. "Molecular systems: Investigating the nature of stability", June 11, 2012.

B. Bapat

28. "Core ionisation and fragmentation of molecules using soft X-rays", October 08, 2012.

D. Chakrabarty

29. "Radar probing of the terrestrial upper atmosphere", Department of Physics, Saurashtra University, Rajkot, March 13, 2013.
30. "Space weather effects over low latitudes: An electric field perspective", Indian Institute of Geomagnetism, Navi Mumbai, March 22, 2013.

K. P. Subramanian

31. "Importance of Saha equation in LIBS algorithm", November 05, 2012.

K. Saha

32. "Understanding unimolecular reaction", April 30, 2012.
33. "Molecular fragmentation : Role of ionization process", May 21, 2012.

M. Sobhita

34. "Theory of Langmuir Probe: Evaluation of plasma parameters", Calicut University, April 26, 2012.

P. Deepa

35. "Electron temperature and density measurements in laser produced plasma using Langmuir Probe", Calicut University, May 03, 2012

P. Kumar

36. "Quantitative elemental analysis using LIBS", Prashant Kumar, October 22, 2012.

R. P. Singh

37. "Phase Singular Beams: A Study of Optical Vortices", University of Hyderabad, October 04, 2012.
38. "Experiments with phase singularities of light", Raman Research Institute, Bangalore, February 12, 2013.

S. P. Gupta

39. "E-region irregularities over low latitude during meteor shower days, rocket based measurements", Department of Earth and Space Science, University of Washington Seattle USA, April 21-May 03, 2012.
40. "Stratospheric conductivity: Balloon based measurements", Department of Earth and Space Science, University of Washington Seattle USA, April 24-May 03, 2012.

S. Ramachandran

41. "Aerosols, clouds and rainfall", Centre for Atmospheric Sciences, Indian Institute of Technology, Delhi, March 12, 2013.

S. Sharma

42. "Satellite and Ground Based Study of Middle Atmosphere over Indian Regions", National Remote Sensing Center (NRSC), Hyderabad, July 13, 2012.
43. "LIDAR: A Versatile Tool to Study Atmosphere", CSSTE-AP Course on Space Sciences, Physical Research Laboratory, and CSSTE-AP course on Satellite- Meteorology (SAT-MET), Space Applications Center, Ahmedabad, August 07, 2012.
44. "Research Avenues in Space and Atmospheric Sciences", PPN Post Graduate College, Chhatrapati Sahu Ji Maharaj University, Kanpur, November 29, 2012.

T. Pradeep

45. "Low energy ion scattering at ice surfaces", IIT, Madras, March 21, 2012.

Geosciences**A.K. Singhvi**

46. "Relevance of geo-sciences in planning the societal future", Indian National Science Academy, Delhi, October 17, 2012.
47. "Future Earth: Societal Relevance of- and Scientific Challenges for- Geosciences as Services", Department of Geology, Delhi University, Delhi, February 28, 2013

48. "Future Earth: Societal Relevance of – and Scientific Challenges for– Geosciences as Services", Birbal Sahni Institute of Paleobotany, Lucknow, March 04, 2013.

J. S. Ray

49. "Third rock from the Sun – the story of the Earth", Sardar Patel University, Ballav Vidyanagar, June 15, 2012.
50. "Learning from volcanoes – the story of Barren Island", Indian Institute of Space Science and Technology, Trivandrum, August 09, 2012.

M. G. Yadava

51. "Long term climate change", CSSTEAP, SAC, Ahmedabad, January 21-24, 2013.(Four Lectures)

R. Ramesh

52. "DST-INSPIRE lecture", K. R. Rangasamy College, Thiruchengodu, August 25, 2012.
53. "Geophysical Fluid Dynamics", Centre for Earth and Space Sciences, University of Hyderabad, September-October 2012.(25 lecture course)
54. "DST-INSPIRE lecture", KIIT, Bhubaneswar, September 15, 2012.
55. "Atmospheric Physics", ISM Dhanbad, November 07-09, 2012.(5 lectures)
56. "DST-INSPIRE lecture", Amity University, Jaipur, January 22, 2013.
57. "DST-INSIPRE lecture", Amity University, Lucknow, January 24, 2013.

R. D. Deshpande

58. "Natkhath monsoon ka raaz", Devilal Kothari Memorial Lecture, Sadbhavna Trust, Banswara, November 25, 2012.

Theoretical and Computational Physics**A. C. Das**

59. "The Solar Wind and Magnetospheric Dynamics", Centre of Atmospheric Studies, Post Graduate Course, Physics Department, Dibrugarh University, March 18-29,2013. (18 lectures)

D. Angom

60. "Computers in modern scientific research", D.D. University, Nadiad, May 12, 2012.

H. M. Mishra

61. "Matter under extreme conditions and chiral symmetry breaking", BITS Pillani, Goa Campus, July 2012.

N. Singh

62. "Charge dynamics in an ideal cuprate $\text{Ca}_2\text{xN axCuO}_2\text{Cl}_2$ using Yang-Rice-Zhang ansatz, Institute of mathematical Sciences (IMSc), Chennai, India, February 14, 2013.
63. "Charge dynamics in an ideal cuprate $\text{Ca}_2\text{xN axCuO}_2\text{Cl}_2$ using Yang-Rice-Zhang ansatz, Raman Research Institute (RRI), Bangalore, India, February 19, 2013.

P. Konar

64. "When Large Hadron Collider (LHC) met Higgs", St.Xavier's College, Ahmedabad on July 21, 2012.
65. "Finding Higgs at Large Hadron Collider (LHC)", Physics department, Sardar Patel University, Vallabh Vidyanagar on August 25, 2012.
66. "Large Hadron Collider (LHC) and Higgs", Gandhinagar Institute of Technology, Ahmedabad on March 05, 2013.

R. E. Amritkar

67. "Extreme events on complex networks", Colloquium, National Chengchi University, Wenshan District, Taipei City, Taiwan, October 15, 2012.

R. Rangarajan

68. "Elementary Particles in Nature and the Search for the Higgs Boson", IIT Gandhinagar, August 16, 2012.
69. "Elementary Particles in Nature and the Search for the Higgs Boson", Vikram A. Sarabhai Community Science Centre, Ahmedabad, August 18, 2012.
70. "Elementary Particles in Nature and the Search for the Higgs Boson", B. P. Baria Science Institute, Navsari, August 24, 2012.
71. "Elementary Particles in Nature and the Search for the Higgs Boson", Ahmedabad University, August 27, 2012.
72. "A Career as a Physicist", Gujarat Science City, Gandhinagar, March 02, 2013.

S. Goswami

73. "Neutrinoless Double Beta decay in TeV scale Left-right symmetric models", Theory Colloquium, TIFR, Mumbai.

U. Sarkar

74. "Neutron-Antineutron Oscillations and Baryogenesis", University of California, Riverside, USA, November 21, 2012.

V. K. B. Kota

75. "First results from Spectral Distribution Method for ^{150}Nd double beta decay nuclear matrix elements", Department of Physics, Laurentian University, Sudbury, Canada, September 20, 2012.

SCIENCE

Astronomy and Astrophysics

The search for Super Earths: Precision Radial-Velocity (RV) measurements on bright G, K Dwarfs (Sun-like stars)

The science observations under the PARAS (PRL Advanced Radial-velocity All-sky Search) project have started since April 2012. PARAS, basically consists of an optical fiber-fed high resolution Echelle spectrograph under temperature ($\delta T \sim 0.3^\circ\text{C}$ at 25.5°C) and pressure (~ 0.045 mbar) controlled environment and is attached to the 1.2 m telescope at Mt. Abu. The spectrograph has achieved appreciable intrinsic stability of 1.35 m/s over a period of several months, and hence, enabled monitoring of stellar jitters or RV variations down to sub- 2 ms^{-1} velocity precision around bright G, K dwarfs (stars brighter than 7^{th} magnitude).

The modelling of RV variation measurements from the stellar spectra enables us to find evidence of a planet around the star. The amplitude of the modulation gives us the mass or rather $m \sin(i)$ of the planet (where i is the angle of inclination with respect to the observer). Since PARAS has achieved a precision of close to 1 ms^{-1} , it thus in principle has the capability of looking for Super-Earths (3 to 10 Earth Mass planets) around Sun-like stars.

We have been monitoring the stellar jitters through precision RV measurements of about a dozen G,K dwarfs and Figures 1 & 2 show examples on two stars σ Draconis (4.7 mag, G9V spectral type) and HD 9407 (6.5 mag, G6V spectral type). Other Radial Velocity groups in US and Europe have earlier monitored many of these stars at a level of 2 to 5 ms^{-1} (see for instance: Wright et. al, 2008, ApJLetters, 683, 63, where they quote a value of 2.5 ms^{-1} for σ Draconis). More recent

work by Bouchy et al. 2013, A&A, 549, 49, quote a value of 1.5 ms^{-1} for a period of 3 months which is statistically similar to our result of 1.7 ms^{-1} over a period of 7 months.

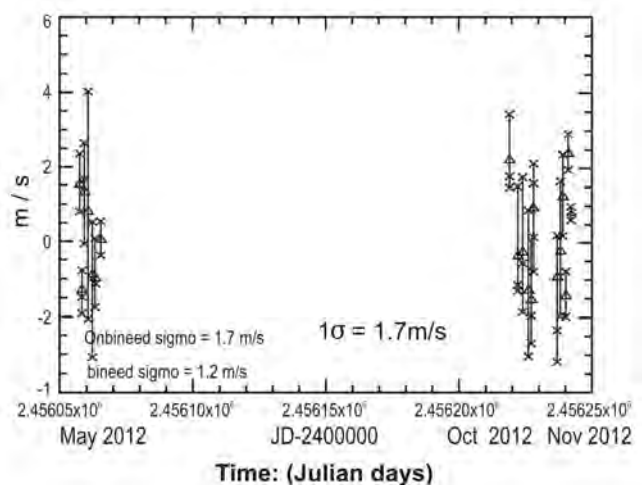


Figure 1: The Star σ Draconis (spectral type G9V, 4.7 mag) shows a stellar jitter of 1.7 ms^{-1} (1.2 ms^{-1} on nightly averages) over a period of seven months. The time line here is from May to November 2012. The x-axis is Time in Julian Days (JD) and the Y-axis is Radial-Velocity (RV) in m/s.

We will thus be in a position to detect the presence of super Earths around such stars after monitoring for a couple of years. We plan to monitor over 30 to 50 such types of stars

over a period of 3 to 4 years at a precision of 2 ms^{-1} or better to find out the presence of Super-Earths. The statistics of such planets along with stellar characteristics like metallicity and mass of host stars will ultimately enable us to understand the process of planet formation.

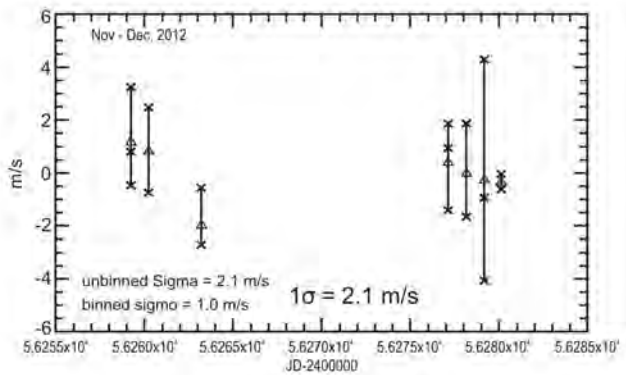


Figure 2: The Star HD 9407 (spectral type G6V) shows a stellar jitter of 2.1 ms^{-1} (1.0 ms^{-1} on nightly averages) over a period of a month. The x-axis is Time in JD - 2400000, here showing a time line between November and December 2012, and the Y-axis is Radial Velocity (RV) in m/s.

(A. Chakraborty, V. Dixit, V. Dongre and P. Chaturvedi)

Extremely high brightness temperature of fast variable sources

Since last 20 years the extremely high brightness temperatures ($>10^{18}\text{K}$) of fast variable sources could be successfully explained in the literature only by invoking coherence within synchrotron sources. But it is now shown that there is a subtle dependence of the gyro-orbit size on the radiating charge energy that will make any coherence to disappear in a time 10^5 to 10^6 times faster than the observed time scales of variability. This virtually rules out a whole class of such coherence based theoretical models.

(A. K. Singal)

Is unified scheme for radio galaxies and quasars valid?

In the currently popular orientation-based unified scheme, a radio galaxy appears as a quasar when its major radio-axis happens to be oriented within a certain angle with respect to the observer's line of sight. Due to geometrical projection, the observed sizes of quasars should therefore appear smaller than those of radio galaxies. It was shown that this simple, unambiguous prediction of the unified scheme is not borne out by the actually observed angular sizes of radio galaxies and quasars. Unified scheme therefore seems falsified.

(A. K. Singal and R. L. Singh)

Giant pulses from the normal pulsars

Giant pulses were for the first time shown to arise from a normal period pulsar. Only a handful of pulsars are known to show giant pulses and they are all fast (millisec) pulsars and the theoretical work till now depends heavily on this fact. But now with evidence of giant pulses from a normal period pulsar it would require a re-thinking on all such models. For example, an idea popular in the literature is that giant pulse emission physics is particularly dependent on the high magnetic field strength at the light cylinder, but this now is completely ruled out.

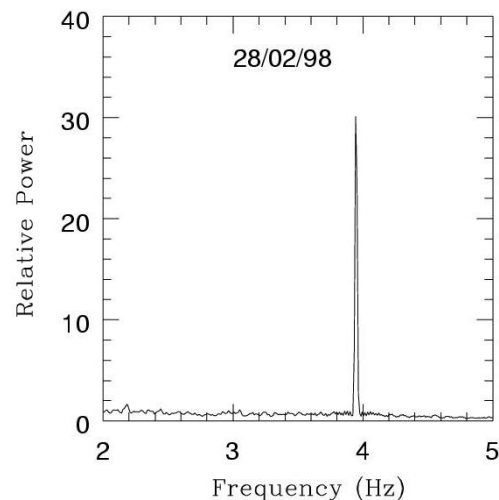


Figure 3: Power-spectrum of giant pulse observations from PSR B0950+08

(A. K. Singal and H. O. Vats)

Triggered Star Formation around Mid-infrared Bubbles in the G8.14+0.23 H II Region

Mid-infrared shells or bubbles around expanding H II regions have received much attention due to their ability to initiate a new generation of star formation. Multi-wavelength observations were made around two bubbles associated with a southern massive star-forming region G8.14+0.23, to investigate the triggered star formation signature on the edges of the bubbles by the expansion of the H II region. Observational signatures were detected of the collected molecular and cold dust material along the bubbles. The $^{12}\text{CO}(J = 3-2)$ velocity map reveals that the molecular gas in the bubbles is physically associated with the G8.14+0.23 region. A total of 244 young stellar objects (YSOs) were detected in the region about 37% of which occur in clusters that are associated with the collected material on the edges of the bubbles. A good agreement was found between the dynamical age of the H II region and the kinematical timescale of bubbles with the fragmentation time of the accumulated

molecular materials. This may indicate possible "collect and collapse" process around the G8.14+0.23 region. However, one cannot entirely rule out the possibility of triggered star formation by compression of the pre-existing dense clumps by the shock wave. It was found that the expansion of the H II region is also leading to the formation of two young massive embedded YSOs (about 10 and 22 solar masses) in the G8.14+0.23 region.

This work was a collaborative effort with L. K. Dewangan (formerly of PRL), D. K. Ojha, S. K. Ghosh and S. Chakraborti of TIFR.

(B. G. Anandarao)

The A–X Infrared Bands of Aluminum Oxide in Stars: Search and New Detections

A search was undertaken for the A-X infrared bands of AIO to better understand the characteristics of this radical. These bands are infrequently encountered in astronomical sources but surprisingly were very prominent in the spectra of two well-known, novalike variables (V838 Mon and V4332 Sgr) thereby motivating us to explore the physical conditions necessary for their excitation. In this study, we present the detection of A-X bands in the spectra of 13 out of 17 stars, selected on the basis of their J - K colors as potential candidates. The majority of the AIO detections are in asymptotic giant branch (AGB) stars, viz., nine OH/IR stars, two Mira variables, and two bright infrared sources. Our study shows that the A-X bands are fairly prevalent in sources with low temperature and O-rich environments. Possible applications of the present study are discussed in terms of the role of AIO in alumina dust formation, the scope for estimating the radioactive ^{26}Al content in AGB stars from the A-X bands, and providing possible targets for further mm/radio studies of AIO which has recently been discovered at millimeter wavelengths.

This work was done in collaboration with W. P. Varricatt, Joint Astronomy Centre, Hawaii and O. Launila, KTH-Albanova, Sweden.

(D. P. K. Banerjee, B. Mathew and N. M. Ashok)

Infrared studies of the Be star X Per

Spectro-photometric results were obtained for the Be star X Per/HD 24534 from near-infrared (near-IR) monitoring in 2010-2011. Comparison of the star's present near-IR magnitudes with earlier records shows the star to be currently in a prominently bright state with mean J, H, K magnitudes of 5.49, 5.33 and 5.06, respectively. The JHK spectra are dominated by emission lines of He I and Paschen and Brackett lines of H I. Lines of O I 1.1287 and 1.3165 μm are also present and since O I 1.1287 is the stronger among the two lines, Lyman beta fluorescence plays an important role in their excitation. Recombination analysis shows that the

H I Paschen and Brackett line strengths deviate considerably from case B predictions. These deviations are attributed to the lines being optically thick, and this supposition is verified by calculating the line centre optical depths predicted by recombination theory. Similar calculations indicate that the Pfund and Humphrey series lines should also be expected to be optically thick, which is found to match observations reported in other studies. The spectral energy distribution of the star is constructed and shown to have an IR excess. Based on the magnitude of the IR excess, which is modelled using a free-free contribution from the disc, the electron density in the disc is estimated and shown to be within the range of values expected in Be star discs.

(B. Mathew, D. P. K. Banerjee, S. Naik and N. M. Ashok)

A Study of the Role of Lyman beta Fluorescence on O I Line Strengths in Be Stars

The possibility of the Lyman beta fluorescence mechanism being operational in classical Be (CBe) stars and thereby contributing to the strength of the oxygen O I 8446 Angstrom line has been recognized for long. However, this supposition needed to be quantified by comparing observed and predicted O I line ratios. In the present work, optical and near-infrared spectra of CBe stars were presented. We analyzed the observed strengths of the O I 7774, 8446, 11287, and 13165 Angstrom lines, which are theoretically known to be good diagnostic lines for identifying the excitation mechanism. We considered and examined the effects of Lyman beta fluorescence, collisional excitation, recombination, and continuum fluorescence on these O I line strengths. From our analysis it is established that the Lyman beta fluorescence process is indeed operative in Be stars.

This work was done in collaboration with Dr. A. Subramaniam of IIA, Bangalore.

(B. Mathew, D. P. K. Banerjee and N. M. Ashok)

Near-infrared properties of classical novae: A perspective gained from Mount Abu Infrared Observatory

In this work we reviewed the near-infrared properties of classical novae in the J, H and K bands at wavelengths between 1.08 to 2.4 microns. A classification system exists for the early post-outburst optical spectra of novae on the basis of the strength of group of non-hydrogen emission lines. A similar scheme for the near-infrared regime, which is not available at present, was presented here. In the optical system there are two principal classes, namely, "Fe II" and "He/N" for novae with either prominent Fe II lines or prominent "He/N" lines. There is also a small subset of the hybrid Fe IIb type. From spectroscopic observations we show the differences and similarities between these classes of novae in the near-infrared. The spectral lines common to the two principal classes arise from H, He, N and O. However, the near-IR features that separate these two classes are the numerous, and often strong, carbon lines

which are seen only in the spectra of the Fe II class of novae. The dust formation process in novae was discussed based on broad-band observations. The first-overtone carbon monoxide (CO) detections in novae were analyzed to understand the formation and evolution of this molecule in the nova ejecta and to discuss the observed $^{12}\text{C}/^{13}\text{C}$ ratio.

(D. P. K. Banerjee and N. M. Ashok)

V496 Scuti: an Fe II nova with dust shell accompanied by Carbon Monoxide emission

Near-infrared (near-IR) and optical observations were presented of the nova Scuti 2009 (V496 Sct) covering various phases - pre-maximum, early decline and nebular - during the first 10 months of its discovery followed by observations in the early part of 2011 April. The spectra follow the evolution of the nova when the lines had strong P Cygni profiles to a phase dominated by prominent emission lines. The notable feature of the near-IR spectra in the early decline phase is the rare presence of first overtone bands of carbon monoxide in emission. Later about 150 days after the peak brightness, the IR spectra show clear dust formation in the expanding ejecta. The light curve shows a slow rise to the maximum and a slow decline indicating a prolonged mass loss. This is corroborated by the strengthening of P Cygni profiles during the first 30 days. In the spectra taken close to the optical maximum brightness, the broad and single absorption components seen at the time of discovery are replaced by two sharper components. During the early decline phase, two sharp dips that show increasing outflow velocities are seen in the P Cygni absorption components of Fe II and H I lines. The spectra in 2010 March showed the onset of the nebular phase. Several emission lines display saddle-like profiles during the nebular phase. In the nebular stage, the observed fluxes of [O III] and H beta lines are used to estimate the electron number densities and the mass of the ejecta. The optical spectra show that the nova is evolved in the PFeAo spectral sequence. The physical conditions in the ejecta are estimated. The absolute magnitude and the distance to the nova are estimated to be $M_V = -7.0 \pm 0.2$ and $d = 2.9 \pm 0.3$ kpc, respectively.

This work was done in collaboration with Prof. U. Munari and his colleagues from the INAF Astronomical Observatory of Padova, Italy.

(A. Raj, D. P. K. Banerjee and N. M. Ashok)

Studies of the dusty bipolar nova V1280 Scorpii and the recurrent nova T Pyxidis

These studies were undertaken by international groups with Mt Abu data contributing to the science campaigns. A striking result, obtained from adaptive optics imaging from the VLT Chile, was the discovery of a dusty hourglass-shaped bipolar nebula around the nova V1280 Sco. The apparent size of the nebula increased from 0.30×0.17 arcseconds in July 2009

to 0.64×0.42 arcseconds in July 2011 allowing a distance estimate to be made and other parameters to be derived. Spitzer Space Telescope and Herschel Space Observatory infrared observations of the recurrent nova T Pyx during its 2011 eruption, complemented by ground-base optical-infrared photometry were done. It was found that the eruption has heated dust in the pre-existing nebulosity associated with T Pyx. This is most likely interstellar dust swept up by T Pyx—either during previous eruptions or by a wind - rather than the accumulation of dust produced during eruptions.

The studies on V1280 Sco and T Pyx were led respectively by Dr. O. Chesneau of the Observatoire de la Côte d'Azur, France and Prof. N. Evans of the Astrophysics Group, Keele University, UK.

(D. P. K. Banerjee and N. M. Ashok)

Ongoing program of Monitoring of Blazars from MIRO

Since blazars are seen at a very small angle to the line of sight, they provide deepest possible access to the central energy source. Therefore, to understand the energy mechanism and structure of AGNs, blazars prove to be very useful tool. We monitor a sample of blazars for variability in optical and near-IR flux using optical CCD (1296×1152 pixels) and NICMOS-3 mounted at the 1.2m telescope of MIRO (Mt Abu InfraRed Observatory). Recently procured 50 cm telescope mounted with EMCCD (1000×1000 pixels) and dedicated to variability study, was also part of the monitoring system. Since blazars vary at various time scales- ranging from years to minutes, in addition to long term monitoring, fast sampling is required to detect microvariations with time scales of few tens of minutes. During the period 2012-13, we monitored 3C66A, 3c279, 3C454.3, S5_0716, PKS 1510, OJ 287, Mrk421, Mrk501 etc for variability in flux and polarization.

(K.S. Baliyan, S. Ganesh and S. Chandra)

CGRaBS J0211+1051: Confirmed as a Low Energy Peaked Blazar

A large number of blazar candidates are being detected in various surveys conducted using Fermi (high energy gamma-ray space observatory) Chandra (X-ray space observatory) and several other facilities. Some of these sources become fairly bright when in outburst phase and can be monitored even by a modest 1.2m telescopes. One such blazar candidate, CGRaBSJ0211+1051 flared in gamma-rays, followed by x-ray and optical wavebands. We monitored it in optical polarized light from Mt Abu Ir Observatory (MIRO) for 5-nights during Jan-Feb 2011. Based on its behaviour, we suggested CGRaBSJ0211+1051 to be low energy peaked blazar (LEBL). However, confirmation for such classification comes only from spectral energy distribution. To ascertain its true nature we analysed multiwavelength data (Gamma-rays: Fermi, X-ray & UV: Swift, Optical: ATVS, radio: MOJAVE & NED) to construct spectral energy distribution of this source. To check whether host galaxy has any significant contribution,

host SED was modeled based on its brightness in I band. The host galaxy was fainter by more than 3 magnitudes and its contribution was found to be less than 2.5%. The SED shows two humps, typical of blazar continuum spectra, synchrotron hump peaking at 10^{14} Hz and IC one lying in gamma-ray regime, confirming CGRaBSJ0211+1051 to be a low energy peaked blazar.

(S. Chandra, K. S. Baliyan and S. Ganesh)

Multiwavelength study of blazar PKS1510-089

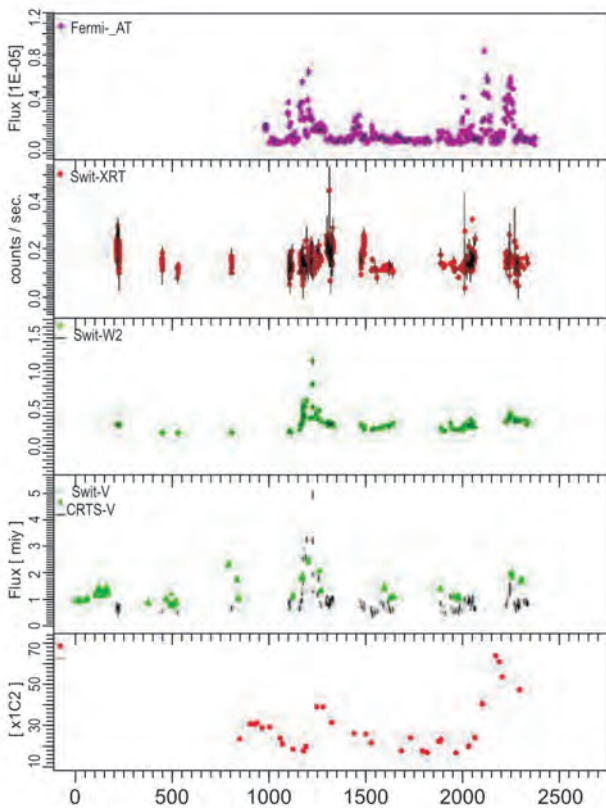


Figure 4: Long-term multiwavelength light curves for FSRQ blazar PKS1510-089 for the duration Jan 2006- May 2012. X-axis: No of days since Jan 1, 2006, Y-axis: flux in various wavebands. These show several flares in almost all the energy regimes, many of them showing significant correlation. Flares originate from the movement of disturbance either in spiral streamline passing through acceleration/collimation zone upstream the core or blobs interacting with stationary or moving cores.

Simultaneous multiwavelength data for longer duration are of great help in understanding the energy generation mechanism in AGNs. The source PKS1510-089 was detected by EGRET at redshift 0.361 and is very active FSRQ blazar which makes it potential candidate for a multiwavelength study. The source is peculiar in the sense that its gamma-ray flux jumped 12 times in few hours in April 2009 while it brightened by 2-magnitude in optical within 3-days in May 2009. For this reason, we analyzed VLBA (2cm:MOJAVE), CRTS (V-band), UVOT and X-ray data of SWIFT and gamma-ray (Fermi) multiwavelength available data during January 1, 2006 to Jun 8, 2012 which encompasses many flares. The multiwavelength

light curves constructed are shown in the figure 4. A large number of flares can be seen in high energy gamma-rays, many of which have counterparts in other energy regimes. 2nd and 3rd sub-flares in gamma-rays are seen with 7 and 13 days delay in optical. Radio lightcurve shows enhanced emission lasting over 6-months. During 2011-2012, 3-Gamma-ray flares are followed in optical, X-ray and onset of outburst in radio. These flares are caused by disturbances moving down the jet and passing through stationary cores, bends or density enhancements. Some of the faster ones could be due to blob moving down the jet in spiral streamline passing through acceleration/collimation zone upstream the core. The exact location of these emission features is now possible to estimate using MOJAVE sub-mm images and polarization information.

(S. Chandra, K. S. Baliyan and S. Ganesh)

Blazar OJ287 and its periodic double peaked outburst

Differential Light Curve OJ287

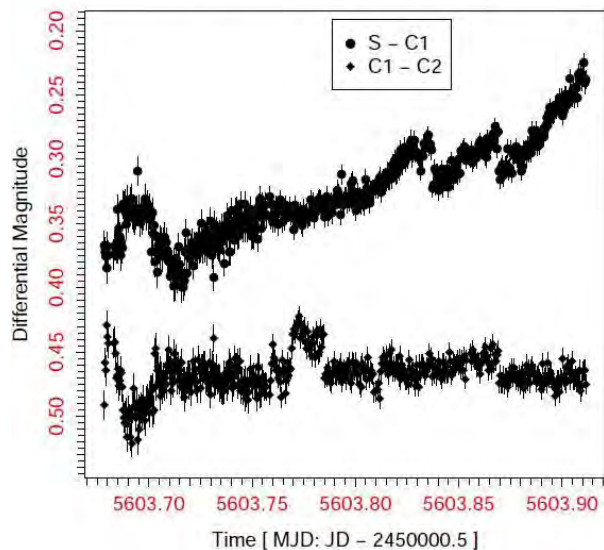


Figure 5: R-band lightcurve for blazar OJ287 on 11 February 2011 showing a change of about 0.18 magnitude in 2.5 hours. Upper curve is differential lightcurve of OJ287 and comparison star C1 (S-C1) while lower lightcurve shows differential magnitudes of two comparison standard stars.

Blazar OJ287 is among the very few blazars which show long-term periodic outburst with a period of about 11.6 years. The outburst is twin-peaked and can be understood by the passage of secondary black hole through the primary black hole accretion disk twice in the period. However, in addition to these two major peaks in the outburst, significant flares are seen just prior to the onset of the outburst. In order to understand the reason behind these 'precursor' flares, multi-observatory observations were conducted in V, B and R optical bands during March-April 2012 while also making use of the old data available in these bands. The nature of the light-curves constructed from the data were used to propose a model where these precursor flares are caused by the secondary black hole hitting the thick disk of the

primary before actual impact on the primary accretion disk. Thus, precursor flares are triggered by secondary black hole gobbling up the gas which eventually brightens its jet. This model can be used to predict next precursor flare towards the end of year 2020. The observations are being made to check the intra-day variability during now and September 2013 while OJ287 is expected to be in low phase. The figure 5 shows intra-night variation during February 11, 2011.

(K. S. Baliyan, S. Chandra and S. Ganesh)

A rare stellar occultation by a large Trans Neptunian Object (TNO) observed at Mt Abu in the Infrared.

Occultation of Stars by Solar system bodies like asteroids with near simultaneity at several positions on earth provides a direct means of accurately determining the size and shape of the body. While stellar occultations by Main belt asteroids are well predicted and frequently observed, occultations involving outer solar system bodies like TNOs and Kuiper Belt Objects are rare mainly due to the difficulty in getting a good ephemeris of these objects for precise predictions. There is usually a large error in the shadow path of these events even after final predictions. One such rare Stellar Occultation event by a large TNO 2003 AZ 84(208996) (about 500 km in size) was successfully recorded at Mt Abu Observatory on February 03, 2012. Predictions of the event were made by a French group and were available only a day before the event. NICMOS IR Imager in the H band (1.65 microns) attached to the 1.2m telescope was used to observe the event. The program star ($V \sim 15.3$) was tracked and images obtained at nearly 5 second intervals. Sixty frames were recorded during the 5 minute window centered on the event from 19:42:56 UT to 19:47:50 UT. Sky conditions were clear but windy. Five frames showed a dip in signal level from the star indicating the occultation event. Another occultation chord of the same event was observed at Girawali IUCAA Observatory and at Weizmaan Observatory in Israel. Other observatories in Europe reported a negative result. From all these observations the maximum chord length has been determined to be 662 ± 50 km. More details regarding the shape of the body will emerge from further analysis.

This work was done in collaboration with the French/European group co-ordinated by Dr R. Duffard (Instituto de Astrofisica de Andolucia, Spain) and several observatory groups including Girawali, IUCAA.

(T. Chandrasekhar, T. Baug, S. Ganesh and J. K. Jain)

Signal to Noise Improvement in K band Lunar Occultation light curves.

During the last few years a large number of lunar occultation (LO) light curves, mainly from galactic late type giants, have been successfully obtained at the 1.2m Mt Abu telescope for high angular resolution studies of these objects. Using NICMOS IR camera in the sub-array mode (10×10 pixels)

corresponding to ($5'' \times 5''$ on sky) permits recording of LO events up to K-magnitude of about 5.0. The main difficulty in observing fainter objects ($K < 3$) is poor signal to noise ratio achieved. The primary sources of noise in the near infrared LO light curves are scintillation noise, and background sky photon noise (variable with lunar phase, position angle of event and variable airglow intensity). For brighter sources ($K < 3$) source-photon noise is invariably present. In addition, in many cases large noise from terrestrial (man made) sources at specific frequencies like power line pick-up (50 Hz) and from the detector and read-out electronics (31 Hz) lowers the Signal to Noise.

A good signal to noise ratio ($S/N > 40$) is essential to extract proper angular diameter information of the source by model fits to the observed occultation light curve. Methods of noise reduction in the observed light curve, post observation, using Fourier transforms or Wavelet transforms or a suitable combination of both has been investigated in this work.

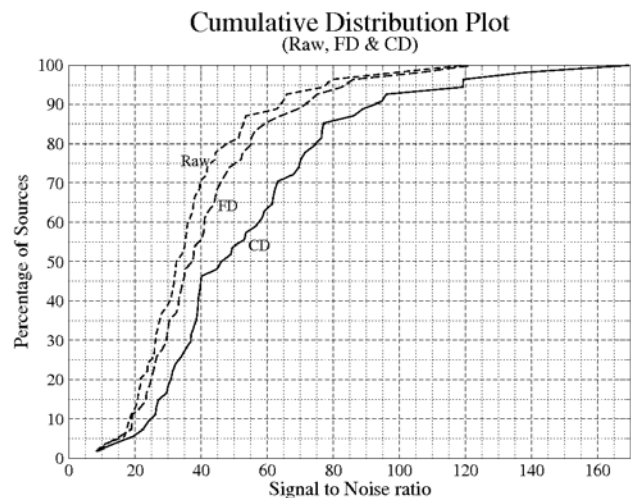


Figure 6: Signal to Noise improvement in LO light curves on applying FT and then combination (CD) of FT and WT methods to raw data. For $S/N < 40$ the improvement from raw to FT is 17% and from FT to CD is a further 9% leading to an overall improvement of 26% for sources with $S/N < 40$. The sample size is 54 light curves.

The sample consisted of 54 light curves up to K-magnitude of ~ 5.0 . All the light curves were observed using sub-array mode of NICMOS camera in the NIR K-band with an integration time of 3 milli-second and a sampling interval of 8.952 milli-second. Using Fourier transforms (FT) well identified specific high frequencies (mainly 31 Hz and 50 Hz) and their sub-harmonics can be completely removed from the light curves. This method is found to be effective in the fainter magnitude regime. Out of the 29 light curves that showed significant improvement (better than 3 sigma) 19 are fainter than K-magnitude of 3.0. In the original sample a total of 38 light curves were below signal to noise of 40. After the application of Fourier transforms the number has reduced to 29 an improvement of about 17%. While using FT a few noise frequencies are removed, fluctuations for a limited period of time may be overlooked by FT and can severely distort the light curve.

Handling of these noisy light curves motivated us to investigate the use of wavelet transforms. After a trial of about 15 different wavelets on a few light curves for suitability, it was found that 'symlet 20' is most effective for filtering of LO light curves. Here also MATLAB environment is used to perform the denoising method. Wavelet transforms (WT) decompose the light curve into different coefficients depending upon the level of decomposition. We mainly targeted to remove the highest frequency coefficients. Cutoff limits were put on those coefficients manually by imposing the condition that the removed components should follow Gaussian distribution. Hence, mainly random noise is removed from the light curves. Though WT show a good improvement in S/N ratio of the light curves, it was often found that power in 50 Hz and 31 Hz remains in the denoised light curves. Also, more importantly for LO analysis, WT tends to slightly smoothen the LO fringes. This motivated us to investigate a combination of FT and WT called CD.

After application of the combination denoising (CD) method almost all the light curves show significant improvement in S/N. The number of light curves with S/N <40 reduced to 29 (53%) from 38 (70%) after application of FT which is further reduced to 24 (44%) after application of CD method. (Figure 6) It may be mentioned that while CD method provides significant improvement in the S/N of LO light curves, model fits to these denoised curves are complicated by the effect of slight distortion and smoothening the fringe region due to WT effects.

(T. Baug and T. Chandrasekhar)

Changes in quasi-periodic variations of solar photospheric fields: Precursor to the deep solar minimum in the cycle 23?

Using both wavelet and Fourier analysis, a study has been undertaken of the changes in the quasi-periodic variations in solar photospheric fields in the build-up to one of the deepest solar minima experienced in the past 100 years. This unusual and deep solar minimum occurred between solar cycles 23 and 24. The study, carried out using ground based synoptic magnetograms spanning the period 1975.14 to 2009.86, covered solar cycles 21, 22 and 23. A hemispheric asymmetry in periodicities of the photospheric fields was seen only at latitudes above $\pm 45^\circ$ when the data was divided, based on a wavelet analysis, into two parts: one prior to 1996 and the other after 1996. Furthermore, the hemispheric asymmetry was observed to be confined to the latitude range 45° to 60° . This can be attributed to the variations in polar surges that primarily depend on both the emergence of surface magnetic flux and varying solar surface flows. The observed asymmetry when coupled with the fact that earlier work has shown that both solar fields above $\pm 45^\circ$ and micro-turbulence levels in the inner-heliosphere have been decreasing since the early to mid-nineties suggests that around this time active changes occurred in the solar dynamo that governs the underlying basic processes in the sun. These changes in turn probably initiated the build-up to the very deep solar minimum at the

end of the cycle 23. The decline in fields above $\pm 45^\circ$ for well over a solar cycle, would imply that weak polar fields have been generated in the past two successive solar cycles viz. cycles 22 and 23. A continuation of this declining trend beyond 22 years, if it occurs, will have serious implications on our current understanding of the solar dynamo.

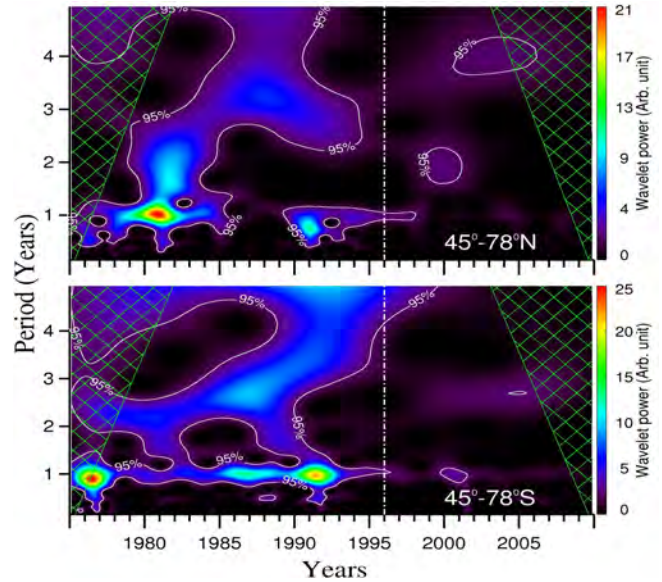


Figure 7: The two panels depict the wavelet power distribution of periodicity in time for the polar field in the north and south. The white contour lines are the significant wavelet power above 95% while the green cross-hatched regions represents the cone of influence (COI) where the power is assumed to reduce by a factor e^2 . A clear transition in periodicities at ~ 1996 (shown by the dotted lines) in both the northern and southern hemisphere, where a discernible decrease in the wavelet power of periods after 1996 compared to those prior to 1996 can be seen.

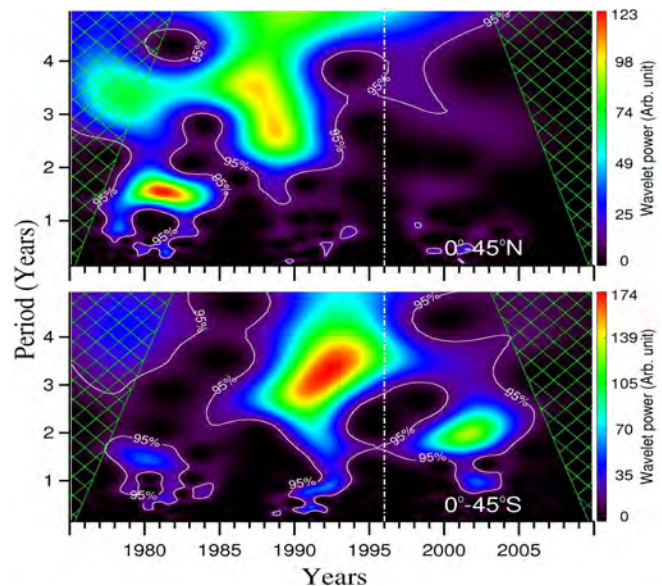


Figure 8: The two panels depict the wavelet power distribution of periodicity in time for the toroidal field in the north and south. The white contour lines are the significant wavelet power above 95% while the green cross-hatched regions represents the cone of influence (COI). A clear transition in periodicities in ~ 1996 (shown by the dotted lines) in both the northern and southern

hemisphere where, a discernible decrease in the wavelet power of periods after 1996 compared to those prior to 1996 can be seen.

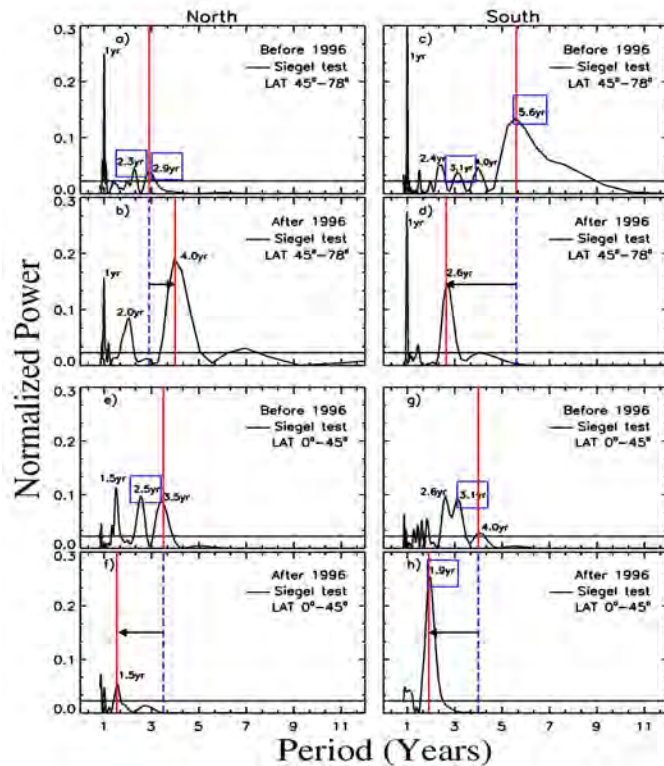


Figure 9: The upper four panels respectively depict the normalized periodograms for the north polar field before 1996, north polar field after 1996, south polar field before 1996, and south polar field after 1996. The solid red lines are drawn through the peak of the component with the largest period and the dotted blue lines, and the black arrows show the direction of the shift in periodicity and Fourier power in all panels revealing the north-south asymmetry in periodicity. Similarly, the lower four panels respectively depict the normalized periodograms for the north toroidal field before 1996, north toroidal field after 1996, south toroidal field before 1996, and south toroidal field after 1996. The blue boxed periods are the new periodicities found.

(S. K. Bisoi, P. Janardhan and D. Chakrabarty)

Thermal and non-thermal energetic of precursor and main phase emission in solar flares:

Study of the spatial, spectral and temporal evolution of thermal and non-thermal emission is performed by employing multi-wavelength observations during various phases of M1.8 flare occurred in NOAA AR 11195 (S17E31) on 22 April 2011. We estimate magnetic-field parameters during 20-23 April 2011 which reveal that energy build-up has started since 20 April 2011 which later released after a critical value of magnetic-field gradient. Spectral analysis performed on RHESSI observations reveals flare plasma parameters viz. T and n to be varying in the range of 13.9-23.2 MK and -5 to -7.3 respectively. Left and right panels of Figure 10 show the spectral fitting performed on the observed X-ray spectra during precursor and main phase respectively. Further, thermal energy during precursor phase is estimated to be $\sim 2\%$ of the total energy released. Temporal correlation study

of H and X-ray emission intensity profile during the precursor phase has revealed the signature of conduction-driven chromospheric evaporation during this phase. We further study the role of the filament dynamics in conjunction with synthesized T and EM maps which enables to propose a unified model of energy release during precursor and main phase. We conjecture that precursor phase emission is originated through conduction front triggered by partial filament eruption. Next, the heated major leftover sigmoid shaped filament has erupted and produced impulsive phase and gradual phase.

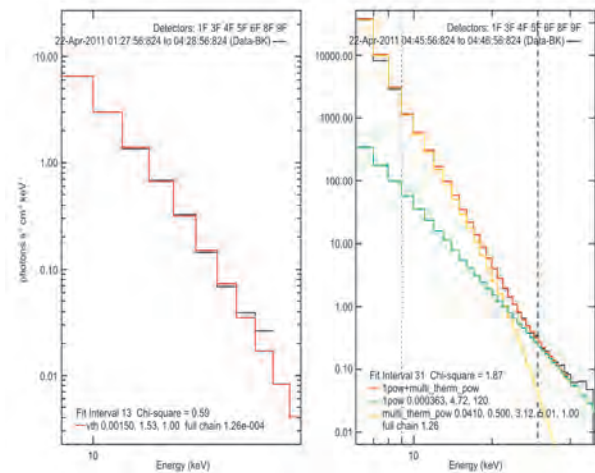


Figure 10: 1 minute integrated photon flux spectrum of 22-Apr-2011 flare event observed during 04:27:00 and 04:39:00UT in left and right panel respectively shown by black line. The spectral fit in left panel is performed employing isothermal photon model function (red line) and that performed in the right panel employing isothermal (yellow line) and broken-power-law (green line) photon models with goodness of fit represented by $\chi^2 = 0.59$ and 1.87 respectively.

(A. K. Awasthi and R. Jain)

Periodicities in the X-ray emission from the solar corona

The time series of full disk integrated soft and hard X-ray emission from the solar corona during January 2004 to December 2008, covering the entire descending phase of the solar cycle 23 from a global point of view has been investigated to study the coronal seismology. We employ the daily X-ray index (DXI) derived from 1s cadence X-ray observations from the Si and CZT detectors of "Solar X-ray Spectrometer (SOXS)" mission in seven different energy bands ranging between 6–56 KeV. X-ray data in the energy band 6-7, 7-10, 10-20 and 4-25 keV from Si detector are considered, while high energy observations in 10-20, 20-30 and 30-56 keV are taken from CZT detector. The daily time series is subjected to power spectrum analysis after appropriate correction for noise. Lomb-Scargle periodogram technique has shown the prominent period of ~ 1.24 year in addition to the other prominent periods of ~ 13.5 , ~ 27 days and near Rieger period of ~ 181 days in all energy bands. Further, other periods like ~ 31 , ~ 48 , ~ 57 , ~ 76 , ~ 96 , ~ 130 , ~ 227 and ~ 303 days are also detected, however

with different power in different energy bands. The measured X-ray periodicities have also been found in other solar-activity parameters, from large to short temporal and spatial scales (e.g., large-scale magnetic evolution, sunspot area, solar flare index). These parameters are the signatures of magnetic flux emergence. The present investigation suggests a scenario of emergence and escape of magnetic flux from the solar convection zone to the interplanetary medium through the photosphere and corona.

(P. Chowdhury, R. Jain and A. K. Awasthi)

X-ray emission characteristics of M class solar flares

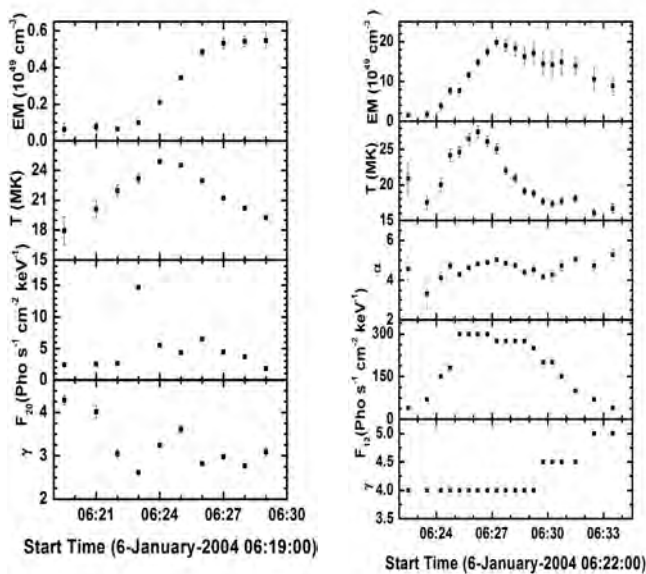


Figure 11: Left: Temporal evolution of spectral parameters for 6 January 2004 solar flare employing SOXS data. From top to bottom: Emission measure (EM), Temperature (T) and Spectral index of multi-thermal plasma and Photon flux at 12 keV (F12) and spectral index (negative power-law). Right: Temporal evolution of spectral parameters for 6 January 2004 employing RHESSI data. From top to bottom: isothermal emission measure (EM); Temperature (T) of the isothermal component; Photon flux at 20 keV (F20) and negative power-law index. Error bars are also shown.

A study of the X-ray emission from ten solar flares of GOES M class observed by "Solar X-ray Spectrometer (SOXS)" as well as RHESSI missions has been conducted. In order to study the thermal and non-thermal X-ray characteristics we characterize the flare plasma in the energy range of 4–100 keV by fitting the spectra with thermal and non-thermal models simultaneously. For SOXS observations, we consider the multi-thermal power-law function for thermal plasma and single power-law function for non-thermal continuum, while for the RHESSI observations; the spectra are fitted using the combination of isothermal component and a single power-law. Shown in Figure 11 is the temporal evolution of the thermal and non-thermal spectral parameters for 6 January

2004 flare obtained from SOXS (left panel) and RHESSI (right panel) respectively. The multi-thermal temperature range of all the flares obtained from SOXS data varies between 14.3 ± 0.15 MK and 43.7 ± 7.9 MK. RHESSI spectra, for the ten selected flares, however, provides isothermal temperature which varies between 18 ± 1.4 MK to 42 ± 1.1 MK. Differential emission measure obtained with SOXS results varies between $0.0018 \pm 0.0008 * 10^{49} \text{ cm}^{-3} \text{ keV}^{-1}$ and $2.05 \pm 1.4 * 10^{49} \text{ cm}^{-3} \text{ keV}^{-1}$. The isothermal emission measure obtained with RHESSI observations varies between $0.016 \pm 0.01 * 10^{49} \text{ cm}^{-3}$ and $0.76 \pm 0.02 * 10^{49} \text{ cm}^{-3}$. Further, the temporal evolution of the measured temperature and emission measure in the flares show that the rise phase of the flare is dominated by thermal conduction, while radiative cooling is dominant mechanism in the post-flare loops. The integrated thermal energy obtained from SOXS observations is found to be varying between ~ 1031 and 1033 ergs. The integrated non-thermal energy in the energy 20–100 keV is estimated to be varying between ~ 1029 to 1030 ergs. The SOXS observations reveal flare plasma to be multi-thermal in contrast to RHESSI observations which suggest isothermal.

(N. J. Bhatt and R. Jain)

Installation of 10-cm aperture Solar flare telescope at Thaltej campus, PRL



Figure 12: Thaltej Solar Flare Telescope of Physical Research Laboratory operating at Thaltej campus. The 10-cm aperture refractor with $f/16$ focal ratio provides 13 mm image at prime focus. The quantum H_2 filter copuled with CCD provides images with a cadence between 10ms to 5s as desired.

An optical facility to observing the full-disk chromosphere

of the Sun has been established at the Thaltej campus. The 10-cm aperture refracting telescope with f/16 focal ratio reveals spatial resolution of ~ 2 arcsec/pixel (~ 1400 km). Currently, in view of space weather research goals, the full-disk observations are of great importance. This Thaltej Solar Flare Telescope, Physical Research Laboratory (TSFT/PRL), shown in Figure 12, may operate at 10 ms to 5 s cadences in H_2 as well as in white light depending on the need of observing goals. The high-temporal cadence observations enable to address the issues viz. cooling of the solar flare plasma, effect of flux-ropes in the solar tornados etc. The professional quantum H_2 filter operates at central wavelength 6562.8 Å and can vary in the range of ± 0.5 Å. It has pass-band ~ 0.3 . This facility has been operational for observing white-light Sun since April 2012 and we have observed a historical astronomical event of Venus transit occurred on 6th June 2012. However, recently, after receiving the H_2 filter, the full-fledged H_2 observations from the TSFT have been started

The Figure 13 shows full disk image (left panel) of the Sun taken by TSFT on 6th March 2013. The active region (AR) shown on right panel has been very complex with an M-shaped filament as shown by arrow. Prominences have been observed at the South-West limb (cf. Figure 13 right panel). The observation of prominences structure shows the stability of the images with this telescope given a long exposure as high as ~ 500 ms. Regular observations have been started with auto-identification of the flare.

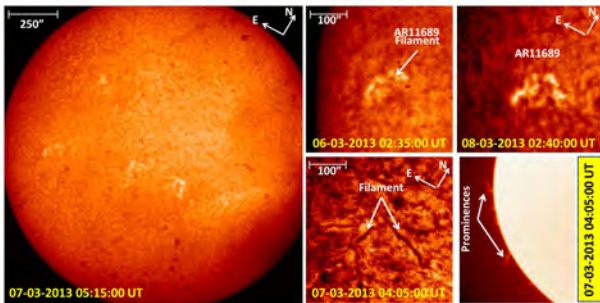


Figure 13: Left panel: Full disk image of the Sun obtained by TSFT/PRL on 07 March 2013 at 05:15:00 UT. Right panel: Images of high-resolution solar chromosphere showing active region, filaments and prominences etc during the observing cadence from 06-08 March 2013.

(R. Jain)

Timing and spectral properties of Be/X-ray pulsar EXO 2030+375 during a Type I outburst

Be/X-ray binaries represent the largest subclass of High-Mass X-ray Binary (HMXB) systems. The compact object in these systems is generally a neutron star (pulsar), whereas the companion is a B⁻ or O⁻ type star that shows Balmer emission lines in its spectra. The binary optical companion lies well within the Roche lobe. The objects in these binary systems

are typically in a wide orbit with moderate eccentricity. Though evolutionary model calculations show that binary systems with a white dwarf and Be star or a black hole and Be star should also exist, clear evidence of the existence of such binary systems has not been found as yet. The neutron star in these Be/X-ray binary systems accretes matter while passing through the circumstellar disk of the companion Be star. The abrupt accretion of matter onto the neutron star while passing through the circumstellar disk of the Be companion or during the periastron passage results in strong X-ray outbursts. During such outbursts, the X-ray emission from the pulsar can be transiently enhanced by a factor of more than ~ 10 . Be/X-ray binary systems generally show periodic normal (type I) X-ray outbursts that coincide with the periastron passage of the neutron star and giant (type II) X-ray outbursts that do not show any clear orbital dependence apart from the persistent low-luminosity X-ray emission during quiescent. The neutron stars in the Be/X-ray binary systems are found to be accretion powered X-ray pulsars, except for a very few cases. We present results from a study of broadband timing and spectral properties of EXO 2030+375 using a Suzaku observation. Pulsations with a period of 41.41 s and strong energy-dependent pulse profiles were clearly detected up to 100 keV. Narrow dips are seen in the profiles up to ~ 70 keV. The presence of prominent dips at several phases in the profiles up to such high energy ranges was not seen before. At higher energies, these dips gradually disappeared and the profile appeared to be single-peaked. The 1.0–200.0 keV broadband spectrum is found to be well described by a partial covering high-energy cutoff power-law model. Several low-energy emission lines such as Si XIII (2.01 keV), Si XIV (2.5 keV), S XV (3.19 keV), Fe K α (6.4 keV), Fe XXVI (6.61 keV) are detected in the pulsar spectrum. We fitted the spectrum using neutral as well as partially ionized absorbers along with the above continuum model yielding similar parameter values. The partial covering with a partially ionized absorber resulted in a marginally better fit. The spectral fitting did not require any cyclotron feature in the best-fit model. To investigate the changes in spectral parameters at dips, we carried out pulse-phase-resolved spectroscopy. During the dips, the value of the additional column density was estimated to be high compared to other pulse phases. While using a partially ionized absorber, the value of the ionization parameter is also higher at the dips. This may be the reason for the presence of dips up to higher energies.

This work was done in collaboration with B. Paul and C. Maitra of RRI, Bangalore.

(S. Naik, G. K. Jaisawal)

Investigation of variability of iron emission lines in Centaurus X-3

Centaurus X-3 (Cen X-3) was the first binary pulsar to be discovered in X-rays. It is an eclipsing HMXB pulsar with a pulse period of ~ 4.8 s and an orbital period of ~ 2.1 days. The binary system consists of a neutron star with a mass of 1.21 ± 0.21 solar-mass accompanied by an O 6-8 III supergiant star (V779~Cen) with a mass and radius of

20.5 ± 0.7 solar-mass and 12 solar-radii, respectively. The distance to the binary system was earlier estimated to be ~ 8 kpc. The high luminosity of the X-ray source suggests that the predominant mode of accretion is via a disc, fed by incipient Roche-lobe overflow, although a strong stellar wind does emanate from the supergiant. The optical light curve supports the presence of an accretion disk, fed by Roche lobe overflow. A comprehensive spectral analysis of the HMXB pulsar Cen X-3 was carried out using data from the XMM-Newton observatory covering eclipse, eclipse-egress and out-of-eclipse phase of the binary period. Three iron emission lines at 6.4 keV, 6.7 keV, and 6.97 keV are clearly detected in the spectrum of the pulsar during the entire observations, irrespective of different binary phases. The properties of these emission lines are investigated at different intensity levels. The flux level and equivalent width of the emission lines change during the eclipse, eclipse-egress and out-of-eclipse orbital phases. Based on the results obtained from the time resolved spectral analysis, it is understood that the most probable emitting region of 6.4 keV fluorescent line is very close to the neutron star whereas the other two lines are produced in a region that is far from the neutron star, probably in the highly photo-ionized wind of the companion star or in the accretion disk corona.

This work was done in collaboration with B. Paul of RRI, Bangalore.

(S. Naik)

Timing and broad band spectroscopy of 1A 1118-61 with Suzaku

1A 1118615 is a hard X-ray transient pulsar which was discovered with Ariel V in an outburst in 1974. The same series of observations revealed X-ray pulsations with a duration of 405.6 s. The optical counterpart He 3–640 (=‘WRA 793’) is a highly reddened Be star classified as an O9.5IV–Ve star. It shows strong Balmer emission lines indicating the presence of an extended envelope. The distance from the source is estimated to be 5 ± 2 kpc from photometric and spectroscopic observations. Ultraviolet observations reveal a P Cygni profile in the C_{IV} line which indicates a stellar outflow with a velocity of the order of 1600 ± 300 km/s. The distance of the binary pulsar and the orbital period of the system were estimated to be ~ 4 kpc and 24 ± 0.4 d, respectively. There have been three giant outbursts so far detected for this source. The first was in 1974, the second was detected in 1992 January. The outburst lasted for ~ 30 d and pulsations with a period 406.5 s were detected up to 100 keV. The source remained in quiescence for about 17 years until 2009 January 4 when a third outburst was detected by Swift. The pulsar was observed with Suzaku twice during this outburst, once at the peak of the outburst and the other 13 days later, at its declining phase. Pulse profiles from both observations exhibit strong energy dependence with several peaks at low energies and a single peak above ~ 10 keV. A weak, narrow peak is detected at the main dip of the pulse profiles from both observations in the energy bands below 3 keV, indicating the presence of a phase-dependent soft excess in the source

continuum. The broad-band energy spectrum of the pulsar could be fitted well with a partial covering cut-off power-law model and a narrow iron fluorescence line. We also detected a broad cyclotron feature at ~ 50 keV from both observations which is a feature common for accretion-powered pulsars with high magnetic field strength. The pulse-phase-resolved spectral analysis shows an increase in the absorption column density of the partial covering component, as well as variation in the covering fraction at the dips of the pulse profiles, which naturally explains energy dependence of the same. The cyclotron line parameters also show significant variation with pulse phase with an ~ 10 keV variation in the cyclotron line energy and a variation in depth by a factor of 3. This can be explained either as the effect of different viewing angles of the dipole field at different pulse phases, or due to a more complex underlying magnetic field geometry.

This work was done in collaboration with C. Maitra and B. Paul of RRI, Bangalore.

(S. Naik)

Constraining the spin of galactic black hole candidate IGR J17091-3624

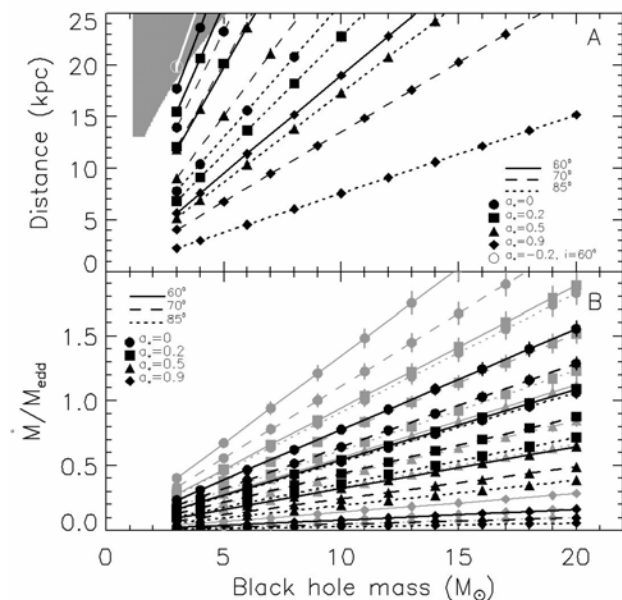


Figure 14: Variation of distance (panel A) and mass accretion rate (panel B) as a function of mass for different inclination angles and spins as shown the legend. For purpose of clarity, the symbols are shown for alternate values of mass and mass accretion rate is shown only for maximum (grey) and minimum (black) of the five values. The grey region in top left corner of panel A shows allowed range for black hole mass and distance from the luminosity argument.

Galactic X-ray binaries are among the brightest X-ray sources in the sky and are known to be variable over time scales ranging from milliseconds to years. However over the intermediate time scale of few minutes to hours these sources,

particularly the black hole binaries are not known to vary significantly. GRS1915+105 was the only black hole binary exhibiting strong systematic and large amplitude variability over the intermediate time scale. Since the source is peculiar in terms of various properties such as highest known BH mass, highest known BH spin, very high local accretion rate etc. it was difficult to identify any specific property, or a specific combination of them, leading to the observed nature. A recently discovered galactic black hole binary IGR J17091-3624 also started exhibiting variability behavior, particularly the 'heartbeat' type variability pattern, much like GRS 1915+105. Despite several similarities in variability patterns, the difference lies in their brightness. GRS 1915+105 is a very bright source whereas IGR J17091-3624 is a faint source. However, in absence of any information on the system parameters such as distance, mass, inclination or spin of the source, it was not possible to draw any specific inferences on the physical origin of the variability behavior. We employed an innovative method phased resolved spectroscopy with constrained system parameters and showed that, it is the high mass accretion rate that is responsible for the observed 'heartbeat' type variability.

We used the only absolute simultaneous observation by RXTE and XMM-Newton of the source in its 2011 outburst was made on 27 March, 2011. Interestingly, RXTE light curve was showing nu-class behavior in this observation with burst period of about 39 seconds. Phase-resolved spectroscopy of bursts was carried out by dividing a burst into 64 phases and co-adding counts from respective phases of all bursts. The 64 phases were grouped into 5 phases before spectral fitting and spectra of 5 phases were fitted simultaneously. We fitted the 0.7-35 keV spectra with 'canonical' model for black hole spectra consisting of an accretion disk and powerlaw (or its equivalent). The simultaneous fitting of spectra from five phases with system parameter tied across the phases could achieve significant constraints on the spin of the black hole indicating very low spin of the black hole. Figure 14 shows the best fit values of distance, D (top panel) and mass accretion rate (bottom panel) for a given combination of mass, inclination angle and spin. The gray shaded region in the top left corner of the top panel indicates only allowed combination of mass and distance from the total observed flux of the source. This clearly shows that the spin of the black hole in IGR J17091-3624 must be very low or even retrograde (rotating in opposite direction of the accretion disk). It is important to note that this was possible despite lack of knowledge of accurate information about black hole mass or distance and inclination of the binary system. This is in stark contrast to GRS 1915+105 which is a maximally rotating black hole ($a^* > 0.99$) with innermost stable orbit going very close to black hole. This can explain the low luminosity of IGR J17091-3624 as compared to GRS 1915+105.

(A. Rao and S. V. Vadawale)

Experimental measurement of lower energy threshold of the plastic scatterer.

The lower limit for the polarization measurement by the Compton polarimeter critically depends on threshold of the

plastic scatterer. There it is essential to have measurement of the scatterer threshold in order to get realistic estimates of the lower energy limit for X-ray polarimetry. However, directly measuring the threshold of the plastic scatterer is very difficult. This is because the extrapolation of measurements with standard radioactive sources with higher energy lines is not feasible due to very poor energy resolution of the plastic scintillator. Also radioactive sources with sufficiently low energy lines are not available. Therefore we have devised a new method to measure the lower energy threshold of the plastic scatterer by employing the principle of Compton scattering.

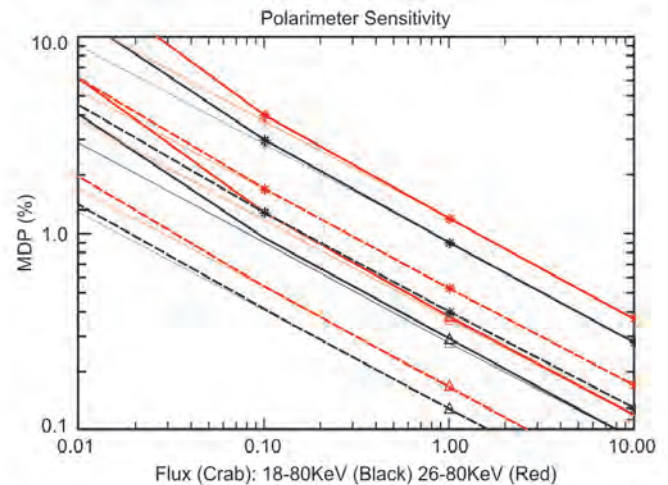


Figure 15: Minimum Detectable Polarization (MDP) for the planned hard X-ray polarimeter as a function of source intensity. Solid lines represent results for single NuSTAR area. Dashed lines refer to 5 times larger NuSTAR area. 1Ms and 100ks exposure time are denoted by triangles and asterisks respectively. The background considered here is 0.5 ph-cc-1-s-1 (thin lines) and 5 cnt-cc-1-s-1 (thick lines).

For incident photons of known energy, the energy deposited in the plastic scatterer can be easily calculated from the knowledge of the scattering angle of the scattered photon. An experimental setup has been designed and fabricated, which allows detection of both the primary Compton scattering event in the plastic scatterer as well as the detection of the scattered photon as different scattering angles while imposing the coincidence time of ~ 5 microseconds. Thus by measuring the scattered photons at different scattering angles, simultaneously with the triggers from the scatterer, provides clean measurement of the energy threshold of the scatterer. Conducting this experiment with multiple energies of incident photons provides independent confirmation of the measurement. Initial results of this experiment are very encouraging and indicate that the threshold is below 1 keV and thus the energy range for Compton polarimetry can be as low as 20 keV.

(T. Chattopadhyay and S. V. Vadawale)

Near-Infrared Monitoring and Modelling of V1647 Ori

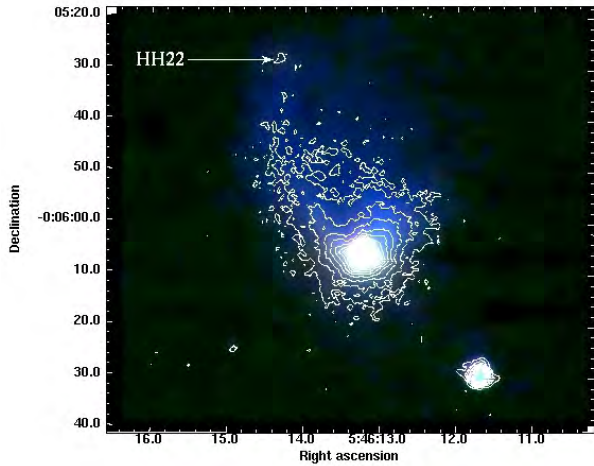


Figure 16: Color composite image of V1647 Ori and the surrounding McNeil's nebula in J (blue), H (green) and K (red) bands taken at Mt. Abu using NICS on 2011 February 4, HH22 is seen at north of V1647 Ori. H band contours (in white) are superposed with the outermost contour representing 20 mag arcsec-2 and each inward contour brightening by 2 mag arcsec-2.

We have been monitoring V1647 Ori, an eruptive young pre-main sequence star (PMS) star located near M 78 in Orion that went in to an outburst during mid-2008 and still on-going. The observed light curves in the JHK bands show period of outburst longer than 3 years indicating a possible similarity with FUors (prototype being FU Orionis). However, the object also shows spectral signatures with Brackett gamma in emission that are characteristic features observed in EXors (prototype EX Lupis). Also, starting from early 2012, the object seems to show a slow fading out with a rate of $\sim 0.06-0.18$ mag per year in the JHK bands. These properties indicate the possibility of a new class of object falling between FUors and EXors having the characteristic features of both the proto-types. Further, the light curves show episodes of mass accretion variation that are indicated by small but significant variations of JHK axes. The star displays positions beyond the T Tauri region during the current outburst in the JHK color-color diagram that are indicative of cold dust. The Herbig-Haro object HH22 situated at about 30 arcsec from V1647 Ori seems to show light fluctuation corresponding to those of the latter confirming that it may be a refection nebulosity triggered by the YSO. Modeling of the Spectral Energy distribution during the quiescent and outburst phases showed an increase in the disk mass and accretion rates

during the outburst phase, while the envelope mass and accretion rates are much lower.

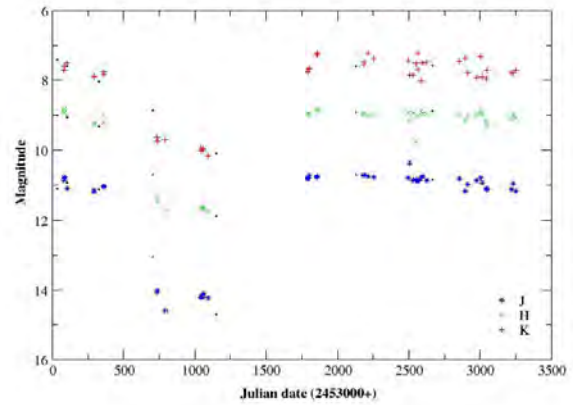


Figure 17: Lightcurves in the J, H, K bands from Mt. Abu observations during 2004-2012. The blue asterisks represent the J band, green crosses represent H band and red pluses represent K band. Observations made elsewhere are shown in black filled circles.

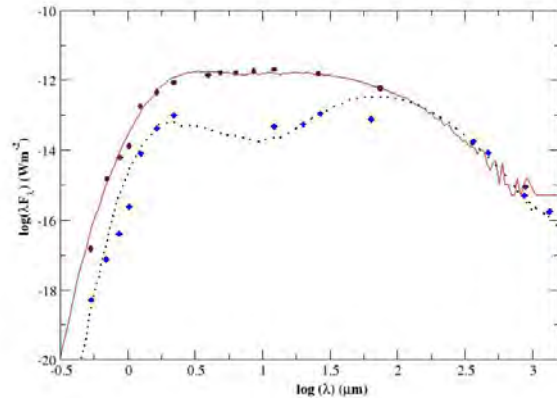


Figure 18: SED model of V1647 Ori during the outburst & quiescent phases. The maroon circles and blue diamonds are photometric fluxes with SED models shown in red and dotted lines for the outburst and quiescent phases.

(V. Venkataraman, B. G. Anandaro and P. Janardhan)

Solar Physics

Injection of Helicity by the Shearing Motion of Fluxes in Relation to Flares and Coronal Mass Ejections

Magnetic helicity is an important magnetohydrodynamic (MHD) quantity to understand the evolution of magnetic fields in solar active regions and energetic transients. We carried out an investigation of helicity injection by photospheric shear motions for two recent active regions, NOAA 11158 and

11166, using LOS magnetic field observations obtained from SDO-HMI. We analyzed the temporal evolution of helicity flux distribution and corresponding accumulation of helicity in conjunction with the observed flares and CMEs. We derived horizontal velocities in the ARs from the differential affine velocity estimator (DAVE) technique. Persistent strong shear motions at maximum velocities in the range of 0.6–0.9 km s⁻¹ along the magnetic polarity inversion line and outward flows from the peripheral regions of the sunspots were observed in the two ARs.

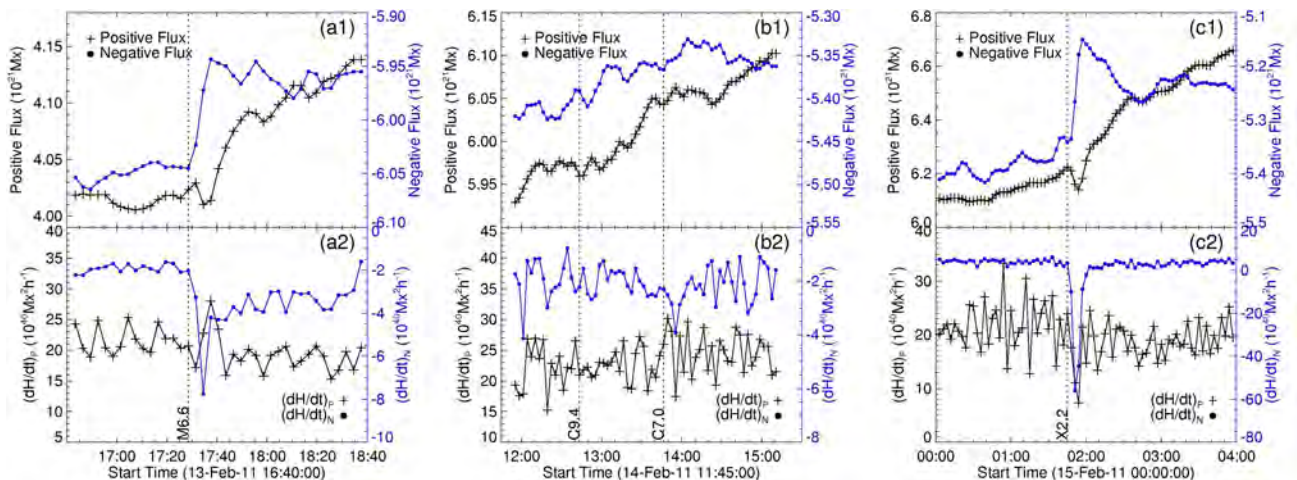


Figure 19 (a): Temporal profiles of magnetic and helicity fluxes during some selected flare events in ARs NOAA 11158 and 11166 on February 13, 14 and 15. Vertical dashed lines indicate onset time of flares as labelled in each panel.

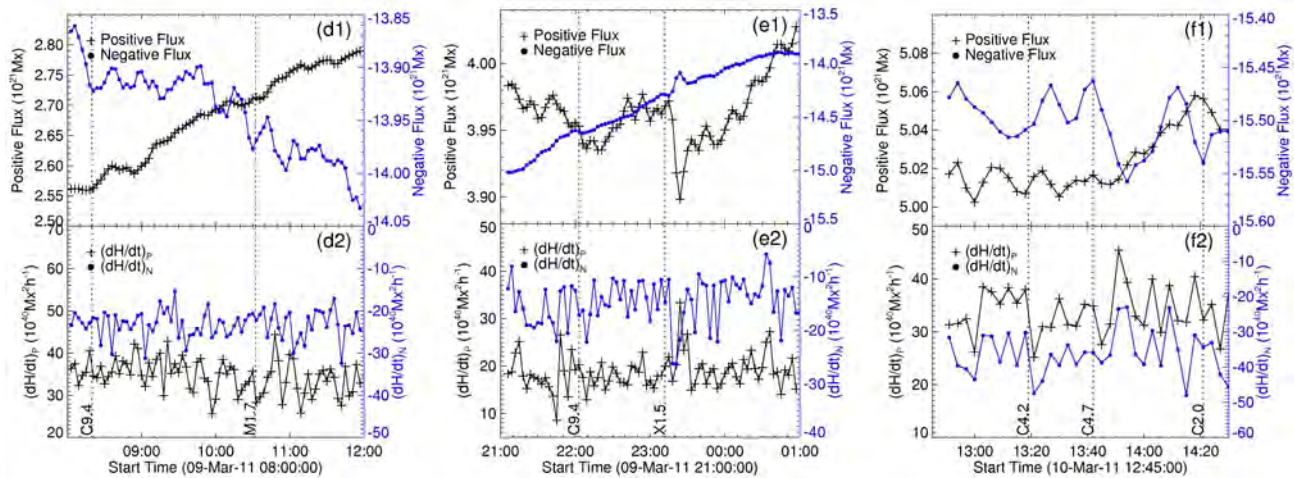


Figure 19 (b): Temporal profiles of magnetic and helicity fluxes during some selected flare events in ARs NOAA11158 and 11166 on March 9 and 10. Vertical dashed lines indicate onset time of flares as labelled in each panel.

The helicity injected in NOAA 11158 and 11166 during their six-day evolution period were estimated at $14.16 \times 10^{42} \text{ Mx}^2$ and $9.5 \times 10^{42} \text{ Mx}^2$, respectively. In both ARs, the flare-prone regions possessed mixed helicities of both signs while the coronal mass ejection (CME) prone regions had helicity flux dominated by a single sign. The temporal profiles of helicity injection showed impulsive variations during some flares/CMEs due to negative helicity injection into the dominant region of positive helicity flux. A marginally significant association of helicity flux was found with CMEs but not with flares in AR 11158, while for the AR 11166, it was the other way round. It revealed evidence of the role of helicity injection at localized sites of transient events. The short-term variations at 3-minute time cadence of helicity flux during some selected flares are examined as shown in Figure 19. The magnetic field measurements appeared to be affected by flare-related effects during the impulsive phase of larger flares (i.e., M6.6, X2.2, and X1.5 flares), which in turn, might have affected the derived helicity rates. However, the results for smaller flares of February 14 at 13:47 UT (C7.0), March 10 at 13:19 UT (C4.2), and 13:42 UT (C4.7) were rather unaffected by any such flare-related effects, and appear to provide “true” transfer of helicity. It is evident that horizontal motion of fluxes played dominant role over emergence term for increasing the complexity of magnetic structures contributing to the accumulated helicity flux. This study suggests that flux motions and spatial distribution of helicity injection are important to understanding the complex nature of the magnetic flux system of the AR, and the conditions favourable for eruptive events.

This work was carried out in collaboration with R. A. Maurya and J. C. Chae of Seoul National University, South Korea.

(P. Vemareddy and A. Ambastha)

Extrapolations of 3-D Magnetic Structure of Active Region NOAA 11158

Magnetic fields in the solar corona are responsible for a wide range of phenomena, however, their direct measurements are very difficult due to lack of suitable spectral lines, weaker magnetic fields, and high temperature. Therefore, extrapolations of coronal magnetic fields using photospheric magnetic field observations as boundary conditions by the force-free assumption are proposed to study the slow evolution of active region (AR) magnetic fields. We obtained 12 minutes cadence SDO-HMI vector magnetograms spanning 4 h duration around an M6.6 flare in AR NOAA 11158 at 17:12UT on 13 February 2011. We constructed coronal magnetic fields using potential, linear force-free (LFF) and non-linear force-free (NLFFF) approximations on $300 \times 300 \times 160$ computational grid representing physical solar dimensions of $219 \times 219 \times 117 \text{ Mm}^3$ encompassing the AR. In order to ascertain how well the extrapolated fields represent the coronal structures, we compared the modelled field lines with coronal plasma loops as seen in SDO-AIA EUV images serving as the proxies of underlying magnetic field lines. It is inferred that long overlying loops in the coronal observations are explained best with the potential and NLFFF models, but the LFF model seems to give the worst approximation.

In Figure 20, we have focused on twisted central region of AR where large shearing motions were present. The field lines are selected at pixels above 800G of $(|B_t|)$ field at one foot point and retained only those landing on the surface (closed field lines). These field lines are drawn using the potential field, LFF and NLFFF models in frames (b) to (d)). For better visualization, we color-scaled the field lines according to LOS field (b) and vertical current(c-d). The blow ups of SDO-AIA observations in EUV channels 171, and 94A are also shown in Figure 20(e-f). The alignment of transverse vectors with the

PIL delineates presence of strong shear that occurred due to continuous foot point shear motion. The consequent stressing of the field lines stored energy in the system. In the potential field case, they simply connected pairs of opposite polarities orthogonally to the PIL. In LFF, the entire region (of one sign) is assigned a constant α , which is obviously not the case in complex ARs. Generally, each field line is expected to have its own twist due to the current flowing along it, and therefore must be specified by different α , rather than a constant α . Such a provision is made with NLFFF algorithm, as field lines having different currents appear as twisted flux bundle above the interface of positive and negative flux regions.

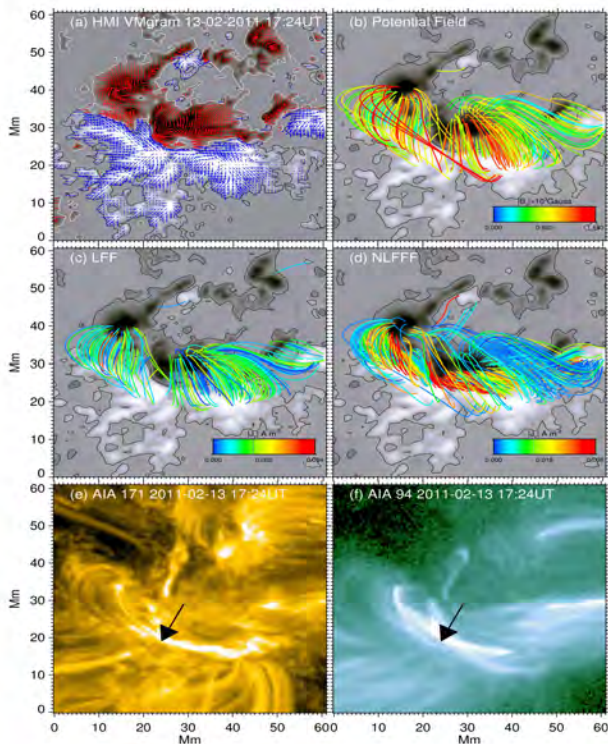


Figure 20: 3-D magnetic field structure of AR 11158 using different models of extrapolations. The computed field lines are overlaid on the plasma tracers observations of the AR in SDO-AIA EUV 171 and 94 Å for comparison. In all 3-models, the foot points of field lines are chosen to be the same and color-scaled according to vertical current (field) at their foot points in panels(c)-(d) ((b)).

The magnetic structure of NLFFF field shows twisted flux system connecting foot points on either side of PIL under the potential field arcade (less current flowing field lines). Such a system represents stored configuration of energy in the form of twist indicated by current flowing along the underlying field lines. Bright plasma emission in EVU channels (pointed by arrow) is observed surrounding this twisted flux system of current. Therefore, highly complex, twisted flux regions are the locations of stored free-energy required to power the flares, and are best reproduced by NLFFF models than the potential and LFF models. We have also computed the magnetic free-energy that is the energy available to the system to power flares above the potential energy state of that system. This is obtained by subtracting potential field

energy (E_p) from NLFFF (E_{NLFFF}) energy. We note that the ratio E_{NLFFF}/E_p decreased from 1.13 before the flare at 17:12UT to 1.10 after the flare at 17:48UT in a step-wise manner. The free-energy released during this M6.6 flare is calculated to be 9.7×10^{30} ergs in the computational domain above the AR. The NLFFF model appear to work reasonably well in reproducing twisted loops, and we plan to use it in our future work for the study of evolution of magnetic structure and explosive phenomena in solar ARs.

This work was carried out in collaboration with T. Wiegmann, Max-Planck-Institut für Sonnensystemforschung, Germany.

(P. Vemareddy and A. Ambastha)

RHESSI and TRACE observations of multiple flare activity in AR 10656 and associated filament eruption

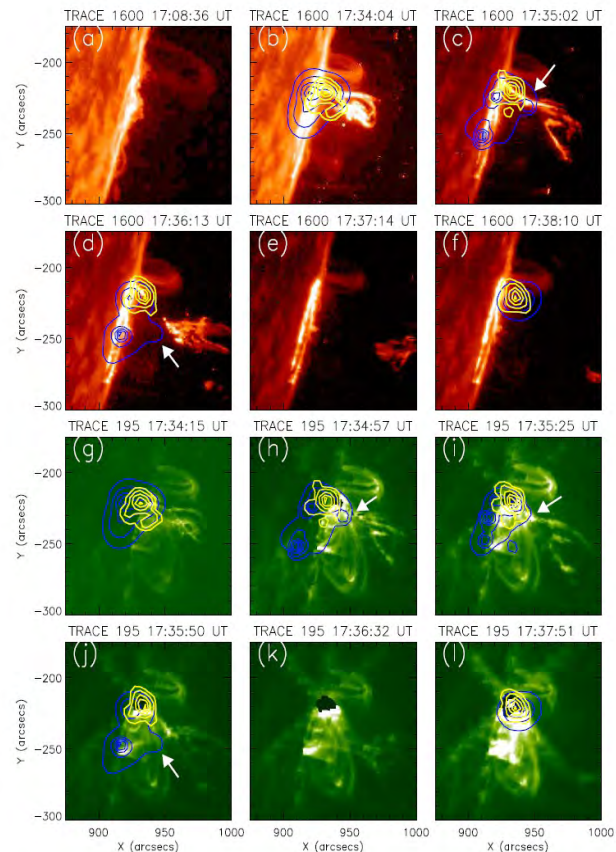


Figure 21: A few representative images taken by TRACE in 1600 Å and 195 Å channels during eruptive X1.8 flare overlaid by co-temporal RHESSI X-ray images in 12–25 keV (yellow) and 50–100 keV (blue) energy bands. It is noteworthy that 50–100 keV HXR coronal source lies over an elongated, bright (E)UV structure formed below the erupting prominence (marked by arrows in panels (c), (h) and (i)). We also note 50–100 keV HXR emission from an extended region in the corona during the phase of detachment of the prominence from the solar source region (marked by arrows in panels (d) and (j)). The RHESSI images are reconstructed with PIXON algorithm.

We have carried out a comprehensive multi-wavelength analysis of RHESSI and TRACE observations of the eruption of a solar filament from the active region NOAA 10656 on 2004 August 18. The phases of activation and eruption of filament are characterized by multiple flare activity over the period of two hours. Out of four successive flares, there were three events of class C while the final event was a major X1.8 solar eruptive flare. The activities during the pre-eruption phase, i.e., before the X1.8 flare, are characterized by three localized episodes of energy release occurring in the vicinity of a filament which produced intense heating along with non-thermal emission. A few minutes before the eruption, the filament undergoes an activation phase during which it slowly rises with a speed of ~ 12 km/s. The filament eruption is accompanied with an X1.8 flare during which multiple HXR bursts are observed up to 100-300 keV energies. We observe a bright and elongated coronal structure simultaneously in EUV and 50-100 keV HXR images formed below the expanding filament during the period of HXR bursts which provides strong evidence for ongoing magnetic reconnection. This phase is accompanied with very high plasma temperatures of ~ 31 MK which is followed by the detachment of the prominence from the solar source region (cf. Figure 21). From the location, timing, strength, and spectrum of HXR emission, we conclude that the prominence eruption is driven by the distinct events of magnetic reconnection occurring in the current sheet below the erupting prominence. These multi-wavelength observations also suggest that the localized magnetic reconnection associated with different phases of the filament in the pre-eruption phase plays an important role in destabilizing the active region filament by tether-cutting process leading to large-scale eruption and X-class flare.

This work has been done in the collaboration with Dr. A. Veronig of University of Graz, Austria and K. S. Cho of Korea Astronomy and Space Science Institute, Daejeon, South Korea.

(B. Joshi and U. Kushwaha)

Multi-wavelength observations of the failed eruption of a filament and associated M6.2 flare

We have analyzed multi-wavelength observations of the failed eruption of a magnetic flux rope that occurred in active region NOAA 10646 on 2004 July 14 using TRACE, RHESSI, and NoRH measurements (cf. Figure 22). The earliest signatures of pre-flare coronal activity are observed in EUV 171 Å images and X-ray observations up to 25 keV in the form of sequential brightening of three coronal loops, overlying the filament. The onset of the filament eruption is accompanied with the impulsive rise of HXR and MW emissions. The impulsive phase is characterized by three prominent peaks observed simultaneously in HXR and MW measurements which are spatially and temporally associated with the fast rise of the magnetic flux rope. Following the flare maximum, the eruption slowed down and was subsequently stopped by the overlying field lines at a height of 5×10^4 km. Our observations indicate that the flare emission is caused due to the reconnection of the rising flux rope and the surrounding low-lying magnetic loops. We further discuss a possible scenario to elucidate HXR and

MW sources associated with different phases of the rising flux rope which finally failed to erupt and provide its implications for models of solar eruptions.

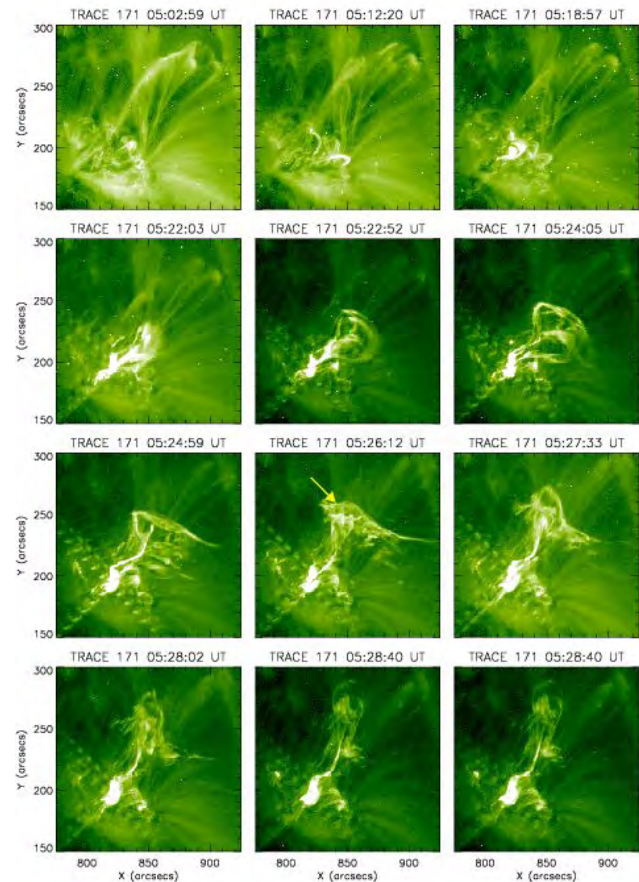


Figure 22: A few representatives TRACE 195 Å images showing failed eruption 2004 July 14 and associated M6.2 flare. The eruption is halted by overlying field lines (indicated by an arrow) and subsequently falls back on the source region.

(U. Kushwaha and B. Joshi)

Analysis of flare associated line profile changes observed in the solar active region NOAA 11158 during an X2.2 class flare

We have analyzed the Dopplergrams and magnetograms obtained by the Helioseismic and Magnetic Imager (HMI) instrument on board Solar Dynamics Observatory (SDO) to examine the photospheric velocity and magnetic field changes associated with a major flare (of class X2.2) that occurred in the NOAA AR 11158 on 2011 February 15 around 01:50 UT. We have identified five locations of velocity transients in the active region during the flare. The magnetic fields associated with these locations show sudden changes later to the velocity transients.

In the absence of spectro-polarimetric observations, it has been always a concern that velocity/ magnetic enhancements observed during the flares could be a result of artifacts arising due to distortions in the line profiles. Hence, we analyze spectro-polarimetric observations obtained from SDO/HMI corresponding to the times of the velocity and

magnetic transients. HMI observes the left circular polarization (LCP) and right circular polarization (RCP) at six wavelength positions in the wavelength range $6173 \pm 172 \text{ m}\text{\AA}$, sequentially, at a cadence of 45s.

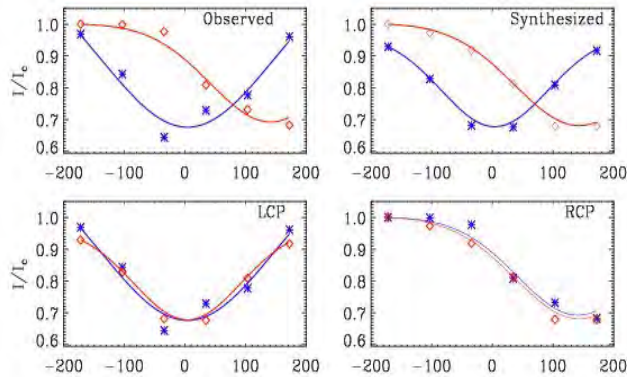


Figure 23: Comparison of observed and synthesized profiles of one of the affected kernels at the epoch before the flare. Top panels: Observed and synthesized profiles of LCP (blue) and RCP (red) and their corresponding Gaussian fit. Bottom panels: Observed (blue) and synthesized (red) profiles of LCP and RCP. Symbols represent the normalized intensity at different wavelength positions and continuous line is for corresponding Gaussian fit.

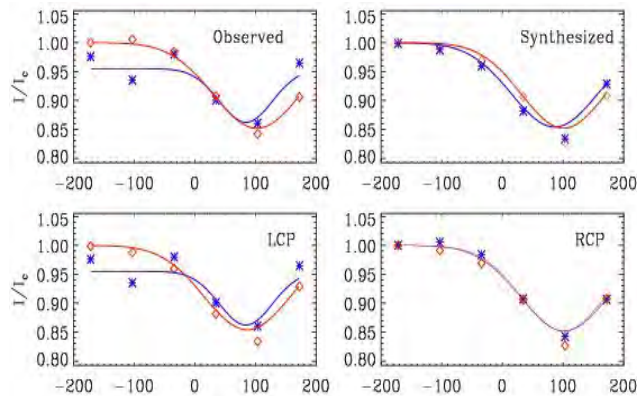


Figure 24: Same as Figure 23, but for the epochs of velocity transient.

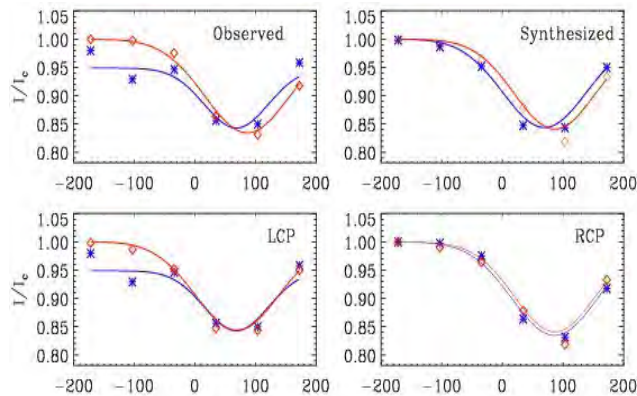


Figure 25: Same as Figure 23, but for the epochs of magnetic transient.

In order to understand the reasons for the line profile changes during the flares, we synthesized the line profiles by forward modelling using the MELANIE code (Milne-Eddington line analysis using an inversion engine; code based on Milne-Eddington solar atmosphere model). We studied the effect of atmospheric parameters on the line profiles by modifying each of the parameters viz., line strength, damping parameter, Doppler width, source function, source gradient, magnetic field strength and Doppler velocity in an optimum range.

With the aforementioned study, we realized that there are two ways of visualizing these observed changes in the line profiles in comparison to pre-flare condition: (a) distortions in the line profiles during the flare are produced on account of time evolution of thermodynamic parameters during the sequential measurements, or (b) distortions in the line profiles are due to the changes in the global atmospheric parameters of the line profiles at the flare kernels.

However, the argument (a) requires a fortuitous time evolution of the thermodynamic parameters to "create" a line distortion that can mimic a magnetic or velocity transient. Thus, we require a minimum of twelve changes in the thermodynamic variables during the sequential observations to mimic the enhancements in velocity/magnetic field relative to pre-flare condition. Whereas, option (b) can show that one require only two changes in the in the dynamical variables to change the pre-flare profile to the one observed during the flare. Applying the principle of "Ocam's Razor" in scientific methodology, we chose the option (b) in preference to option (a).

Atmospheric parameters are obtained by inverting the near simultaneous Stokes I, Q, U, and V profiles of one of the affected kernels for the epoch before the flare. These parameters were adjusted to match with the observed LCP and RCP. The synthesized line profiles along with observed ones are shown in Figure 23. The atmospheric parameters that fit the observed LCP and RCP at the epoch before the flare were adjusted in such a way that it closely matches the observed profiles of LCP and RCP at the time of velocity and magnetic transients. The dominant changes seen are the change in magnetic field strength of about 1400 G and change in velocity of about 1100 m/s in addition to change in line strength and source function. The synthesized line profiles along with observed ones at the time of transients are shown in Figure 24 and 25.

Similar analysis for distorted line profiles at other kernels also show that a significant change in magnetic field strength and Doppler velocity relative to pre-flare condition are necessary in achieving the correlation between observed and synthesized profiles at all the kernels. However, this conclusion is subject to the caveat that there are no variations of the thermodynamic parameters during the sequential sampling of the line profile. This emphasizes the importance of simultaneous measurements of LCP and RCP at a better cadence. The best case scenario would be obtaining observations from a slit-based spectrograph with the flaring locations coinciding with the the slit.

This work has been done in collaboration with B. Ravindra of IIA, Bangalore, S. Mathur of High Altitude Observatory, Boulder, USA, and R. A. Garcia of Laboratoire AIM, CEA/DSM-CNRS, Université Paris, IRFU/SAP, Centre de Saclay, Gif-sur-Yvette, France.

(A. R. Bayanna, B. Kumar, P. Venkatakrishnan, and S. K. Mathew)

On the relation between intensity oscillations and magnetic field parameters in the solar active region NOAA 10953

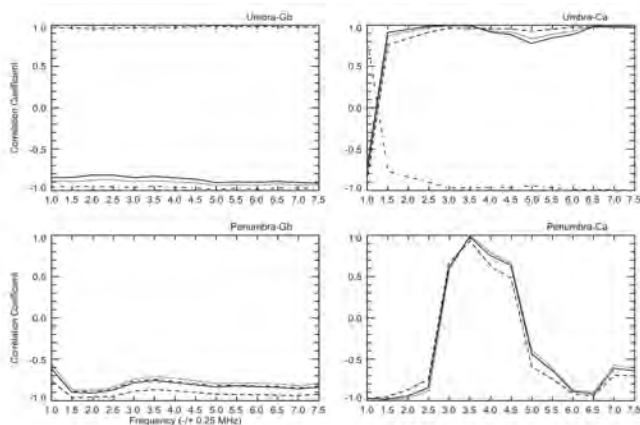


Figure 26: Plots of correlation between photospheric magnetic field parameters and intensity oscillatory power of umbra (top panels) and penumbra (bottom panels) in G-band (left panels) and Ca II H (right panels) in different frequency bands. Correlation between $B_{0\phi}$ vs. power (solid line), B_t vs. power (dashed line), B_l vs. power (dotted), and inclination vs. power (dot-dashed line) are shown here.

We have analyzed the filtergrams obtained by SOT instrument on-board Hinode spacecraft to study the properties of intensity oscillations in the solar active region NOAA 10953. The observations consist of near simultaneous G-band, and Ca II H line intensity images. This allows us to compare intensity oscillations in the magnetic and non-magnetic regions simultaneously in the solar photosphere and chromosphere. From the acoustic power maps, it is observed that G-band intensity oscillatory power decreases with increase in magnetic field strength at all frequencies, while Ca II H umbra shows enhanced power at higher frequencies. Enhancement of power is also seen at low frequencies across the light bridge in Ca II H and at the boundaries of umbra-penumbra and sunspot-quiet Sun in G-band. Former coincides with the chromospheric brightening across the light bridge while the latter could be due to the continuous flow of plasma along the magnetic field lines. We have also used near simultaneous spectro-polarimetric observations of the active region from Hinode SOT/SP to study the relation between various magnetic field parameters and the intensity oscillatory power in the photosphere and the chromosphere. We performed the correlation analysis between the power and various parameters of photospheric magnetic field as a function of frequency in umbra and penumbra separately. We observe that in the penumbra the chromospheric height

power is correlated with the magnetic parameters at 3-4.5 MHz range while it is anti-correlated at all other frequencies. The penumbral power in photosphere shows anti-correlation with magnetic parameters at all frequencies. Photospheric umbral power shows anti-correlation with magnetic field strength, line-of-sight magnetic field and inclination while it shows correlation with transverse magnetic field. In the chromospheric umbra, we observe a reverse behavior except at very low frequencies (Figure 26).

This work has been done in collaboration with R. E. Louis of Leibniz-Institut für Astrophysik, Potsdam, Germany.

(A. R. Bayanna, S. K. Mathew, B. Kumar and P. Venkatakrishnan)

Reconstructing CME in inner heliosphere by its continuous tracking in imaging observations taken by STEREO

Coronal Mass Ejections (CMEs) are episodic expulsions of magnetised plasma from the solar corona in to the heliosphere. One of the main interests of solar-terrestrial researchers is to understand CMEs, their nature of propagation and predict their arrival time at the Earth, since they drive the strongest disturbances in the Earth's magnetosphere. The dynamics of CME changes throughout its journey from Sun to Earth due to dominant role of different driving forces near the Sun and beyond. Since last two decades, several studies have been carried out to relate the remote sensing observations of CMEs to near Earth consequences. Majority of these studies were aimed at understanding the kinematics of CMEs and predicting their arrival time at the Earth based on exploitation of white light observations taken near the Sun. For an improved estimation of the arrival time of CMEs and their kinematics, we selected CMEs which were observed in remote sensing as well as in in-situ observations. Since twin STEREO provide two view directions of heliosphere from their locations away from the Sun-Earth line, they enable 3D study of evolution and propagation of CMEs. For continuous tracking of CMEs in the heliosphere, we constructed the time elongation maps (J-maps) using images taken by instruments, coronagraph COR2 (FOV: 2.5-15 R_s) and heliospheric imager HI1 (FOV: 15-90 R_s) & HI2 (FOV: 70-330 R_s) on-board STEREO. The evolution of CME of 12 December 2008 in STEREO Behind COR2 and HI FOV is shown in Figure 27. We implemented the geometric triangulation technique which requires the measured elongation angles of selected CME features from two view directions as inputs, to estimate its propagation direction and speed of CME in the heliosphere. In the selected CMEs, for the distance where CMEs could not be tracked unambiguously, we used the kinematics obtained from geometric triangulation technique as inputs in the Drag Based Model (DBM) to predict the transit velocity and arrival time of CMEs at the in-situ spacecraft near 1 AU. The adopted DBM is based on the assumption that beyond a distance of 20 R_s , in the corona, the dynamics of a CME is governed solely by its interaction with ambient solar wind.

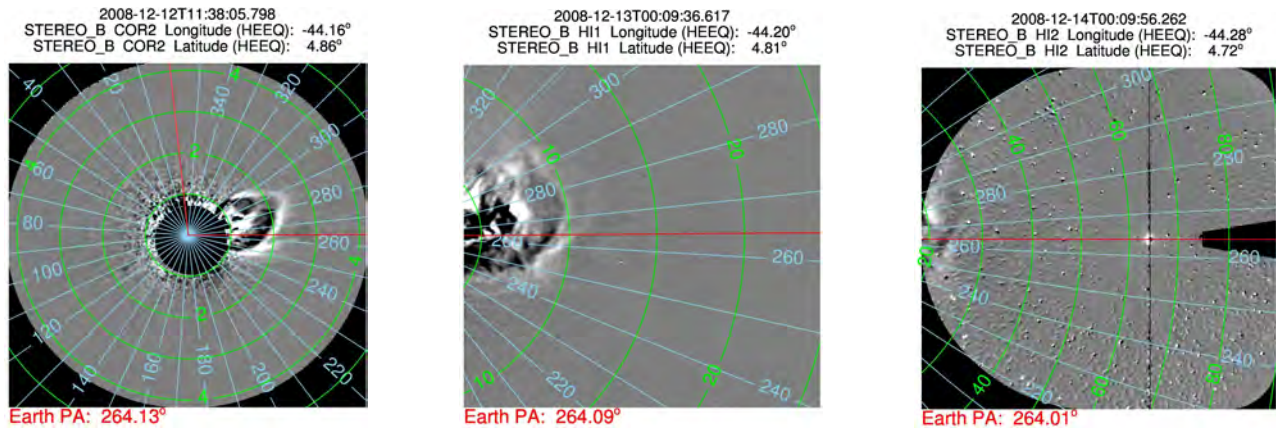


Figure 27: Left, middle and right figures show the running difference images of COR2, HI1 and HI2 respectively, taken by STEREO/SECCHI Behind spacecraft. Contours of elongation angle (green) and position angle (blue) are overdrawn on images. The vertical red line shows the zero degree position angle and horizontal red line shows the position angle of Earth.

We identified the CME boundaries in in-situ data and marked the actual arrival time of tracked feature. We also estimated the errors in the predicted arrival time of CME from its actual arrival time. In our study of 8 selected CMEs observed during 2008-2010, we found a better accuracy in predicted arrival time of CMEs, using both COR2 and HI observations than using only COR2 observations. Our study reveals that kinematics of CMEs estimated by exploiting wide angle imaging observations of STEREO combined with DBM improves prediction of arrival time of CMEs with errors of 3 to 9 hours. Our study also underlines the possibilities of changes in CME dynamics due to its interaction with fast solar wind from the coronal hole.

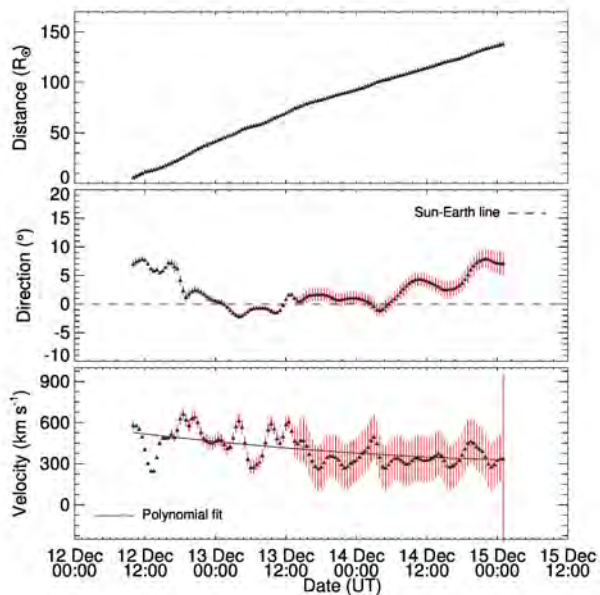


Figure 28: From top to bottom, panels show the distance, propagation direction and velocity of 12 December 2008 CME. Vertical red lines show the estimated error bars.

(W. Mishra and N. Srivastava)

Cradle-to-grave study of January 5, 2005 CMEs

One of the major aims of solar and heliospheric research is to reveal the mechanisms of the initiation, evolution and near-Earth response to the solar eruptive events; all together in the domain of space weather studies. These solar eruptive events or coronal mass ejections (CMEs) expel huge amount of plasma, magnetic flux and helicity in the interplanetary medium. About 70% of CMEs are associated with solar filaments, which are low temperature and high density structures that remain suspended by magnetic fields in the corona and are observed along the polarity reversal lines between regions of oppositely directed photospheric magnetic fields. On 5 January 2005, SoHO/LASCO observed 2 successive CMEs associated with the filaments (active region & quiescent). The eruptions resulted in two distinct magnetic clouds whose embedded flux rope topology was modelled using Grad-Shafranov (G-S) reconstruction technique. Filament plasma remnants in these magnetic clouds were identified by using a combination of in-situ plasma, magnetic and composition signatures.

Multiple Earth-directed CMEs, during propagation in interplanetary space, might interact, transferring momentum and energy between the two flux systems through magnetic reconnection. These interactions can produce or enhance southward magnetic fields which can induce storms and substorms at Earth's magnetosphere. In-situ spacecraft (ACE & Wind) measurements during 7-9 January 2005, suggest interaction between two magnetic clouds (MC1 & MC2) with complex magnetic structures (R1 & R2) at interface region; separated by magnetic holes (H1 & H2). These features impacted the Earth's terrestrial magnetosphere - ionosphere system and resulted in a moderate geomagnetic storm (peak Dst \sim -96 nT). During the main phase of this storm on 7 January 2005, polarity reversals in the Y-component (dawn-to-dusk) of interplanetary electric field triggered two major auroral substorms with concomitant changes in the polar ionospheric electric field. However, similar polarity reversal on 8 January 2005 during the recovery phase of the storm did not trigger any auroral substorm activity.

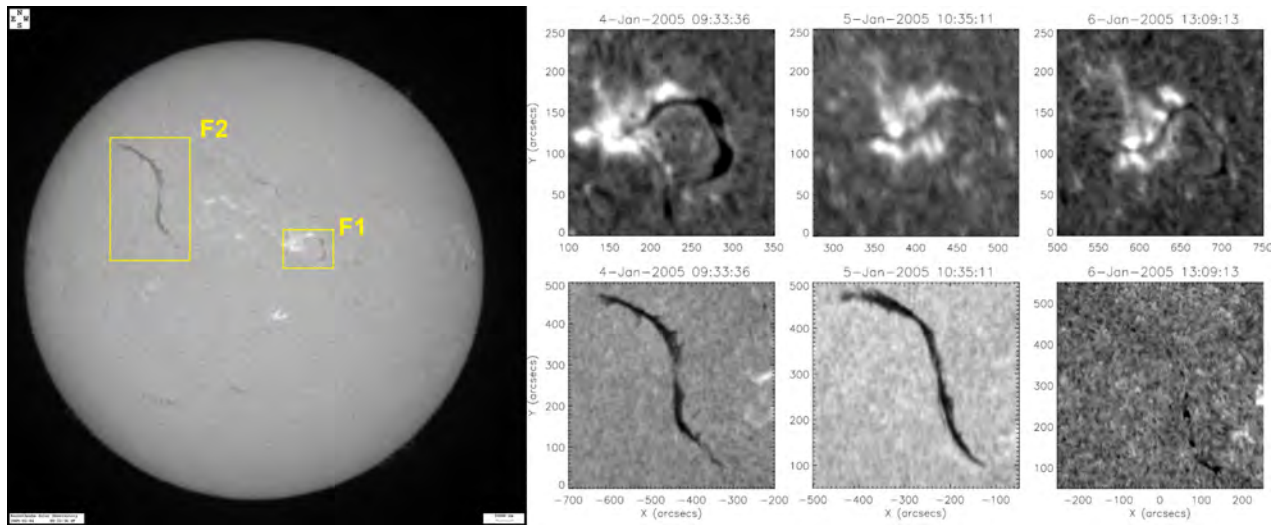


Figure 29: Left: H α image from KSO taken on 4 January, 2005. Right: Upper panels shows H α observations of filament (F1) before eruption on 4 January at 09:33 UT; 5 January at 10:35 UT & on 6 January at 13:09 UT. Lower panels show H α observations of filament (F2) before (4 January) and after the eruption (6 January).

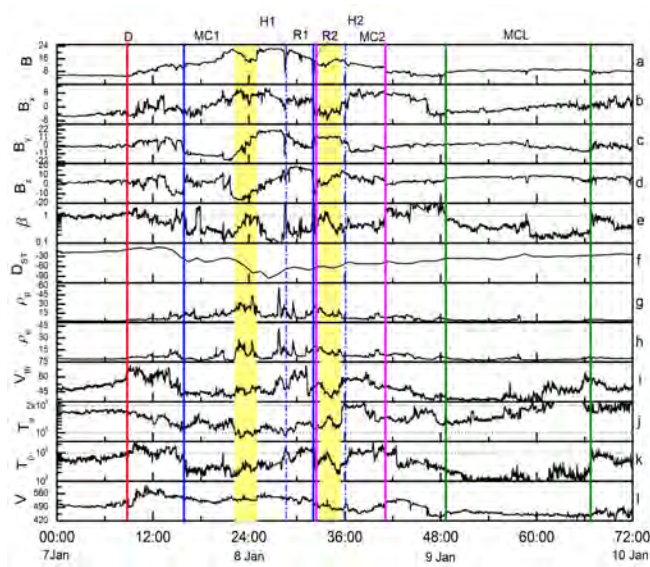


Figure 30: A plot of magnetic (a-e) and plasma (g-l) parameters from January 7-10, 2005. (top to bottom) the magnetic field strength (B), magnetic field components (B_x , B_y , B_z), plasma beta obtained from Wind spacecraft and 1-hour averaged Dst index. Measurements of proton density (ρ_p), electron density (ρ_e), proton thermal velocity (V_{th}), electron temperature (T_e), proton temperature (T_p) and solar wind bulk velocity (V), indicating the boundaries of MC1, R1, MC2, R2 and MCL from 7-10 January, 2005. Arrows indicate the location of magnetic holes (H1 and H2). Shaded portion is filament plasma region.

Our study of remote sensing and in-situ observations of two CMEs associated with eruptive filaments on 5 January 2005 shows that these eruptions caused two distinct but slow ICMEs travelling at different velocities that interacted in interplanetary medium and resulted in complex magnetic

structures. These structures coupled with Earth's space and terrestrial environment and triggered a series of substorms in the main phase of a moderate geomagnetic storm. Our study provides a unique opportunity to combine different observations and analysis techniques to understand causative interplanetary magnetic and plasma structures associated with complex storm-substorm phenomenon.

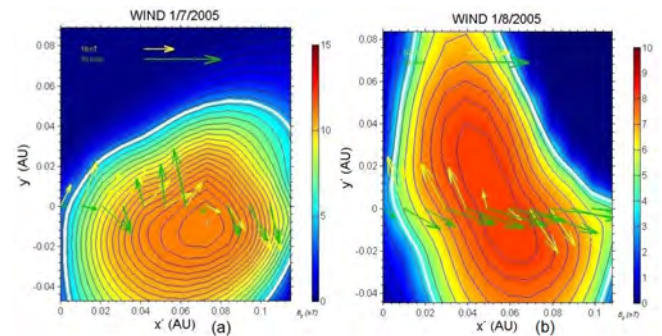


Figure 31: Cross section of G-S reconstructed magnetic flux rope associated with magnetic clouds (a:MC1 & b:MC2). Black contours show transverse magnetic field lines while the colors show the axial magnetic field distribution. Yellow arrows denote measured transverse magnetic field while green arrows are residual velocities in deHoffmann-Teller frame at Wind spacecraft.

This work is done in collaboration with C. Moestl of Institute of Physics, University of Graz and Q. Hu of Center for Space Plasma and Aeronomic Research, The University of Alabama, Huntsville.

(N. Srivastava, R. Sharma and D. Chakrabarty)

On the formation of magnetic discontinuities through the superposition of two linear force-free magnetic fields

The magnetic flux across an arbitrary fluid surface remains conserved in a fluid with infinite electrical conductivity. The magneto-fluid then can be partitioned into contiguous sub-volumes of fluid each of which entraps its own subsystem of magnetic flux. During dynamical evolution of the magneto-fluid, these sub-volumes may press into each other and in the process two such sub-volumes may come into direct contact while ejecting a third interstitial sub-volume. Depending on the orientations of magnetic

fields of the two interacting sub-volumes the magnetic field at the common surface of interaction may become discontinuous and a current sheet is formed there. This process of current sheet formation and their subsequent decay is believed to be a plausible mechanism for coronal heating and may also be responsible for various eruptive phenomena at the solar corona. In this work, we explore this theoretical concept through numerical simulations of a viscous, incompressible magneto-fluid characterized by infinite electrical conductivity where the initial magnetic field is prescribed by the superposition of two linear force-free fields with different twists.

(D. Kumar and R. Bhattacharyya)

SCIENCE

Planetary Sciences and PLANEX Program

The Planetary Sciences Division focuses on isotopic investigations of meteorites to understand presolar and early solar system processes and timescales, and the evolution of terrestrial planets and their atmospheres. The PLANEX Program aims at the understanding of surface features and processes on Moon and Mars using remote sensing data from lunar and Mars missions. Another important objective of the PLANEX Program is to develop science payloads for planetary missions to Moon and Mars. Some progress on the recently initiated planetary astronomy program is also reported.

Planetary Sciences

Constraining Water Content in Low-Ti Mare Basalt, 15555

The Moon was believed to be "bone dry" based on the earlier analysis of returned lunar samples. Infrared mapping by Moon Mineralogy Mapper on Chandrayaan-1 resulted in the detection of hydroxyl (OH) and water on the uppermost few millimetres of the lunar surface. Analyses of Apollo 14 rock samples of volcanic origin has revealed that parts of the lunar mantle are likely to be more rich in volatiles than previously thought. However, it is unclear whether the measured water contents from different minerals (glass, apatite and melt-inclusions) in various lunar rocks are representative of the entire lunar mantle.

In this study, volatile content is measured from late-crystallizing apatite grains and the early entrapped melt inclusions in magnesian olivine within lunar sample 15555. This mare basalt is considered to be representative of a parent-magma in the low-Ti mare basalt suite and crystallised in a closed system at 0.85-1.2 GPa pressure range (170-240 km depth). The water content in melt-inclusions is observed to be ~ 200 -300 ppm, whereas in apatites, the range of measured water content is ~ 2500 -9500 ppm. The measured water content in melt-inclusion is equivalent to parent melt of 15555, whereas the estimated H₂O content in parent melt is ~ 100 -380 ppm (assuming apatites appeared at 99% crystallization level). Both the values are complementing each other, demonstrating that 15555 has undergone closed-system crystallization. At least a few percent of melting is needed at source region to accumulate enough melt to provide momentum and leave the source. Assuming 5-20% partial melting, which is needed to form mare basalts as shown using highly siderophile elements and isotopic modelling, and a range of partition coefficients ($D=0.005$ -0.01), we calculate 10-60 ppm water from melt-inclusion in the source region of low-Ti mare basalts. The water content in source region in our studied rock yields eight to ten times lower value than that measured in melt-inclusions of volcanic glass, which originated at deeper mantle (500-600 km depth). This study shows that budget and distribution of volatiles in the Moon varies in different water-rich reservoirs. This difference must have an important role in the magma evolution and eruption on the Moon.

(A. B. Sarbadhikari, K. K. Marhas, Sameer and J. N. Goswami)

Presence of ^{60}Fe in QUE97008 and implication towards stellar source incorporating Short lived nuclides in Early Solar System

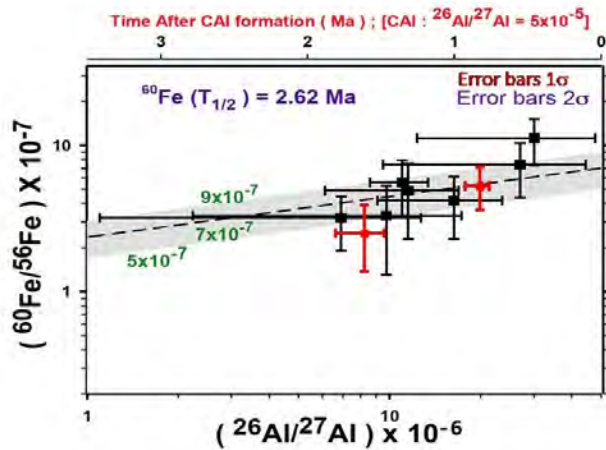


Figure 32: Variation of initial $(^{60}\text{Fe}/^{56}\text{Fe})$ with initial $(^{26}\text{Al}/^{27}\text{Al})$ at the time of formation of unequilibrium ordinary chondrules analysed using Nanosims and existing SIMS data (Mishra et al. 2010). The expected correlation if ^{60}Fe and ^{26}Al were co-injected from the same source is shown. Time of formation of the chondrules, relative to CAIs is shown in the top panel.

The determination of initial solar system abundances from measurements of extinct radionuclides is important for constraining the astrophysical setting of solar system formation. ^{60}Fe ($t_{1/2} = 2.62$ Myr), a short-lived radionuclide which decays to ^{60}Ni , is important since it is a unique product of stellar nucleosynthesis, and is a potential heat source (along with ^{26}Al) for early thermal metamorphism of planetesimals. An accurate estimation of the solar system initial abundance of ^{60}Fe is important to determine the stellar source of this nuclide. After initial attempts in CAIs and differentiated meteorites, investigations were carried out in-situ in Fe-rich phases in chondrules and matrices. The inferred solar system initial (SSI) values from the in-situ studies using SIMS suggested values in the order of 10^{-7} to $\sim 10^{-6}$, while the bulk analysis carried out in differentiated meteorites, using MC-ICPMS indicated a value $\leq 10^{-8}$.

We present results of Fe-Ni isotope systematics in chondrules from one of the least altered ordinary chondrite Que 97008 (LL 3.05). O- primary ion beam of 4 nA was focussed to $\sim 10\mu\text{m}$ to generate positive secondary ions of Fe and Ni. A typical analytical protocol lasting for a couple of hours involved measuring ^{57}Fe , ^{60}Ni , ^{61}Ni , ^{62}Ni for 10 seconds in each cycle in three magnetic field settings in multicollection mode using nanoSIMS 50 at Physical Research Laboratory. Terrestrial olivine and NBS 610 were used to assess the instrumental mass fractionation.

The results are in agreement with the earlier measurements and support the possibility of a large mass stellar source as the provenance of SLNs with shorter half-life. The Initial Solar System $[(^{60}\text{Fe}/^{56}\text{Fe})_{\text{SSI}}]$ estimate from the two chondrules is $(7.2 \pm 2.5) \times 10^{-7}$ (wt. average). The correlation between

^{26}Al and ^{60}Fe records in chondrules (Figure 32) observed suggest that these nuclides are co-genetic and a high mass supernova appears to be the most plausible source that delivered short-lived nuclides into the protosolar cloud.

(K. K. Marhas, R. K. Mishra and Sameer)

Noble gases in the martian meteorite Tissint

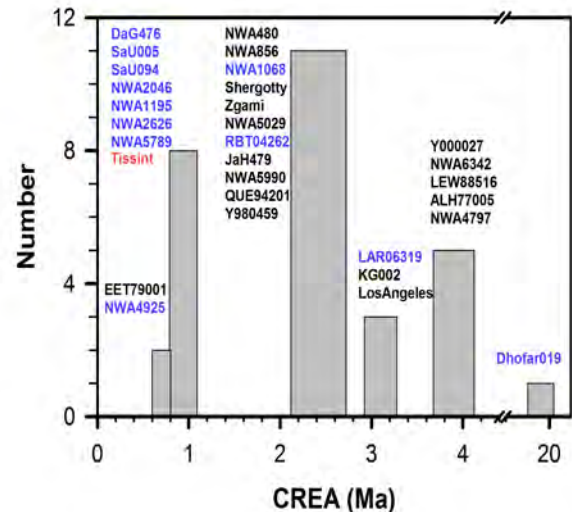


Figure 33: Comparison of cosmic-ray exposure ages of Shergottites

Tissint is only the fifth witnessed meteorite fall from Mars. It fell in Morocco on July 18, 2011, and has been classified as olivine-phyric shergottite. We have analysed noble gases and nitrogen in Tissint to decipher its cosmic ray exposure age and composition of trapped gases. Our sample comes from an unknown piece of Tissint and consisted of eleven interior grains (total weight ~ 100 mg). We analysed all the noble gases and nitrogen, extracted in two pyrolysis steps (800°C and 1700°C), on a multi collector noble gas mass spectrometer using standard procedures. Though the meteorite fell in July, it has been collected after a few months, exposing it to the hot desert environment, resulting in pickup of some terrestrial atmospheric gases, as clearly seen in Xe isotopic composition.

The elemental ratios of the trapped component ($^{84}\text{Kr}/^{132}\text{Xe}$) and ($^{36}\text{Ar}/^{136}\text{Xe}$) are 4.9 and 100 respectively indicating a contribution from Mars interior. However, the ($^{129}\text{Xe}/^{132}\text{Xe}$) of 1.140 ± 0.003 clearly shows a contribution from Mars atmosphere as well. The observed cosmogenic ratio $(^{82}\text{Kr}/^{83}\text{Kr})_c$ is 1.32, higher than the pure spallation ratio of 0.78 ± 0.02 , indicating a contribution to $^{82}\text{Kr}_c$ from (n, γ) reactions on Br. This requires that the minimum pre-atmospheric size of Tissint should be > 22 cm. Ne is purely cosmogenic, and the high $(^{22}\text{Ne}/^{21}\text{Ne})_c$ ratio of 1.313 is typical of most shergottites, due to compositional effects, and hence is not a good shielding parameter. We obtain ^{21}Ne based cosmic ray exposure age of 1.0 ± 0.1 Ma, for a production rate calculated using average shielding depth and the chemical composition of Tissint. The available

exposure ages of shergottites (excluding Dhofar 019) fall under different clusters, in the range of 0.73 Ma to 4.7 Ma. Tissints exposure age matches with seven other olivine-phyric shergottites (Figure 33), suggesting that they are all ejected in a single event from the Martian surface.

(R. R. Mahajan and S. V. S. Murty)

Solar gases in Washington County iron meteorite

Iron meteorites can be broadly classified into two groups; magmatic irons, formed as cores of early differentiated planetesimals and non magmatic irons. The latter group are presumed to be younger and their formation process is yet to be understood. The focus of our work is to understand the origin of non magmatic irons through studies of their trapped noble gases. Noble gases in most irons are dominated by cosmic-ray produced component, in particular for He, Ne and Ar. It has been found that in non magmatic irons that have silicate, troilite and graphite inclusions, trapped noble gases of Q composition have been observed. But in the unique case of Washington County (WC), an ungrouped iron meteorite, solar composition of noble gases has been detected, but with an ambiguity about the sample location (i.e. surface/interior). We have obtained a rectangular slab of WC, one end of which represents the fall surface and the other end, the interior. Three samples from this slab, representing the fall surface (S) and interior (A and B) have been analysed for noble gases by stepwise pyrolysis (800°C, 1200°C and 1700°C) in an all metal resistance heater and analysed in a multi-collector noble gas mass spectrometer by standard procedures.

The systematics of He, Ne and Ar for all the three samples of WC indicate the presence of trapped components. In the Ne three isotope plot, the data for both surface and interior samples fall along the mixing line of solar wind (SW) and cosmogenic end members (Figure 34). The peak release at maximum temperature (1700°C) for both trapped and cosmogenic components illustrate that the trapped SW gases are volume correlated, similar to the cosmogenic gases. Presence of surface correlated SW gases is possible only if the measured sample is from the actual unablated surface of the meteorite. Samples were taken from three different locations longitudinal to the rectangular slab of WC. Using the elemental ratio of the cosmogenic isotopes ($^{38}\text{Ar}/^{21}\text{Ne}$)_c, location of the measured surface sample can be estimated to be below around 11 cm in the pre-atmospheric meteoroid, suggesting that the present surface is not the actual surface of the meteorite where solar gases can be surface implanted. The present result clearly demonstrates the presence of volume correlated SW gases in WC meteorite. It is inferred that the SW gases must have been acquired by WC during the formation of its parent body and not lost subsequently. Formation of WC parent body in a local melt pool by an impactor carrying SW gases consistently explains the above results.

(P. M. Ranjithkumar and S. V. S. Murty)

Metallographic cooling rate of Iron meteorite

Iron meteorites, being essentially made of Fe- Ni alloy, cool very slowly in the order of a few degree to few hundred degree centigrade per million years (Ma). Considering various constraints like presence of non- metals and their impinge effect during growth in the melt, cooling of melt in the closed/open system, metallographic cooling rates (CR) were estimated for two iron meteorites-Raghnunathpur (IIAB) of India (fall of 1986) and Nyaung (IIIAB) of Myanmar (fall of 1939). Estimation of CR helps to assess the nature of fractionation in open or closed system and the size of the parent bodies.

Raghnunathpur comprises large plates of kamacite (Ni- 4.3 wt%) with homogeneous distribution of microrhabdites and rhomb rhabdites in the matrix (Figure 35a). In addition, there are considerable proportions of platy lamellar schreibersite and very long, acicular needle schreibersite. Most significant features of this hexahedrite are the presence of Daubreelite (FeCr₂S₄)-Troilite (FeS) nodules where these two sulphides exist as exsolution texture. Neumann lines (at least three sets) observed within kamacite imply a shock pressure of 130 kb. In absence of Widmansttten pattern and taenite lamellae, growth of schreibersite lamellae in the kamacite matrix has been used to determine the rate of cooling. Employing calibrated experimental data (after Randich & Goldstein, 1978), CR of Hexahedrite based on Ni- content and phosphide band width is estimated to be 4°C/Ma which corresponds to a parent body diameter of 78.2 km. This estimate is slightly higher than mean CR of 2°C/Ma because of the effect of Cr bearing sulphide nodules in the melt.

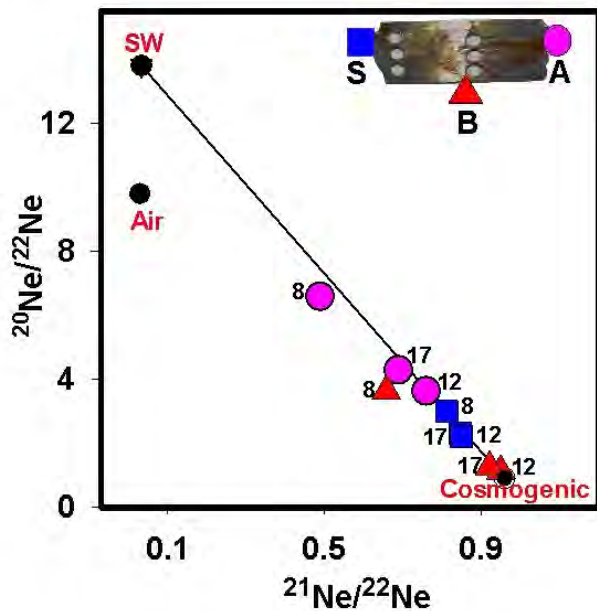


Figure 34: Neon three isotope plot for WC samples. S is a surface sample, whereas A and B are interior samples. The numbers besides data points indicates temperature in units of 100°C

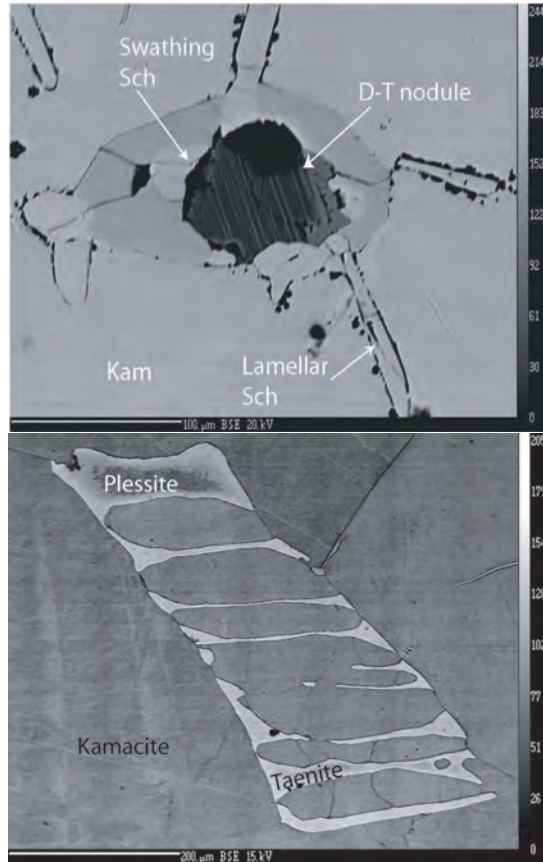


Figure 35: (a) BSE image of Raghunathpur IIAB. Sawthing Schreibersite is seen to occur as a rim around Daubreelite Troilite (D-T) nodule. (b) (right) shows the BSE image of Nyaung IIIAB. Plessite is seen within the taenite lamellae.

Nyaung has been structurally classified as Medium Octahedrite (Om) based on the estimation of true bandwidth of kamacite (Ni-6.23 wt%) which clearly define Widmansttten pattern. Besides taenite lamellae (Ni- 33.45 wt%) and several types of plessites (very fine grained kamacite-taenite mixture) Daubreelite nodules occur as inclusions (Figure 35b), along with exsolved lamellae of troilite. Presence of multiple sets of Neumann lines and their recrystallized nature at places suggest a shock pressure of 130 kb and thermal annealing to some extent. Ni-profiling across taenite lamellae provides a good estimate of cooling rate when plotted in the calibrated CR curves (CRC) in the space defined by taenite half width and its Ni- content. CR data of Nyaung spread within the 100 to 200°C/Ma range with a mean CR of 150°C/Ma, very similar to Bella Roca Octahedrite.

(S. Ghosh, D. Ray and S. V. S. Murty)

Aerodynamic Morphology and Geochemistry of Impact Spherules from Lonar Crater, India

The ~570 ka old Lonar impact crater, India, is one of the few known terrestrial impact craters that was excavated in the basaltic targets of the Deccan Traps (~65 Ma). This impact crater of ~1.8 km diameter is a unique terrestrial analog for the large number of craters on planetary bodies in our

solar system having basaltic crusts. The typical Lonar impact glasses that occur only within the ejecta around the rim of the Lonar crater include impact-melt bomb and spherules.

The aerodynamically shaped, mm-sized spherules are characteristically black, spherical to ellipsoidal droplets and vary in size from 2-5 mm (Figure 36a). The BSE image of a whole spherule shows that it is almost homogeneous, non-crystalline at the central part but vesicular close to the margin (size ~0.4 mm). The partially digested plagioclase xenocrysts are highly vesicular (Figure 36b). The central part of the spherules are generally devoid of any remnant of partially-melted xenocrysts (plagioclase, pyroxene and magnetite), which is commonly present towards the marginal part of the grains.

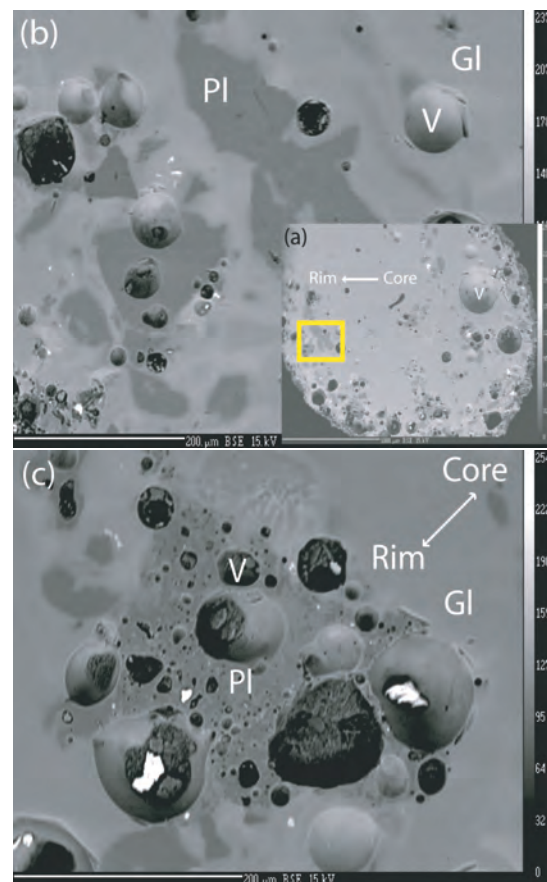


Figure 36: (a) BSE image of mm-sized spherule (inset); (b) BSE image of enlarged view of marginal part of spherule shows partially digested plagioclase. Pl, V and Gl indicate plagioclase, vesicle and glass respectively. (c) shows partially digested plagioclase at the marginal part of spherules.

The average mm-sized Lonar impact-spherules are marginally enriched in SiO₂ and significantly in K₂O, and depleted in MgO and Na₂O over target-basalt, these spherules have ~1.5 times higher Ni over the target basalt. In comparison to sub-mm sized spherules, the mm-sized spherules are generally acidic and enriched in SiO₂, Na₂O, K₂O and P₂O₅, and depleted in FeO_{total}, MnO, MgO, and in all transitional trace elements (Cr, Co, Ni) and Zn.

Generally the absence of vesicles and smooth surface texture characterize the sub-mm sized spherules, whereas presence of vesicles could be taken as a characteristic feature of the mm-sized spherules. Occurrence of vesicles especially along the marginal zone of the mm-sized spherules suggests the evolution of these quenched liquid droplets (that solidified in atmosphere during their flight) must be associated with high volatile pressure. The morpho-chemical differences between the sub-mm and mm-sized spherules suggest different modes of their formation from the impact plume. Pre-dominance of schlieren and impactor components, and near absence of vesicles in the sub-mm sized spherules suggest these quenched liquid droplets could have been produced from the impactor-rich, hotter central part of the plume, whereas the morpho-chemistry of the mm-sized spherules suggests possibility of their formation from the relatively cool outer part of the same plume.

(D. Ray)

U-Pb and Lu-Hf isotope records of eastern and western Dharwar craton

U-Pb ages and Lu-Hf isotope systematics of detrital (metasedimentary) and magmatic (orthogneissic) zircons from the eastern and western Dharwar craton provided new insight on tectonomagmatic evolution of this ancient craton in the Indian shield. Five samples (three from the western and two from the eastern blocks) that yielded reasonable number of zircons were analyzed. The antiquity and nature of the source magma (juvenile or recycled) sampled by these zircons provide a better understanding of evolutionary history of the craton. U-Pb ages for detrital zircons suggest presence of 3.4 Ga crustal components in both the western block and the eastern block of the Dharwar craton. Magmatic zircon from the western block yielded ages ranging between 3.1 to 3.2 Ga while those from the eastern block show a bi-modal distribution with records of older components (3.0 to 3.2 Ga) and presence of younger events (overgrowth at 2.7 and 2.5 Ga). Magmatic and detrital zircons of western Dharwar block exhibit positive ϵ_{Hf} values (+1 to +5) and Hf model ages of 3.25 to 3.45 Ga suggesting formation of juvenile crust during this epoch. The age data for majority of the detrital and few magmatic zircons from the eastern Dharwar craton suggest formation of juvenile crust (ϵ_{Hf} values ranging between +1 to +4) during 3.2 to 3.6 Ga. The combined U-Pb and Hf isotope studies strengthen the view that crust formation processes in both western and eastern blocks of the Dharwar craton took place contemporaneously.

This study is a collaborative effort with B. Maibam of Manipur University and A. Gerdes of Institute of Geoscience, Goethe-University, Frankfurt.

(J. N. Goswami)

Understanding Moon and Mars through remote sensing

Aeolian morphology and processes studied for Nicholson crater on Mars

The Martian surface has evolved from geological and morphological processes including volcanism, impacts, fluvial, glacial and wind action. Presently, aeolian activity is the most active and dynamic geological processes occurring in the non-polar areas. Aeolian landforms mainly include sand dunes, wind streaks, yardangs and deflation pits which have been observed in various high resolution images.

Our study region comprises of a ~ 100 km diameter Nicholson crater (0.1°N and 164.5°W). Nicholson crater is of particular interest due to its prominent central peak and a massive central high mound of debris which rises above the crater floor by ~ 3.5 km and the horizontal extent is roughly 54 km. High Resolution Imaging Science Experiment Data (HiRISE) images having 25 cm/pixel spatial resolution and Mars Reconnaissance Orbiter CTX (context camera) data having 6m/pixel spatial resolution were used.

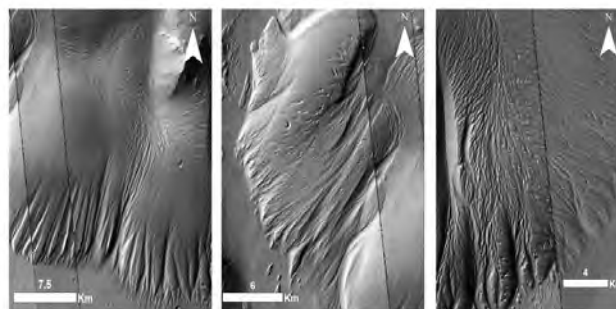


Figure 37: Different classes of yardangs (types 1, 2 and 3); arrows indicate the probable wind direction and yardang orientation.

Two prominent morphologies were observed and studied, namely yardangs and slope streaks. Yardangs, one of the most prominent formations on Mars, are the resultant erosional patterns formed due to strong unidirectional wind currents. They are commonly found in regions with strong wind supply and less or total absence of water. We observed three distinct classes of Yardangs in our study region: smooth linear yardangs, linear to curvilinear yardangs, and rough textured yardangs (Figure 37).

The study revealed that the yardangs falling in type 1 are more or less linear with a distinct NE-SW orientation, type 2 shows a combination of linear to curvilinear nature and the orientation is mainly in the NE-SW direction. The type 3 yardang represents a very rough textured classes of yardangs prominently presenting a bidirectional characteristic with a combination of all three classes. The bidirectional nature can be attributed to the gradual or a sudden change in wind speed and wind direction that played a major role in carving these features.

The region also shows presence of numerous slope streaks which are believed to be formed during the later stages of dust storm and do not require constant wind conditions over a long period of time. One unique characteristic about these features is that they fade with time due to the further settling of dust from the atmosphere and the adjoining areas or due to the gradual down slope movement of the material. Considering this aspect we characterized three types of slope streaks; recent, intermittent and old depending on their tonal variation. We could delineate around 117 streaks on the left mound portion out of which 65 are almost completely faded, suggesting they are the oldest ones, 47 are intermittent and only 5/6 represent recent or newer formed ones. From our studies we observe that these features were a reflection of the prevailing wind conditions.

(A. J. Desai and S. V. S. Murty)

Evidences of extensive glaciation in Deuteronilus Mensae, Mars

In this study, we examine the existence of multiple episodes of glacial activities on Mars from the analysis of high resolution remote sensing images acquired by Mars Reconnaissance Orbiter (MRO) Context Camera (CTX). The investigated portion of northern mid-latitude is centered at 44.6°N and 28.8°E in the Deuteronilus Mensae and lies ~200 km southerly from the largest crater (Lyot) of northern plains. We have investigated the features on the surface of regional aprons and suggested a possible process by which these formations would have resulted. The entire morphology of the surface was mapped using CTX data sets for developing a general idea about the class of landforms and their extent. The topographic characteristic of the region was derived from Mars Orbiter Laser Altimeter (MOLA) data sets to assess the down-slope flow of ice-debris mixture and the local slope-variations were also determined to interpret the flow of small-scale features. The degradational extent of craters lying on the surface of LVF flow was systematically explained to account for the presence of ice in the surface beneath the debris apron.

The flow-features on the apron surface were examined and compared with their terrestrial glacial analogues for deducing the possible reason for the variation in pattern of LVF flow. Processes resulting in similar type of glacial landforms as on Earth were widely identified and attributed to be the major cause that has led to shape the fretted terrain on Mars. From these observations, we ascertain that Mars has experienced extensive glaciation during the past, and has preserved the landforms on its surface resulting from multiple glacial activities. We have also attempted to classify the Martian glacial activity as different stages of glaciation, based on the nature of landforms observed in the study region.

(R. K. Sinha and S. V. S. Murty)

Geomorphic signatures of glacial activity in Alba Patera volcanic province: Implications for recent frost accumulation on Mars

Recent geomorphic studies have shown numerous evidences for abundant glacial and periglacial landforms in the craters lying in northern mid-latitude of Mars. A closer look at these landforms have led to the identification of two mechanisms for their formation, (1) intermittent melting of atmospherically emplaced snow/ice during past spin-axis/orbital conditions and (2) melting of debris covered ice-rich deposits on interaction with hot ejecta materials. The potential ice/snow-rich features that have been recognized in craters include thermal-contraction crack polygon, gully, arcuate ridge, and viscous flow lobe. The consistent occurrence of these ice/snow-rich features on the wall and floor of craters lying in the latitude above 45°N have suggested independent emplacement of atmospherically derived ice/snow during the past. In the craters located within < 40-45°N, the maximum presence of these ice/snow-rich features were observed on the pole-facing slope, thereby indicating that pole-facing slope was the preferred site for ice/snow accumulation. However, the lack of observation of these features in the craters lying within < 40°N, have suggested that the accumulation concentrated mainly on the pole-facing slope. In this study, we have investigated the craters lying in Alba Patera volcanic province in the latitudinal bands between 45°–32.4°N. We confirm from our observations that the past inferences derived for accumulation of ice/snow on Mars are even unswerving for craters that are lying on a volcanic terrain.

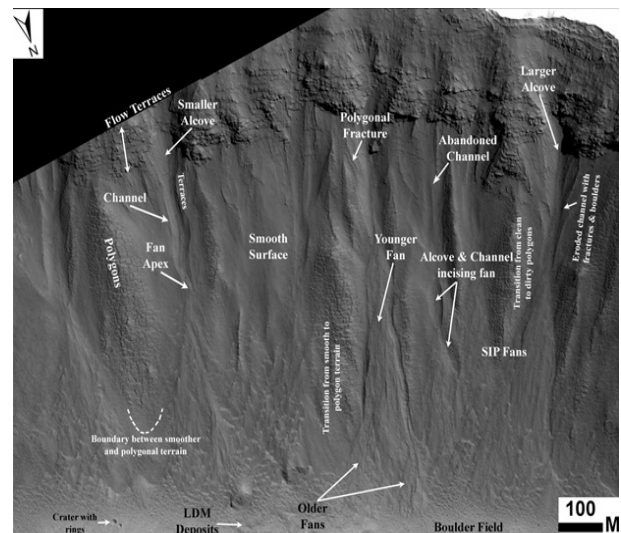


Figure 38: Gully-polygon-fan system found on the pole-facing wall of central crater (Image Id: PSP_007958.2250_RED.JP2). The ~350-400 m gullies observed here exhibit classical characteristics with the presence of alcove, channel, polygons, and fan-shaped depositions.

We have analysed morphological variations among 35 craters using datasets from past and ongoing remotely sensing missions. The formation and evolution of ice/snow-rich features were found to exhibit distinct characteristics as

inferred from our morphological comparison of craters lying between 45° - 40° N and 40° - 32.4° N. An example of the typical morphological characteristics of landforms that were commonly observed from the pole-facing wall of a crater located on the edifice of Alba Patera volcanic province is shown in Figure 38. For each of the specified craters in our study region, we have analyzed the relation between the observed features and simultaneously attempted to propose their plausible formation mechanism. Based on our morphological comparisons, we show that formation of ice/snow-rich feature was dependent on accumulated ice/snow on the pole-facing slopes as well as on the pre-existing debris-covered glacial deposits in this volcanic province. The lower latitudinal limit identified from our survey for the accumulation of ice/snow on the pole-facing wall of craters lying in the Alba Patera region is 39° N. Our results suggest that the period of ice/snow accumulation activity in Alba Patera occurred throughout Amazonian and lasted until the recent past, i.e. 2.1-0.4 Ma.

(R. K. Sinha and S. V. S. Murty)

Unique Viscous Flows found on Lowell Crater floor, Orientale Basin: Impact Melts or Young volcanic Flows?

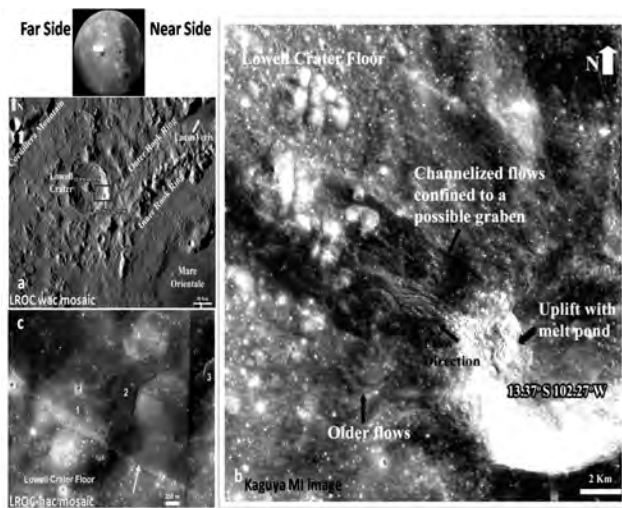


Figure 39: (a) A Wide Angle Camera image of the NW portion of the Orientale basin showing geologic context of the recently built re-surfacing; (b) A view of the flows from Kaguya MI image showing morphological details; (c) A high resolution view of a portion of the resurfacing showing flows of multiple generations

Topographic, morphological and spectral reflectance studies have been carried out for a distinct resurfacing spotted inside Copernican aged Lowell crater (12.9° S 103.1° W), Orientale basin, using high resolution MI-VIS, LROC-NAC, LOLA and M³ data from Kaguya, Lunar Reconnaissance Orbiter (LRO) and Chandrayaan-1 missions. The resurfacing is predominantly gabbroic/basaltic in composition and is confined to a nearly linear ~ 17 km long, 3-6 km wide and

~ 100 m deep channel, possibly a graben. It is characterized with distinct surface features such as small uplift with melt pond, several lava like flows, up to decimeter sized cracks, 20-80 m pits/craters with small central uplift or depression and ~ 100 m craters emanating liquid etc (Figure 39). A minimum of three generations of flows have been identified within the unit, the youngest one being less viscous and the subsequent ones showing well developed lobes due to high viscosity. There is a conspicuous absence of primary impact crater on the later flows suggesting their fresh nature. On the basis of these integrated observations, it has been hypothesized that the younger portions of this carved and resurfaced unit might be composed of magmatic flows erupted from single or multiple sources subsequent to the emplacement of impact melts from a ~ 9 km diameter crater on the edge of Lowell crater. Gabbroic/basaltic signatures have also been identified at several other locations inside Lowell crater indicating that it would have impacted on a pre-existing basaltic surface or a gabbroic pluton. These findings have implications to lunar magmatism and understanding of the genesis of young flows on lunar surface.

This work is done in collaboration with R. P. Gupta of IIT Roorkee.

(N. Srivastava and D. Kumar)

Extensive exposures of Mg-spinel anorthosite in the Orientale Basin

Mg-spinel anorthosite is a new addition to the inventory of lunar crustal lithology. Their formation and distribution on the lunar surface is not well understood. Several hypotheses such as differentiation/meltwall rock reaction in plutons or differentiation in the impact melt sheet have been proposed. Identification of exposures across the lunar surface and deciphering their geologic setting is important to test these hypotheses. In this study, Mg-spinel rich rocks without mafic silicates have been identified in the Orientale basin on the Moon using Chandrayaan-1 M³ data. The spatial distribution of these Mg-spinel dominant rocks and their associations observed in non-mare highland units of Orientale basin, particularly in the Inter Rook Ring (IRR), indicates absence of deep-seated pervasively spinel rich layer in the primordial crust. Further, the co-existence of spinel, anorthosite exposures and pyroxenes in adjoining areas at several locations of the Orientale basin suggests that Mg-spinel was present alongside pyroxene and anorthosite at a comparatively lesser depth, and were excavated during the Orientale forming impact. This scenario is likely if the spinels were produced before due to melt-wall rock reaction during ancient pre-Orientale magmatism.

This work is done in collaboration with R. P. Gupta of IIT Roorkee.

(N. Srivastava)

Microwave Remote Sensing of Lunar Surface

The use of microwave has several advantages in the planetary remote sensing and can provide the information, which may not be possible using the infrared or other wavelengths. Active microwave remote sensing has been used for the lunar surface to detect water ice present in polar regions. In case of passive microwave remote sensing, the microwave radiometers provide the thermal emission of a planetary surface, and it can be used at any time without relying on the source such as the sun. The microwave emission from the planetary object is primarily dependent upon its temperature and dielectric properties. We have recently started analysing the passive microwave data of lunar surface from Change-1 moon mission. A conditional correlation is defined for the brightness temperature with the iron content on the lunar surface and passive microwave data from Change-1 mission has been used in the analysis. This result will be used for modelling the lunar emissivity in microwave range. Also, an analysis of lunar temperature data from the DLRE instrument on LRO mission has been initiated to derive microwave emissivity model of the moon.

(J. P. Pabari)

Development of payloads for planetary exploration missions

Alpha Particle X-ray Spectrometer on-board Chandrayaan-2 Rover

The objective of the Alpha Particle X-ray Spectrometer (APXS) instrument is to analyse several soil/rock samples along the rover traverse for the major elements with characteristic X-rays in 1 to 25 keV range. The working principle of APXS involves measuring the intensity of characteristic X-rays emitted from the sample due to Alpha Particle Induced X-ray Emission (PIXE) and X-ray fluorescence (XRF) processes using suitable radioactive sources, allowing the determination of elements from Na to Br, spanning the energy range of 0.9 to 16 keV. For this experiment ^{244}Cm radioactive source has been chosen which emits both alpha particles (5.8 MeV) and X-rays (14.3 keV, 18 keV) respectively.

Presently the APXS payload is configured as a single package which is mounted under the rover chassis at a height of 180 mm from the lunar surface. Motor based shutter mechanism is also incorporated in the new design to protect the sources and the detector from the lunar dust while landing on the lunar surface. The expanded view of the APXS package is shown in Figure 40. The APXS package consists of six alpha sources mounted on the circular head and the detector at the centre. The sources are collimated such that they view about 220 mm sample diameter, and the detector viewing area is kept larger than the source viewing area. The inner side of the shutter will be coated with calibration target for on-board calibration. It also consist of stack of three PCBs accommodating Charge

Sensitive Pre-Amplifier, Shaping amplifier, Peak detector, A/D converter, HV circuit and Peltier controller circuits. The payload look alike model has been fabricated and tested for its performance, and the energy resolution has been observed to be ~ 150 eV at 5.9 keV for the pulse peaking time of 3 μs .

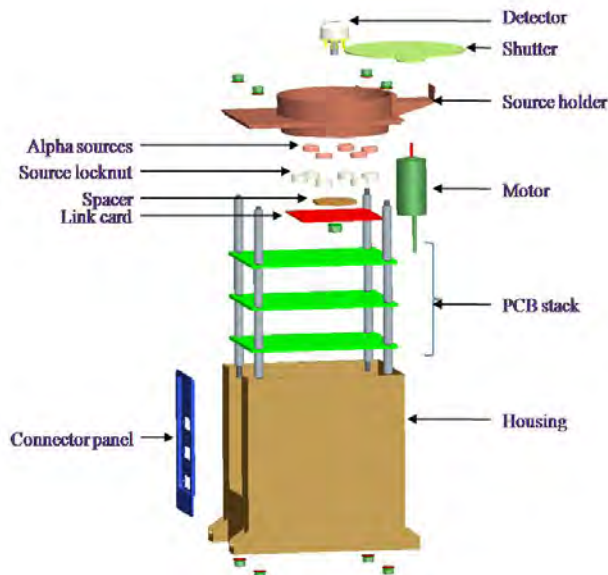


Figure 40: Expanded view of Alpha-particle X-ray spectrometer package

The Field Programmable Gate Array (FPGA) based data readout ground check out system has been developed simulating the actual data packet readout configuration as planned on-board rover. The detector performance is also tested for various temperatures and shown that the SDD based spectrometer provides energy resolution of ~ 150 eV for the detector temperatures $\leq -35^\circ\text{C}$. A PCB with flexi cable interface between the detector and the charge readout system has been designed and testing is in progress. This interface will minimize the noise level to further improve the APXS spectral performance. We plan to make a model incorporating the flexi interface and the motor based shutter mechanism. This payload setup will be tested for fluorescence measurements as planned on the rover.

(M. Shanmugam, S. K. Goyal, A. Patel, B. Shah, Y. B. Acharya and S. V. S. Murty)

Solar X-ray Monitor for Chandrayaan-2 Orbiter

Remote X-ray Fluorescence spectroscopy is a powerful technique to investigate the elemental abundances, particularly the major surface constituent elements such as Mg, Al, Si, K, Ca, Ti and Fe, in the atmosphere-less planetary bodies. A typical remote X-ray fluorescence experiment consists of two components, a Moon viewing X-ray detector to measure the fluorescent spectra and a Sun viewing X-ray detector to measure direct solar X-ray spectra. At PRL, we are involved in developing XSM payload for Chandrayaan-2 Orbiter.

The XSM instrument consists of two packages namely XSM sensor package and XSM processing electronics package. The XSM sensor package houses SDD detector module, analog with front-end electronics for charge to voltage conversion and pulse shaping, Peltier controller to maintain the stable detector temperature during the payload operation. The overall size of the XSM sensor package is about $60 \times 140 \times 40 \text{ mm}^3$ and total weight of the sensor package is about 450 gm. XSM processing electronics package consists of Field Programmable Gate Array (FPGA) based control and data readout system, DC-DC converters, power switching circuits based on tele command and driver circuits for linear motor based mechanism. The overall size of the XSM processing electronics is $130 \times 130 \times 45 \text{ mm}^3$ and the weight is $\sim 800 \text{ gm}$.

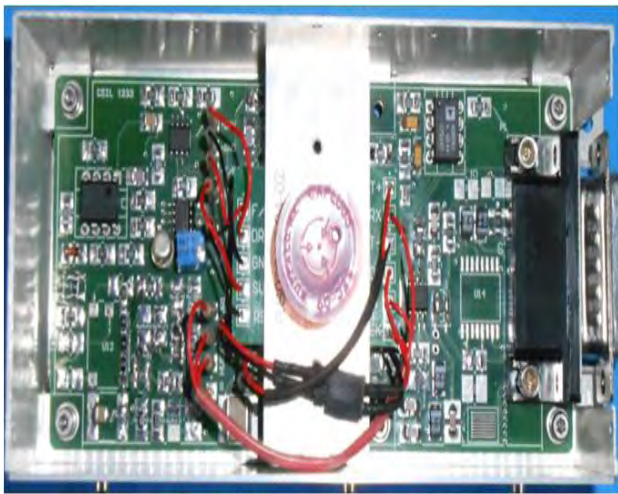


Figure 41a: Photograph of XSM sensor package including front-end-electronics subsystems



Figure 41b: Photograph of XSM processing electronics subsystem

Fabrications of both the packages are completed for making payload like model for laboratory tests and performance evaluation. The photographic views of the fabricated

packages are shown in Figures 41a and 41b. In this laboratory setup, we have achieved the energy resolution of about 170 eV at 5.9 keV for the pulse peaking time of $1 \mu\text{s}$. The performance of the experiment is being evaluated for high count rates using X-ray gun. A PCB with flexi cable interface between the detector and the charge readout system has been designed and testing is in progress to further minimize the noise level for improved spectral performance. The near future plan is to make a qualification model of the payload and subsequently the flight model.

(M. Shanmugam, S. K. Goyal, A. Patel, B. Shah, Y. B. Acharya and S. Vadawale)

Development of a LaBr_3Ce Gamma Ray Spectrometer (GRS)

An important technique for remote sensing studies of chemical composition of planetary surfaces is gamma ray spectroscopy which has been used previously to study surface composition of the Moon, Mars and Asteroids at various spatial resolutions. We are developing a LaBr_3Ce gamma ray spectrometer for a future planetary mission. A 3 inch LaBr_3Ce crystal was procured along with a 3.5 inch PMT and a preamplifier to check its suitability. We have previously checked the specifications of LaBr_3Ce crystal using a pulse shaping amplifier, and an Ortec MCA card. Further amplification was provided by a pulse shaping amplifier whose coarse gain was set to 20 and fine gain to 0.5. The pulse shaping time was initially chosen to be $2 \mu\text{s}$. Pulses with a pulse height between 0 and 10 V were recorded with a Ortec multi channel analyser.

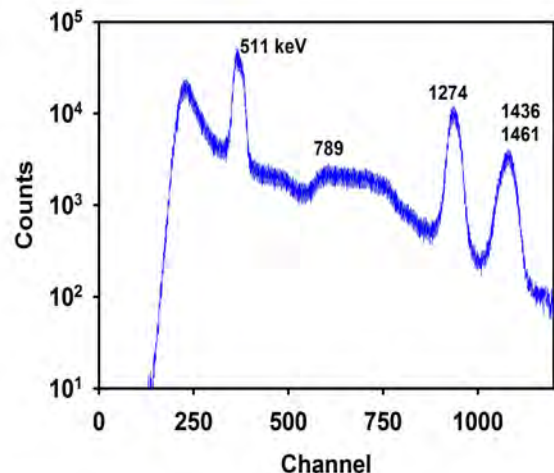


Figure 42a: Response of LaBr_3Ce gamma ray spectrometer to ^{22}Na . The photopeak at 1436 keV arises from intrinsic gamma ray emissions of contaminant ^{138}La

After testing the performance of the detector, different individual subsystems including shaping amplifier, peak detection, analog to digital conversion and high voltage

unit were developed. Once these modules were tested individually, we developed the bread board model for shaping-peak detector-ADC. The $\text{LaBr}_3:\text{Ce}$ detector requires high voltage of 720 V DC, which is being presently provided using an Aplab High Voltage unit. The bread board model of high voltage module is under progress. The shaping amplifier and peak detector were designed with hybrid components. Tests were performed using a shaping time of $3\mu\text{s}$. This unit has been set to the gain of ~ 3.5 , and is used to change and amplify the pre-amplifier output to Gaussian shaped output. We have used a parallel ADC of 12-bit resolution.

The control signal for peak detector and ADC are being generated through FPGA program. The realization of the newer version of bread board model for processing electronics has been done by using Actel A3PE250 FPGA. Along with the FPGA, the processing electronics sub-system consists of a discriminator unit for synchronization of shaping pulses with digital acquisition, a reference generator unit for ADC, line drivers for the signal compatibility of FPGA and 12-bits parallel ADC. The ADC digitized data is given to Data Acquisition Software developed in Labview. At present with the data acquisition software we are able to get the counts from the bread-board model.

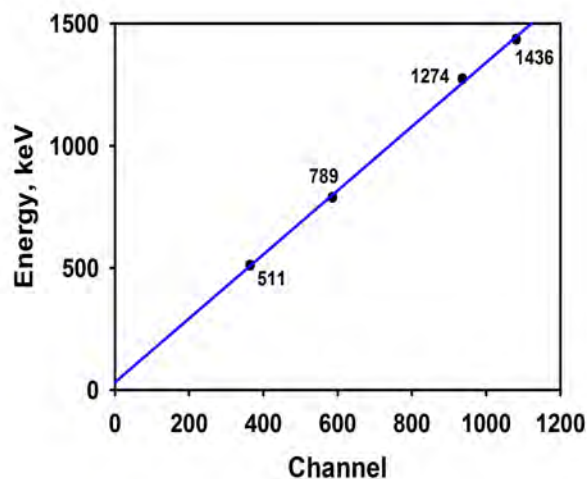


Figure 42b: Variation of gamma-ray energies with ADC channel for GRS

The performances of the shaping amplifier and the processing electronics sub-systems have been tested with the $\text{LaBr}_3:\text{Ce}$ detector. The energy resolution at 1.274 MeV was measured using a ^{22}Na radioactive source (Figure 42a) and is estimated to be $\sim 3.2\%$. The linearity of the developed GRS has been checked by plotting the variation of ADC channel with gamma ray energy (Figure 42b). An excellent linear correlation is observed between variation in channel with energy for the energy range ~ 0.2 -1.5 MeV. We are working on reduction of electronic noise to further improve the energy resolution. The design and fabrication of a 4 inch thick Pb shield has been initiated recently.

(D. K. Panda, D. Banerjee, A. Patel and S. K. Goyal)

Micro-channel Plate (MCP) detectors for PACE)

The Plasma and Current Experiment (PACE) aims to probe the Martian atmosphere. It is a plasma analyzer instrument consisting of one Electron Spectrometer (ES) and one Ion Mass Spectrometer (IMS). Each spectrometer is composed of electrostatic analyzer coupled with the end detectors as the micro-channel plate (MCP). We received three MCPs, one with single anode and two with 16 split anodes. The MCPs were packed in the dry nitrogen and therefore at initial stage were stored in the dry nitrogen environment. More recently, we have opened up packages and transferred the MCPs to vacuum chamber in order to test their vacuum compatibility.

We plan to test the electron spectrometer and therefore the power supplies have also been developed. This experiment requires about ± 2.1 kV bias supply with application rate not exceeding 100 volt/s for micro-channel plate (MCP) detectors. This supply has been developed using HV dc-dc converter module from M/s HVM and has specifications: Bias voltage: ± 2.1 kV; Load current: $14\mu\text{A}$; Ripple: 0.018% (~ 450 mVpp at rated voltage and current); Soft start time: ~ 160 sec; Input power consumption: 250 mW at rated load (Input voltage, current: 5V, 50mA). The development of other high voltage supplies is in progress, including accelerating and deflection voltage for carbon mesh and tungsten harp of time-of-flight (TOF) ion mass spectrometer (-15kV, -14kV, -12kV), and sweep voltage for electrostatic analyzer (ESA) for electrons & ions (± 5 kV).

This work is done in collaboration with A. R. Srinivas, R. Dev and D. Subramaniam from Space Application Center, Ahmedabad.

(R. Jain, Y. B. Acharya, A. B. Shah, P. Adhyaru, G. P. Ubale and V. D. Patel)

Development of an imaging polarimeter module for PRL 's 50 cm telescope

PRL's operates a 50 cm telescope at the Mt. Abu observatory. This telescope is equipped with an EMCCD based area imaging detector (field of view = $13' \times 13'$) and standard astronomical filters. The optical filters are contained in a computer controlled filter wheel. In order to study the spatial distribution of polarization in extended objects, such as comets, we have designed and constructed an imaging polarimetric module for this telescope. This module consists of a rotatable wheel with multiple positions. Operationally this is identical to the filter wheel already present in the instrument. Three of the positions are occupied by optical quality polaroid sheets with relative angular positions of the optic axis oriented at 0° , 45° and 90° respectively. Additional positions in the wheel are left empty for direct imaging in non-polarimetric mode. The wheels were commercially sourced while a new spacer had to be designed and was built at PRL to include the polaroid wheel in the optical train. A photograph of the instrument at the focus of the 50 cm telescope is shown in Figure 43. Imaging polarimetric measurements consist of imaging observations through each of the three polaroids in

sequence. Linear polarization (% polarization and position angle) is then calculated from the resulting images after standard CCD data reductions using scripts written in the IRAF software. Test observations have been taken with the setup in anticipation of bright comets expected to reach perihelion in 2013.

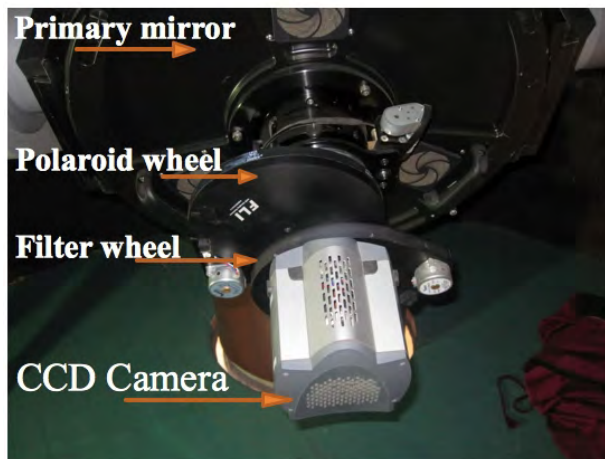


Figure 43: Photograph of the imaging polarimeter module at the focus of the 50cm telescope

(S. Ganesh and A. Kalyaan)

Development of a Novel Light Sensing Module for Planetary Exploration and Stellar Photometry

A novel and versatile light sensing device with wireless networking capability has been designed and tested for stellar and planetary photometric observations. The developed battery operated device weighing ~ 50 g is capable of measuring extremely low light intensities of the order of microlux with a wide dynamic range ($<10^{-5}$ to 10^5 lx). In order to assess the performance of the designed modules and their applicability with diverse applications, a series of experiments were carried out. These experiments include monitoring light intensities for different conditions such as daylight, twilight, moon light and night sky etc., which demonstrate the dynamic range of measurement of the designed devices. The designed

module was also employed to detect fine variations in night sky background at two stations, Ahmedabad and Mt. Abu, representing noisy (more light polluted) and clear sky (less light polluted) respectively.

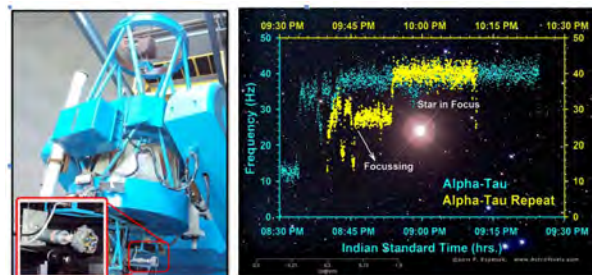


Figure 44: Observation of a star by coupling the light sensing module to Mount Abu telescope.

In order to demonstrate the sensitivity and capability of the designed module for stellar photometric observations, the designed node is coupled with 1.2 m telescope at Gurushikar, Mt. Abu, Rajasthan. The telescope is focused to collect the light from the Star. The device transmits the intensity data wirelessly to the remote coordinator which is displayed and logged by means of custom-developed software in real-time. The experimental set up and intensity measured from Alpha-tau star is shown in Figure 44. Incident flux from a star (alpha-tau) has been quantified in terms of detector frequency which gives the calibration for this type of star. Similar measurements from various known sources will provide a calibration for quantifying the light from various celestial sources which is planned with future observations. Illumination of Moon during waxing phase is also measured. A Wireless Sensor Network using these devices is further capable of spatio-temporal investigations of sky background intensities. Such a network can also be used to effectively monitor certain astronomical events (lunar eclipse, asteroid occultation etc.) simultaneously from several locations. The capability of the device, level of miniaturization and its versatility makes it a potential tool for many photometric applications.

(K. Durga Prasad, S. V. S. Murty and T.Chandrasekhar)

SCIENCE

Space, Atmospheric, Molecular and Laser Physics

Size segregated aerosol chemical composition over an urban region in India

Single particle aerosol size distribution in real time, and their chemical composition in the sub-micron and micron size ranges have been measured using an aerosol time-of-flight mass spectrometer over Ahmedabad. Aerosols sampled have been classified into major aerosol species and components. The size segregated aerosol chemical composition analysis (May 2010 is drawn as an example) shows that in the sub- and super-micron size ranges aerosol species such as dust, sea salt, elemental carbon and organic carbon are dominant and they exist as mixed in the atmosphere (Figure 45). These associations among the different aerosol species and the speciation information are impossible to obtain from bulk aerosol measurements. Aerosols, which result due to biomass burning (identified by K), are found throughout the year over Ahmedabad. Mineral dust in coarse mode increases in June. During August (monsoon) sulfate and sea salt aerosols dominate contributing >55% to total aerosol particles because of hygroscopic growth and higher relative humidity. The winter season shows higher amount of elemental and organic carbon as compared to pre-monsoon season due to increase in biomass burning and decrease in boundary layer height. The chemical speciation and the associations among different aerosol species will ultimately determine the radiative properties of aerosols. Single scattering albedo (SSA) (ratio of aerosol scattering to extinction) is higher (~0.8) when size segregated aerosol chemical composition is used (Figure 45), as compared to the SSA (~0.7) obtained assuming external mixing (no physical and/or chemical interactions among different aerosol species). This information is useful

in constraining the uncertainty in aerosol radiative effects because aerosol radiative forcing is non-linearly related to SSA.

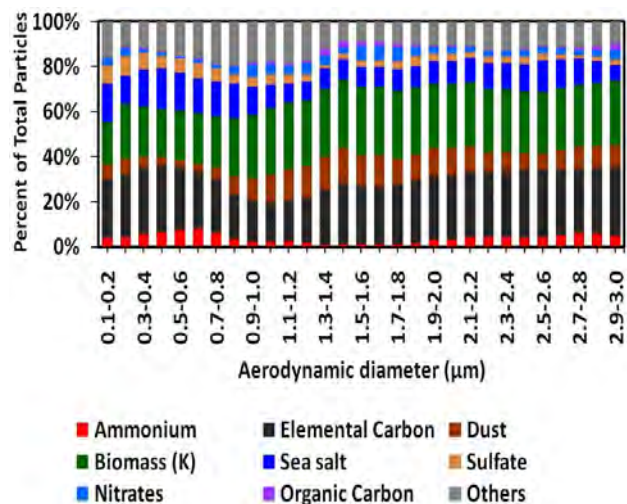


Figure 45: Size segregated aerosol chemical composition in the 0.1-3.0 μm aerodynamic size range in May 2010 measured using an aerosol time-of-flight mass spectrometer in Ahmedabad. Aerosols sampled are classified into eight major aerosol types and components. Lead and unclassified components are included in 'others'.

(S. Ramachandran and T.A. Rajesh)

Aerosol, cloud and rainfall characteristics over India

radiative effect of aerosols. Frequency distribution histogram revealed that 80% of CER in northwest India, and 30% of CER over All India in July 2002 are $<14\mu\text{m}$, which is the precipitation threshold critical CER. Northeast India shows contrasting features of correlation among aerosols, clouds and rainfall when compared to the rest of the country. These results will be important while examining the inter-annual variation in aerosols, cloud characteristics, rainfall and their trends.

This work was done in collaboration with S. Kedia, Centre for Development of Advanced Computing, Pune.

(S. Ramachandran)

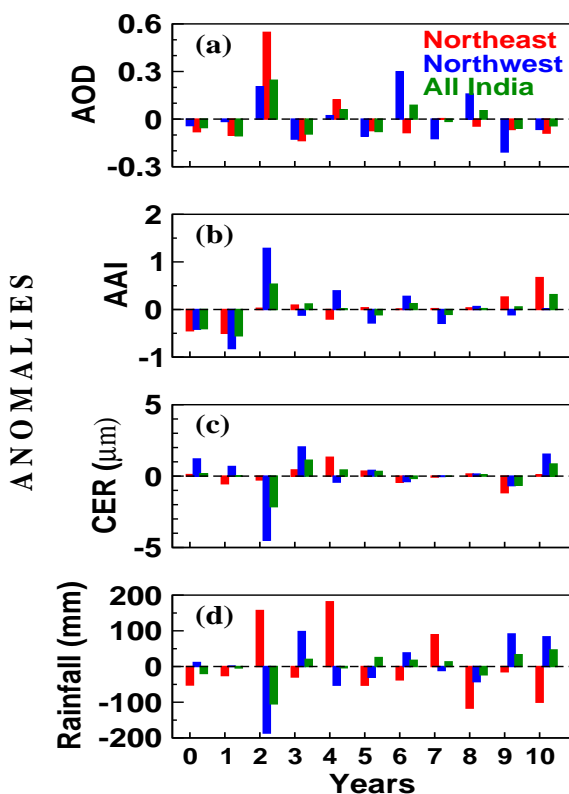


Figure 46: Anomalies in aerosol optical depth (AOD), aerosol absorbing index (AAI), cloud effective radii (CER, μm) and rainfall (mm) over the homogeneous rainfall zones of Northeast, Northwest and All India for July from year 2000 (0) to 2010 (10). The anomalies are calculated with respect to the 11-year (2000-2010) mean.

During these interruptions aerosols can build up over a region and contribute to an increase in AODs. This finding is supported by the occurrence of higher positive anomalies in AOD, AAI and negative anomaly in rainfall over India in July 2002 (Figure 46). Aerosols, cloud characteristics and rainfall exhibit large regional variations. Cloud effective radii (CER), cloud optical thickness and columnar water vapor over India are the lowest in July 2002. CER decreases as AOD and AAI increase, providing an observational evidence for the indirect

Periodicity and phase in aerosol optical depths over India

Aerosol characteristics exhibit periodic or cyclic variations depending on natural and anthropogenic sources over a region, which can get modulated by synoptic meteorological parameters such as winds, rainfall, relative humidity, and long-range transport. Information on periodicity and phase in aerosol properties assumes significance in prediction as well as to examine the radiative and climate effects of aerosols including its association with changes in cloud properties and rainfall. Periodicity in aerosol optical depth is determined using continuous wavelet transform over 35 locations (capitals of states and union territories) in India. Continuous wavelet transform is used in the study, because it is better suited than Fourier transform to extract the periodic and local modulations present at various frequencies. Monthly mean aerosol optical depths (AODs) from MODerate Resolution Imaging Spectroradiometer (MODIS) on board the Terra satellite at $1^\circ \times 1^\circ$ resolution from January 2001 to December 2012 are used. Annual and quasi-biennial oscillations (QBO) in AOD are evident in addition to the weak semi-annual (5-6 months) and quasi-triennial oscillations (~ 40 months). The semi-annual and annual oscillations are consistent with the seasonal and yearly cycle of variations in AODs. QBO type periodicity in AOD is found to be non-stationary while the annual period is stationary. The 40-month periodicity indicates the presence of long term correlations in AOD. The observed periodicities in MODIS Terra AODs are also evident in the ground-based AOD measurements made over Kanpur in the Indo-Gangetic Plain. The phase of the periodicity in AOD is stable in the mid-frequency range (corresponding to 12 month period), while local disturbances in the high-frequency range (6 month period) and long term changes in the atmospheric composition give rise to unstable phases in low-frequency range (corresponding to greater than 24 month time period). The presence of phase relation among different locations reveals that modulations in AOD over a location/region can influence aerosol characteristics over other locations/regions.

This work was done in collaboration with P. K. Panigrahi, Indian Institute of Science and Education Research, Kolkata.

(S. Ramachandran)

Retrieval of cirrus cloud properties from sun photometry

Cirrus clouds are important modulators of the Earth-atmosphere radiation budget and continue to be one of the most uncertain components in weather and climate modeling. Sun photometers are widely accepted as one of the most accurate platforms for measuring clear sky Aerosol optical Depth (AOD). However, interpretation of AOD measurements is ambiguous in the presence of cirrus clouds. Earlier work on derivation of a valid AOD under cirrus conditions was focused on correction factors, rather than on derivation of cirrus cloud optical thickness (COT). In the present work a new approach has been proposed that uses the total measured irradiance to derive cirrus COT and ice particle effective diameter (D_{eff}). For this approach, lookup tables of total transmittance for the sunphotometer field of view due to the direct and scattered irradiance over the spectral range of 400-2200 nm are generated, for a range of cirrus COT (0-4), and ice cloud effective diameters (10-120 μm) using explicit cirrus optical property models for (a) cirrus only and (b) a two-component model including cirrus clouds and aerosols. The new approach is tested on two cases (airborne and ground-based) using measured transmittances from the 14-channel NASA Ames Airborne Tracking Sunphotometer. The relative uncertainties in COT are found to be much smaller than those for D_{eff} . This study shows that for optically thin cirrus cases ($\text{COT} < 1.0$), the aerosol layer between the instrument and the cloud plays an important role, especially in derivation of D_{eff} .

This work was done in collaboration with M. Segal-Rosenheimer, NASA Ames Research Center, USA.

(S. Ramachandran)

Intrusion of stratospheric ozone over the northern Arabian Sea

Measurements of vertical distribution of ozone were made over several locations in the Arabian Sea as part of the Integrated Campaign for Aerosols, Gases and Radiation Budget (ICARB) conducted from 12 April to 9 May, 2006. A total of 16 balloon ascents were made covering almost the entire Arabian Sea. Vertical profiles of ozone, pressure, relative humidity and temperature were obtained using balloon borne ozonesondes and radiosondes. Ozone profiles during 4-7 May, in particular on 5th May (Figure 47), show enhanced values in the 8-12 km height. Higher ozone values on these days are attributed to the downward transport of ozone-rich air from the stratosphere as indicated by potential vorticity (PV) map wherein PV values > 2 units were observed. Tropospheric PV values of greater than 1.6 indicate stratospheric intrusion. These higher PV values along with back trajectories suggest that the observed ozone peaks were associated with air of stratospheric origin from higher latitudes. Results such as these have a great potential in gaining insight into the stratosphere-troposphere exchange process.

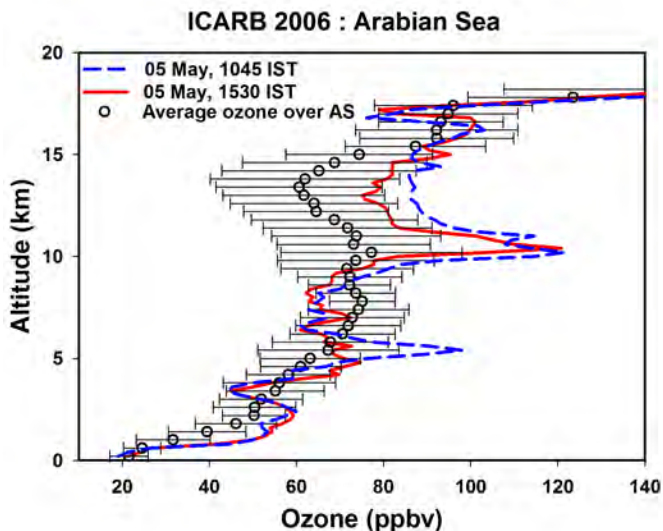


Figure 47: Vertical distribution of ozone on the 5th May 2006 (morning and afternoon) over the Arabian Sea (AS) during ICARB. Average ozone profile along with one sigma standard deviation obtained from the 16 balloon ascents over the AS is also shown.

This work was done in collaboration with scientists from ARIES, Nainital.

(S. Lal, S. Venkataramani, S. Srivastava and C. Mallik)

Variability in ozone and its precursor gases over the Bay of Bengal during post-monsoon

Trace gas measurements were conducted over the Bay of Bengal (BOB) to study the role of dynamics and chemistry in the marine atmospheric boundary layer. Continuous measurements of O_3 , CO and NO_x were supplemented by intensive, sampling based measurements of $\text{C}_2\text{-C}_5$ NMHCs, CH_4 and CO, onboard the ORV Sagar Kanya during 28 October - 17 November, 2010. The cruise track is shown in Figure 48.

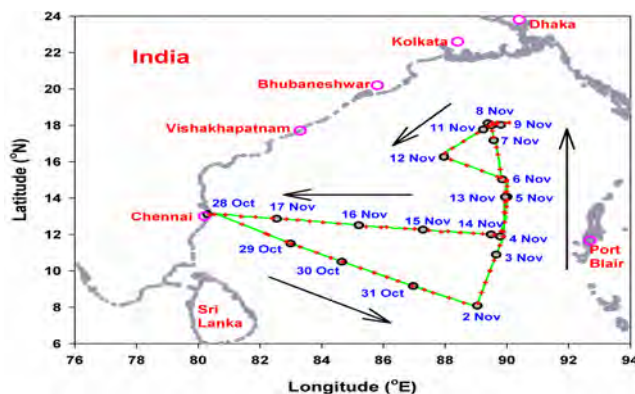


Figure 48: The cruise track of Sagar Kanya (SK-277) during 28 October - 17 November, 2010.

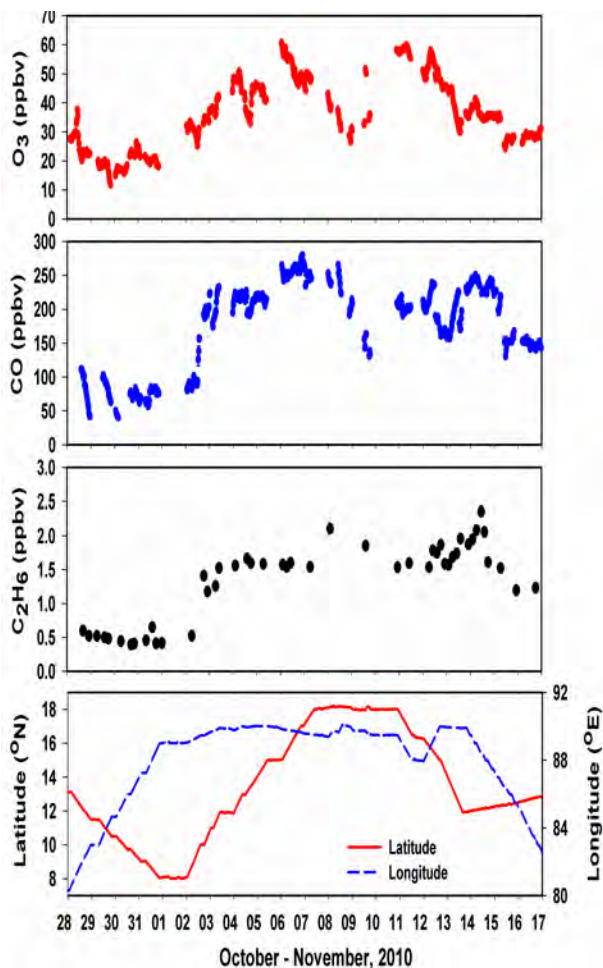


Figure 49: Variations of O_3 , CO and C_2H_6 aboard ORV Sagar Kanya during 28 October - 17 November, 2010.

A wide range of O_3 concentrations were encountered from as low as 11 ppbv in the open ocean (29 October) to over 60 ppbv in the North BoB (11 November) (Figure 49). Both O_3 and CO showed sharp latitudinal gradients (increasing towards northern BoB), which were higher than those obtained by earlier studies conducted during other periods. This is most likely due to different air mass regimes prevailing over the north and south BoB during post-monsoon. Residence time analysis showed higher levels of ozone and its precursors when the air masses spent more time over land, particularly in the northern region. Various signatures of emissions in the air masses were identified using proxies derived from inter-relationships between O_3 , CO, NO_x and NMHCs. These results indicated predominance of biofuel/biomass burning in air masses from South-East Asia, while the air masses coming from Bangladesh, India and North-West Myanmar were influenced mostly by urban/industrial sources. Variations of surface O_3 show effects of advection, entrainment and photochemistry. This was corroborated by simulations using a photochemical box model. The model is able to simulate the observed daytime O_3 reduction in pristine oceanic air masses and photochemical buildup in polluted air masses. The model simulated diurnal variations were found to be highly sensitive to background NO_2 , O_3 levels and as well as to entrainment.

This work was done in collaboration with the scientists from ARIES, Nainital.

(C. Mallik, S. Lal and S. Venkataramani)

Variability in tropospheric carbon monoxide over an urban site in Southeast Asia

MOZAIC (Measurements of Ozone aboard Airbus in-service airCrafft) data of carbon monoxide (CO) profiles over Bangkok were analyzed to investigate the seasonality in vertical distribution of CO during 2005-2006. The mixing ratios of CO were enhanced in the lower troposphere and highest in winter followed by summer and wet seasons. During all the seasons, the mixing ratio of CO decreased rapidly and remained low in the middle troposphere. At higher altitudes (6-12 km), CO shows enhanced values particularly during wet and early winter seasons. The strong seasonality in CO was caused by the shift in the patterns of the long-range transport and biomass burning in South and Southeast Asia. Flow of cleaner air and negligible biomass burning resulted in the lowest mixing ratio of CO in the wet season. In addition to anthropogenic influence, the longrange transport and biomass burning gave rise to higher CO in winter and summer seasons, respectively. Despite extensive local biomass burning activities in Thailand during the summer season, the moderate levels of CO observed were attributed to the dilution due to flow of cleaner marine air from the Indian and Pacific oceans. The observations were also compared with the Model for Ozone And Related Chemical Tracers (MOZART) simulations. Mostly the observations lie between the MOZART-2 and MOZART-4 simulations as they underestimate and overestimate the observed CO, respectively. In the middle and upper troposphere, both the observed and simulated mixing ratios of CO during September-November of 2006 were higher by 15-30 ppbv due to the impact of El Niño induced extensive biomass burning in Indonesia compared to the same period of 2005.

(L. K. Sahu and V. Sheel)

Emission characteristics of black carbon in anthropogenic and biomass burning plumes over California during ARCTAS-CARB 2008

The impact of aerosols on regional air quality and climate necessitates improved understanding of their emission and microphysical properties. The size distributions of black carbon (BC) and light scattering particles (LSP) were measured with a single particle soot photometer on board the NASA DC-8 aircraft during the ARCTAS mission 2008. Air sampling was made in the air plumes of both urban and forest fire emissions over California during the CARB (California Air Resources Board) phase of the mission. A total of eleven plumes were identified using SO_2 and CH_3CN (acetonitrile) tracers for fossil fuel combustion and biomass burning, respectively. The enhancements of BC and LSP in biomass burning plumes were significantly higher (by a factor >2) compared to those in fossil fuel plumes. Distinctly

different emission ratios of BC/CO₂, BC/CH₃CN, CH₃CN/CO, and CO/CO₂ and microphysical properties of BC and LSP were observed in the plumes from these two sources. The BC count median diameter of 115±5 nm in fossil fuel plumes was smaller compared to 141±9 nm in the biomass burning plumes. BC aerosols were thickly coated in the biomass burning plumes, the average shell/core ratios were 1.47 and 1.24 in biomass burning and fossil fuel plumes, respectively. In the total mass of sub-micron sized aerosols, organic aerosols constituted about 67% in the fossil fuel plumes and 84% in biomass burning plumes. The contribution of sulfate was also significant in the fossil fuel plumes.

This work was done in collaboration with Y. Kondo of University of Tokyo, Japan. The ARCTAS mission was supported by NASA.

(L. K. Sahu)

Detection of long-lived neutral hydrated clusters in laboratory simulation of ionospheric D region plasma

Existence of hydrated cluster ions is known through in situ measurements in the D region of the ionosphere and laboratory simulation experiments. A series of experiments were conducted at Sagami-hara, Japan with the intention of detecting some of the hydrated cluster ions, which, though predicted, had eluded detection in laboratory simulation. The other motivation was to look for heavier ions in laboratory simulations, in conditions close to those in the D region. With the availability of better ion mass spectrometers, these could supposedly be detected by rocket measurements. Results of these experiments pointed to a new aspect, namely the production of a neutral hydrated cluster molecule, which (a) has ionization potential of less than 10.2 eV, (b) has life times in excess of 90 minutes and (c) is formed within a limited pressure range. As this neutral cluster molecule has the mass number of 102, most probably it is NO·(H₂O)₄. A number of other important ions, which were detected earlier in laboratory experiments, were also seen in our data. It was also found that, like the earlier experiments, the concentration of most of the hydrated ions showed an oscillatory behavior. The ion formation was observed only within a limited pressure range, which corresponds to the 50 to 100 km altitude range of the terrestrial atmosphere.

This work was done in collaboration with K. I. Oyama of Institute of Space and Astronautical Sciences, JAXA, Japan and S. Watanabe of Faculty of Science, Hokkaido University, Hokkaido, Japan.

(H. S. S. Sinha)

Impact of low intensity solar flares on the equatorial electrojet

In order to unambiguously isolate the imprint of lesser rank X-ray solar flares in the equatorial electrojet (EEJ), 9

M-class, 3 C-class and 1 B-class flares are chosen from the years 2005, 2007 and 2010. During these flares, the enhancements in the X-ray and EUV fluxes are significantly correlated which suggest weaker EUV absorption in the solar atmosphere. These flares occurred during magnetically quiescent conditions during the deep minimum of solar cycle 23/24, when the active regions were extremely sparse, making the EUV contributions from the non-flaring active regions almost negligible. Using ground-based magnetic data with high cadence and precision, it is shown that the enhancements in the strength of the EEJ current corresponding to these flares are unambiguous when the effects of external electric fields (other than arising due to the global dynamo action driven by tidal winds) are completely avoided. However, the magnitudes of increase in the EUV flux and the strength of the EEJ current are significantly correlated irrespective of local time only if the enhancements are normalized to their respective pre-flare levels. The normalization procedure, in a way, accounts for the local time variation of the quiet time electric field (associated with the global dynamo action) embedded in the EEJ current. The flare events caused enhancements in the EEJ strength irrespective of normal or counter electrojet (CEJ) conditions, further indicating that these enhancements in the EEJ strength are due to the enhancements in the E-region ionization density.

This work was carried out in collaboration with B. M. Pathan of Indian Institute of Geomagnetism.

(D. Chakrabarty, M. S. Bagiya, S. V. Thampi, and R. Sekar)

Investigations on vertical coupling of atmospheric regions using combined multiwavelength optical dayglow, magnetic, and radio measurements

Systematic investigations of optical dayglow emissions at OI 557.7 nm, OI 630.0 nm, and OI 777.4 nm have been carried out simultaneously over a large field-of-view of 140°. A high-spectral resolution multi-wavelength imaging echelle spectrograph (MISE) was used to obtain these emission intensities during January-March in the years 2011 and 2012 from Hyderabad, (7.5°N, 78.5°E), India. Spectral analyses of all the dayglow emission intensities are performed and their association with lower atmospheric planetary wave type periodicities and direct solar forcings are investigated. This analysis revealed that periods near the atmospheric free-normal modes of 5, 10, and 16 days (that are produced mainly in the troposphere) are found to register their presence in the upper atmospheric emission intensities as shown in figure 50. In an earlier study during high solar activity (2001), sunspot numbers (SSN) and OI 630.0 nm dayglow intensities were seen to be co-varying. In contrast, the variability in the dayglow emission intensities during relatively low solar activity epoch (2011) show no or weaker correlation with that of the SSN but a greater similarity with that of the equatorial electrojet (EEJ) strength. Periodicities of both lower atmospheric normal modes and those related to sunspots are found during moderate solar activity (2012). Based on this analysis, it is inferred that the wave dynamics of upper atmosphere are influenced by the lower atmospheric forcing when the SSN<50, and by the direct solar forcing when

SSN > 60, and from both the lower and solar forcings in the intermediary epoch of SSN 50–60.

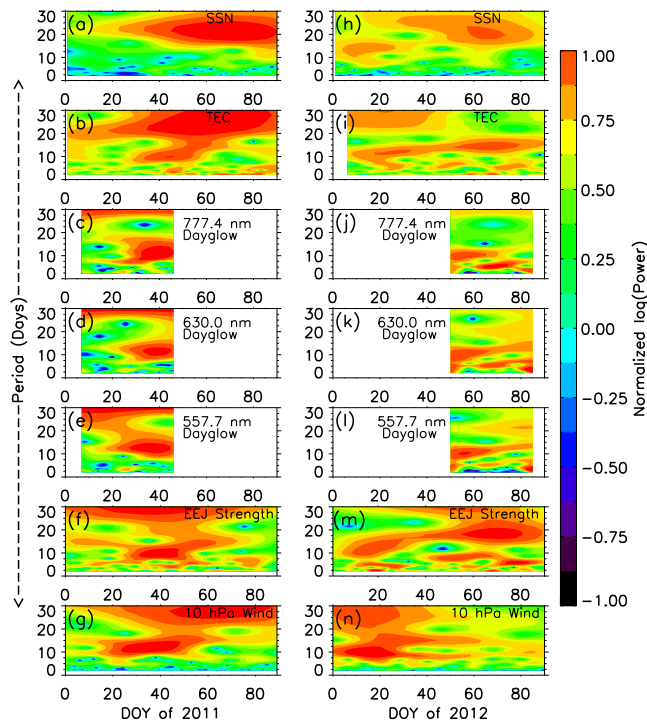


Figure 50: Wavelet spectra showing the temporal occurrence of the periods in SSN, TEC, OI 777.4, 630.0, 557.7 nm dayglow emissions, EEJ strength and zonal wind at 10 hPa level for the years 2011 (left panel) and 2012. The colour scale indicates the normalized (log) power. One can note that the 5-6, 8-11, and quasi-16 day periodicities occur in the same time duration in all the lower and upper atmospheric parameters in 2011 indicating vertical coupling from below. In 2012 5-6 and 8-10 day periodicities are present during DOYs 51-86 in all the atmospheric parameters. The concomitant occurrence of quasi-16 day period between DOY 5-35 in 10 hPa wind, EEJ, TEC, and SSN implies a possible mixed influence from both solar and lower-atmosphere on the upper atmosphere in 2012.

This work was carried out as part of PRL– Jawaharlal Nehru Technological University, Hyderabad, collaboration with T. V. Lakshmi, and B. M. Pathan of Indian Institute of Geomagnetism, Navi Mumbai, and S. Chakrabarti, University of Massachusetts, Lowell, USA.

(F. I. Laskar and D. Pallamraju)

Absence of streaming plasma waves around noontime over Thumba in recent times

Systematic ground-based magnetometer measurements from Thumba (8.47°N, 76.6°E) and Tirunelveli (8.73°N, 77.8°E) revealed a movement of the magnetic dip equator towards the south. The magnetic dip angle measured over Thumba increased by about 2° during 1985-2010. In view of the movement of the dip equator over Thumba, the dependence of the generation of streaming plasma waves on the dip angle is examined. An order of magnitude calculation using the

results obtained from the thin-shell model of the electrojet is performed. The calculation suggests that the streaming waves over Thumba during magnetically quiet periods at noontime exist when the dip angle is <1.5° and that these waves are generally absent whenever the dip angle is ≥1.5°. Evidence based on rocket measurements (Figure 51) and ground-based radar observations is provided.

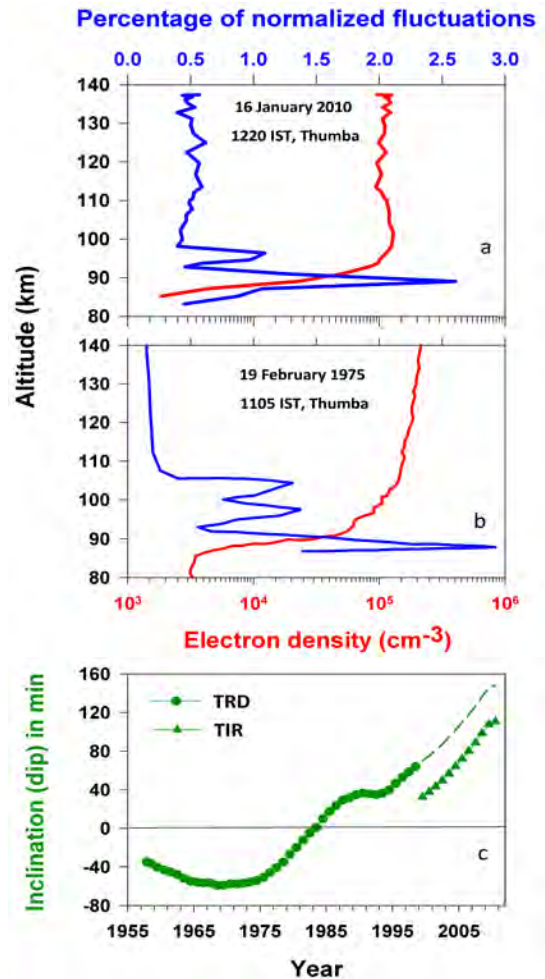


Figure 51: (Left) Altitude profiles of electron densities and percentage amplitudes of plasma waves measured over Thumba (a) on 16 January 2010 at 1220 IST and (b) on 19 February 1975 at 1105 IST as obtained by Langmuir probe measurements. Comparison of (a) and (b) plots reveals two peaks below 100 km in the normalized fluctuations in the electron densities that correspond to the presence of gradient drift waves on these two occasions. However, the absence of the third peak in the amplitudes of fluctuations at 105 km in the top plot clearly indicates the absence of the streaming waves on 16 January 2010, (C) The annual mean of the measured dip angle from Thumba (TRD) and Tirunelveli (TIR, 8.73°N) are represented by black circles and triangles, respectively. The projected dip angle over TRD after 1999 - 2010 is denoted by a dashed line.

This work was carried out in collaboration with scientists from IIG and SPL, VSSC.

(R. Sekar, S. P. Gupta, Y. B. Acharya, D. Chakrabarty, and D. Pallamraju)

On the wave dynamics in the lower thermosphere: Results from the Balloon-borne Investigations of Regional-atmospheric Dynamics (BIRD) experiment

Analysis of the data obtained from the joint INDO-US collaborative experiment on the investigations of Mesosphere Lower Thermosphere (MLT) wave dynamics using balloon-borne optical airglow emission measurements revealed an assay of neutral waves that are present in the daytime MLT region. Ultraviolet OI 297.2 dayglow nm emissions were obtained from low-magnetic latitudes. These measurements were enabled by a high spectral resolution (0.2 nm at 297.2 nm) and large field-of-view of 80° ultraviolet spectrograph which was operated from on-board a high-altitude balloon wherein emission intensities were obtained along the zonal direction. The balloon-based measurements were complemented with that of ground-based optical, radio, and magnetometer data. Ground-based OI 557.7 nm dayglow emission intensities were obtained over 140° field-of-view along the magnetic meridian. Spectral analysis on the measurements obtained from these two orthogonal directions revealed the presence of scale sizes ranging from 20–50 km in the zonal direction and around 200 km along the meridian. The resultant wave characteristics of the waves measured in these two orthogonal directions seems to be propagating in a direction away from East by about 14° towards North. In conjunction with the ground-based OI 557.7 nm dayglow emission intensity measurements where in the periodicities have been minutes, the speeds of these waves are estimated to be in the range of 10–55 ms⁻¹. Waves of such periodicities were also seen to be present over equator in the equatorial electrojet strengths on that day indicating the presence of neutral fluctuations of gravity wave origin in the equatorial electrojet. It is envisaged that waves of such scale-sizes and speeds at these heights are capable of propagating upward to the ionosphere and are potentially capable of forming the seeds for the generation of equatorial plasma irregularities.

This work was carried out in collaboration with S. Chakrabarti, University of Massachusetts, Lowell, USA, and T. K. Pant, SPL.

(D. Pallamraju, F. I. Laskar, R. P. Singh and R. Narayanan)

Response of equatorial electrojet during the super geomagnetic storm of April 2000

A major geomagnetic storm associated with coronal mass ejection occurred with sudden commencement (SC) at 1636 UT on 6 April 2000 and minimum of Sym/H index of -300 nT at 0000 UT on 7 April 2000. The event is unique with IMF Bz remaining southward from around 1630 UT till almost midnight. The event is studied in the data obtained along a chain of ground magnetometers in the Indian and Pacific longitude sectors and those that are present at other low latitude stations. The amplitude of SC in the horizontal component (H) at low latitude stations was the highest at Huancayo (around local midday) with a value of about 150 nT and about 45 nT at Tirunelveli in the Indian sector (night time). The amplitude of SC in H in the night side Indian sector

showed an increase with latitude from a value of about 45 nT near dip equator and increasing to about 85 nT near Sq focus. Counter electrojet was seen on the following day from 04 to 11 UT (maximum value of -70 nT) in the Indian sector and the ionograms at Thumba showed disappearance of Es-q at 05 UT (1130 LT) and its reappearance at 1100 UT (1630 LT). The long duration counter electrojet in the Indian sector is likely due to disturbance dynamo electric fields.

(R. G. Rastogi and H. Chandra)

Critical assessment of the forecasting capability of L-band scintillations over the magnetic equatorial region – Campaign results

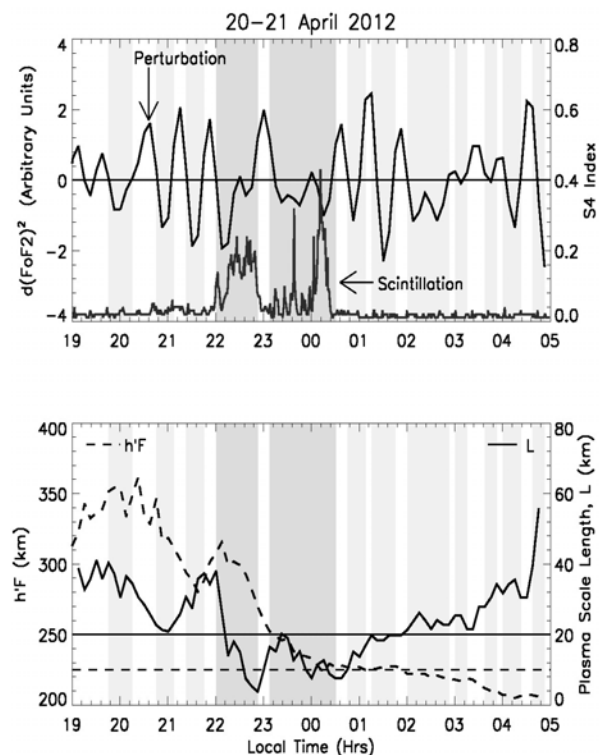


Figure 52: Forecasted density perturbations $[d(f_0F_2)^2]$ along with the actual S_4 index from GSAT observations and $h'F$ (base height) of F-region and plasma scale length L variations during 1900 to 0500 LT on 20–21 April 2012. The dark shaded regions show the time windows where scintillation forecast has been successful.

A critical assessment has been made on the forecast of L-band scintillations during a special campaign conducted from Trivandrum (8.5°N, 76.91°E, dip latitude 0.5°N) in the month of April– May 2012 using a new method suggested by us earlier. A threshold upward velocity for the evening (1730–1830 LT) F-region has been gleaned out to be 5 ms⁻¹ for the ESF to get triggered. While the zonal velocity of the perturbations has been evaluated using GSAT and GPS data, the daytime f_0F_2 data from ground-based digital ionosonde provided clues on the characteristics of the perturbation.

Maintaining the relative amplitudes and integrity of phase, the perturbations have been extended throughout the night. Invariably (>95%) the scintillation patches occurred in the predicted time windows (Figure 52), vindicating the role of perturbations in the evolution of the phenomenon and making it useful for issuing necessary alerts. The non-occurrence of scintillations has also been understood based on the changes in the background conditions.

This work was done in collaboration with S. Sunda of Airport Authority of India, L. Jose, T. K. Pant, and R. K. Chaudhary of SPL, VSSC.

(M. S. Bagiya and R. Sridharan)

Pre-assessment of the strength and latitudinal extent of L-band scintillation – a case study

Forecasting the strength of night time L-band scintillations well in advance of their actual occurrence by making use of the background conditions has been attempted over the Indian zone with an eye on generating operational forecasting capability. It has been shown that the base height of the equatorial F-region as early as 1930 LT shows a linear relation to the maximum altitudinal extent of medium scale irregularities (Figure 53a) that are responsible for the L-band scintillation during the course of the night. As these in turn get mapped to latitudes away from the equator, this indicates the latitude range that gets affected by their presence. On the other hand, the maximum strength of scintillations represented by S_4 index on a given day and location is dependent on the average value of the Vertical TEC (V_{TEC}) between 1830 and 1930 LT at that location (Figure 53b).

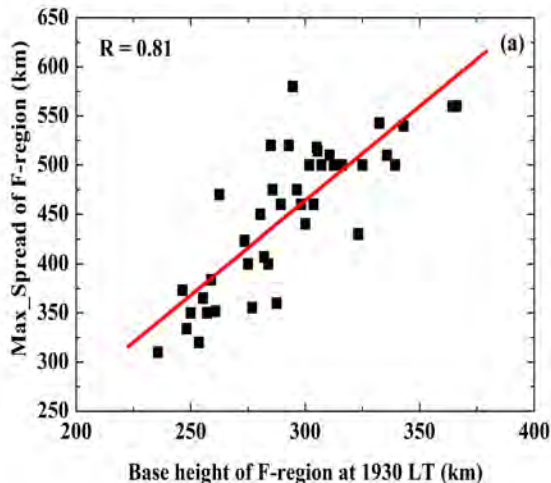


Figure 53a: The relation between the h'F at 1930 LT and the maximum reflection altitude for given h'F at 1930 LT as seen in an ionogram over the magnetic equator during the course of the night gives clues on the possible latitudinal extent that is likely to be affected by the generation of irregularities.

Although this analysis has been carried out for an equatorial station Trivandrum, it is still applicable to other latitudes as

well. Having demonstrated the control of the background ionospheric - thermospheric conditions, it has been shown that the averaged V_{TEC} around the pre-reversal enhancement (during 1830 - 1930 LT) along with the actual base height information at 1930 LT over the magnetic equator would enable one to forecast the maximum possible S_4 in a given latitudinal region as early as 1930 LT and issue necessary forewarning alerts wherever needed.

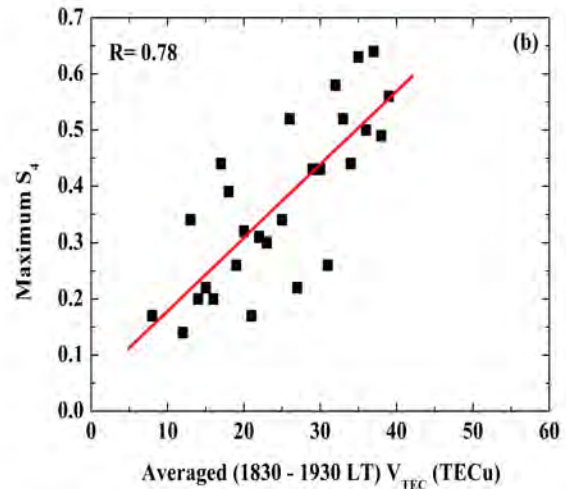


Figure 53b: The relation between the absolute maximum S_4 for a given V_{TEC} (av) (averaged between 1830 and 1930 LT on a given day) gives clues on the maximum strength of the scintillation that is likely to be observed during the course of the night.

This work was done in collaboration with S. Sunda of Airport Authority of India.

(M. S. Bagiya and R. Sridharan)

Spatial heterogeneity in the radiogenic activity of the lunar interior: Inferences from CHACE and LLRI on Chandrayaan – 1

In the past, clues on the potential radiogenic activity of the lunar interior have been obtained from the isotopic composition of noble gases like Argon. Excess Argon (40) relative to Argon (36), as compared to the composition of solar wind, is generally ascribed to the radiogenic activity of the lunar interior. Almost all the previous estimates were based on, on-the-spot measurements from the landing sites. Relative concentration of the isotopes of ^{40}Ar and ^{36}Ar along a meridian by the Chandra's Altitudinal Composition Explorer (CHACE) experiment, on the Moon Impact Probe (MIP) of India's first mission to Moon, has independently yielded clues on the possible spatial heterogeneity in the radiogenic activity of the lunar interior in addition to providing indicative antiquity of the lunar surface along the ground track over the near side of the moon. These results are shown to broadly corroborate the independent topography measurements by the Lunar Laser Ranging Instrument (LLRI)

in the main orbiter Chandrayaan-1. The unique combination of these experiments provided high spatial resolution data while indicating the possible close linkages between the lunar interior and the lunar ambience.

This work was done in collaboration with S. M. Ahmed of Hyderabad Central University, Hyderabad, T. P. Das, G. Supriya, A. Bharadwaj, of SPL, VSSC, Trivandrum and J. A. Kamalakar of LEOS, Bangalore.

(R. Sridharan)

Ionization by GCRs compared to SEPs in the lower ionosphere of Mars

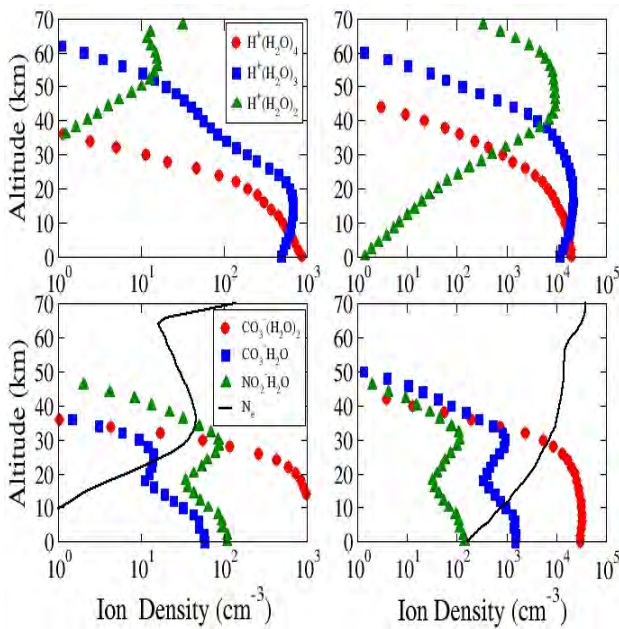


Figure 54: Density profiles of positive ions (top) and negative ions (bottom) simulated by the PRL ion-neutral model with ionisation sources as: GCRs (left) and SEPs (right).

Galactic cosmic rays (GCRs) are a major source of ionization in the lower atmosphere of Mars. Steady-state ion-neutral model of the lower atmosphere, developed in PRL, was used to simulate the density profiles of 35 ions and electrons, with GCRs as the main source of ionization. In this model, the ion-neutral chemistry consists of 12 neutral species (CO_2 , N_2 , Ar , O_2 , H_2 , CO , H_2O , O , O_3 , NO , NO_2 and HNO_3), the densities of which are derived from observations of neutral air density by the Mars Global Surveyor. Initially, the galactic cosmic rays ionise the neutral species, creating positive ions like CO_2^+ . These ions then interact through 101 reactions incorporated in the ion-neutral model, resulting in hydrated ions as the most dominant ones at lower altitudes, such as $\text{H}_3\text{O}^+(\text{H}_2\text{O})_n$, for $n = 1, 2, 3$, and 4 . Amongst the negative ions, electrons play an important role above 40 km, while below this height, water clusters like $\text{CO}_3^-(\text{H}_2\text{O})_n$ and $\text{NO}_2^-(\text{H}_2\text{O})_n$, (for $n = 1$ and 2) are dominant ions. In another

case study, the source of ionisation is taken as high energy solar energetic protons (SEPs) of 29 September 1989. Our model predicts that the major ion densities increase by an order of magnitude during SEP event (Figure 54f). Electron densities below 100 km increase from 10^2 cm^{-3} to 10^4 cm^{-3} . Such enhancements in electron densities could explain the blackouts observed in MARSIS data as the radio waves were strongly attenuated.

(V. Sheel and S. A. Haider)

Response of dust storm in the ionospheric D region of Mars

The model to estimate ion concentrations in the D region produced by absorption of galactic cosmic rays in the Martian ionosphere, has now been extended to include dust aerosols to study dust storms in Martian atmosphere. The model suggest that water cluster ions $\text{H}^+(\text{H}_2\text{O})_n$, $\text{NO}_2^-(\text{H}_2\text{O})_n$, and $\text{CO}_3^-(\text{H}_2\text{O})_n$ are most dominant. The ion concentrations and conductivity are reduced by 2 orders of magnitude in the presence of aerosols in the dust. As the atmospheric pressure on Mars is lesser than that on the Earth, galactic cosmic rays penetrate deeper into the Martian atmosphere and form the D layer at lower altitudes at 25 km, as opposed to around 60 km on Earth. The conductivity near Martian surface has been calculated to be $\sim 10^{-11}$ and $10^{-13} \text{ ohm}^{-1}\text{m}^{-1}$ in absence and presence of dust aerosols, respectively. Further, the total ion concentration (without dust) on Mars is lower than that on Earth by a factor of ~ 5 at 25 km.

(V. Sheel and S. A. Haider)

Nighttime ionosphere of Mars and its causative mechanism

Radio science experiment onboard Mars Express observed three plasma layers in the nighttime ionosphere of Mars at altitudes ~ 80 - 100 km, ~ 120 km and ~ 160 km. These layers have been reproduced by model calculations and are found to be due to impact of meteoroid, solar wind protons and electrons, respectively. The densities of 21 ions (Mg^+ , Fe^+ , Si^+ , MgO^+ , MgCO_2^+ , MgO_2^+ , MgN_2^+ , FeO^+ , FeO_2^+ , FeN_2^+ , FeCO_2^+ , SiO^+ , SiCO_2^+ , SiN_2^+ , SiO_2^+ , CO_2^+ , N_2^+ , O^+ , O_2^+ , CO^+ , and NO^+) have been computed between altitude 50 km and 200 km. The model shows that all atmospheric ions (CO_2^+ , N_2^+ , O^+ , CO^+ , O_2^+ and NO^+) are produced above 100 km due to solar wind electron and proton impact ionizations. The metallic ions are formed between 50 km and 100 km due to ablation of micrometeoroids. It is found that mass $\sim 3.0 \times 10^{-4}$ g of incoming meteoroid is sufficient for meteor ablation and its characteristic flux $\sim 4.0 \times 10^{-15} \text{ cm}^{-2}\text{s}^{-1}$ could produce the nighttime metallic layer observed by Mars Express.

This work was carried out in collaboration with B. Pandya, C. U. Shah College, Ahmedabad.

(S. A. Haider)

Martian Ionosphere during quiet and disturbed conditions

Radio occultation data obtained from Mars Global Surveyor (MGS) at high latitudes (65.3° - 65.6°N, 69.3° - 69.6°N and 74.6° - 77.5°N) were used to study the effects of X-ray flares in the E-region of Martian ionosphere in response to solar events that occurred on 29 and 31 May, 2003 and 17 January and 13 May, 2005. Modeling of flare induced solar X-ray fluxes, ion production rates and electron densities were carried out in each case using GOES measured X-ray data. The estimated electron densities are compared with the MGS observations during quiet conditions when there are no solar flares. As a sample an average of several electron density profiles obtained on one day (31 May 2003; Figure 55) is shown. It is noted that measured electron density profiles cannot be reproduced completely by the model. This is due to the fact that E and F layers are produced in the Martian ionosphere at ~ 90 – 110 km and ~130 – 140 km due to absorption of both solar X-ray and EUV radiations, respectively. In the present calculation only X-ray fluxes were used as input, which produced E-region of the Martian ionosphere. It is found that the modeled E layer peak height compares well with that of the MGS observations (during quite times). During Solar flares the peak electron densities are higher by a factor of 5–6 than the quite time modeled values.

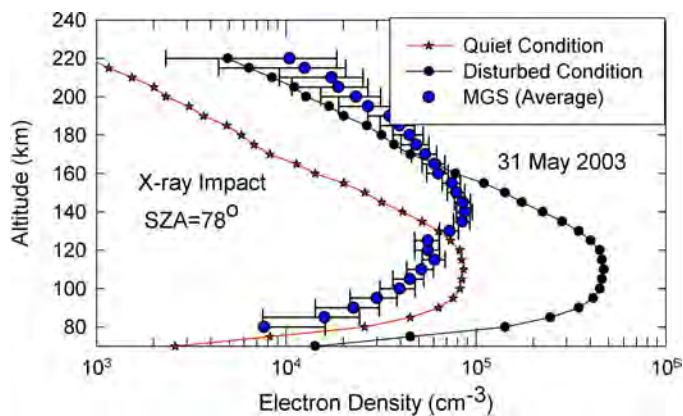


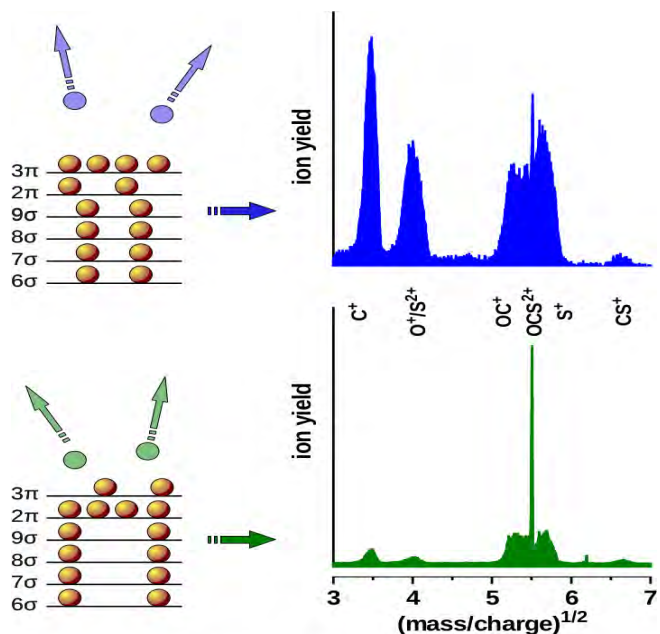
Figure 55: MGS derived electron density profiles for 31 May 2003 showing E- and F-region of Martian ionosphere. The computed electron density profile using GOES X-ray flux data as input shows a reasonable match with one day averaged electron density profile. For 31 May 2003 solar flare, computed electron density profile shows a factor of 5–6 enhancement when compared to the quiet condition. Calculations and measurements were performed at solar zenith angle (SZA) of 78°.

(S. A. Haider)

Study of shell specific ionization and non-radiative relaxation processes in molecules

Electron relaxations in molecules are much faster than vibrational and rotational relaxations. However, the coupling of the electronic perturbation to the vibrational motion is

substantially larger for inner shell ionization as compared to the valence shell ionization. Therefore, these two classes of ionization are expected to lead to different break-up pathways, which would be characterized by differences in the angular distributions of, and energy sharing between, the fragments. By performing electron-ion coincidence measurements in which electron energies are selected to capture Auger electrons, inner shell ionization can be isolated. A cylindrical mirror analyzer (CMA) for electrons was built for this purpose and was integrated with the existing recoil-ion momentum spectrometer (RIMS). Experiments were performed on sulphur bearing molecules CS₂, OCS and SF₆. Soft x-ray photons from the Indus-1 synchrotron were used to ionize the L-shells of sulphur. Photoelectron spectra of CS₂ molecules, when ionized with photons of energies below and at the L_{1,2,-3} edges of sulphur showed remarkable differences. By setting the bandpass of the CMA at different electron energies, ion momentum measurements were made. The pathways as well as kinematics during fragmentation of the molecules studied in the experiment demonstrated discernible differences in fragmentation pathways of the transient photo-ions created by inner-shell ionization vis-à-vis valence shell ionization.



When electrons from different energy levels in a molecule (OCS in this example) are ejected, the resulting fragment ion distributions exhibit a dramatic contrast.

Figure 56: Electron Spectrum with newly functional CMA.

This experiment was done in collaboration with the Indus-1 Group of RRCAT, Indore.

(K. Saha, S.B. Banerjee, P. Kumar, K.P. Subramanian and B. Bapat)

Experimental investigation and theoretical modelling of charge symmetric dissociation of doubly ionized N₂ and CO

Multiple ionization of molecules generally affects their stability and unstable molecular ions proceed to fragmentation via many channels. The channel to which a molecule will fragment is largely controlled by the excited state in which the transient ion is populated. The structures appearing in the kinetic energy release in dissociation (KERD) measured in kinematically complete measurements indicate the excited states in which the transient ions are populated. The KERD measured for the break-up of di-cations of isoelectronic molecules N₂ and CO under 2 keV electron impact showed significant differences. To understand the differences in detail, the excited states of the transient di-cations of N₂ and CO were theoretically modelled under Born-Oppenheimer approximation using MOLPRO codes at the level of cc-p5dZ basis set. The measured differences in the KERD of the two molecular ions could be satisfactorily explained on the basis of the computed potential energy curves, the state overlaps and the excitation energy function. The dissociation pathways could be identified, and contrasted in the two cases.

This work has been carried out in collaboration with K. R. Shamsundar of IISER, Mohali.

(A. Pandey and B. Bapat)

A new algorithm for calibration-free laser induced breakdown spectroscopy

A new calibration free algorithm for retrieval of elemental concentrations using Laser Induced Breakdown Spectroscopy has been proposed. This is a simple and improved version of other ratio-based algorithms as it needs only one trial parameter to estimate all other concentrations. The plasma temperature was determined using Boltzmann plot for constructed from the neutral line intensities in LIBS spectrum. From the ionic emission line present in the spectrum, the electron density of the plasma plume was determined, and ionization yields up to fourth degree ionization of the plume elements were determined. The electron densities were re-calculated applying the plasma quasi-neutrality condition, and iterations were continued till electron number densities determined by Saha equation and by plasma neutrality conditions were in agreement. Present algorithm has been used to estimate the composition of a brass sample and the results agree within 1% with Electron Probe Micro Analyzer measurements.

This work has been carried out jointly with A. Kumar and R. Singh of IPR, Gandhinagar

(P. Kumar and K. P. Subramanian)

Mass spectroscopy of clusters produced by supersonic expansion

An experimental set-up has been developed to study atomic and molecular clusters using time-of-flight mass spectrometry. The system is equipped with a two-field time-of-flight mass spectrometer and a nozzle expansion cluster source for gases. An Nd:YAG laser at two wavelengths, 1064 nm and 355nm, (peak power 10^{10} Wcm⁻²), is used to create cluster ions. Xeⁿ⁺ ($n=1-50$) clusters have been detected. The present investigation on Xenon clusters reveals the dependence of cluster ion production on the laser wavelength, gas pressure and the delay between the expansion of the gas and its interrogation by the laser. The dependence of clustering tendency, quantified by the ratio of the dimer to the monomer, and the formation of multiply charged ions on stagnation pressures has been investigated.

This work has been carried out with A. Kumar and R. K. Singh of IPR, Gandhinagar.

(A. Saxena, S. B. Banerjee, P. Kumar, K. P. Subramanian and B. Bapat)

Spatial distribution of Spontaneous Parametric Down-Converted Photons

Spontaneous parametric down-conversion (SPDC) is a non-linear process which has served as a good source of entangled photon pairs for experimental studies related to quantum physics and quantum information. In this process, a photon is split into two lower frequency photons. The distribution of down-converted photons follows energy and momentum conservation rules.

The study of spatial distribution of down-converted photons holds a very important place in quantum information processing as it helps in optimizing the experimental setup for the maximum collection of entangled photons. We have investigated spatial distribution of the down-converted photons for a Gaussian pump beam along with vortex beams. We observe that the spatial extent of these photons forming a ring increases linearly with increase in size of the pump beam. However, the SPDC of an optical vortex contains two bright rings following its classical intensity distribution, the separation between these rings increases with increase in the order of the vortex. The experimental observations have been verified with numerical calculations.

(S. Prabhakar, S. G. Reddy, A. Aadhi, A. Kumar, G. Samanta and R. P. Singh)

High-power, continuous-wave, solid-state, tunable source for the ultraviolet

Study of photon entanglement is of great importance due to their immense need in many quantum information protocols such as cryptography, teleportation and quantum computing. Spontaneous parametric down conversion (SPDC) of a high

energy pump source into a pair of low energy photons is the most direct route to generate entangled photons. Due to the highest quantum (detection) efficiency of the silicon based detectors in the visible wavelength region, the down converted photons are preferably generated in the visible wavelength range using blue or ultraviolet pump sources. However, these pump sources suffer from various limitations of the performance parameters including low power, wide spectral width, and poor spatial beam quality. Therefore, it is imperative to device alternative pump sources in the blue and ultraviolet spectral region with improved performance parameters.

We developed a high-power, continuous-wave, solid-state UV source tunable across 355.4 - 418.1 nm based on single-pass, intra-cavity second harmonic generation of green-pumped optical parametric oscillator (OPO), providing single-frequency ultraviolet output power of 770 mW and line-width of ~ 12.5 MHz at 398.2 nm. This source can be used for generation of entangled photons and their related studies

(A. Aadhi, R. P. Singh and G. K. Samanta)

Continuous-wave, two-crystal, singly-resonant optical parametric oscillator: Theory and experiment

Coherent optical sources of multiple wavelengths with wide and arbitrary tuning and high output power can be of great interest for many fields including spectroscopy, microscopy, frequency metrology, short- and long-wavelength nonlinear conversion, and THz generation. Optical parametric oscillators (OPOs), where a high energy pump photon converts into two low energy photons known as signal and idler, have long been recognized as versatile sources of widely tunable radiation in spectral regions inaccessible to lasers. However, due to the coupling of the signal and idler waves through energy conservation and phase-matching, the generation of truly arbitrary signal-idler wavelength pairs with independent tuning control is not possible using conventional OPOs.

We have demonstrated a novel OPO architecture based on two-crystal, singly-resonant OPO (T-SRO) comprising two identical nonlinear crystals in a four-mirror ring cavity and pumped with two separate pumps to generate truly arbitrary tunable dual-wavelength beams with independent control. Solving the coupled amplitude equations under undepleted pump approximation, we calculate the maximum threshold reduction, parametric gain acceptance bandwidth and closest possible attainable wavelength separation in arbitrary dual-wavelength generation and compare with the experimental results. We verified coherent energy coupling between the intra-cavity resonant signal waves resulting Raman spectral lines. Based on the T-SRO scheme, we also demonstrated a new technique to measure the temperature acceptance bandwidth of the single-pass parametric amplifier across the OPO tuning range.

This work was done in collaboration with Prof. M. E. Zadeh from the Institute of Photonic Sciences, Barcelona.

(A. Aadhi and G. K. Samanta)

Topological charge dependent propagation of optical vortices under quadratic phase transformation

We make optical vortices of different topological charge and diffract them through a quadratic phase mask using the same spatial light modulator. This phase mask shows the diffraction in which the positive diffracted order has different dynamics than the negative diffracted order. The diffraction pattern and its orientation depend on the charge of the vortex as well as its sign. The experimental results are verified with exact analytical results.

(P. Vaity and R. P. Singh)

Propagation of vortex beams through self-assembled photonic crystal

This study describes a new and simple approach to produce multiple optical vortices (OVs) using three-dimensional polymeric photonic crystal (PhC). The crystals are fabricated by well-known inward-growing self-assembly technique using polystyrene micro-particles of particle sizes 990 and 1900nm. This fabrication technique provides the cubic lattice arrangement to the spheres with the $\langle 111 \rangle$ plane parallel to the substrate. When a Gaussian beam from a He-Ne laser at 633nm is diffracted through the crystal of particle size 990nm, six bright spots along with a central spot are observed on the screen. Diffractions are observed up to third-order in the case of 1900nm particle size PhC. Multiple OVs arise when vortex beam with unit topological charge is diffracted through such a crystal. The diffraction pattern shows similar arrangement of bright spots as for the Gaussian beam except now the diffracted spots contain the property of incident OV, i.e. the central dark core. The diffraction is recorded using a charge coupling device camera.

(S. Kedia, A. Kumar and R. P. Singh)

Manifestation of coherence decay of optical vortices on scattering through photorefractive SBN crystal

We have investigated scattering of optical vortices via beam fanning as they propagate in photorefractive SBN crystal. The measurements show that the power decay of the vortex through the crystal depends on the order of the vortex. This decay for optical vortices is compared with that of the

Gaussian laser beam and it is found to be faster than the vortices. The experimental results are explained using the dependence of the two-wave mixing or beam coupling in the photorefractive materials on the degree of coherence. Furthermore, the coherence dependence of the beam fanning has been verified with partially coherent light.

(P. Vaity, A. Kumar and R. P. Singh)

Measuring the topological charge of an optical vortex by using a tilted convex lens

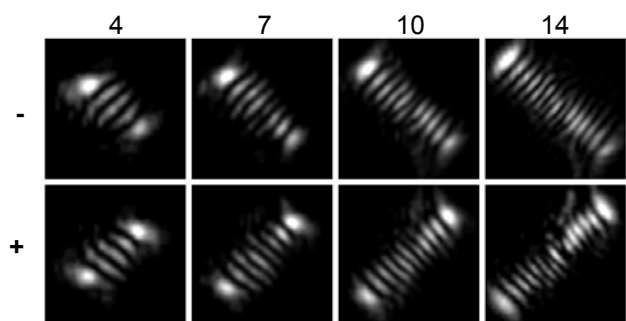


Figure 57: Observed intensity distributions at $z = 60$ cm for vortices of topological charge (from left to right) $|m| = 4, 7, 10$ and 14 respectively for both negative (top row) and positive (bottom row) charges.

We demonstrate, analytically and experimentally, a simple, but effective method to determine the topological charge of an optical vortex by using a spherical bi-convex lens, a ubiquitous optical element found in any optics laboratory. Just by tilting the lens and recording the intensity distribution of a propagating vortex at a predicted position past the lens, we have been able to measure both the sign and the magnitude of the topological charge m up to $m = \pm 14$. Our experimental results (Figure 57) are in excellent agreement with analytical predictions (Figure 58).

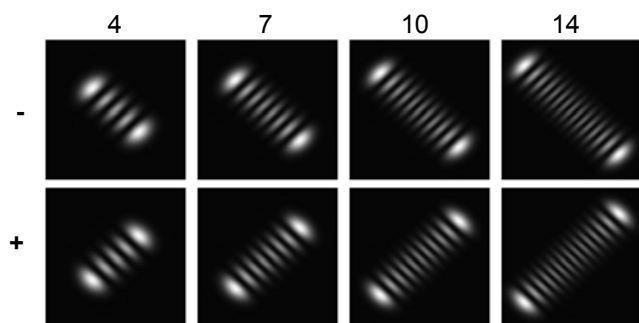


Figure 58: Theoretically predicted intensity distributions at $z = 59.6$ cm. All other details are same as in Figure 57.

(P. Vaity, J. Banerji and R. P. Singh)

Electron ionization of exotic molecular targets CN, C₂N₂, HCN, HNC and BF - Theoretical cross sections

Total ionization cross sections (Q_{ion}) of the electron impact on exotic but lesser known targets CN, C₂N₂, HCN, HNC and BF have been calculated at incident energies E_i from ionization threshold to 2 keV, by employing the Complex potential ionization contribution (CSP-ic) method. Since most of the present results are new, comparable theoretical data are obtained by Additivity Rules and by generating the BEB (Binary Encounter Bethe) values through the Quantemol-N package at the Sardar Patel University, Vallabh Vidyanagar. A good accord is found among the present and the other results, except in BF. Benchmarking of calculated ionization cross sections on HCN, HNC and BF is done by comparison with the available data on iso-electronic, i.e. 14-electron systems, N₂, CO and C₂H₂. Moreover in $e^- \rightarrow \text{HCN}$ scattering, the relative contributions of various allowed scattering channels are analyzed at the energy of the peak of ionization (70 eV) and presented in figure 59 as a bar chart. This chart serves to give a comprehensive picture of electron scattering with HCN at the peak ionization energy. The present work is relevant due to its importance in mass spectrometry and in planetary environments.

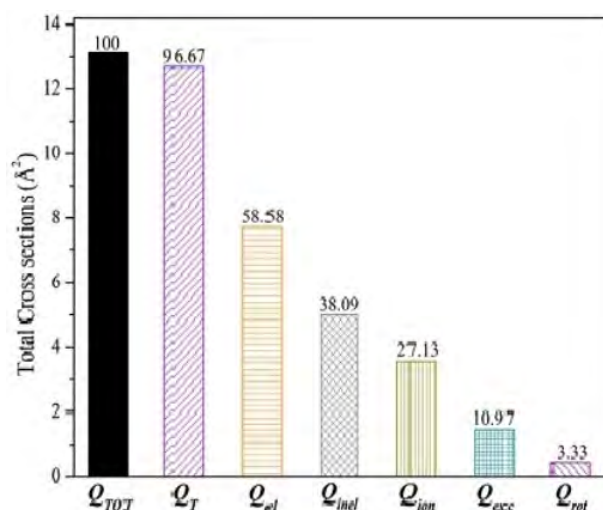


Figure 59: Percentage contributions of various scattering channels for eHCN scattering at the peak of ionization (70 eV).

This work is done in collaboration with Prof. K. N. Joshipura, Mr. S. Pandya, Ms. F. A. Shelat at Sardar Patel University, Vallabh Vidyanagar.

(B.G. Vaishnav)

Electron inelastic mean free paths in solids: A theoretical approach

Inelastic mean free path (IMFP) of electrons passing through a medium has been a subject of longstanding interest in view of its important role in the physics of surface thin films and various solids. When external electrons

interact with a bulk medium, the inelastic processes result in energy loss. Accurate scattering surface analysis by Auger electron spectroscopy and x-ray photoemission spectroscopy requires the IMFP which is also useful in determining surface sensitivity. Energetic photons of radiation interacting with solids as well as living organisms liberate secondary electrons which can induce excitations and ionization, and other interaction processes can also occur depending on the impact energy. Matter in condensed forms is also presented in various solar system objects (planets, the moon, asteroids with almost no atmosphere) and outer-space environments, and it is exposed to energetic electrons from sources like solar wind, etc. In short, the electron IMFP plays an important role in any experiment or a situation which involves motion of electrons through solids or condensed matters, and this includes as well the electron diffraction, Bremsstrahlung spectroscopy, and so on. The inelastic mean free path (IMFP) of incident electrons is calculated as a function of energy for

silicon (Si), oxides of silicon (SiO_2), SiO, and Al_2O_3 in bulk form by employing atomic/molecular inelastic cross sections derived by semi-empirical quantum mechanical method. A general agreement of the present results is found with the most of the available data. It is of great importance that we have been able to estimate the minimum IMFP which corresponds to the peak of inelastic interactions of incident electrons in each solid investigated. New results are published for SiO for which no comparison is available. The present work is important in view of the lack of experimental data on IMFP in solids.

This work is done in collaboration with Prof. K. N. Joshipura and Mr. S. Pandya at the Sardar Patel University, Vallabh Vidyanagar.

(B.G. Vaishnav)

SCIENCE

Geosciences Division

Infrared Radioluminescence studies on K-feldspar

Natural ubiquitous minerals like quartz and feldspar extracted from sediment samples have been used for the dosimetry of natural radiation environment for geochronometry. Radioluminescence (RL) in Infrared (IR) and Ultraviolet - Visible (UV-VIS) was explored as a possible tool to measure the stored palaeodose as it has

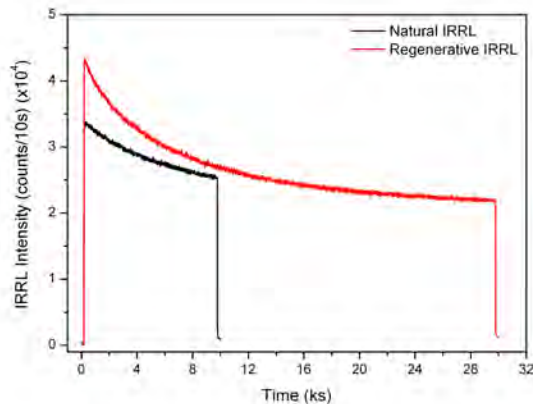


Figure 60: IRRL decay curve for naturally dosed sediment feldspar. Natural IRRL is displaced over regenerative to estimate equivalent dose in sample.

dose dependent characteristic and prospect of higher onset of saturation dose. Infrared Radioluminescence (IRRL) is

defined as luminescence in IR region, emitted by radiative trapping of electrons stimulated by irradiation (dose). As the stimulating dose increases, the probability of next successive electron for trapping at trapping centers decreases and IRRL intensity decreases with dose (time), leading to a decay curve (Figure 60). IRRL prominently observed in K-feldspar (microcline and orthoclase) having an emission peak at ~865 nm. We established IRRL system with an aim to explore its geochronological applications further. A major difficulty has been the sensitivity changes during read out cycles. We therefore examined the sensitivity change and proposed a revised protocol for the estimation of palaeodose.

Parameters like bleaching of IRRL signal, phosphorescence associated with the signal, pause for charge equilibration after irradiation and sensitivity changes in mineral as well as sediment K-feldspar were studied. Both, multiple measurements on single aliquots and multiple aliquots for single measurement were carried out. Experimental observations suggested an optimization of bleaching time to 800 s (using 395 nm UV LED of power 700mW/cm²) and that a pause for 60 min after bleaching was not required as phosphorescence decays steeply to its minimum during bleaching, (Figure 61). Further repetitive cycles of Bleach-IRRL indicated sample dependent sensitivity changes. The changes were negligible for mineral samples and significant for sediment samples. Thus, a 5 cycle of Bleach-IRRL was included in the dating protocol. Using a spline fitting for sensitivity changes, a sensitivity correction factor F_s ($IRRL_1/IRRL_0$) was calculated which when multiplied to natural signal for the estimation of palaeodose led to improved results for control samples (Figure 62).

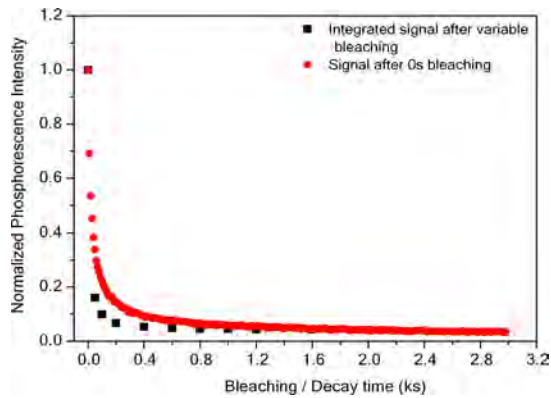


Figure 61: Phosphorescence versus bleaching/decay (measurement) time is plotted. Red points represent signal immediately after 800 Gy dose (without bleaching). Black points represent the integrated signal (0–1 ks) of phosphorescence after variable bleaching time represented by x-axis. Both the curves are normalized with respect to the initial intensity = 1.

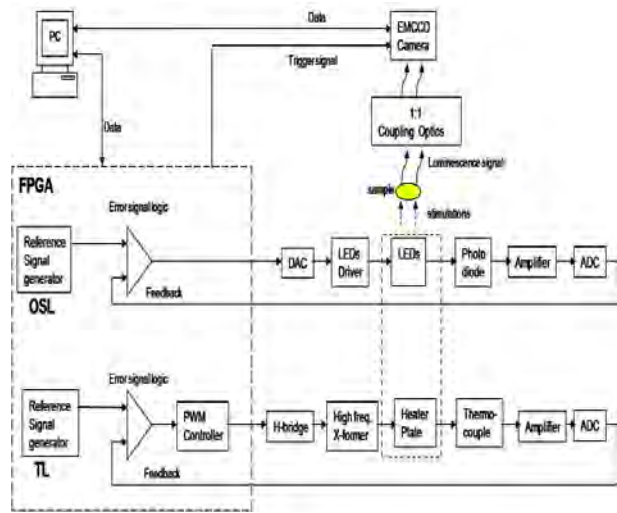


Figure 63: Block diagram of FPGA based TL-OSL system.

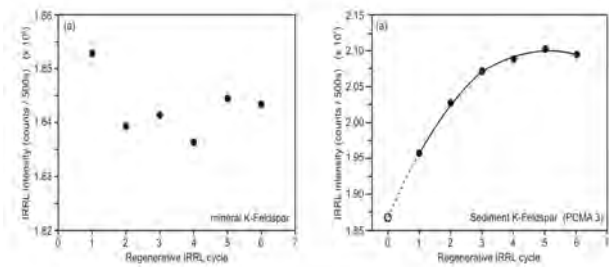


Figure 62: Regenerative IRRL intensity plotted against regenerative cycle for (a) mineral which shows no trend, while (b) sediment samples (PCMA 3) showing an increasing sensitivity which is then spline fitted to calculate F_s .

(V. Varma, R. H. Biswas and A. K. Singhvi)

Development of an FPGA based TL-OSL System with EMCCD camera for Spatial Analysis

An FPGA (Field Programmable Gate Array) based prototype system has been developed to provide programmed thermal and optical stimulation for Spatially Resolved Luminescence (SRL) dating studies. Further for a possible future development of a portable system for such studies, a compact design was achieved using a high frequency transformer for resistive heating of Kanthal strip and a thermocouple spot welded for feedback control. The light stimulation was obtained using a string of blue LEDs mounted in an aluminum holder and a photodiode as a light sensing element for feedback loop to ensure a stable/programmable illumination.

A high sensitivity back illuminated EMCCD camera (Electron Multiplying CCD camera) was interfaced to the system for detecting and resolving the luminescence signal as an X-Y array. This camera was optically coupled to the sample using a specially designed optics module such that an imaging ratio of $\sim 1:1$ could be maintained.

Analogous to any conventional control system this instrument also used a feedback mechanism for programmed heating and optical stimulation. However, its processing was done digitally to identify and apply the most suitable algorithm for higher performance and reduced hardware. A LabVIEW based software program enables the user to set the parameters like final heating temperature, heating rate and duration for Thermo-luminescence (TL) measurements and similarly the linear power ramp rate and duration for Optically-Stimulated-Luminescence (OSL). A selection of different modes of operation like step/ramp TL, step/ramp OSL and its combinations are possible. The set parameters are transferred from PC to FPGA using a RS232 protocol. The FPGA (Spartan 3A) provides the controlling signals for the thermal and optical cycling of the sample as per the parameters set in the LabVIEW program. The signal processing is done in a parallel manner at the hardware level by the FPGA which was programmed using VHDL programming language and Xilinx tools. FPGA also activates EMCCD camera at specific temperature to integrate and capture luminescence images. The acquired data is then transferred to PC via camera data acquisition system.

This system enables heating of sample up to 500°C with heating rate from 1°C/s to 10°C/s and hold time up to 3600 seconds. It also allows the intensity of light to go up to 100% (equivalent to 20mA current in LED string) at rate up to 2%/second with hold time up to 3600 seconds. The system block diagram is shown in Figure 63.

This study was done in collaboration with J. Mundupuzhakar, St. Xaviers College and B. Chakrabarty of M.S. University, Vadodara

(P. Adhyaru, N. Chauhan, H. Vaghela, Y. Acharya and A. K. Singhvi)

Chronology of coastal Red dunes in South India and contemporary paleo-environment

Red sand dunes occur in the coastal plains of Tamil Nadu in the south coast of India between 8°00' to 9°30' N; 77°18' to 79°00' E (Figure 64a). While most of the dunes in east and west coast of India are white and were deposited since middle-late Holocene (<5 ka), it is suggested that the red dune sands were deposited during earlier times. To understand their evolution chronology and contemporary environment, sections up to 12 m reaching up to the basement were excavated and samples for optically stimulated luminescence dating, geochemistry, grain size and magnetic susceptibility measurements were collected. Some of the specific questions we address to, were, i) the timing of the onset of dune accumulation, ii) radiation dosimetric aspects of dune reddening and, iii) changes in weathering index and geochemical proxies for reconstruction of environmental changes during the past.

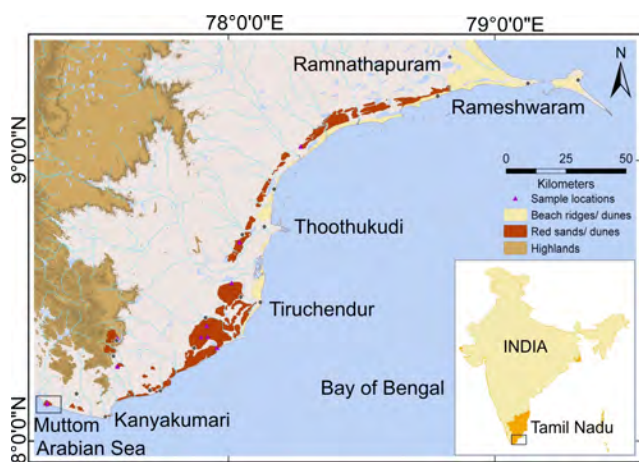


Figure 64a: Occurrence of red dunes sands and beach ridges between Ramnathapuram and Kanyakumari.

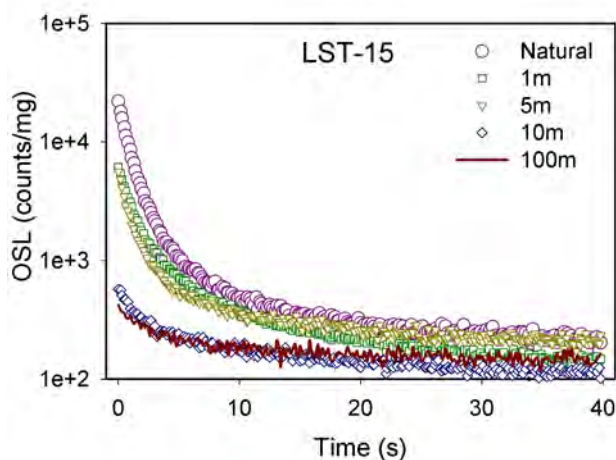


Figure 64b: Effect of day light exposure on the OSL of red sands to determine the status of bleaching prior to deposition.

Bleaching experiments to understand attenuation of light due to the red coating on the sand grains indicated that daylight exposure bleached the luminescence signals to a near background level within 10m of exposure (Figure 64b).

Dating of a 12m section comprising of partly consolidated sand at the base capped by thin (~1m) loose sand at Muttom ($N 8^{\circ}07'56''$; $E 77^{\circ}19'84''$) (Figure 64a), an elevated promontory overlooking a low lying coastal plain indicated that the sand aggradation started at ~25 ka and stopped at ~9 ka. The sand aggradation here was primarily controlled by sand availability from the on-shore source during low sea-level stands. Cessation of accumulation was associated with sea level rise by about ~9–8 ka. In the west coast, the upper part of section showed two intervals of humid climate between 17 and 14 ka, as evidenced from the units of increased clay, higher organic matter and enhanced magnetic susceptibility (Figure 65). The lower part of the section comprised finer sands with little organic matter, reduced clay content and magnetic susceptibility, indicating a drier period with reduced vegetation and absence of soil formation. Red sands at Kachanavilai ($N 8^{\circ}33'51.9''$; $E 78^{\circ}00'43.0''$) in the east coast were underlain by fluvial deposits of ~27ka residing on a lateritic bed rock. OSL ages of samples indicate that here the sands started accumulating around ~24ka.

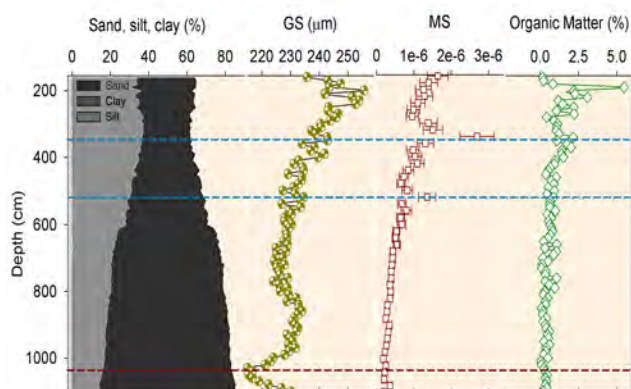


Figure 65: Down profile variation in sand-silt-clay (%), grain-size (GS), magnetic susceptibility (MS), organic matter (OM) are shown. Intervals of enhanced MS values, OM and clay content is marked with blue hatched lines.

This study was done in collaboration with Prof. P. Serlathan, Cochin University, Dr. S. Srinivasalu, Dept. of Geology, Anna University and Dr. P. Morthekai, NGRI, Hyderabad.

(L. Alappat, A. D. Shukla and A. K. Singhvi)

Al₂O₃:C blue and UV emissions

Al₂O₃ is now a well established Thermoluminescence (TL) and Optically Stimulated Luminescence (OSL) dosimeter for personnel, environmental, space and medical applications. It has two principle emissions, in blue (360 - 480 nm) and in UV (315 - 370 nm) regions due to F and F⁺ centers respectively. The present work aimed to see the effect of blue (470 nm) stimulation on TL corresponding to the main dosimetric trap (MDT) in blue (384 - 445 nm) and UV (340 - 372 nm) emission windows. On blue optical stimulation, the

TL peak temperature (T_m) shifted to higher temperature and the full width at half maximum (FWHM) increased, implying the MDT was not a single trap and comprised a distribution of traps. The low temperature part of the TL dosimetry trap peak bleached faster than the high temperature part of the TL peak, suggesting that the traps responsible for the low temperature part of the TL glow curve have higher photo-ionization cross-section for OSL. Both illumination and phototransferred TL (PTTL) experiments suggest a wide distribution of traps and increase of FWHM with T_m . Partial annealing experiment using continuous wave OSL (CW-OSL) suggests that the traps responsible for the lower temperature part of the TL peak are responsible for the fast component (higher photo-ionization cross-section). The similar behaviours are observed in both the emission windows.

This work was done in collaboration with Prof. B. C. Bhatt of BARC.

(R. H. Biswas and A. K. Singhvi)

Band-tail states in anomalous fading of feldspars

Infra-red stimulated luminescence (IRSL) of feldspar is a potential signal to extend the datable range of luminescence dating. However, IRSL suffers from anomalous (athermal) fading over geological timescales which hinders the dating of older samples. The presence and the participation of band-tail states in IRSL production mechanism in feldspar were recently reported. We examined the role of band-tail states in anomalous fading. Towards this several feldspars of diverse origin, museum feldspars (orthoclase, albite and plagioclase), sediment K-feldspar and volcanic feldspar, were examined. The band-tail depth of each feldspar type was measured using the temperature dependence of IRSL intensity. The stimulation temperature-dependent IRSL intensity exhibited super-Arrhenius kinetics and was analyzed using quadratic plot (inset of the Figure 66) to derive the temperature dependent thermal activation energy (E_{th}).

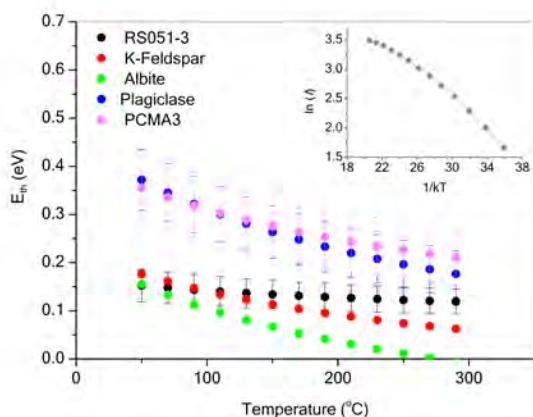


Figure 66: Temperature dependency of thermal activation energy. The inset of figure 66 shows super-Arrhenius plot ($\ln I$ vs. $1/kT$) of IRSL signals of one feldspar sample.

The temperature dependency of E_{th} of different samples was different (Figure 66), and for a particular temperature E_{th} of the post infrared IRSL (pIR-IRSL) signal was 3-4 times higher than the IRSL signal. The anomalous fading rate (g-value in %/decade) of the IRSL signal of different samples ranged between 4-11 %/decade. The anomalous fading rate was correlated with the degrees of temperature dependency of E_{th} . The observation of temperature dependency of E_{th} , being higher E_{th} for the pIR-IRSL signal than IRSL signal for a fixed temperature, and the correlation between anomalous fading rate and temperature dependency of E_{th} suggests that the IRSL mechanism depends not only thermally assisted movement towards conduction band, rather it also depends on diffusion in the lattice for recombination.

This work was done with Dr. P. Morthekai of NGRI Hyderabad.

(R. H. Biswas and A. K. Singhvi)

PM_{2.5}, EC, OC and aerosol organic mass-to-organic carbon ratio in atmospheric outflow from the Indo-Gangetic Plain

Temporal variability in the mass concentrations of PM_{2.5}, mineral dust, OC, EC, water-soluble organic carbon (WSOC) and inorganic species (WSIS) has been studied in the atmospheric outflow from a downwind site [Kharagpur: 22.02°N, 87.11°E] in the Indo-Gangetic Plain. Based on diagnostic ratios of carbonaceous species [OC/EC \approx 7.0 \pm 2.2, WSOC/OC \approx 0.6 and K⁺/EC \approx 0.48 \pm 0.17], we document the impact of biomass burning emissions (wood-fuel and post-harvest agricultural-waste burning) from source regions in the Indo-Gangetic Plain. The high abundance of sulphate (SO₄²⁻ \approx 6.9 – 25.3 μ g m⁻³; SO₄²⁻/ Σ WSIS = 45-77 %) and characteristic ratios of nss-SO₄²⁻/EC (3.9 \pm 2.1) and nss-SO₄²⁻/OC (0.61 \pm 0.46) provide useful information on absorption/scattering properties of aerosols. Based on the quantitative assessment of individual components of PM_{2.5}, we document aerosol organic mass-to-organic carbon (OM/OC) ratio centring at 1.5 \pm 0.2 in the atmospheric outflow from the Indo-Gangetic Plain. The aerosol composition from the downwind oceanic region (Bay of Bengal) shows striking similarity with diagnostic ratios documented for the atmospheric outflow from the Indo-Gangetic Plain. Relatively high OM/OC ratio (2.0 \pm 0.8) over the Bay of Bengal is attributed to oxidation of organic aerosols during long-range transport.

(B. Srinivas and M. M. Sarin)

Characterization and emission budget of carbonaceous aerosols from agricultural-residue burning emissions

Characterization and emission budget of carbonaceous aerosols from two distinct post-harvest agricultural-residue (paddy- and wheat-residue) burning emissions from a sampling site (Patiala: 30.2°N, 76.3°E; 250 m amsl) in the

Indo-Gangetic Plain (Northern India) are reported here. The $PM_{2.5}$ mass concentration varies from 60–390 $\mu\text{g m}^{-3}$ during paddy-residue burning (October–November) with dominant contribution from organic carbon (OC \approx 33%); whereas contribution from elemental carbon (EC) centers at \sim 4%. Water-soluble organic carbon (WSOC) accounts for about 50% of OC. The mass concentration of $PM_{2.5}$ is relatively low during the period of wheat-residue burning (April–May), varying from 18–123 $\mu\text{g m}^{-3}$ with higher contribution of EC (7%) and lower OC (26%). The diagnostic ratios of OC/EC (11 ± 2), WSOC/OC (0.52 ± 0.02), nss-K⁺/OC (0.06 ± 0.00) and Σ PAHs/EC (4.3 ± 0.7 mg/g) from paddy-residue burning emission are significantly different than those from wheat-residue burning emission (OC/EC: 3.0 ± 0.4 ; WSOC/OC: 0.60 ± 0.03 ; nss-K⁺/OC: 0.14 ± 0.01 and Σ PAHs/EC: 1.3 ± 0.2 mg/g). The emission budget of OC, EC and PAHs from post-harvest agricultural-waste burning in the Indo-Gangetic Plain are estimated to be 580 ± 120 Gg/y, 80 ± 11 Gg/y and 180 ± 18 Mg/y, respectively. Emissions from crop-residue burning in Northern India contribute significantly (50% of OC and 30% of EC) to the global emission scenario for agricultural-waste burning

(P. Rajput and M. M. Sarin)

Contribution of atmospheric nitrogen deposition to new production in the nitrogen limited photic zone of the northern Indian Ocean

Primary productivity in the sunlit surface layers of tropical oceans is mostly limited by the supply of reactive nitrogen (N_r) through upwelling, N_2 fixation by diazotrophs, riverine flux and atmospheric deposition. The relative importance of these processes varies from region to region. Using recent data on the nitrogen content of aerosols over the ocean and marine new production in parts of the northern Indian Ocean for the period 1994–2006 CE, a quantitative assessment of the contribution of atmospheric deposition to new production in the two biogeochemically different basins of the northern Indian Ocean, viz., the Arabian Sea and the Bay of Bengal, is presented. By suitably converting the measured concentrations of aerosol nitrogen into fluxes and comparing them with ^{15}N tracer-based direct new and primary production measurements, it is inferred that the contribution of atmospheric deposition to new production in the northern Indian Ocean could at best be \sim 3%. Our estimate of \sim 1.39 Tg N year⁻¹ of N_r flux into the northern Indian Ocean through aerosols is a step toward significantly reducing the uncertainty in the global nitrogen budget.

(N. Gandhi, R. Ramesh and A. Singh)

Zonal variability in primary production and nitrogen uptake rates in the southwestern Indian Ocean and the Southern Ocean

Hydrographic parameters along with the primary and new production measurements were carried out during the austral summer, 2009, in the southwestern Indian Ocean and Indian sector of the Southern Ocean (SO). The production varies

from 185 to 4900 $\text{mgCm}^{-2}\text{d}^{-1}$ in different zones of SO. The zonal variations in production accompany variations in SST, salinity and nutrients. Further, the new production (0.3 to 4.1 $\text{mmol Nm}^{-2} \text{d}^{-1}$) covaries with the overall production, while the uptake of reduced forms of nitrogen (both NH_4 and urea) show opposite trends. In the NO_3 limiting environment (north of subtropical convergence), NH_4 uptake dominates the total regenerated production, whereas, urea uptake dominates the regenerated production under Si, light and micronutrient (e.g., Fe) limiting conditions (found between the subtropical convergence and Antarctica). On the basis of the C and N uptake data, the studied region can be divided into five zones (from the south to the north) viz., located between (i) the Antarctic continent and the polar front (Antarctic zone; ANZ), (ii) the polar and subantarctic fronts (SAF) (Polar frontal zone; PFZ), (iii) SAF and Agulhas Retroreflection fronts (ARF) (South Subtropical front; SSTF), (iv) subtropical frontal zone (STFZ), and (v) ARF and the north subtropical front (Subtropical zone; STZ). Except at SSTF, regenerated production dominates in all the zones. From the south to the north, this could be due to different reasons e.g., light, grazing by zooplankton, supply of key micronutrients (probably Fe), Si-limitation, or NO_3 -limitation. In the absence of such limitations, the maximum possible f-ratio in SO could be as high as 0.78 ± 0.12 and under such conditions the region could export most of the total production to the deep. Supply of micronutrients through the Agulhas return current and from the Crozet Island supports the higher Chl a, C uptake and new production at the 48°E transect relative to the 57.5°E transect. The C:N assimilation ratio is found to be 5.64, marginally lower than the canonical Redfield ratio. This slight difference is likely due to the variation in the composition of phytoplankton and NO_3 -limitation in some zones. A comparison with earlier results shows that seasonal and spatial variations in f-ratios in these zones are much higher than its inter-annual variability.

This work was done in collaboration with NCAOR, Goa.

(N. Gandhi, A. H. Laskar and R. Ramesh)

Changes in litter decomposition and soil organic carbon in a reforested tropical deciduous cover (India).

Soil organic carbon (SOC) up to 1 m depth originates from contemporary vegetation cover dating from past millennia. Deforestation and reforestation with economically important species is influencing soil carbon sequestration. An attempt has been made in this study to evaluate the impact of vegetation cover change (due to replacement of natural heterogeneous cover by teak and bamboo) on SOC using carbon isotopes ($\delta^{13}\text{C}$, ^{14}C) in a tropical system (India). A litter decomposition study was carried out to understand the impact of differences in vegetation characteristics (specifically of leaves) on decomposition. Both experiments were carried out to look at the impact of changes in vegetation characteristics (specifically of leaves) on litter decomposition, and how these influence near term litter decomposition rates (k values) and long-term SOC content of the soil system beneath. Leaves of teak, bamboo and eight other species were selected for this study. The proportion of structural carbohydrates (lignin and

cellulose) in leaves significantly % (at 5% level) influenced k values. The SOC and carbon isotope data collected in this study indicate that C vegetation cover in the study area could be contemporary and dominant for the past few centuries. This can be extended up to 2,200 years from the recorded ^{14}C values of teak cover. The study confirms that k values of leaf litter influence SOC present beneath the vegetation cover at the decadal/century time scale.

This work was done in collaboration with M.S. University of Baroda, Vadodara.

(A. H. Laskar, R. Ramesh and M. G. Yadava)

Internal cycling of dissolved barium in water column of the Bay of Bengal.

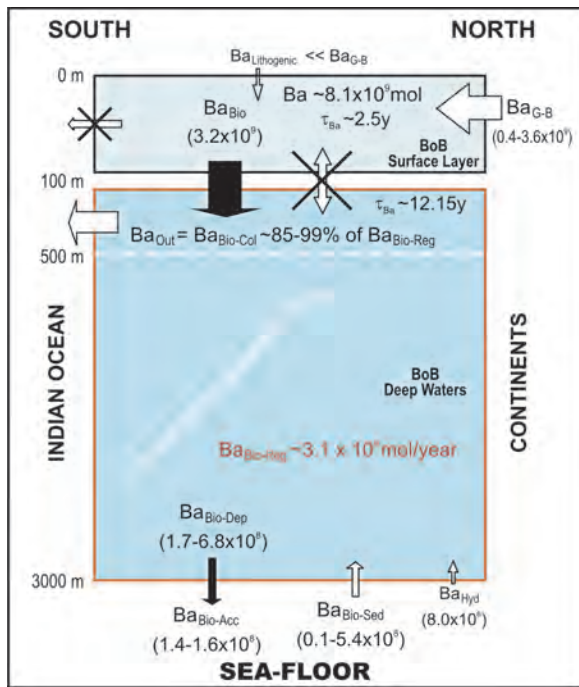


Figure 67: Two box model of the Bay of Bengal explaining dissolved Ba distribution.

Dissolved barium concentrations in water column of the Bay of Bengal along the 87°E transect (~6°N to ~21°N) have been measured to track the dispersion of its large influx from the Ganga–Brahmaputra river system and the outflow to the equatorial Indian Ocean. A typical barium concentration depth profile shows relatively higher Ba concentration in surface waters (depth ≤5 m) followed by a minimum in the depth interval ~50–150 m, which further increase with depth. The barium concentrations in surface waters (depth ≤5 m) of the Bay of Bengal vary from ~34.9 nmol/kg at the southernmost station 0806 to ~112.8 nmol/kg close to mouth of the Hooghly estuary (station 0816). The Ba data in upper layers (depth ≤100 m), excluding the very high Ba at station 0816, generally show a strong and significant inverse correlation with salinity ($R^2 = 0.75$; $P < 0.0001$). This indicates the southward flow of dissolved Ba from the GB river system that also includes its

contributions by particle release and SGD. The subsurface Ba minimum found in this study is ubiquitous and most probably is a result of Ba uptake on settling particulates. On the other hand, the Ba concentrations in deep waters (depth ≥500 m) is controlled dominantly by water mixing as suggested by a very strong and significant inverse correlation with salinity ($R^2 > 0.95$; $P < 0.0001$). Exceptions to this conservative behavior are the "hot-spots" of dissolved Ba in bottom waters, which are probably resulted by the dissolution of sediments at and/or below the sedimentwater interface.

Attempts were made to budget the Ba abundance in the Bay of Bengal using a two box model approach (Figure 67), surface (top ~100 m) and deep water (below ~100 m). Under the steady state the annual Ba influx from the Ganga–Brahmaputra river system seems to be balanced through its removal via sinking particulates as a result there is no lateral outflow of dissolved Ba from the GB to the equatorial Indian Ocean through top ~100 m of the BoB. Most of this sinking particulate Ba (~95%) is regenerated again in the lower box, preferentially in the intermediate waters ~100–500 m. Therefore, frequently ventilated intermediate waters of the Bay of Bengal, receiving a large input of dissolved Ba through particle remineralization can be a significant source of dissolved Ba to the Indian Ocean.

(S. P. Singh, S. K. Singh and R. Bhushan)

Impact of various water masses and dust deposition on Nd concentration and isotopic composition of the waters of the Arabian Sea

The concentration and isotopic composition (ϵ_{ND}) of dissolved Nd in the water column of the Arabian Sea along with inverse model calculation indicate a negligible riverine contribution to the Arabian Sea surface waters and reaffirms the supply of surface waters from the Bay of Bengal to the Arabian Sea during winter monsoon. The contribution of North Indian Intermediate Water (NIIW) is significant north of 10°N, while the existence of North Indian Deep Water (NIDW) is significant south of 8°N in the Arabian Sea.

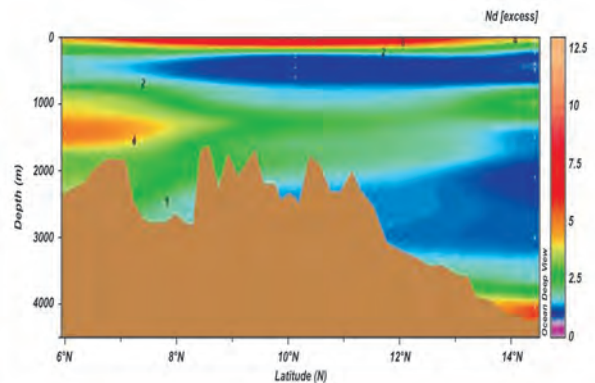


Figure 68: Excess Nd in the surface water of the Arabian Sea is derived from dust.

The North Atlantic Deep Water (NADW) and Antarctic Bottom Water (AABW) both show a north-south transport in the Arabian Sea. The presence of Chagos-Laccadive ridge significantly reduces the flow of deeper water masses from the Arabian Sea to the Bay of Bengal. This study highlights the significant dust deposition over the Arabian Sea resulting in considerable amount of dissolved Nd in its surface water (Figure 68). The dust deposition flux over this oceanic basin is estimated to be $8 \pm 2 \text{ g m}^{-2} \text{ y}^{-1}$ contributing ~ 40 million gram Nd annually to the Arabian Sea, about two order magnitudes higher compared to its riverine supply.

(V. Goswami, S. K. Singh and R. Bhushan)

Molybdenum isotope composition in Narmada and Tapi estuaries

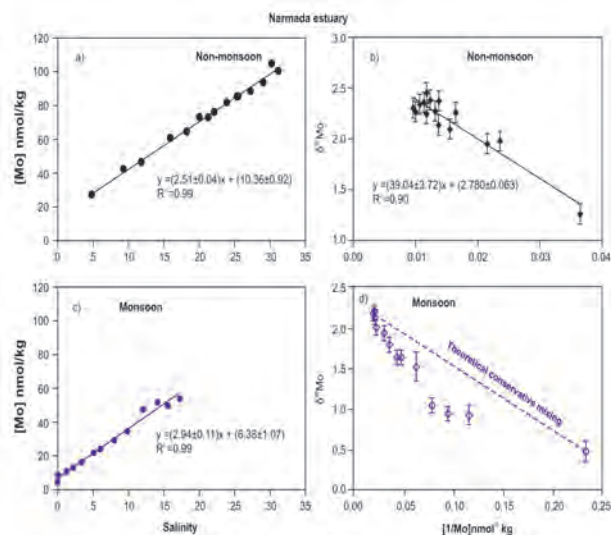


Figure 69: Mo isotope displays non-conservative behaviour in the Narmada Estuary indicating supply of lighter Mo either from particulates or from submarine groundwater discharge.

Temporal variation in Molybdenum (Mo) isotope composition of seawater is being used as an important proxy to determine the spatial extent of paleo-redox condition of oceans. The quantitative interpretation of Mo isotope records in terms of redox conditions of ancient oceans is critically dependent on inputs of Mo and its isotope composition to the oceans through rivers which are poorly constrained. This study tries to characterize the riverine Mo isotope composition and its behaviour in rivers and estuaries. Towards this, Chemical extraction and measurement technique of Mo isotope composition using double spike and MC-ICP-MS have been successfully established in our laboratory. Dissolved Mo isotope compositions have been studied in the Narmada and the Tapi rivers and estuaries from the Arabian Sea. $\delta^{98}\text{Mo}$ of dissolved Mo of these rivers display higher values

compared to that of the basalt, the major lithology of these rivers indicating adsorption of lighter Mo on Fe, Mn oxy-hydroxide during riverine transport. On the other hand, in the Narmada estuary, lighter Mo being contributed either by particle desorption or from submarine groundwater discharge (Figure 69). In the Tapi estuary, lighter Mo is being supplied by anthropogenic activities such as steel industry situated nearby. This study underscores the need to characterize the Mo isotope composition of global rivers and estuaries before using it as a proxy of paleo-redox condition.

This study was done in collaboration with Dr. Waliur Rahaman, NCAOR, Goa.

(S. K. Singh and V. K. Rai)

GEOTRACES intercalibration of neodymium isotopes and rare earth element concentrations in seawater: reproducibility of results for the international intercomparison

As a part of International GEOTRACES programme, we participated in the intercalibration of Nd isotope composition of the seawater. During the GEOTRACES intercalibration cruise, conducted in the Atlantic ocean, two samples one each from surface and deep water were collected from Barmuda Time Series station and distributed to 15 laboratories over the globe. We received 10 l of each sample.

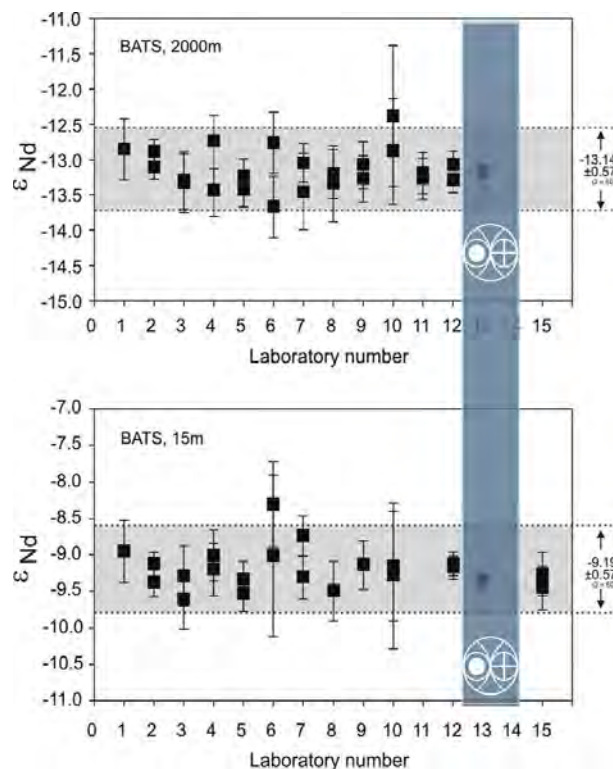


Figure 70: Intercalibration of Nd isotope measurement. Values obtained by PRL is indicated with PRL emblem

Nd was extracted from these waters and measured in our laboratory and results were reported to the scientist incharge

for intercalibration. The results reported from PRL (Figure 70) are among the best values reported from all laboratories indicating our high quality measurement capability of Nd isotopes in dissolved phase.

(V. Goswami and S. K. Singh)

Diurnal Characteristics PM_{2.5} over the Indo-Gangetic Plain during Biomass Burning Emissions: Evidences of Secondary Aerosol Formation

Emissions from large-scale biomass burning with winter type meteorological condition is thought to be the major cause of wintertime haze/fog over the Indo-Gangetic Plain (IGP); however, the understanding on corresponding particulate composition is meager. Further, the emissions from biomass and fossil fuel burning sources produce large amount of secondary aerosol precursors, and under favourable meteorological conditions secondary aerosols are formed; however, experimental evidences are scarce over Indian region. The diurnal characteristics of carbonaceous species (elemental carbon (EC), organic carbon (OC), and water-soluble organic carbon (WSOC)) and inorganic species (such as SO₄²⁻, NO₃⁻, NH₄⁺, K⁺) in ambient PM_{2.5} have been studied over Patiala, a site located in the source region of biomass burning emissions over IGP. The study was carried out during October 2011 to March 2012, a time span covering periods dominated by emissions from post harvest paddy-residue burning (October-November, P1), from fossil fuel, wood, and bio-fuel burning (December-February, P2) and from various regional sources (March, P3) with different meteorological conditions. The contribution of OC and EC to PM_{2.5} ranged from 30 to 45% during the study period with higher values during P1. Striking diurnal differences were observed in PM_{2.5} mass, as well as in the concentrations major carbonaceous and inorganic species during P1, with ~30 to 300% higher nighttime concentrations. On average, OC/EC ratios for the daytime samples were ~8.7, 6.5 and 3.1, and, for the nighttime samples were ~13, 7.3, and 3.9 during the P1, P2 and P3, respectively; suggesting that the relative contribution of EC (absorbing species) was significantly lower in P1 and increases subsequently.

The diurnal behavior of species was used as evidence of secondary organic and inorganic aerosol formation. The averaged WSOC/OC ratios for daytime samples were ~0.60, 0.69 and 0.68, and for nighttime samples were 0.44, 0.53 and 0.47 during the P1, P2 and P3, respectively, suggesting the enhanced daytime secondary organic aerosols formation in all seasons. Further, the contribution of WSOC and SO₄²⁻ to total water-soluble species in PM_{2.5} was decreased by 20% to 30%, and that of nitrate was increased by almost a factor of three (from 8% to 22%) in nighttime samples during P1. These observations indicate the prominent formation of secondary nitrate during nighttime, and that of WSOC and SO₄²⁻ during daytime. These results have implications in understanding the impact of biomass burning emissions on regional air quality and climate change, and designing appropriate mitigation strategies.

Logistic support for the sample collection was provided by Mr. A. Singh and Prof. D. Singh (Punjabi University, Patiala).

(N. Rastogi)

Role of anthropogenic activities on nitrogen and carbon cycling of a tropical estuary and adjacent coastal waters

Situated at the interface of rivers, ocean, atmosphere and dense human settlement, estuaries are subjected to large number of natural and anthropogenic forcings. These forcings, including high pollutant loads, lead to significant ecological and biogeochemical changes within an estuary. Cochin estuary is one such example in India, which processes high pollutant loads emanating due to anthropogenic activities. However, the scientific understanding of how the pollutant loads lead to ecological changes and affect the rates of biogeochemical processes in this estuary, and tropical estuaries around the world, is poorly understood.

In order to answer some of the intriguing questions vis-a-vis tropical estuaries, we undertook three short-term field campaigns to Cochin estuary and adjacent coastal waters (off Cochin and Mangalore) during April, September, and December 2012. Experiments to measure nitrogen (N) and carbon (C) uptake rates using stable isotope technique were performed along with sample collection for natural stable isotopic studies in particulate matter. Results obtained from the April campaign (remaining analyses are underway) provided some interesting insights with respect to the estuarine ecosystem. In general, N uptake rates at all locations within the estuary were very high compared to open ocean bloom conditions. Interestingly, N uptake rates at coastal transect off Cochin were higher compared to off Mangalore, suggesting that the pollutant loads from the Cochin estuary may be affecting the N cycling of the adjacent coastal waters. Another significant finding of the study is a very strong relationship between salinity, pH and N uptake rates, indicating that under nutrient replete conditions, parameters like salinity and pH may play a significant role in modulating N cycling.

This work is being done in collaboration with Dr. G. V. M. Gupta of Centre for Marine Living Resources and Ecology, Cochin, India.

(S. Kumar and P. S. Bhavya)

Deciphering nitrogen uptake potential under projected climatic conditions using a mesocosm experiment

Increase in sea surface temperature and precipitation in future, as projected by climate projection models, may alter nutrient cycling in coastal regions due to potential changes in phytoplankton community structure and their ability to assimilate nitrogen (N) and carbon (C). An experiment simulating different temperature and salinity conditions (28°C

- 35, 28°C - 31, 31°C - 35 and 31°C - 31) in mesocosms containing 1000 L of coastal seawater was performed and N uptake rates were measured using ^{15}N tracer technique on the 3rd, 6th, 8th and 11th day of the experiment. The results show that, under all conditions, the total N (nitrate + ammonium) uptake rates were lower on the first and the last day of the tracer experiment, while it peaked up in the middle, consistent with chlorophyll concentration. Total N uptake was considerably lower under ambient temperature-lower salinity condition (28°C-31) than the others. This indicates that the lowering of salinity in coastal regions due to excessive rainfall in future may affect the N uptake potential of the plankton resulting into potential changes in the C and N budget. Recently (March 2013), another mesocosm experiment involving different set of temperature and salinity conditions and newer phytoplankton community structure has also been performed.

This work was done in collaboration with Dr. A. Godhe of University of Gothenburg, Sweden.

(S. Kumar, P.S.Bhavya and R. Ramesh)

Inorganic ionic constituents of $\text{PM}_{2.5}$ over Arabian Sea: Results from online measurements

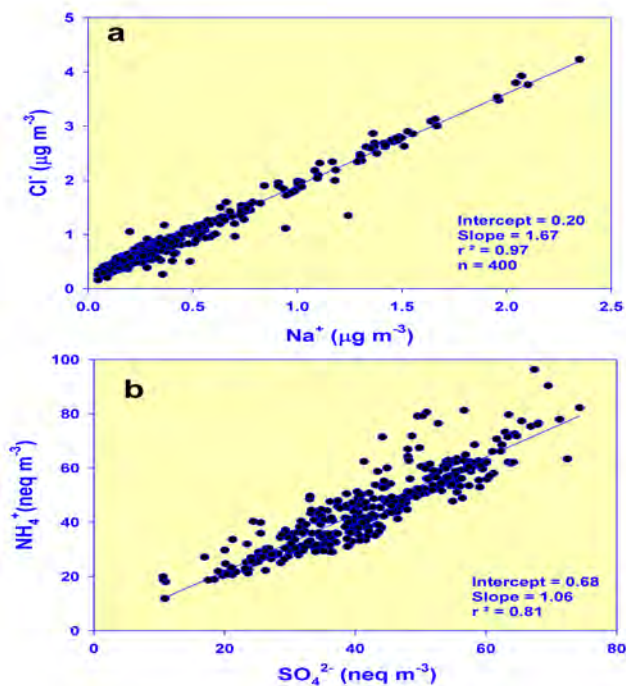


Figure 71: Plot showing (a) Cl^- and Na^+ are significantly correlated with sea-salt proportions and (b) strong linear relation of NH_4^+ with SO_4^{2-} for the samples collected from the Arabian Sea.

Real time measurement of water-soluble ionic constituents (Cl^- , NO_3^- , SO_4^{2-} , Na^+ , NH_4^+ , K^+ , Mg^{2+} and Ca^{2+}) of $\text{PM}_{2.5}$

aerosols over Arabian Sea atmospheric boundary layer has been done using Ambient Ion Monitor (AIM) onboard Sagar Sampada during the cruise from March 18 to 13 April 2012. AIM is equipped with a steam jet aerosol collector and two ion chromatographs for simultaneous on-line measurement of cations and anions in $\text{PM}_{2.5}$ with hourly time resolution. Concentration of NO_3^- and NH_4^+ were found 1.03 and 0.8 $\mu\text{g m}^{-3}$, respectively, which are higher compared to earlier reported values using off line filter based measurements on total suspended particulate samples during March-April months. A strong linear relation of NH_4^+ with SO_4^{2-} (Figure. 71b) indicates existence of fine particulate $(\text{NH}_4)_2\text{SO}_4$ and/or NH_4HSO_4 . Deposition flux of inorganic nitrogen calculated based on these measurements is $\sim 0.8 \text{ mg N m}^{-2} \text{ d}^{-1}$. Cl^- and Na^+ are significantly correlated (Figure 71) with sea-salt proportions and discernable depletion of chloride is not observed. Such assessment of chemical constituents with real time measurements is essential for better understanding on effect of continental outflow on marine atmosphere and surface ocean biogeochemistry.

(A. K. Sudheer, R. Rengarajan, D. Deka, R. Bhushan and S. K. Singh)

Seasonal characteristics of aerosol ionic constituents over an urban atmosphere: Results from semi-continuous measurements

Variation of aerosol constituents, number concentration and mass concentration may have significant impact on diurnal trend in aerosol optical depth and single scattering albedo. Hence incorporation of real time measurement data and delineation of controlling factors of variability in such radiative transfer calculations may result aerosol forcing estimates more realistic. Measurement of aerosol composition with hourly time resolution enables to study diurnal variation in chemical constituents and factors controlling these variations. Water-soluble ionic constituents of $\text{PM}_{2.5}$ were measured at Ahmedabad during winter (December 2011–January 2012) and summer (May–June 2012) using Ambient Ion Monitor in order to study the secondary aerosol formation and influence of meteorological factors on ambient aerosol. The average diurnal trend of various constituents during winter as well as summer seasons are depicted in Figure 72(a) and Figure 71(b) respectively. During winter-time typical diurnal trend indicates chemical constituents largely affected by boundary layer changes. During summer season after noon maximum coincide with the high wind speed and elevated photochemical production of secondary aerosol. During summer, constituents like Ca^{2+} and Mg^{2+} increased in the afternoon by about 30-50% while the increase in secondary aerosols like NO_3^- and SO_4^{2-} is almost a factor of two or more. Since relative humidity is also low during afternoon period which reduces the hygroscopic growth of soluble particles and subsequent removal by dry deposition compared to night time may cause increase in concentration.

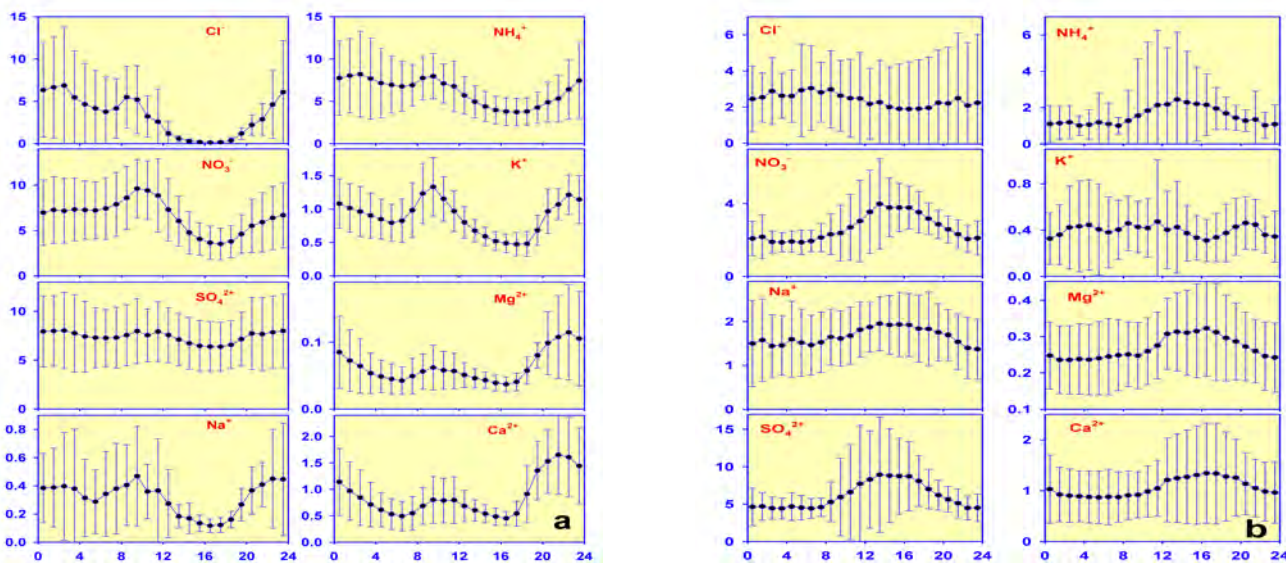


Figure 72: The average diurnal trend of various water-soluble inorganic constituents ($\mu\text{g m}^{-3}$) during (a) winter and (b) summer.

(A. K. Sudheer, R. Rengarajan, D. Deka, R. Bhushan and S. K. Singh)

Aerosols over arid and semi-arid regions in India: enhanced secondary organic aerosol

Carbonaceous aerosol, comprise of elemental carbon (EC) and organic aerosol (OA) constitute a substantial fraction of fine particulate matter. The primary sources of carbonaceous aerosols are incomplete combustion processes, either fossil fuel or biomass, and OA has also secondary sources. OA produced from sources other than primary emission is estimated to be higher and large uncertainty exists associated with these estimates. The uncertainties in OA estimates are due to poor understanding of secondary organic aerosol (SOA) formation, their spatio-temporal variations and controlling factors. Hence, it is essential to constrain OA sources in order to assess the environmental impact of carbonaceous aerosol in regional and global scales. In this context, we have studied carbonaceous species in atmospheric aerosol samples collected from Ahmedabad and Jodhpur to evaluate SOA formation over this region. EC and OC concentrations are expected to exhibits linear relationship if they are originated from similar sources. They show considerable scatter during the observation at both Ahmedabad and Jodhpur, suggesting large fraction of OC is not associated with primary combustion emission. The average OC/EC ratio in PM_{10} samples is 7.3 at Ahmedabad with a range of 3.6 to 17.2. The average value at Jodhpur during September-October 2011 is 32 with wide range from 5.7 to >100, indicating that non-combustion sources of organic aerosol predominate (Figure 73). SOC contribution calculated by EC-tracer method suggests almost 70% carbon is of secondary in origin, which varies from 9% to >90%. The corresponding value at Ahmedabad is only 12%. OC abundance ratio in $\text{PM}_{2.5}$ to PM_{10} at Ahmedabad is ~ 0.52 and that at Jodhpur is ~ 0.30 , suggesting that fine mode organic aerosol is only about 30% where as 70% OC exists in coarse particles. In general secondary aerosols produced from gaseous precursors are expected to be present largely on

fine mode and on the contrary at Jodhpur its size distribution is conspicuously different. This difference in size distribution of organic aerosol could be due to the role of mineral dust on heterogeneous reactions of precursor volatile organic compounds leading to SOA formation on coarse particles.

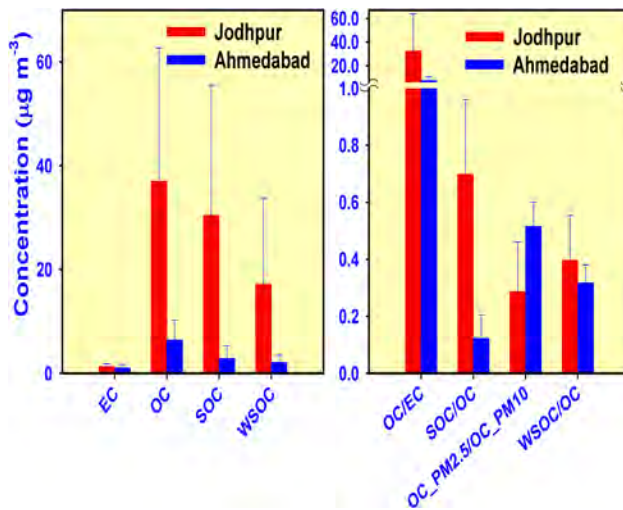


Figure 73: Average EC, OC, SOC, WSOC and their ratios in $\text{PM}_{2.5}$ and PM_{10} collected from Ahmedabad and Jodhpur.

This work was done in collaboration with Prof. J. S. Rathore from J.N.V university, Jodhpur.

(A. K. Sudheer, R. Rengarajan, R. Bhushan and S. K. Singh)

Weak monsoon event at ~ 2.1 ka registered in the sedimentary deposits

The late Holocene climate and vegetation of the Lower Narmada valley, Gujarat, western India is inferred from stable

carbon and oxygen isotopic compositions ($\delta^{13}\text{C}$ and $\delta^{18}\text{O}$) of sedimentary carbonates and the associated organic carbon (OC). The alluvial plain from the surface to a depth of ~ 2 m consists of the late Holocene sediments, deposited during last ~ 3 kyr, probably by large historic and paleofloods. $\delta^{13}\text{C}$ of both carbonates and OC in the sediments suggest that climate was sub-humid throughout the late Holocene (~ 3 kyr) as it is today, and the vegetation was of mixed C_3 - C_4 type with little change in their relative proportions. The modern vegetation mostly comprises shrubs and scattered distribution of woody plants (C_3) with a little grass (C_4) at some places. The recent change in vegetation is attributable to anthropogenic disturbance: the natural grasslands (C_4) are replaced by shrubs and woody plants (C_3). Two comparatively drier events at ~ 2.1 ka and ~ 1.3 ka are observed, consistent with widespread proxy paleoclimatic records and are attributed to a weaker southwest monsoon rain.

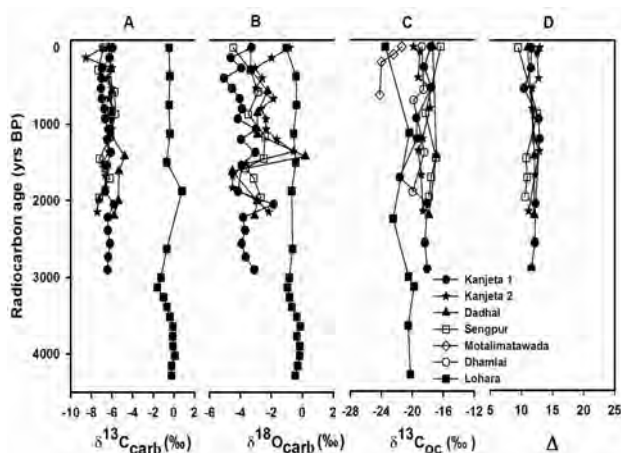


Figure 74: Variation of stable isotopic composition with radiocarbon ages in the sediment profiles: (A) $\delta^{13}\text{C}$ in carbonate, (B) $\delta^{18}\text{O}$ in carbonate and (C) $\delta^{13}\text{C}$ in organic matter. (D) Difference between $\delta^{13}\text{C}$ values in carbonate and organic carbon ($\Delta = \delta^{13}\text{C}_{\text{carb}} - \delta^{13}\text{C}_{\text{oc}}$).

(A. H. Laskar, R. Ramesh and M. G. Yadava)

Weak monsoon event at ~ 2.1 ka indicated by a stalagmite from Andaman Islands

As oxygen isotopic composition ($\delta^{18}\text{O}$) of precipitation in the tropics has amount dependence, past rainfall conditions could be reconstructed using carbonate archives such as speleothems, which preserve records of paleo-monsoonal rainfall variations. Two stalagmites from Baratang cave in Andaman Islands are being investigated for their temporal variations in $\delta^{18}\text{O}$ to reconstruct Indian Summer Monsoon (ISM). We have further improved radiocarbon chronology and added new O and C stable isotope measurements in stalagmites investigated earlier which extends now up to the last ~ 4 ka. We find that ' ~ 2.1 ka' seems to be a unique dry event in the last 4kyr of the Andaman Islands. It seems to be widespread and weakest of monsoon episode in the last 4kyr of the monsoon reconstructed from Andaman Islands. During 1800-2000 cal yr BP, identified as the Roman Warm Period,

a strong reduction in the ISM is observed, the wide-spread nature of which is confirmed by diverse proxy records from other areas influenced by the ISM. Reduction in the ISM is also observed around 1500 and 400-800 cal yr BP, the latter period is the transition from the Medieval Warm Period to the Little Ice Age. The strongest monsoon in the last ~ 4 kyr is observed during 800-1200 cal yr BP, the Medieval Warm Period.

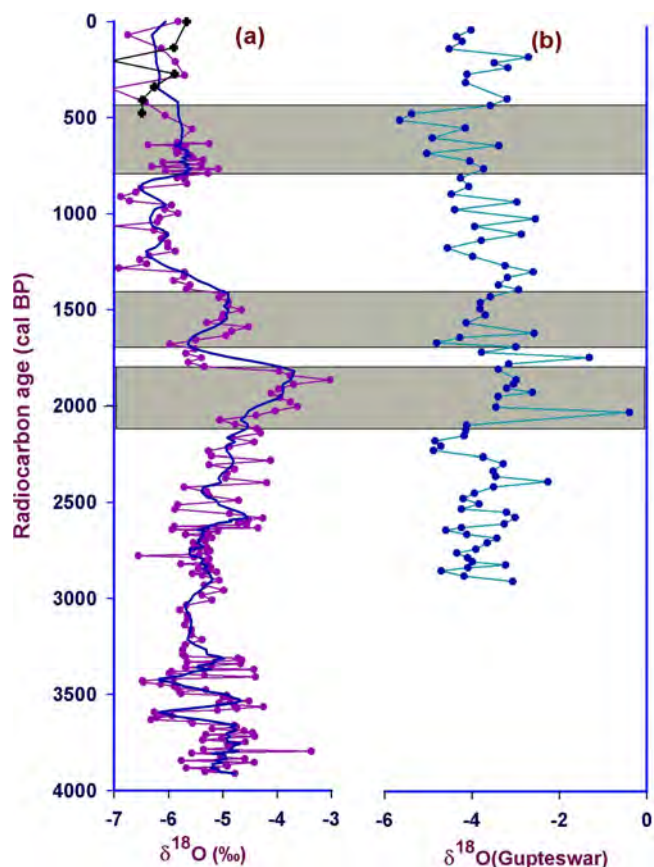


Figure 75: (a) Stalagmite O variation from Baratang Island, thick line shows five point running average. Another recently grown speleothem shows similar value of $\delta^{18}\text{O}$ (black circles). (b) Stalagmite $\delta^{18}\text{O}$ variation from Gupteswar cave. Dark gray patches show century scale relatively arid phases. Uncertainty in the chronology varies between 100 and 200 yrs.

(A. H. Laskar, R. Ramesh and M. G. Yadava)

Automation of ' CO_2 preparation line' in Radiocarbon (C_{14}) Laboratory

Radiocarbon dating method is used to estimate age of ancient carbon containing material by measuring residual radiocarbon activity in a sample. Standard procedure requires conversion of carbon sample first into carbon dioxide (CO_2), then into acetylene and finally into benzene. The current set up consists of open-loop heating system and manual displacement of heaters which requires continuous monitoring by the operator. Automation of this involves programmable

temperature control and motorized displacement of heaters, PC based control system, wireless communication between PC and experiment-control section and remote access of the system through network communication.

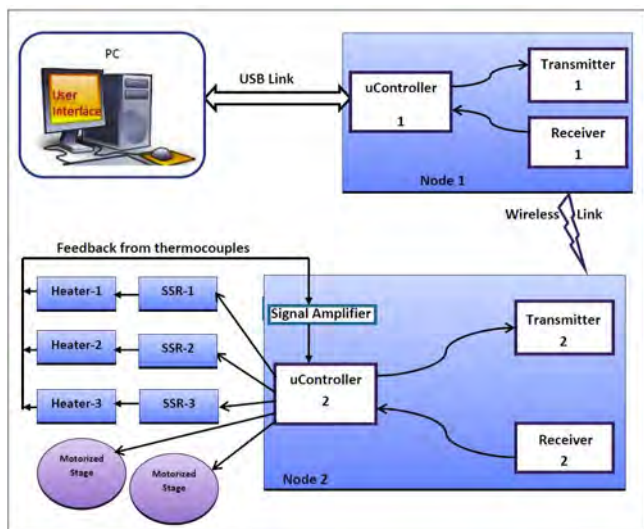


Figure 76: Block diagram of the system

We have designed a prototype module to accomplish these tasks. The system consists of a PC, two wireless nodes, heaters and motorized stages as shown in block diagram (Figure 76). The system can be controlled and monitored from PC through graphical user interface developed in LabView software. As PC and experiment setup location are at some distance, wireless communication link is established between PC and experiment-control section using RF modules. The temperature and displacement of the heaters are controlled according to the received commands from the user. The PWM (Pulse Width Modulated) pulses are generated through PI (Proportional-Integration) technique and given to solid state relay for controlling heating power to achieve desired temperature. Type-K thermocouple is used for giving feedback of temperature value to microcontroller for each heater. The current values of temperature are logged into the separate excel file throughout the experiment. For movement of heater, in-house single axis linear motion system is designed and developed. For precision movement stepper motor is used and driver circuit is designed such that it can operate independently. The system software is developed for network communication, which provides control of the system from any PC connected in the LAN. At present, the prototype module has been tested successfully as per the requirement; shortly it will be attached to the actual experiment setup for verification of the automated operations.

Instrument controller and data logger based on Wind Direction/Speed sensor

Hi-volume air samplers are operated during the ship cruises for collecting aerosol samples in order to study the various chemical constituents of marine aerosol. The samples need to be collected only when the relative wind direction is from the fore side of the ship to avoid contamination from ship's exhaust. To achieve this, an automated system (Figure 77) based on microcontroller has been designed which continuously monitors wind direction/speed using the sensor and actuates the sampler. Facility to log the data of sensor and status of the instrument has also been added for future reference.

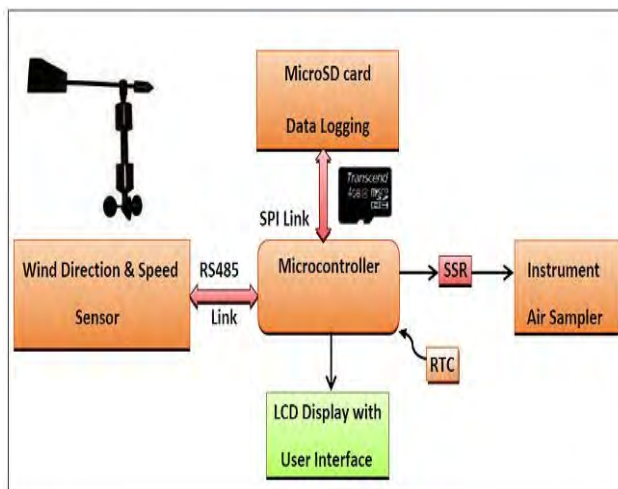


Figure 77: Block diagram of the system

The system includes AVR series microcontroller having 128KB of program memory and can support up to 16 MHz clock operation. It communicates with wind direction/speed sensor through RS485 communication link which supports long distance transmission. The wind direction and speed are obtained as an angle from 0 to 360 degree and in meter/second respectively. To log the sensor data, Micro SD card has been interfaced through Serial Peripheral Interface (SPI) bus of microcontroller. The software core is developed such that data is written in file format like ".xls", ".txt" etc. and saved in the memory card. The system has been tested successfully with 8 GB card which can store this data type for more than 3 years. For ease of access, alphanumeric LCD and keypad are also interfaced to monitor and enter the system parameters. The Air sampler instrument is connected to microcontroller through 'solid state relay' (SSR) and it is controlled by programmed logic defined by user. The system can be used as an independent data logger and also accommodate different types of sensors with minor modifications. This system has been tested onboard Sagar Sampada cruise in the Arabian Sea with satisfactory results.

Age of Barren Island Volcano

Barren Island of Andaman Sea is the only active volcano in the Indian subcontinent. While the volcano has erupted sporadically many times over the last ~ 70 ka, it is not known when it formed and breached the sea surface. To provide estimates for the timing of these events, we dated two tephra (ash) layers older than 42 ka and generated by this volcanism in a previously studied marine sediment core collected ~ 32 km southeast of the island using the newly established modern ^{40}Ar - ^{39}Ar facility in India. The ^{40}Ar - ^{39}Ar plateau ages of plagioclase separates from successive tephra layers at 310 and 375 cm are 1.8 ± 0.4 (2σ) Ma and 1.5 ± 1.8 (2σ) Ma, respectively. We interpret the more robust age of 1.8 Ma as the time of crystallization of plagioclase grains. As this age is very much older than the depositional age of the tephra layer (~ 61 ka), we infer that it represents the age of older rocks present in the plumbing system of the volcano that were blown out with later pyroclastic eruptions and therefore sets a strict younger limit to the time of formation of the volcano.

This work was done in collaboration with K. Pande of IIT Bombay.

(J. S. Ray and N. Awasthi)

Geochemistry of fluids in Mud Volcanoes of Andamans

Mud Volcanoes (MV) of Andaman accretionary prism have been generated as a consequence of lateral tectonic compression between slowly converging Indian and Burmese plates leading to rise of a mixture of fluidized mud and hydrocarbon gases that travel upward from the décollement to the surface through the fault networks of the forearc. These MVs emit thermogenic CH_4 ($\delta^{13}\text{C} \geq -42\text{‰}$), C_2H_6 ($\delta^{13}\text{C} \geq -29\text{‰}$) and CO_2 ($\delta^{13}\text{C} < -3.0\text{‰}$), low chlorinity water ($\text{Cl}^- = 45\text{--}135$ mM) having distinct δD and $\delta^{18}\text{O}$ isotopic compositions ($\delta\text{D} = 1.1 \pm 0.9$; $\delta^{18}\text{O} = -21.2 \pm 2.8$) and young (< 40 kyr) argillaceous sediments (smectite-illite-kaolinite-chlorite dominated). We infer these to have been derived from the marine sediments and altered oceanic crust of the Indian slab at shallow depths (2 km–6 km) of the Andaman subduction zone. Using diameter and bursting frequency of bubble trains in gryphons we conservatively estimate that the annual emission of methane from the MVs of Andaman Islands could exceed 110 tonnes, which could be significant to the atmospheric methane budget and hence to the global climate models. As suggested by the trace element contents and $\delta^{18}\text{O}$ and δD isotopic compositions, the mud volcano water is a mixture of sediment pore water (ancient seawater) and water released from dehydration of clay minerals. The $^{87}\text{Sr}/^{86}\text{Sr}$ of water confirms the above inference and points out that altered oceanic crust plays a significant role in controlling the chemistry of water expelled at MVs at convergent zones.

This work was done in collaboration with D. J. Patil and A. M Dayal of NGRI.

(J. S. Ray, A. Kumar, A. K. Sudheer, R. D. Deshpande, D. K. Rao, N. Awasthi and R. Bhushan)

Role of precipitation and temperature during the Holocene glaciations in Dunagiri valley, Central Himalaya, India

It has been suggested that monsoon is the major driver of glaciation in Himalaya, however, the exact mechanisms, timing and geographical extent of monsoon influence in glaciation is still debated. In order to improve our understanding of monsoon-glaciation relationship, a monsoon dominated Dunagiri valley located in the Dhauliganga valley of the Central Himalaya has been investigated.

Reconstruction based on moraine stratigraphy supported by optical and radiocarbon dating suggests that the oldest and longest valley glaciation named as BGS-I occupied ~ 50 km². This glaciation began during the Younger Dryas (YD; ~ 12 ka) cooling and persisted until around the early Holocene (~ 9 ka) intensified monsoon. We speculate that the lowered temperature required to sustain the BGS-I glaciation beyond the YD cooling event until the early Holocene climatic optimum could have been achieved by the ice-albedo feedback mechanism which probably reduced radiative heating. Therefore, although there was an increase in precipitation, it was the lowered temperature that drove and sustained the BGS-I glaciation. The second glacial advance viz. BGS-II is dated between 7.5 ka and 4.5 ka. During this period, there was a $\sim 30\%$ reduction in glacier area compared to the BGS-I glaciation. We ascribe it to the gradual decrease in precipitation during the mid-Holocene as indicated by other studies that during the mid-Holocene, increased snow accumulation due to high precipitation was much smaller than reductions in ablation caused by lower temperatures. Our data suggest that although the rainfall was low during the mid-Holocene, glaciation was sustained by low temperatures. After the mid-Holocene, a renewed phase of glacier advance occurred in Dunagiri valley during the Late Holocene (~ 1 ka; (BGS-III). Morphology of the lateral moraines indicates appreciable thinning of the ice volume which is ascribed to an increase in temperature. Following this, a marginal increase in the ice cover occurred during the cool and moist Little Ice Age (LIA) before the glacier receded to its present position.

This study was carried out in collaboration with S. P. Sati, N. Rana, Y. P. Sundriyal, HNB Garhwal University and Falguni Bhattacharya, Institute of Seismological Research, Gandhinagar

(S. N. Ali, R. Bhushan, A. D. Shukla and N. Juyal)

Summer monsoon verses mid-latitude westerlies in driving Late Quaternary glaciations in the Goriganga valley, Central Himalaya, India

The Himalayan glaciers are fed by two major weather systems viz. the Indian Summer Monsoon (ISM) and the mid-latitude westerlies. The glaciers located in the southern and eastern part of Himalaya receive moisture from the summer precipitation, whereas, the mid-latitude westerlies are the major contributors for snow accumulation in the

north-west Trans-Himalaya and Tibet. However, the existing chronological suggests that the late Quaternary glacier mass balance was strongly influenced by the insolation driven monsoon variability with little contribution from the westerlies even in the westerlie dominated areas. Considering that mid-latitude westerlies are an important component of the circulation system, and the same was known to be intensified during the Last Glacial Maximum (LGM), the present study is an attempt ascertains whether the intensified mid-latitude westerlies contributed to the glacier dynamics in the Central Himalaya during the LGM. Towards this, we selected the Goriganga valley in the Central Himalaya which is located in a transitional zone between the dry steppe of the Tibetan plateau in the north and the sub-humid Himalayan climate in the south.

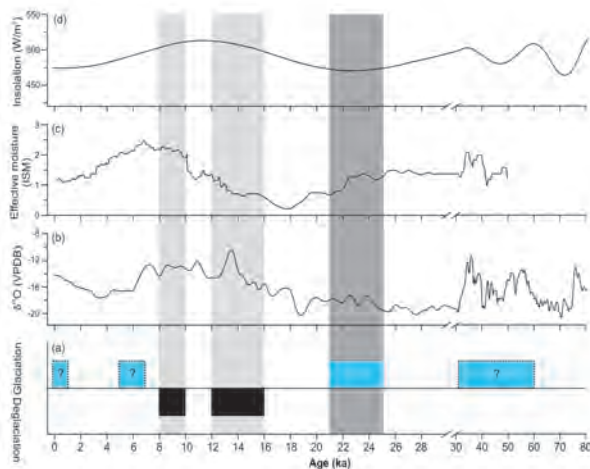


Figure 78: Comparison of the events of glaciations and deglaciations with the palaeoclimate records. Note that during the Last Glacial Maximum (LGM), glacier in Dhauliganga expanded during period of weak summer monsoon (b and c) and low solar insolation (c).

Our study suggests that the oldest and longest glaciation which was assigned to Marine Isotopic Stage-3 (MIS-3; 50–30 ka) occupied ~44 km² area. This we attribute to a lowered temperature and marginally enhanced summer monsoon. But the most important aspect of the study was for the first time, multiple ages obtained on lateral moraine suggests that the monsoon dominated Central Himalaya responded to the global LGM (MIS-2) when the valley glaciers were significantly lowered from their present position. This we ascribed to a combination of enhanced mid-latitude westerlies and lowered temperature.

The study has implications towards reevaluating our understanding about the eastward extent of westerlies and their contribution in the glacier mass balance during the cold periods in Himalaya.

(S. N. Ali, R. H. Biswas, A. D. Shukla and N. Juyal)

Reactivation of the South Tibetan Detachment System in the Central Himalaya during the last 20 ka: implication for compressional tectonics

Two important structural features, with very different characteristics, that developed in the Himalayan orogen are (i) north dipping thrusts (compressional structures) such as the Main Central Thrust (MCT) and the Main Boundary Thrusts (MBT); and (ii) north dipping normal faults (extensional structures) the South Tibetan Detachment System. The South Tibetan Detachment System (STDS) developed near the crest of the Higher Himalaya along the southern margin of the Tibetan plateau to accommodate crustal thickening and elevated topography arising from the subducting Indian lithosphere. Studies suggested that the STDS came into existence along with the MCT during the Miocene. Several studies show that the terrain that lies between the MCT and the Himalayan Frontal Thrust (HFT) witnessed episodic tectonic activity during the Late Quaternary. Compared to this, the structural and geochronological data indicate that the STDS was active during the Miocene but its subsequent activity remains poorly understood.

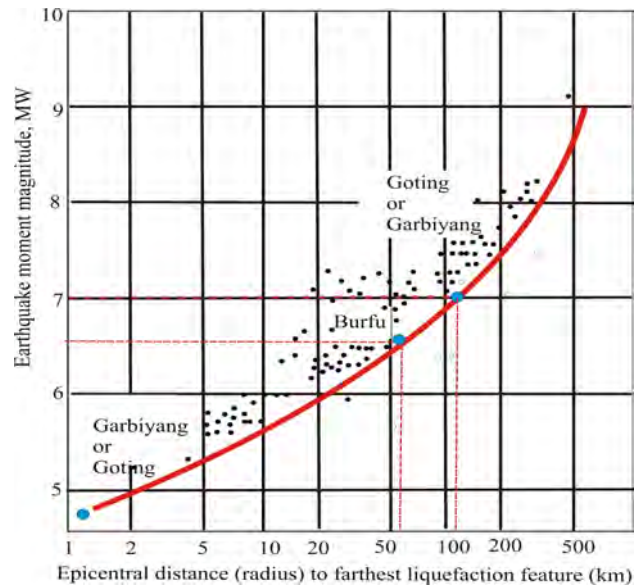


Figure 79: Reconstruction of palaeo-earthquake magnitude based on plotting the SSDS observed at Goting, Burfu and Garbiyang lakes on the global data curve which indicate that the deformation were caused by an earthquake of magnitude ranges between 6.5 and 7 Mw respectively.

We demonstrate based on the occurrence of the Soft Sedimentary Deformation Structures (SSDS) in three relict lake sequences (Goting, Burfu and Garbiyang) located in the upper reaches of the Dhuli Ganga, Gori Ganga and Kali Ganga valleys (Central Himalaya, Uttarakhand) that the STDS was active during the last 20 ka. Geomorphological expression of the activity along the STDS is the obstruction caused by the rising footwall of the STDS as a result; the

southward extrusion of valley glaciers was prevented. The lakes which are studied developed on the hanging wall of the STDS following the retreat of the glaciers. Considering above, it is reasonable to consider that the SSDS preserved in these lakes are associated with the reactivation of the STDS during the Late Quaternary for the following reasons. (i) The presence of deformed layers caused due by liquefaction, fluidization in a stress field within the undeformed layers. (ii) Their occurrences at three locations ~ 130 km apart in a similar geological and hydrological setting. (iii) The deformation events in the three lakes clustered between 13.5 ka and 17 ka implies that they were triggered by common earthquake. Based on, a global data curve on known earthquake magnitude and the distance of SSDS from the epicenter of shallow and deep-focused earthquakes in various tectonic and sedimentary settings, the unknown earthquake magnitude is estimated. In the present case the deformations that occurred during 17 ka to 13.5 ka, were caused by an earthquake of magnitude between Mw 6.5 and >7 Mw having an epicenter in the vicinity of the STDS.

The present study has implication towards the suggestion that movement along the STDS did not end in the middle Miocene but persisted episodically or continuously into the Quaternary. The MCT and the STDS are the coupled structures and the recent geodetic study in central Nepal has shown that 80% of the modern crustal shortening rate of 17–18 mm/yr is concentrated near the surface trace of the MCT implying that the MCT is still active. In view of this, the late Quaternary activity of the STDS as observed in the present study is an expression of providing accommodation space to the ongoing crustal shortening arising due to north-south compression in the Himalaya during the late Quaternary.

This study was carried out in collaboration with N. Rana of HNB Garhwal University, F. Bhattacharya of Institute of Seismological Research, Gandhinagar, N. Basavaiah of Indian Institute of Geomagnetism, Mumbai and R. K. Pant, retired PRL scientist.

(N. Juyal)

Mid-Holocene sedimentation and landscape evolution in the western Great Rann of Kachchh, India

The Great Rann of Kachchh (~ 300 km in length and 80–100 km in width) is a unique landscape in western India, which gets inundated during the monsoon by wind driven marine storm surges and continental fluvial influxes. Sedimentation in the Great Rann was controlled by the interplay between the continental and marine processes. Occurrence of clay and silt with sandy lenticles are interpreted as the deposition under the tidal flat low energy environment during the period when the Great Rann probably was occupied by shallow marine gulfs. Similarly, occurrences of fluvial sand rich Bets indicate the combined contribution from the Indus and Nara Rivers. In addition to this, there are references to suggests existence of a mighty river called the Saraswati receiving water and sediment from the Himalaya and draining through the Western

Great Rann into the Kori Creek. Further the landform evolution is considered to have significantly influenced by infrequent earthquakes in the past the most recent one was the 1819 Allah Bund earthquake.

Although the above studies, suggests that the Great Rann sedimentation was driven both by the marine and continental processes, however, these studies did not adequately dwell upon the role of terrain instability in the sedimentation and landform evolution. Similarly, argument towards the existence of mighty river called Saraswati based more on the morphological features inferred through remote sensing data, and not based on the field and sedimentological evidences. Considering above we investigated the Western Great Rann to understand (i) the processes responsible for spatial and temporal changes in the pattern of sedimentation, (ii) ascertain the role of terrain instability in the landform evolution, and (iii) develop a model of landform evolution of the western Great Rann.

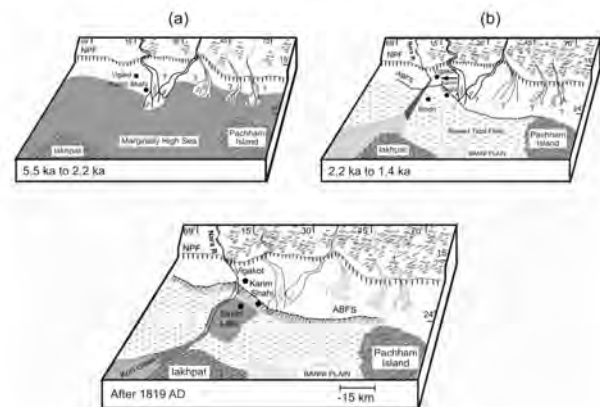


Figure 80: Block diagrams depicting the evolutionary stages of the western Great Rann since the last 5.5 ka. (a) Tidal flat sedimentation dominated during 5.5 and 2 ka (b) A major transformation in the landform and earth surface processes took place after 2.2 ka, a major earthquake between 2.2 ka and 1.4 ka brought the land surface above the intertidal influence along with the westward shift of the Nara River. Probably the surface expression of the Allah Bund Fault Scarp (ABFS) appeared during this earthquake. (c) The present land configuration was achieved after 1819 Allah Bund earthquake.

The study based on field stratigraphy, sedimentology, geochemistry, optical and radiocarbon dating suggests that (i) major part of the western Great Rann was under the influence of tidal flat sedimentation during the last 5.5 ka to 2 ka implying marginally high sea level. (ii) The low energy fluvial sedimentation was limited to the north and north-eastern margins by the streams originating north of the Nagar Parkar Fault. Our study negates the suggestion for the existence of a mighty river called Saraswati that was receiving waters from the Himalaya and were flowing through the Great Rann of Kachchh into the Kori Creek. (iii) We support the suggestion that the Allah Bund Fault Scarp (ABFS) is cumulative scarp at least created by two major earthquakes. The older earthquake

which is radiocarbon dated between 2.2 ka and 1.4 ka not only led to the westward shift of the Nara river channel but also led to the complete withdrawal of the marginally high sea from the region. (iv) The present day landforms owe its genesis to the 1819 Allah Bund earthquake which completely disrupted the Nara river system and pushed the creek zone to its present position.

This study was carried out in collaboration with A. K. Tyagi, Institute for Plasma Research, Gandhinagar, P. S. Thakker, Space Application Centre, Ahmedabad, M. G. Thakkar, K.S.K.V. Kachchh University, Bhuj.

(A. D. Shukla, R. Bhushan and N. Juyal)

Continental and marine interaction during the last 1400 years: evidence from the Western Great Rann Kachchh

In the near coastal environment, river channels respond to changing land-sea configuration by spatial and temporal changes in the sedimentation pattern which in turn can be used to reconstruct the past climate tectonic history. The western Great Rann of Kachchh is currently an extensive saline mudflats and salt encrustation area, part of it is inundated due to storm induced tidal surges during the monsoon particularly the narrow trench zone. Fluvial processes are virtually absent except during the occasional major floods in the Indus River, northwestern Great Rann is flooded. The western Great Rann opens into the Arabian Sea through a macrotidal dominated Kori creek, which serves as a conduit for seawater to seasonally enter inland and flood. The existing chronometric data suggests that although the tidal flat sedimentation terminated from the major part of the western Great Rann, however, in the narrow confined Nara River channel, the only river in the western Great Rann, sedimentation continued until around 1 ka.

Our study indicate that during the last 1.4 ka to 1 ka yr BP, (a period of 400 years), Nara river experienced at least four relatively high discharge events punctuated by equal number of low discharge events. This led to the fluctuations in the sedimentation pattern along the course of the Nara river. We hypothesize that large freshwater flux routed through the Nara river limited the tidal influence hence the tidal flat sedimentation proximal to the Kori Creek. It was only during the low fluvial discharges that the landward ingress of tidal surges occurred that facilitated the intertidal sedimentation. Absence of sediments after 1 ka on the Nara river bed can be attributed to a combination of natural and anthropogenically induced changes. Particularly, after 1766 AD, the construction of bunds has significantly reduced both the water and sediment flux into the western Great Rann. Finally, the 1819 Allah Bund earthquake induced uplift of the Nara river bed completely defunct the river system

This study was carried out in collaboration with M. Ngangom and M.G. Thakkar, K.S.K.V. Kachchh University, Bhuj.

(R. Bhushan and N. Juyal)

1819 Allah Bund Earthquake and its impact on landforms in the Western Great Rann of Kachchh

The present observations are pertaining to the geomorphological changes that have occurred after 1819 earthquake (7.9 M_w) in the western Great Rann. Although the broad morphological changes in the vicinity of the Allah Bund earthquake are known such as the development of ~80 km long and 3 to 6 m high linear scarp and coseismic submergence of the Sindri fort in the south of the scarp, the detailed geomorphological changes and its westward impact on the Great Rann was remained uncertain.

Our preliminary observations in the Western Great Rann indicate that the earth surface processes are in the embryonic stage. In arid and semi-arid areas, if the terrain is tectonically active one can have high concentration of juvenile streams with high incision rate. Although the lateral variability of the 1819 scarp is not mapped in detail, however, the field observations indicate that the scarp that was created during 1819 earthquake was <4 m high and was probably the result of multiple earthquake (cumulative scarp). In addition to this, the lateral spread of the damage caused to the build areas after the 1819 earthquake indicate that the silty-clay dominated footwall of the Allah Bund fault suffered mega scale (10³ of km) flexure buckling which was responsible for not only the submergence of Sindri Fort but also the Basta Bunder Fort that was located ~60 km west of the Allah Bund scarp.

This study was carried out in collaboration with M. Ngangom and M.G. Thakkar, K.S.K.V. Kachchh University, Bhuj and P. S. Thakkar, Space Application Centre, Ahmedabad.

(N. Juyal)

IWIN National Programme

The National Programme on Isotope Fingerprinting of Waters of India (IWIN) progressed successfully along a predetermined trajectory, crossing a landmark of 20,000 new isotope data ($\delta^{18}\text{O}$ and δD) generated exclusively at IWIN-IRMS laboratory at PRL. Interpretation of this isotope data has yielded important new insights about various components of hydrological cycle. Two important studies are briefly described in the following.

Surface Water dynamics of the Bay of Bengal

The spatio-temporal variation in $\delta^{18}\text{O}$ and salinity in the surface water samples from the Bay of Bengal (BOB) has been investigated together with published data. A broad geographical correspondence between seasonal variation in spatial distribution of $\delta^{18}\text{O}$ and salinity is observed. In general, $\delta^{18}\text{O}$ and salinity have lower values in north and northeast part of the BOB which progressively increase in southwest direction in all the three seasons (March to May, June to October, and November to February). During winter months of November to February, surface water with low values of salinity (<30) and $\delta^{18}\text{O}$ (< -1 ‰) extends south of ~ 10°N, particularly on the east coast of India. This is interpreted

as due to influence of NE monsoon river discharge from Peninsular India together with steady southward dispersal of fresh water from Himalayan Rivers advected by the prevailing southward moving (East India Coastal Current).

In spite of the observed broad geographical correspondence between $\delta^{18}\text{O}$ and salinity during different seasons, the $\delta^{18}\text{O}$ -S plot for all available data pairs considered together shows no significant relationship between the two parameters though such relationships for different seasons and sub-regions of the BOB have been observed by earlier workers. The most prominent $\delta^{18}\text{O}$ -salinity relationship is seen (See Figure 81) for samples collected during June to October when the Himalayan river influx dominates. When this influx decreases in other seasons the $\delta^{18}\text{O}$ -salinity relationship is poor. This is because fresh water influx from different rivers modifies the $\delta^{18}\text{O}$ (and salinity) of the surface waters of the BOB differently in different regions. In particular, the $\delta^{18}\text{O}$ of Himalayan Rivers and that resulting from winter precipitation in Peninsular India is significantly lower than the riverine discharge from Peninsular Rivers during SW summer monsoon, whereas, in comparison to sea water, the salinity of all riverine sources is essentially similar. This difference in the spatial and temporal characteristics of riverine discharge in terms of $\delta^{18}\text{O}$, in contrast to near similar salinity characteristics, seems to be responsible for lack of strong $\delta^{18}\text{O}$ -S relationship when the BOB as a whole is considered as a single unit. This may have important implications for palaeoclimatic studies.

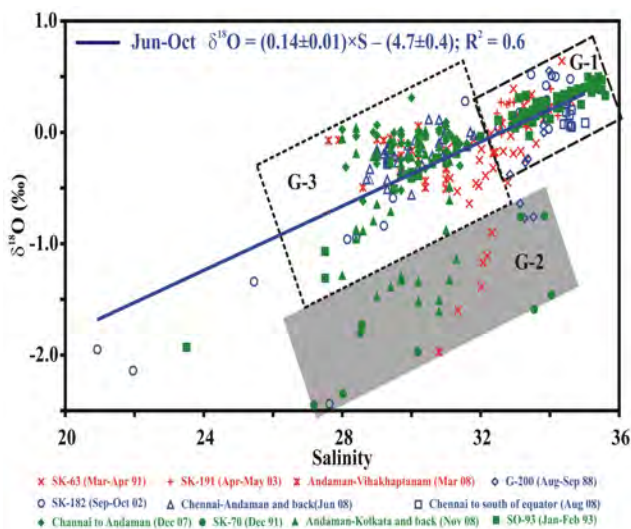


Figure 81: The $\delta^{18}\text{O}$ -S plot of all the samples from the surface waters of the BOB. The three groups (G-1, G-2 and G-3) of samples represent different geographical region of the BOB. Note: The regression line shown is based on samples collected during June-October only.

The $\delta^{18}\text{O}$ -D regression plot of samples north of $\sim 10^\circ\text{N}$ is similar in slope to the Global Meteoric Water Line and is ascribed to a stratified nature of meteoric water dominating the surface waters of the BOB, and the strong role of direct precipitation. However for samples south of $\sim 10^\circ\text{N}$, the $\delta^{18}\text{O}$ - $\delta^{18}\text{D}$ regression line has a significantly lower slope

and compares well with the subset of global oceans data between 10°N to 10°S and small discharge of Peninsular Rivers during summer monsoon. This implies that world surface ocean water line is not applicable to regions which do not receive significant amount of meteoric water either by direct precipitation or continental runoff.

In general variations in salinity and isotopes are related to the balance between evaporation and precipitation but this study highlights that the seasonal distribution of $\delta^{18}\text{O}$ and salinity over the northern BOB is dominantly governed by the spatial and temporal variation in the $(P+R|E)$; $\sim 4000 \text{ km}^{-3} \text{ a}^{-1}$ in spite of the fact that both Summer Moonsoon Current and Winter Monsoon Current transfer more than 75 times water between the Arabian Sea and the BOB. This confirms the dominant role of a shallow stratified layer of meteoric water over the BOB in restricting vertical mixing. This aspect needs to be considered when using $\delta^{18}\text{O}$ -S relationship for the palaeoclimatic reconstructions from sediment cores in the BOB.

Earlier studies have indicated that formation of this stratified meteoric water layer is important to maintain the threshold SST over the BOB for charging the cloud-base air-mass with the required moist static energy for sustenance of large scale deep convection in the atmosphere during the summer monsoon. Significant holding back of continental runoff in response to societal requirements or melting away of glaciers due to global warming, therefore, may limit the formation of this stratified meteoric water layer leading to possible undesirable consequences for rainfall over south Asian region. This aspect needs to be further investigated.

This study was done in collaboration with H. Achyuthan of Anna University and her colleagues and A. S. Maurya of IIT, Roorkee.

(R. D. Deshpande and S. K. Gupta)

Isotopic investigation of Megacryometeor

Unusually large icy conglomerates, sporadically falling from a clear sky even when there are no clouds or precipitation, are known as megacryometeors, and are different from hailstones. The formation mechanism for megacryometeors is poorly understood due to unpredictability of location and time of fall, logistic difficulties of spontaneous sample collection and proper preservation. Four such megacryometeors, weighing several kilograms fell, in Western India during October-November 2010, of which samples from three could be retrieved. The oxygen and hydrogen isotopic composition ($\delta^{18}\text{O}$ and δD), chemical composition and γ -activity were measured to investigate the origin and formation mechanism of these megacryometeors. No γ -activity from cosmogenic radionuclide ^{26}Al , characteristic of extraterrestrial matter, was detected in the ice, melt water and inherent dust. The chemical parameters of these samples were within the normal range of variation in rainwater in western India, except for chloride and Electrical Conductivity. The $\delta^{18}\text{O}$ and δD values

were within the range of variation for local precipitation. The slope and intercept of $\delta^{18}\text{O}-\delta\text{D}$ regression line were comparable to that of local meteoric water line (See Figure 82).

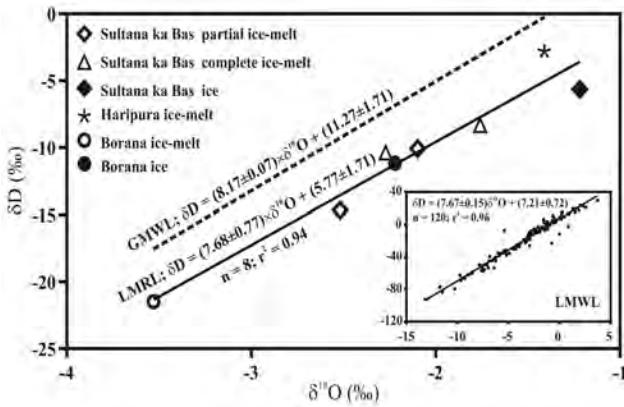


Figure 82: The $\delta^{18}\text{O}-\delta\text{D}$ regression line for ice and melt water samples of the investigated megacrymeteors (LMWL) that fell at different locations in western India. Also shown is the Global Meteoric Water Line (GMWL) and the Local Meteoric Water Line (LMWL) for Ahmedabad (inset). The $\delta^{18}\text{O}$ and δD values are within the range of variation for local precipitation. The slope and intercept of $\delta^{18}\text{O} - \delta\text{D}$ regression line are comparable to those of local meteoric water line

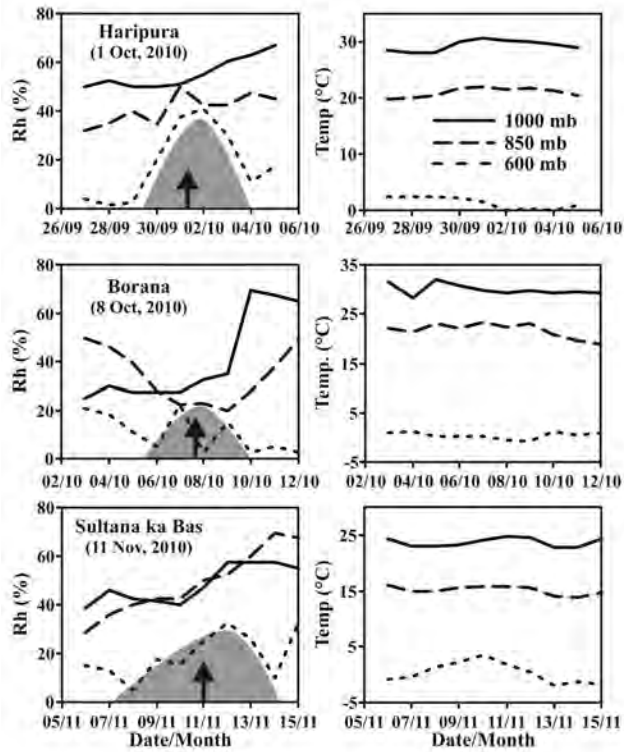


Figure 83: Temporal variation in relative humidity and temperature at three pressure levels during a few days before and after the day of the megacrymeteor fall, marked by an arrow. A conspicuous increase in the relative humidity at 600 mb (~4 km) is observed at all the locations. The plot is based on NCEP Reanalysis data provided by the NOAA/OAR/ESRL PSD, Boulder, Colorado, USA, from their Web site at <http://www.esrl.noaa.gov/psd/>.

These observations indicated that water molecules in the sampled megacrymeteors could be of atmospheric origin. However, the three fall locations lie below one of the busiest air-corridors in western India. This coupled with the observed (See Figure 83) increase in the relative humidity at above 4 km elevation, during a few days before and after the fall, suggested that perturbations in atmospheric parameters and/or mediation of aircrafts may be responsible for their formation in the present cases.

This study was done in collaboration with A. S. Maurya of IIT, Roorkee and R. C. Angasaria of PHE, Rajasthan.

(R. D. Deshpande, M. Dave, A. D. Shukla, N.Bhandari and S. K. Gupta)

Helium Anomalies in ground waters along Narmada river

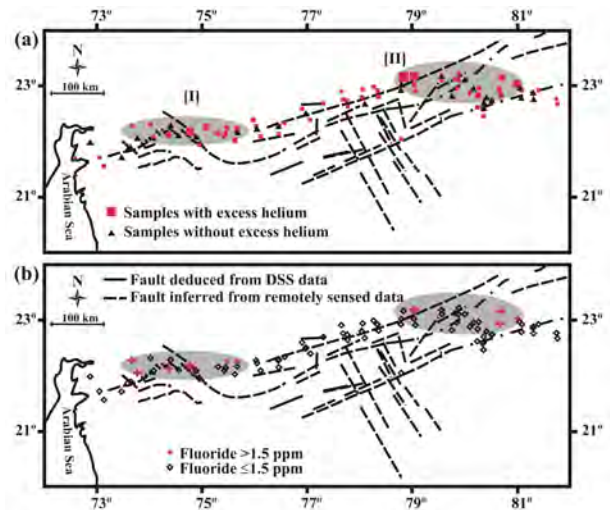


Figure 84: (a) Geographic locations of groundwater samples having ~5.3 ppmAEU helium (black triangles) corresponding to atmospheric equilibration and those having >5.3 ppmAEU (red squares). The size of red squares varies following square root scaling method. Note that samples with very high helium concentrations (>10 ppmAEU) are also located in two broad regions enclosed in clusters I and II indicating plumes of high helium concentration being injected into shallower groundwater in these regions, possibly facilitated by some faults and fractures. (b) Geographical locations of the groundwater samples with fluoride concentration ≤ 1.5 ppm (open black diamonds) and those with >1.5 ppm (red crosses). Note that groundwater samples having >1.5ppm of fluoride remarkably correspond to the locations of the two clusters I and II of excess helium.

A survey of dissolved helium, fluoride and electrical conductivity in groundwater from across the main stem of the Narmada River, between Bharuch in the west and Amarkantak in the east, was undertaken with a view to identify active tectonic regions, based on locations of high helium concentrations, interpreted as indicative of upward migration of deep fluids. Existence of deep fluids in this region has been hypothesised earlier based on various geophysical studies in

the Narmada Rift Basin-a major tectonic feature in central India. Our study revealed that samples with high helium concentration are clustered in two broad regions (See Figure 84) with known intersecting faults, indicating the possibility of plumes with high helium concentration being injected into shallower groundwater in these regions, facilitated by these faults and fractures. It is noteworthy that the epicenter of the devastating earthquake at Jabalpur in 1997 is located in the Cluster II of anomalous helium. Locations of groundwater samples having excess fluoride remarkably correspond to these two clusters of excess helium. This suggests a possible commonality between the causal factor of excess helium and higher fluoride in groundwater, which needs to be further investigated.

(R. D. Deshpande and S. K. Gupta)

Rare Earth Element (REE) study of Permo Triassic Sediments from Spiti Valley, India

The Permo-Triassic transition witnessed the most severe extinction event in the history of life on Earth. This most severe biotic crisis wiped out nearly 90% of all the species in the ocean and about 70% of the vertebrate families on land on Earth and occurred around 251 Ma ago. Several attempts have been made to understand the environmental changes which could possibly have brought this devastation, including volcanic eruption, global climate change, ocean anoxia and extraterrestrial impacts.

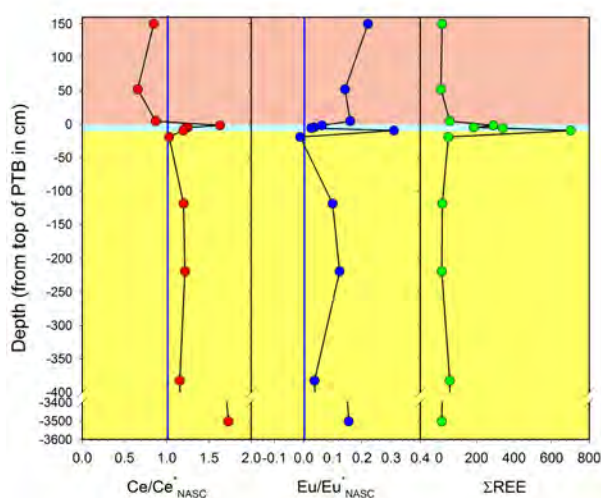


Figure 85: $(Ce/Ce^*)_{NASC}$, $(Eu/Eu^*)_{NASC}$ and ΣREE data of PT sedimentary section from Spiti valley.

In our continuing effort to understand environmental conditions which led to PT extinction, we studied the rare earth elements (REE) with the aim to understand the depositional environment before, during and after extinction event. Nearly 10-20 mg of aliquots of finely powdered samples from P-T section were digested in HF-HCl-HNO₃ in microwave

oven. Digested solutions were diluted appropriately and analyzed by ICPMS at PRL. The results are plotted in Figure 85. It can be seen that the ΣREE are higher in the ferruginous boundary layer as compared to sediments above and below. The enrichment of REE is also accompanied by Eu and Ce anomalies [Where $(Ce/Ce^*)_{NASC} = 2 \times Ce_{NASC} / (La_{NASC} + Pr_{NASC})$ and $(Eu/Eu^*)_{NASC} = \log \{ 2 \times Eu_{NASC} / (Sm_{NASC} + Gd_{NASC}) \}$] which are redox sensitive. The ferruginous layer is not only enriched in REE but also fractionated relative to chondrite with enriched LREE and nearly flat to HREE. Whereas shale below the boundary shows very different pattern with enrichment of LREE and HREE and depletion in MREE.

(V. K. Rai and A. D. Shukla)

Decadal variations in oceanic properties of the Arabian Sea since GEOSECS

This study attempts to decipher the temporal changes in the measured oceanic geochemical properties of the Arabian Sea by reoccupying several stations nearly after two decades investigated during the GEOSECS expedition (1977-78). The observed differences in the concentration of nutrients, DIC and oxygen could be affected by the water mass mixing and the remineralization processes taking into account denitrification and anthropogenic CO₂. On comparison with GEOSECS data, depth-profiles of nitrate and dissolved oxygen show significant variations while silicate and phosphate show only marginal changes. Differences in the nutrients since GEOSECS indicate increase in productivity in the Arabian Sea during two decades.

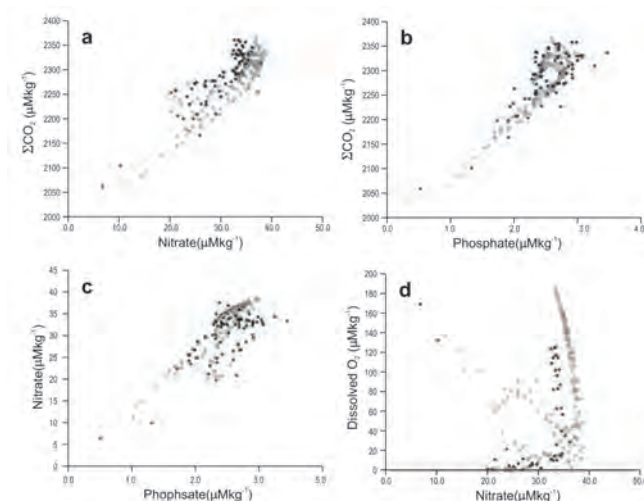


Figure 86: Relative changes in two decades for ΣCO_2 , nutrients (nitrate and phosphate) and dissolved oxygen for GEOSECS (open circles) and SS-164 cruise (filled circles) in the Arabian Sea. (a) ΣCO_2 versus nitrate showing reduction of nitrate mainly in deeper water; (b) ΣCO_2 versus phosphate showing no discernible shift; (c) nitrate versus phosphate; and (d) dissolved oxygen versus nitrate showing distinct reduction in deep water nitrate.

Increased inventory of radiocarbon in the top 1000 m can be understood in terms of atmosphere-ocean transfer and vertical diffusion of bomb radiocarbon due to the penetration of bomb radiocarbon since 1950's. This study indicates increase in the biological pump due to the nutrient delivery via ocean circulation.

This work was carried out along with Dr. K. Dutta, presently at Northwestern University, Evanston, USA and Dr. R. Agnihotri presently at National Physical Laboratory, Delhi, India.

(R. Bhushan, R. Rengarajan and S. P. Singh)

Radiocarbon dating of groundwaters from Jaisalmer, Rajasthan

Radiocarbon is an important tool for dating of groundwaters. The age of dissolved inorganic carbon cannot be directly translated into the age of the groundwater and thus a correction must be applied to obtain the age of the groundwater. The correction is required for hydrochemical effects of dilution of soil CO₂ by non-radiogenic

carbon and by precipitation and dissolution of carbonate minerals. The present research work is aimed to reconstruct paleotemperature (past-temperature) records from groundwater samples of Rajasthan in India to understand the discrepancy existing for glacial-interglacial temperature changes between continental and other records. Some of the oldest dated groundwater in India has been found in Rajasthan, which are very suitable for such studies. In this work concentrations of He, Ne, Ar, Kr and Xe would be used to determine the temperature of recharge in groundwaters. The different models used for correction of radiocarbon ages were based on isotope mixing (Pearson), NETPATH model and Vogel's model. Some of the preliminary results from the radiocarbon dating of groundwaters from the Jaisalmer district of Rajasthan shows that corrected radiocarbon ages based on these models range from ~800 to 25000 years with corrections of 1400-6700 years.

This work is carried out along with Mr. D. Balaji presently at M.S. University of Baroda, Vadodara and with Dr. J. S. Rathore from Department of Chemistry J.N. Vyas University, Jodhpur.

(R. Bhushan and A. K. Sudheer)

SCIENCE

Theoretical and Computational Physics

Nuclear charge radii of Ra isotopes

Nuclear charge radii in a number of radium (Ra) isotopes due to proton distribution are evaluated to 5% accuracy by combining the recently measured isotope shifts in Ra ion with our atomic structure calculations using the relativistic coupled-cluster (RCC) method. Also, the effects of nuclear deformations, a more realistic nuclear Fermi distribution, and higher-order effects have been accounted in this investigation. Our obtained values of relative root mean square charge radii of the considered isotopes will be very useful for the studies of atomic parity violation in a chain of Ra isotopes.

This work is done in collaboration with L. Wansbeek, S. S. Schlessler, A. E. L. Dieperink, C. J. G. Onderwater, and R. G. E. Timmermans of KVI, University of Groningen, The Netherlands.

(B. K. Sahoo)

Determination of Nuclear Moments

We have reported nuclear octupole moment (Ω) of ^{137}Ba for the first time. Hyperfine structure constants are measured to very high precision in the $5d\ ^2D_{3/2}$ state of $^{137}\text{Ba}^+$ ion. Combining these results with the corresponding diagonal and off-diagonal matrix elements of the hyperfine interaction Hamiltonian, we obtained $\Omega = -0.04885(53)\ \mu N \times b$. This value significantly differs from the nuclear shell-model predicted value $\Omega = +0.0385\ \mu N \times b$ along with its sign. Similarly,

we have reexamined the nuclear quadrupole moments of ^{39}K , ^{40}K and ^{41}K , the three stable isotopes of potassium atom, combining our theoretical calculations with the available experimental values of the hyperfine structure constants and ratios of nuclear quadrupole moments (Qs) in the above isotopes. Our analysis reveals that $Q(^{39}\text{K})$, $Q(^{40}\text{K})$ and $Q(^{41}\text{K})$ values are $0.0614(6)\ b$, $-0.0764(8)\ b$ and $0.0747(7)\ b$, respectively, against the previously reported their corresponding literature values as $0.0585(6)b$, $-0.0749(19)b$ and $0.0733(18)b$, respectively. We also argued from our analysis that some of the reported experimental hyperfine structure constants are not correct within their error bars.

This work has been carried out in collaboration with N. C. Lewty, B. L. Chuah, R. Cazan and M. D. Barrett of Centre for Quantum Technologies and Department of Physics, National University of Singapore, Singapore.

(B. K. Sahoo, Y. Singh and D. Nandy)

Magic wavelengths for alkali atoms

Knowledge of magic wavelengths for alkali-metal atoms is very important for trapping and manipulating these atoms by the gradient forces of light waves. By studying the dynamic polarizabilities for the linearly and circularly polarized lights in the ground and first two excited states in Li, Na, K and Rb atoms, we have predicted many magic wavelengths for these atoms. We have explicitly demonstrated the cases where the linearly and/or the circularly polarized lights will be useful. We found that circularly polarized light is not

suitable for trapping Li atoms. We also proposed the use of a switch trapping scheme for the magic wavelengths at which the state-insensitive trapping is supported only for either positive or negative m_j sublevels.

This work is carried out in collaboration with B. Arora of Department of Physics, Guru Nanak Dev University, Punjab, India and B. P. Shah of Department of Physics, University of Baroda, Vadodra, India.

(B. K. Sahoo, D. Nandy and Y. Singh)

Theoretical insight to the inconsistent experimental results of the ground state quadrupole polarizability of Ba^+

(N. Singh)

We carried out analysis of the calculated and experimental results of the ground state quadrupole polarizability in Ba^+ . We found that all three reported measurements of this quantity are not reliable enough to test the validity of the calculated results. On the basis of different physical considerations, we propose new theoretical and experimental studies of the quadrupole polarizabilities of the 5D states of this ion to test the accuracies of the E2 matrix elements between the ground and the 5D excited states. These results can be used further to find the most precise value of the ground state quadrupole polarizability of Ba^+ .

This work is carried out in collaboration with B. P. Das of Indian Institute of Astrophysics, Bangalore, India.

(B. K. Sahoo)

An Investigation on the microscopic origin of YRZ theory

We are investigating the microscopic foundation of the Yang-Rice-Zhang phenomenological model of the pseudogap state of high T_c cuprate superconductors. To this end we are analyzing the Pole-Zero mechanism proposed by a Japanese theorist Imada which has support from numerical studies also. There are deep connections between Pole-Zero mechanism and YRZ ansatz and we are analyzing them with the calculations of various observable properties of the pseudogap state like, density of states, spectral function, behaviour of Green's function etc.

This study was done in collaboration with G. Bhaskaran of IMSc, Chennai.

(N. Singh)

Yang-Rice-Zhang (YRZ) phenomenological theory

Optical conductivity of the cuprate $Ca_{2-x}N_xCuO_2Cl_2$ (CNCOC) was computed using Kubo formula using an

analytical form of electron Greens function proposed (ansatz) by Yang-Rice-Zhang (YRZ) for the underdoped cuprates based on their previous renormalized mean field theory. Our theoretical analysis done on a specific experimental work (K. Waku et al. 2004 [1]) shows that YRZ model does not reproduce experimentally observed doping and temperature evolution of various Drude-Lorentz parameters (in some cases not even qualitatively). However, it does reproduce the shifting of pseudogap peak to lower energy scale with increasing doping as captured by Lorentz frequency. Our analysis shows that YRZ phenomenological model although quite successful in photoemission spectroscopy needs further improvements in addressing the charge transport in CuO_2 planes.

Generalized top-spin analysis and new physics in e^+e^- collisions with beam polarization

A generalized top-spin analysis proposed some time ago in the context of the Standard Model and subsequently studied in varying contexts is now applied primarily to the case of $e^+e^- \rightarrow t\bar{t}$ with transversely polarized beams. This extends recent work with new physics couplings of scalar (S) and tensor (T) types. A comprehensive analysis assuming only the electron beam to be transversely polarized is carried out which eliminates any azimuthal angular dependence due to standard model or new physics of vector (V) and axial-vector (A) type interactions. New physics of the general four-Fermi type with V and A interactions with both beams transversely polarized is then studied including implications with longitudinal polarization. The generalized spin bases are investigated in the presence of either longitudinal or transverse beam polarization to look for appreciable deviation from the SM prediction in case of the new physics. It is found that beamline basis combined with transverse polarization provides an excellent window of opportunity both for S , T and V , A new physics. The helicity basis is shown to be the best in case of longitudinal polarization to look for new physics effects due to V and A interactions.

This work was done in collaboration with B. Ananthanarayan, J. Lahiri and M. Patra of CHEP, Indian Institute of Science, Bangalore.

(S. D. Rindani)

Colour electric and magnetic dipole couplings of the top quark and signals at hadron colliders

The top quark, which is copiously pair produced at hadron colliders serves as a useful tool for studying possible new physics. The possibility of measuring at hadron colliders anomalous couplings of the top quark to gluons which are of the chromoelectric or chromomagnetic type is examined. Analytic expressions are obtained for parton level

top polarization in the presence of anomalous couplings. Asymmetries which can separately measure the CP-even magnetic and CP-odd electric couplings are suggested for the Tevatron ($p\bar{p}$) and the LHC (pp) colliders. The sensitivities for realistic energies and luminosities are obtained in each case.

This work was done in collaboration with S. Biswal of the Orissa University of Agriculture and Technology, Bhubaneswar, and P. Sharma of KIAS, Seoul, S.Korea.

(S. D. Rindani)

On the power spectrum generated during inflation

Recently there have been differing viewpoints on how to evaluate the curvature power spectrum generated during inflation. The primordial curvature power spectrum is the seed for structure formation and provides a link between observations and inflationary parameters. Therefore it is important to resolve any disagreements over the expression for the power spectrum. We have studied the differing viewpoints and indicated inconsistencies in these recently proposed approaches. We then provide arguments as to why the standard expression is valid.

This work was done in collaboration with Arjun Berera of University of Edinburgh, UK and Mar Bastero-Gil of Universidad de Granada, Spain.

(N. Mahajan and R. Rangarajan)

Neutrino Mass Hierarchy and Octant Determination with Atmospheric Neutrinos

The recent discovery by the Daya-Bay and RENO experiments, that the third lepton mixing angle is nonzero and relatively large, significantly impacts existing experiments and the planning of future facilities. In many scenarios, the nonzero value of the third angle implies that 2-3 mixing is likely to be different from 45 degrees. Additionally, large detectors will be sensitive to matter effects on the oscillations of atmospheric neutrinos, making it possible to determine the neutrino mass hierarchy and the octant of the 2-3 mixing. We show that a 50 kT magnetized liquid argon neutrino detector can ascertain the mass hierarchy with a significance larger than 4 sigma with moderate exposure times, and the octant at the level of 2-3 sigma with greater exposure.

This work was done in collaboration with Vernon Barger from University of Wisconsin, R. Gandhi and P. Ghoshal from Harish Chandra Research Institute, D. Marfatia from University of Kansas, S. Prakash, S. Raut and S. Umasankar from Indian Institute of Technology, Mumbai.

(S. Goswami)

Two Zero Mass Matrices and Sterile Neutrinos

Recent experimental data is indicative of the existence of sterile neutrinos. The minimal scheme that can account for the data and is consistent with cosmological observations is the 3+1 picture which consists of three predominantly active and one predominantly sterile neutrino with the fourth neutrino being heavier than the other three. Within this scheme there are two possibilities depending on whether the three light states obey normal or inverted hierarchy. In this paper we consider the two zero textures of the low energy neutrino mass matrix in presence of one additional sterile neutrino. We find that among 45 possible two zero textures for this case, 15 are consistent with all current observations. Remarkably, these correspond to the two-zero textures of a three active neutrino mass matrix. We discuss the mass spectrum and the parameter correlations that we find in the various textures. We also present the effective mass governing neutrinoless double beta decay as a function of the lowest mass.

(S. Goswami, M. Ghosh and S. Gupta)

Vacuum Stability constraints on the minimal singlet TeV Seesaw Model

We consider the minimal seesaw model in which two gauge singlet right handed neutrinos with opposite lepton numbers are added to the Standard Model. In this model, the smallness of the neutrino mass is explained by the tiny lepton number violating coupling between one of the singlets with the standard left-handed neutrinos. This allows one to have the right handed neutrino mass at the TeV scale as well as appreciable mixing between the light and heavy states. This model is fully reconstructible in terms of the neutrino oscillation parameters apart from the overall coupling strengths. We show that the overall coupling strength for the Dirac type coupling between the left handed neutrino and one of the singlets can be restricted by consideration of the stability bounds on the electroweak vacuum. Incorporating this bound, the overall coupling strength of the small lepton number violating coupling can also be constrained from neutrino oscillation data. In this scenario the lepton flavor violating decays of charged leptons can be appreciable which can put further constraint on the coupling, for right-handed neutrinos at TeV scale. We discuss the combined constraints on the coupling strength for this scenario from the process muon going to electron and photon from the consideration of vacuum stability constraints on the Higgs self coupling. We also briefly discuss the implications for neutrinoless double beta decay and possible signatures of the model that can be expected at colliders.

This work was done in collaboration with S. Roy from IACS, Kolkata.

(S. Goswami and S. Khan)

Octant sensitivity in atmospheric and long baseline neutrino experiment

One of the unknown parameters in neutrino oscillations is the octant of the 2-3 mixing angle. We studied the possibility of determining the octant of this angle in the long baseline experiments T2K and NOvA in conjunction with future atmospheric neutrino detectors, in light of non-zero value of the third mixing angle measured by reactor experiments. We consider two detector technologies for atmospheric neutrinos - magnetized iron calorimeter and non-magnetized Liquid Argon Time Projection Chamber. We present the octant sensitivity for T2K/NOvA and atmospheric neutrino experiments separately as well as combined. For the long baseline experiments, a precise measurement of the third angle, which can exclude degenerate solutions in the wrong octant, increases the sensitivity drastically. For favourable parameters 2 sigma sensitivity can be achieved by T2K+NOvA for all values of CP phases for both normal and inverted hierarchy. For atmospheric neutrinos, the moderately large value of the third angle measured in the reactor experiments is conducive to octant sensitivity because of enhanced matter effects. A magnetized iron detector can give a 2 sigma octant sensitivity for 500 kT yr exposure for a 2-3 mixing angle of 39 degrees and normal hierarchy. This increases to 3 sigma for both hierarchies by combining with T2K+NOvA. A Liquid Argon detector for atmospheric neutrinos with the same exposure can give higher octant sensitivity, due to the interplay of muon and electron contributions and superior resolutions.

(S. Goswami, P. Ghoshal and S. Raut)

$\mu - \tau$ symmetry and recently measured reactor angle

Viability of the $\mu - \tau$ interchange symmetry imposed as an approximate symmetry (1) on the neutrino mass matrix $\mathcal{M}_{\nu f}$ in the flavour basis (2) simultaneously on the charged lepton mass matrix M_l and the neutrino mass matrix M_ν and (3) on the underlying Lagrangian is discussed in the light of recent observation of a non-zero reactor mixing angle θ_{13} . In case (1), $\mu - \tau$ symmetry breaking may be regarded as small (less than 20-30%) only for the inverted or quasidegenerate neutrino mass spectrum and the normal hierarchy would violate it by a large amount. The case (2) is more restrictive and the requirement of relatively small breaking allows only the quasidegenerate spectrum. If neutrinos obtain their masses from the type-I seesaw mechanism then small breaking of the $\mu - \tau$ symmetry in the underlying Lagrangian may result in a large breaking in $\mathcal{M}_{\nu f}$ and even the hierarchical neutrino spectrum may also be consistent with mildly broken $\mu - \tau$ symmetry of the Lagrangian. Neutrinoless double beta decay provides a good means of distinguishing above scenarios. In particular, non-observation of signal in future experiments such as GERDA would rule out scenarios (1) and (2).

This work was done in collaboration with Ketan M. Patel, TIFR, Mumbai and Shivani Gupta, Yonsei University, Seoul, Korea.

(A.S. Joshipura)

Pseudo-Dirac neutrinos via mirror-world and depletion of UHE neutrinos

We propose a possible explanation of the non-observation of muon neutrino events at IceCube coincident with GRB gamma ray at the rates predicted by the standard Bahcall-Waxman model, in terms of neutrino oscillations. Our model is based on assuming that (a) all neutrinos are pseudo-Dirac particles and (b) there exists a mirror world interacting gravitationally with the observed world. This scenario has three sterile neutrinos associated with each flavour of ordinary neutrinos. Very tiny mass splitting between these neutrinos is assumed to arise from lepton number violating dimension five Planck scale suppressed operators. We show that if a mass splitting of 10^{-15}eV^2 is induced between the four mass eigenstates of a given species, then its flux will be suppressed at IceCube energies by a factor of 4 which could be the explanation of the IceCube observation that the muon neutrino flux is lower than the Waxman-Bahcall limit by at least a factor of 3.7. Hierarchies in mass splitting among different flavours may result in different amount of suppression of each flavour and based on this, we predict a difference in the flavour ratios of the observed neutrinos which is significantly different compared to the standard three flavour prediction which could serve as a test for this model.

This work was done in collaboration with S. Pakvasa, University of Hawaii, U.S.A.

(A.S. Joshipura and S. Mohanty)

Explanation for the low flux of high energy astrophysical muon-neutrinos

We consider the possibility that some exotic neutrino property is responsible for reducing the muon neutrino flux at high energies from distant neutrino sources; specifically, we consider (i) neutrino decay and (ii) neutrinos being pseudo-Dirac particles. This would provide a mechanism for the lack of high energy muons in the Icecube detector.

This work was done in collaboration with S. Pakvasa, University of Hawaii, U.S.A.

(A.S. Joshipura and S. Mohanty)

Can Neutrinos travel faster than light?

The OPERA collaboration at Gran Sasso, Italy claimed that energetic neutrinos have superluminal speeds, which prompted many activities to interpret this data without conflicting with our basic notion of causality. It was argued that if there is violation of Lorentz invariance in nature, then neutrinos can have maximum attainable velocity, which is different from that of light. In that case neutrinos can be superluminal without violating causality principle. We then used the conservation of energy and momentum and the cosmic ray data from Ice-Cube and Baksan, to show that if the neutrinos are superluminal, then the decays of the pions could not have produced the neutrinos that have been observed at OPERA. In other words, our analysis show that the stringent constraint on the superluminal speed of the neutrinos from pion decay is much stronger than what is required to explain the OPERA result, and hence, OPERA could not have seen any superluminal neutrinos. We strengthened our result by estimating the matrix elements for the pion decays for superluminal neutrinos and improved the bound. Our result have been subsequently confirmed by the next run of the OPERA experiment.

This work has been carried out in collaboration with R. Cowsik and T. Madziwa-Nussinov, Washington University in St. Louis, U.S.A. and S. Nussinov, Tel Aviv University, Israel.

(U. Sarkar)

Proton decay induced baryogenesis

The grand unified theories predicted proton decay, which could also explain the baryon asymmetry of the universe. But subsequently it was shown that this proton decay conserves baryon-minus-lepton number violation, and hence, the sphalerons will erase the generated asymmetry. A successful baryogenesis theory requires a baryon-minus-lepton number violation for this to work before the electroweak phase transition. We show that the baryon-minus-lepton number violation could also exist in some proton decay modes, which in turn, can generate the cosmological baryon asymmetry. Specifically, the mechanism for the generation of the baryon asymmetry of the universe requires a baryon-minus-lepton number violation that can also mediate a testable proton decay.

This work has been carried out jointly with P. Gu, Max-Planck-Institut für KernPhysik, Heidelberg, Germany.

(U. Sarkar)

Domain growth in chiral phase transition: role of inertial dynamics.

We investigate the kinetics of phase transitions for chiral symmetry breaking in heavy-ion collisions. We use a Langevin

description for order-parameter kinetics in the chiral transition. The Langevin equation of motion includes *dissipation* and an *inertial term*. We study the ordering dynamics subsequent to a quench from the massless quark phase to the massive quark phase, and discuss the effect of inertia on the growth kinetics.

This work is being pursued in collaboration with A. Singh and S. Puri from School of Physical Sciences, Jawaharlal Nehru University, New Delhi.

(H. Mishra)

Bulk and Shear viscosities of hot and dense quark matter

The viscous coefficients of hot and dense quark matter is estimated using Kubo formula for the transport coefficient. We have estimated this within Polyakov loop extended Nambu-Jona Lasinio model (PNJL) with the effect of confinement being included in the four fermion interaction model. The coefficients are calculated using relaxation time approximation. The effect of polyakov loops at finite temperature and chemical potential on these transport coefficients is investigated.

(P. Deb and H. Mishra)

Bulk and Shear viscosity coefficient in Hadron gas.

The results for quark matter viscos coefficients have been complemented by an estimation of the same using hadron resonance gas model. We estimate this both at finite temperature and chemical potential. This will be relevant for viscos hydrodynamics calculations for the expansion of matter following a heavy ion collision for the beam energy scan experiments in RHIC as well as heavy ion collision experiments at FAIR at GSI, Darmstadt.

This work was done in collaboration with A. Mishra of IIT, New Delhi.

(G. Kadam and H. Mishra)

Thermal conductivity of quark matter.

One of the important transport coefficient of quark matter at finite baryon density is the thermal conductivity apart from the other dissipative transport coefficients like viscosity. We estimate the thermal conductivity of quark matter using a spectral function approach in the ambit of PNJL model.

(P. Deb, R. Mohapatra, A. Mishra and H. Mishra)

Synchronization of coupled nonidentical dynamical systems

We analyze the stability of synchronized states for coupled nearly identical dynamical systems on networks by deriving an approximate Master Stability Function (MSF), which allows us to calculate the stability of synchronized state on a network. Using this MSF we treat the problem of designing a network having the best synchronizability properties. We find that the edges which connect nodes with a larger relative parameter mismatch are preferred and the nodes having values at one extreme of the parameter mismatch are preferred as hubs.

(S. Acharyya and R. E. Amritkar)

Experimental evidences of synchronization of time-varying dynamical network

We investigate synchronization of time-varying networks and derive stability conditions. We derive interesting relations between the critical coupling constants for synchronization and switching times for time-varying and time average networks. The relations are based on the additive property of Lyapunov exponents and all are verified experimentally in electronic circuit. This is the first experimental demonstration of synchronization in time varying networks.

This work was done in collaboration with S.K.Bhowmick and S.K. Dana of Central Instrumentation, CSIR-Indian Institute of Chemical Biology, Kolkata.

(R. E. Amritkar)

Extreme event-size fluctuations in biased random walks on networks

Random walk on discrete lattice models is important to understand various types of transport processes. Using random walk model for transport extreme events, defined as exceedences of the flux above a prescribed threshold, have been studied recently in the context of complex networks. This is motivated by the extreme events such as the traffic jams, floods, power black-outs that take place on networks. In this work, we study the extreme events in a generalized random walk model in which the walk is preferentially biased by the network topology. The walkers preferentially choose to hop toward the hubs or small degree nodes. In this setting, we show that the probability for the occurrence of extreme events on any node in the network depends on its 'strength', a measure of the ability of a node to attract walkers, which is a function of the degree of the node and that of its neighbours. We obtain analytical and simulation results for the probability of extreme events on the nodes of a network using the generalized random walk model. The result reveals that the nodes with larger value of strength, on an average, display lower probability for the occurrence of extreme events compared to the nodes with lower value of strength. In particular, we obtain the distribution of event sizes on the network. This shows that extremely large fluctuations

in event-sizes are possible on small degree nodes when the walkers are biased toward the hubs.

This work was done in collaboration with M.S. Santhanam of IISER, Pune.

(V. Kishore, R. E. Amritkar)

Amplitude death in complex networks induced by environment

We present a mechanism for amplitude death in coupled nonlinear dynamical systems on a complex network having interactions with a common environment-like external system. We develop a general stability analysis that is valid for any network topology and obtain the threshold values of coupling constants for the onset of amplitude death. An important outcome of our study is a universal relation between the critical coupling strength and the largest non-zero eigenvalue of the coupling matrix. Our results are fully supported by the detailed numerical analysis for different network topologies.

This work was done in collaboration with V. Resmi, G. Ambika IISER, Pune and G. Rangarajan of IISc, Bangalore.

(R. E. Amritkar)

Embedded Unitary Ensembles with $U(\Omega) \otimes SU(r)$ Embedding generated by Random Two-body Interactions with $SU(r)$ Symmetry

Following the earlier studies by PRL group on embedded unitary ensembles generated by random two-body interactions [EGUE(2)] with spin $SU(2)$ and spin-isospin $SU(4)$ symmetries, developed is a general formulation, for deriving lower order moments of the one- and two-point correlation functions in eigenvalues, that is valid for any EGUE(2) and BEGUE(2) ('B' stands for bosons) with $U(\Omega) \otimes SU(r)$ embedding and generated by two-body interactions preserving $SU(r)$ symmetry. Using this formulation with $r = 1$, we recover the results derived by Asaga et al [Ann. Phys. (N.Y.) **297**, 344 (2002)] for spinless boson systems. Going further, new results are obtained for $r = 2$ (this corresponds to two species boson systems) and $r = 3$ (this corresponds to spin one boson systems). This work unifies all the work done before in deriving analytical results for EGUE and BEGUE and has generated several additional new results.

This work was done in collaboration with Dr. (Mrs) Manan Vyas (Washington State University, Pullman, USA.)

(V. K. B. Kota)

Deformed Shell Model Results for Neutrinoless Positron Double Beta Decay of ^{64}Zn , ^{74}Se , ^{78}Kr and ^{84}Sr nuclei

Nuclear matrix elements for the neutrinoless positron double beta decay ($0\nu\beta^+\beta^+$ and $0\nu\beta^+EC$) for ^{64}Zn , ^{74}Se , ^{78}Kr and ^{84}Sr , that are the only candidate nuclei in the $A=60-90$ region, are calculated within the framework of the deformed shell model (DSM) based on Hartree-Fock states. DSM was developed by PRL-Berhampur group many years back. Experimental searches are in progress for these nuclei in some laboratories in Europe, Russia and South Korea. For ^{64}Zn , GXPF1A interaction in $1f_{7/2}$, $2p_{3/2}$, $1f_{5/2}$ and $2p_{1/2}$ space with ^{40}Ca core is employed. Similarly for ^{74}Se , ^{78}Kr and ^{84}Sr nuclei, a modified Kuo interaction in $2p_{3/2}$, $1f_{5/2}$, $2p_{1/2}$ and $1g_{9/2}$ space with ^{56}Ni core is employed. Spectroscopic properties such as energy spectra, electric quadrupole and magnetic dipole transitions strengths and occupancies of single particle orbitals are first studied using DSM. Going further, the deduced half-lives, assuming neutrino mass is 1eV , are $\sim 10^{28}$ for $\beta^+\beta^+$ mode and $\sim 10^{27}$ for β^+EC mode. These are first predictions for neutrinoless double beta decay for positron modes in $A=60-90$ region using DSM.

This work was done in collaboration with R. Sahu, (Berhampur University, Berhampur, Orissa).

(V. K. B. Kota)

Quantum Phase Transitions in a Class of Interacting boson models of nuclei.

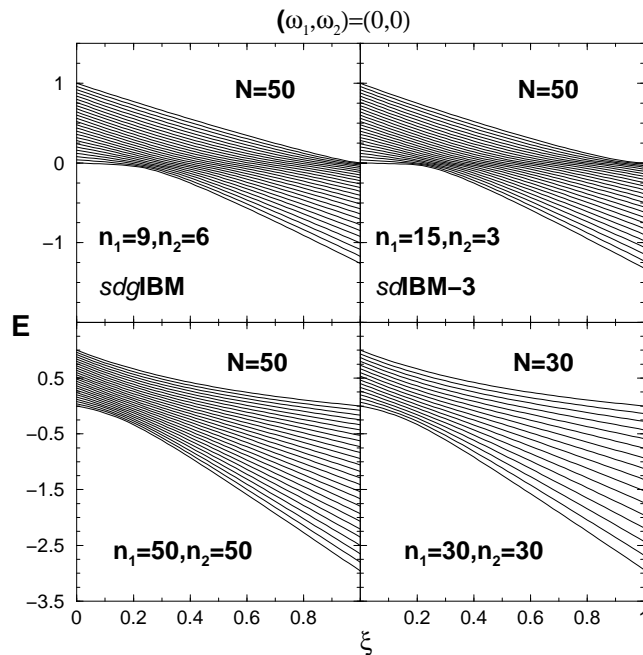


Figure 87: Spectra as a function of the mixing parameter ξ for: (i) $(n_1, n_2)=(9,6)$ and $(15,3)$ with $N=50$; (ii) $(n_1, n_2) = (50,50)$ with $N = 50$; (iii) $(n_1, n_2) = (30,30)$ with $N = 30$. All results are shown for $(\omega_1, \omega_2) = (0, 0)$. The two figures in the upper part show QPT and those in the lower part show no QPT.

Quantum phase transitions (QPT) - that is phase transitions that occur at zero temperature as a function of a coupling

constant - have become very important as the concept of QPT can be used in mesoscopic systems, that is systems with finite number of particles such as nuclei, molecules, atomic clusters and so on. These are being studied in nuclei employing interacting boson models (IBMs). Starting with $U(n)$ spectrum generating algebra (SGA), one general group structure admitted by large class of IBMs of nuclei including $sdIBM$, $spIBM$, $spdIBM$, $sdgIBM$, $sdpfIBM$, $sdgpfIBM$, $sdIBM-2$ (proton-neutron IBM), $sdIBM-3$ [IBM with bosons carrying isospin $T = 1$ degree of freedom] and $sdIBM-4$ [IBM with bosons carrying spin-isospin (ST) degrees of freedom with $(ST) = (10) + (01)$] is: $U(n) \supset G \supset SO(n_1) \oplus SO(n_2) \supset K$ where $n = n_1 + n_2$ with (A) $G = U(n_1) \oplus U(n_2)$ or (B) $G = SO(n)$. A simple Hamiltonians preserving $SO(n_1)$ and $SO(n_2)$ quantum numbers ω_1 and ω_2 respectively [combined they are denoted by (ω_1, ω_2)] but mixing (A) and (B) algebras consists of the number operator for $U(n_1)$ [or $U(n_2)$] and the pairing operator that is invariant with respect to $SO(n)$. A mathematical formulation developed many years back by PRL group is used to carry out numerical calculations as a function of the mixing parameter ξ for many different values for (n_1, n_2) and the boson number N . Some results are shown in Figure 87. Results show that for $N \gg n_1 + n_2$ the systems exhibit second order QPT, i.e. only in the dense limit boson systems exhibit QPT. Let us add that the importance of the dense limit of boson systems was also brought out by the work in the last decade by PRL group on quantum chaos and random matrix theory. Second order QPT seen in the upper part of Figure 87 was also verified by constructing a generalized coherent state for the system. Proceeding further, QPT in IBMs with $U(n) \supset G' \supset SO(n_1) \otimes SO(n_2) \supset K'$ where $n = n_1 n_2$ and (C) $G = U(n_1) \otimes U(n_2)$ or (D) $G = SO(n)$ algebras, is being analyzed using a Hamiltonian mixing (C) and (D) with fixed $SO(n_1)$ and $SO(n_2)$ quantum numbers.

(V. K. B. Kota)

Higher order correlations in the spectra of interacting trapped bosons

Continuing with the study reported last year, for a interacting trapped boson system with parameters appropriate for ^{87}Rb atoms in JILA trap, measures for higher order correlations in spectral fluctuations are studied this year. For 5000 bosons and focusing on lowest 100 levels, calculated is the q -th order correlation function $C_q(n)$ for $1 < q \leq 10$ using a two-fold averaging. Numerical results clearly showed that the level fluctuations follow GOE random matrix predictions even to higher orders, i.e. logarithmic correlation structure is seen instead of multi-scaling structure in the $C_q(n)$ results. This result is significant as interacting trapped boson systems are of experimental relevance.

This work was done in collaboration with Dr. (Mrs) Barnali Chakrabarti (Kalyani University, Kolkata.)

(V. K. B. Kota)

Large Shell Model Description of Sulfur isotopes

Neutron rich Sulfur isotopes exhibit quadrupole collectivity (deformation and γ -soft structure), shape coexistence, erosion of $N=28$ (N is neutron number) shell gap and so on. Following this, most recently available experimental data on low-lying energy levels of Sulfur isotopes ^{35,37,39,41}S have been interpreted by performing large shell model calculations using the modern $sd - pf$ interaction SDPF-U from the Madrid-Strassburg group. For the S isotopes protons and neutrons are restricted to the sd shell for $N < 20$ and neutrons start filling fp shell for $N > 20$. The low-energy spectra and electric quadrupole transition probabilities are successfully reproduced by employing $0p - 0h$ excitations (i.e. only in-shell mixing) for normal parity states and $1p - 1h$ excitations (i.e. inter-shell neutron excitations) for opposite parity states.

This work was done in collaboration with P.C. Srivastava (Instituto de Ciencias Nucleares, UNAM, Mexico.)

(V. K. B. Kota)

Curl-free vector potential observation on the macro-scale and a new dimension to the Lorentz trajectory

The recently reported curl-free vector potential observation on the macro-scale, which has been attributed to a macro-scale matter wave associated with the quantum modulation of the de Broglie wave along the magnetic field is seen to be in apparent contravention with the Lorentz equation of classical electrodynamics which as a descriptor on the macro-scale takes no cognizance of a curl-free vector potential. The two different formalisms— a deterministic one 'a la Lorentz and a probabilistic one by the quantum modulation—both existing on the macro-scale and, though in apparent contravention, complement each other and are essential for a complete description of all phenomena relating to charged particle dynamics. The quantum modulations which arise in consequence of transition across Landau levels appear as 'hole' auto-excitations in the Lorentz trajectory involving internal inelastic scattering. This lends a new dimension to the Lorentz trajectory which, though on the classical macro-scale, acts like a 'quantum resonator' and can now exist in a number of self-excited states labelled by the Landau level interval involved in the excitation, and which are of quantum origin and on the macro-scale, with the quantum modulations being the excitations.

(R.K. Varma)

A novel interferometric mass spectrometry concept

A novel mass spectrometry concept is presented here which is based on interferometric principle using a newly discovered matter wave on the macro-scale for charged particle moving in a magnetic field. The wave length of the matter wave involves

the mass of the ions which feature can be used for mass discrimination in the same manner as photon interferometry is used for discriminating the different wave lengths of light. The concept involves injecting the ions of a given sample consisting of isotopes of a certain element to be discriminated, along a uniform magnetic field and varying the magnetic field which sweeps through the various interference peaks. The different masses are then identified through the location of their interference peaks which are mass dependent because of the mass dependence of the associated macro-scale matter wave lengths.

(R.K. Varma)

A one-dimensional macro-scale matter wave dynamics embedded in the classical Lorentz trajectory

A rather curious revelation has come about whereby some observed phenomena in charged particle dynamics in a magnetic field on the macro-scale have been found to correspond very closely to one dimensional quantum phenomena pertaining to passage of particle over one-dimensional potential humps. Both the transmitted and reflected currents exhibit characteristics which bear close similarity to the quantum mechanical transmission and reflection coefficients as a function of the particle energy, when the energy exceeds the height of the potential hump. The observed characteristics have already been identified as macro-scale matter wave interference effects. Also observed is a curl-free vector potential on the macro-scale and in one dimension, which has not yet been recognized as being observable quantum mechanically. Well known as the Aharonov-Bohm effect, it is known to require a minimum of two dimensions. It thus stands revealed, quite curiously and paradoxically, that there exists embedded in the classical Lorentz trajectory a matter wave dynamics on the macro-scale.

(R.K. Varma)

Kelvin-Helmholtz instability in a strongly coupled dusty plasma medium

The Kelvin-Helmholtz (KH) instability in the context of strongly coupled dusty plasma medium has been investigated. In particular, the role of transverse shear and the compressional acoustic modes in both the linear and nonlinear regimes of the KH instability has been studied. It is observed that in addition to the conventional nonlocal KH instability, there exists a local instability in the strong coupling case. The interplay of the KH mode with this local instability shows up in the simulations as an interesting phenomenon of recurrence in the nonlinear regime. Thus, a cyclic KH instability process is observed to occur. These cyclic events are associated with bursts of activity in terms of transverse and compressional wave generation in the medium.

This work was done in collaboration with S. K. Tiwari, A. Das, B.G. Patel and P.K. Kaw from IPR.

(D. Angom)

(D. Angom)

Electric dipole polarizability from perturbed relativistic coupled-cluster theory: Application to neon

We develop a method based on the relativistic coupled-cluster theory to incorporate a perturbative interaction to the no-pair Dirac-Coulomb atomic Hamiltonian. The method is general and suitable to incorporate any perturbation Hamiltonian in a many-electron atom or ion. Using this perturbed relativistic coupled-cluster (PRCC) theory, we calculate the electric-dipole polarizability of neon. The linearized PRCC results are in very good agreement with the experimental value. However, the results of the nonlinear PRCC theory show larger uncertainty, but they are consistent with the observations from earlier works.

This work was done in collaboration with B. K. Mani of University of South Florida.

(S. Chattopadhyay and D. Angom)

Observation of the nuclear magnetic octupole moment of ^{173}Yb from precise measurements of the hyperfine structure in the 3P_2 state

We measure hyperfine structure in the metastable 3P_2 state of ^{173}Yb and extract the nuclear magnetic octupole moment. We populate the state using dipole-allowed transitions through the 3P_1 and 3S_1 states. We measure frequencies of hyperfine transitions of the $^3P_2 \rightarrow ^3S_1$ line at 770 nm using a Rb-stabilized ring cavity resonator with a precision of 200 kHz. Second-order corrections due to perturbations from the nearby 3P_1 and 3P_1 states are below 30 kHz. We obtain the hyperfine coefficients as $A = 742.11(2)$ MHz and $B = 1339.2(2)$ MHz, which represent a two orders-of-magnitude improvement in precision, and $C = 0.54(2)$ MHz. From atomic structure calculations, we obtain the nuclear moments quadrupole $Q = 2.46(12)$ b and octupole $\Omega = 34.4(21)$ b $\times \mu_N$.

This work was done in collaboration with Alok Singh and Vasant Natarajan from IISc.

Perturbed coupled-cluster theory to calculate dipole polarizabilities of closed-shell systems: Application to Ar, Kr, Xe, and Rn

We use perturbed relativistic coupled-cluster (PRCC) theory to calculate the electric dipole polarizability of the noble-gas atoms Ar, Kr, Xe, and Rn. We also provide a detailed description of the nonlinear terms in the PRCC theory and consider the Dirac-Coulomb-Breit atomic Hamiltonian for the calculations. We find that the largest contribution from the Breit interaction to the electric dipole polarizability is 0.1%, in the case of Rn. As we go from Ar to Rn, based on the pattern in the random-phase-approximation effects, the contraction of the outermost $p_{1/2}$ orbitals due to relativistic corrections is discernible without any ambiguity.

This work was done in collaboration with B. K. Mani of University of South Florida.

(S. Chattopadhyay and D. Angom)

Formation and stability of coreless vortex dipoles in phase-separated binary condensates

We study the motion of the Gaussian obstacle potential created by a blue detuned laser beam through a phase-separated binary condensate in the pancake-shaped traps. We show that phase-separated binary condensates like ^{85}Rb – ^{87}Rb , with appropriate interaction parameters, can be used experimentally to create obstacle assisted droplet and coreless vortex dipoles. We theoretically analyze the energetic stability of condensates with normal and coreless vortices. We confirm our analytic and semi-analytic results by numerical solutions of coupled Grossa-Pitaevskii equations.

This work was done in collaboration with S. Gautam of IISc and P. Muruganadam of Bharathidasan University, Tiruchirapalli.

(D. Angom)

PUBLICATIONS

Publication in Journals

Astronomy and Astrophysics

1. Banerjee, D. P. K., Varricatt, W. P., Mathew, B., Launila, O., and Ashok, N. M., 2012, "The A-X infrared bands of Aluminum Oxide in stars—search and new detections", *ApJ. Lett.*, v. 753, p. L20, pp. 1-14.
2. Chesneau, O., Banerjee, D. P. K., Ashok, N. M., et. al. 2012, "The expanding dusty bipolar nebula around the nova V1280 Scorpi", *J. Astronom. Astrophys.*, v. 545, p. A63, pp.1-10.
3. Dewangan, L. K., Ojha, D. K., Anandarao, B. G., Ghosh, S. K., and Chakraborti, S., 2012, "Triggered Star Formation around Mid-infrared Bubbles in the G8.14+0.23 H II Region", *ApJ.*, v. 756, p. 151-162.
4. Evans, A., Banerjee, D. P. K., and Ashok, N. M., et. al. 2012, "Infrared observations of the recurrent nova T Pyxidis—ancient dust basks in the warm glow of the 2011 outburst", *Mon. Not. R. Astron. Soc.*, v. 424, p. L69–L73.
5. Maitra, C., Paul, B., and Naik, S., 2012, "Timing and broad band spectroscopy of 1A1118-61 with Suzaku", *Mon. Not. R. Astron. Soc.*, v. 420, p. 2307-2317.
6. Mathew, B., Banerjee, D. P. K., Naik, S., and Ashok, N. M., 2012, "Infrared studies of the Be star X Per", *Mon. Not. R. Astron. Soc.*, v. 423, p. 2486-2491.
7. Mathew, B., Banerjee, D. P. K., Subramaniam, A., and Ashok, N. M., 2012, "A Study of the Role of Ly β Fluorescence on O I Line Strengths in Be Stars", *ApJ.*, v. 753, p. 1-13.
8. Naik, S., and Paul, B., 2012, "Investigation of variability of iron emission lines in Centaurus X-3", *BASI*, v. 40, p. 503-514.
9. Naik, S., Maitra, C., Jaisawal, G. K., and Paul, B., 2013, "Timing and spectral properties of Be/X-ray pulsar EXO 2030+375 during a Type I outburst", *ApJ.*, v. 764, p. 158, pp. 1-9.
10. Pihajoki, M., Chandra, S., Ganesh, S., Baliyan, K. S., et. al. 2013, "Precursor Flares in OJ 287 P", *ApJ.*, v. 764, p. 1-5.
11. Provencal, J. L., Baliyan, K. S., Vats, H. O., et. al. 2012, "Empirical Determination of Convection Parameters in White Dwarfs. I. Whole Earth Telescope Observations of EC14012-1446", *ApJ.*, v. 751, p. 91-107.
12. Raj, A., Ashok, N. M., Banerjee, D. P. K., Munari, U., Valisa, P., and Dallaporta, S., 2012, "V496 Scuti(2012), an Fell nova with dust shell accompanied by CO emission", *Mon. Not. R. Astron. Soc.*, v. 425, p. 2576-2588.
13. Rao, A., Vadawale, S. V., 2012, "Why is IGR J170913624 So Faint? Constraints on Distance, Mass, and Spin from 'Phase-resolved' Spectroscopy of the 'Heartbeat' Oscillations", *ApJ. Lett.*, v. 757, p. L15, pp. 1-5.
14. Singal, A. K., 2012, "Gyro-Orbit Size, Brightness Temperature Limit and Implausibility of Coherent Emission by Bunching in Synchrotron Radio Sources", *AJ.*, v. 143, p. 1-5.
15. Singal, A. K., 2013, "Comment on Exact Expression for Radiation of an Accelerated Charge in Classical Electrodynamics", *Found. Phys.*, v. 43, p. 267-270.
16. Singal, A. K., and Singh, R. L., 2013, "Unification scheme of radio galaxies and quasars falsified by their observed size distributions", *ApJ.*, v. 766, p. 37-42.

17. Singal, A. K., and Vats, H. O., 2012, "Giant-pulse Emission from PSR B0950+08", *AJ.*, v. 144, p. 1-8.

Solar Physics

18. Kilpua, E. J., Mierla, M., Rodriguez, L., Zhukov, A., Srivastava, N., and West, M., 2012, "Estimating travel times of solar minimum coronal mass ejection from the Sun to near 1 AU using multi-spacecraft forward modelling", *Solar Phys. J.*, v. 279, p. 477-496.
19. Sharma, R. and Srivastava, N., 2012, "Presence of solar filament plasma detected in interplanetary coronal mass ejections by in-situ spacecraft", *J. Space Weather and Space Clim.*, v. 2, p. A10, pp. 1-13.
20. Vemareddy, P., Ambastha, A., and Maurya, R. A., 2012, "On the Role of Rotating Sunspots in the Activity of Solar Active Region NOAA 11158", *ApJ.*, v. 761, p. 60, pp. 1-13.
21. Vemareddy P., Ambastha A., Maurya R. A. and Chae J., 2012, "On the injection of helicity by shearing motion of fluxes in relation to Flares and CMEs", *ApJ.*, v. 761, p. 86, pp. 1-18.

Planetary Sciences and PLANEX Program

22. Chauhan, P., Kaur, P., Srivastava, N., Bhattacharya, S., Ajai., Kiran Kumar, A. S., and Goswami, J. N., 2012, "Compositional and morphological analysis of high resolution remote sensing data over central peak of Tycho crater on the moon : implications for understanding lunar interior", *Current Sci.*, v. 102, p. 1041-1046.
23. Das, J. P., Goswami, J. N., Pravdivtseva, O. V., Meshik, A. P., and Hohenberg, C. M., 2012, "Cosmogenic neon in grains separated from individual chondrules: Evidence of precompaction exposure in chondrules", *Meteor. Planet. Sci.*, v. 47, p. 1869-1883.
24. Durga Prasad, K., Bhattacharya, A., and Murty, S. V. S., 2012, "An ambient light sensing module for wireless sensor networks for planetary exploration", *Planet. Space Sci.*, v. 70, p. 10-19.
25. Gohil, V. M., Pabari, J. P., Panchal, S. R. and Nayak, V. H., 2012, "Effect of Electrode Resistance and Stray Capacitance on Measurement of Soil Properties", *IOSR J. of Engg.*, v. 2, p. 837-843.
26. Jadhav, M., Amari, S., Zinner, E., Maruoka, T., Marhas, K. K., and Gallino, R., 2012, "Multi-element isotopic analyses of presolar graphite grains from Orgueil", *Geochim. Cosmochim. Acta.*, v. 113, p. 193-224.
27. Jain, R., Awasthi, Arun K., Tripathy, Sharad C., Bhatt, Nipa J., Khan, and Parvaiz A., 2012, "Influence of Solar Flare X-rays on the habitability on the Mars", *Icarus.*, v. 220, p. 889-895.
28. Pabari, J. P., Acharya, Y. B., Desai, U. B. and Merchant, S. N., 2012, "Concept of wireless sensor network for future in-situ exploration of lunar ice using wireless impedance sensor", *Adv. Space Res.*, v. 52, p. 321-331.

29. Senthil Kumar, P., Keerthi, V., Senthil Kumar, A., Mustard, J., Gopala Krishna, B., Amitabh., Ostrach, L. R., Kring, D. A., Kiran Kumar, A. S., and Goswami, J. N., 2013, "Gullies and landslides on the Moon: Evidence for dry-granular flows", *J. Geophys. Res.*, v. 118, p. 206-223.
30. Shanmugam, M., Murty, S. V. S., Acharya, Y. B., Goyal, S. K., Arpit, R. P., Shah, B., Hait, A. K., Patinge, A. and Subramanyam D., 2013, "Alpha particle X-ray spectrometer on board Chandrayaan-2", *J. Adv. Space Res.*, v. , p. 1-11.
31. Shuanggen, J., Arivazhagan, S., and Araki, H., 2013, "New results and questions of lunar exploration from SELENE", *Chang'E-1, Chandrayaan-1 and LRO/LCROSS*, *J. Adv. Space Res.*, v. 52, p. 285-305.
32. Takamasa, A., Nakai, S., Sato, F., Toyoda, S., Banerjee D. and Ishibashi, J., 2013, "U-Th radioactive disequilibrium and ESR dating of a barite-containing sulfide crust from South Mariana Trough", *J. Quat. Geochronol.*, v. 15, p. 38-46.

Space, Atmospheric, Molecular and Laser Physics

33. Aggarwal, M., Joshi, H. P., Iyer, K. N., Kwak, Y. S., Lee, J. J., Chandra, H., and Cho, K. S., 2012, "Day-to-day variability of equatorial anomaly in GPS-TEC during low solar activity period", *J. Adv. Space Res.*, Vol. 49, p. 1709-1720.
34. Bagiya, M. S., Sridharan, R., and Sunda, S., 2013, "Pre-assessment of the strength and latitudinal extent of L-band scintillation - a case study", *J. Geophys. Res. Space Physics.*, v. 118, p. 488-495.
35. Bapna, M., Sunder Raman, R., Ramachandran, S., and Rajesh, T. A., 2013, "Airborne black carbon concentrations over an urban region in western India-temporal variability, effects of meteorology, and source regions", *Environ. Sc. and Pollution Res.*, v. 20, p. 1617-1631.
36. Bhatt, J., Kumar, A., Jaaffrey, S., and Singh, R. P., 2012, "Controlling the Flow of Microscopic Particles The Role of Beam Size", *Optics and Photonics J.*, v. 2, p. 294-299.
37. Chakrabarty, D., Bagiya, M. S., Thampi, S. V., and Iyer, K. N., 2012, "Solar EUV flux (0.1-50 nm), F10.7 cm flux, sunspot number and the total electron content in the crest region of equatorial ionization anomaly during the deep minimum Between solar cycle 23 and 24", *Ind. J. of Radio & Space Phys.*, v. 41, p. 110-120.
38. Chandra, H., Sinha, H. S. S., Patra, A. K., Das, U., Misra, R. N., Selvaraj D., and Datta, J., 2012, "Low-latitude mesospheric turbulence investigated using coordinated MST radar and rocket-borne observations from India", *J. Geophys. Res.*, v. 117, p. D22109, pp. 1-15.
39. Choudhary, R. K., Kunjukrishnapillai Rajeev, Krishna Moorthy, K., and Sridharan, R., 2013, "Ionospheric impact on the geopotential height profile of the temperature by balloon-borne GPS radiosondes?", *Geophys. Res. Lett.*, v. 40, p. 239-244.

40. Haider, S. A., 2012, "Role of X-ray flares and CME in the E region ionosphere of Mars: MGS observations", *Planet. Space Sci.*, v. 63, p. 56-61.
41. Haider, S. A., Mckenna-Lawlor, S. M. P., Fry, C. D., Jain, R. and Joshipura, K. N., "Effects of solar X-ray flares in the E region ionosphere of Mars: First model results", *J. Geophys. Res.*, v. 117, p. A05326, pp. 1-13.
42. Mundupuzhakal, J., Acharya, Y., Adhyaru, P., and Chakrabarty, B., 2012, "A Feasibility Study of Analogue and Digital Silicon Photomultiplier as an Alternative to PMT for Low Light Level Applications", *Sensors & Transducers J.*, v. 139, p. 52-62.
43. Kanaya, Y., Taketani, F., Komazaki, Y., Liu, X., Kondo, Y., Sahu, L. K., Irie, H., and Takashima, H., 2012, "Comparison of black carbon mass concentrations observed by multi-angle absorption", *Aerosol Sc. and Tech.*, v. 47, p. 1-10.
44. Kedia, S., Ramachandran, S., Rajesh, T. A., and Srivastava, R., 2012, "Aerosol absorption over Bay of Bengal during winter: Variability and sources", *Atmos. Environ.*, v. 54, p. 738-745.
45. Kedia, S., Kumar, A., and Singh, R. P., 2012, "Investigation of local structural properties of self-assembled photonic crystals by optical diffraction", *App. Phys. B*, v. 108, p. 903-907.
46. Kedia, S., Kumar, A., and Singh, R. P., 2013, "Propagation of vortex beams through self-assembled photonic crystal", *Journal of Expe Nanoscience*, v. 8, p. 249-253.
47. Kondo, Y., Ram, K., Takegawa, N., Sahu, L. K., Morino, Y., Liu, X., and Ohara, T., 2012, "Reduction of black carbon aerosols in Tokyo: Comparison of real-time observations with emission estimates", *Atmos. Environ.*, v. 54, p. 242-249.
48. Kumar, A., Banerji, J., and Singh, R. P., 2012, "Hanbury BrownTwiss-type experiments with optical vortices and observation of modulated intensity correlation on scattering from rotating ground glass", *Physical Review A*, v. 86, p. 013825, pp. 1-7.
49. Lal, S., Venkataramani, S., Srivastava, S., Gupta, S., Mallik, C., Naja, M., Sarangi, T., Acharya, Y. B., and Liu, X., 2013, "Transport effects on the vertical distribution of tropospheric ozone over the tropical marine regions surrounding India", *J. Geophys. Res., Atmos.*, v. 118, p. 1513-1524.
50. Mallik, C., Lal, S., Naja, M., Chand, D., Venkataramani, S., Joshi, H., and Pant, P., 2013, "Enhanced SO₂ concentrations observed over northern India: role of long-range transport", *Int. J. of Remote Sensing*, v. 34, p. 2749-2762.
51. Mallik C., Venkataramani, S., and Lal, S., 2012, "Study of a high SO₂ event observed over an urban site in western India, Asia-Pacific", *J. of Atmos. Sci.*, v. 48, p. 171-180.
52. Manju, G., Sridharan, R., Ravindran, Sudha., Madhav Haridas, M. K., Pant, T. K., Sreelatha, P., and Mohan Kumar, S. V., 2012, "Rocket borne in-situ Electron density and Neutral Wind measurements in the equatorial ionosphere – Results from the January 2010 annular solar eclipse campaign from India", *J. Atmos. Sol. Terr. Phys.*, v. 86, p. 56-64.
53. Ojha, N., Naja, M., Singh, K. P., Sarangi, T., Kumar, R., Lal, S., Lawrence, M., Butler, T., and Chandola, H. C., 2012, "Variabilities in ozone at a semi-urban site in the Indo-Gangetic Plain region: Association with the meteorology and regional processes", *J. Geophys. Res.*, v. 117, p. D20301, pp. 1-19.
54. Pandya, B. M., and Haider, S. A., 2012, "Meteor impact perturbation in the lower ionosphere of Mars: MGS observations", *Planet. Space Sci.*, v. 63, p. 105-109.
55. Pandya, S. H., Vaishnav, B. G., Joshipura, K. N., 2012, "Electron inelastic mean free paths in solids: A theoretical approach", *Chin. Phys. B.*, v. 21, p. 093402, pp. 1-7.
56. Pandya, S. H., Shelat, F. A., Joshipura, K. N., Vaishnav, B. G., 2012, "Electron ionization of exotic molecular targets CN, C₂N₂, HCN, HNC and BF-Theoretical cross sections", *International Journal of Mass Spectrometry*, v. 323-324, p. 28-33.
57. Ramachandran, S., and Kedia, S., 2012, "Radiative effects of aerosols over Indo-Gangetic Plain: environmental (urban vs. rural) and seasonal variations", *Environ. Sc. and Pollution Res.*, v. 19, p. 2159-2171.
58. Ramachandran S., Srivastava, R., Kedia, S., and Rajesh T.A., 2012, "Contribution of natural and anthropogenic aerosols to optical properties and radiative effects over an urban location", *Environ. Res. Lett.*, v. 7, p. 034028, pp. 1-11.
59. Ramachandran, S., Ghosh, S., Verma, A., and Panigrahi, P. K., 2013, "Multiscale periodicities in aerosol optical depth over India", *Environ. Res. Lett.*, v. 8, p. 014034, pp. 1-8.
60. Rastogi, R. G., Chandra, H., Condori, L., Abdu, M. A., Reinisch, B., Tsunoda, R. T., Maruyama, T., Khurshid Ahmed, Pant, T. K., and Prasad, D. S. V., 2012, "Abnormally large magnetospheric electric field on 9th November 2004 and its effects on the ionosphere around the world", *J. Earth Syst. Sci.*, v. 121, p. 1145-1161.
61. Rastogi, R. G., Chandra, H., Das, A. C., Sridharan, R., Reinisch, B. W., and Khurshid Ahmed, 2012, "Space weather event of 25-26 June 1998: Effects on equatorial ionosphere in midday and midnight sectors", *Earth Planet and Space*, v. 64, p. 353-360.
62. Rastogi, R. G., and Chandra, H., 2012, "Response of equatorial electrojet during the super geomagnetic storm of April 2000" *Ind. J. Radio & Space Phys.*, v. 41, p. 524-535.
63. Rastogi, R. G., Chandra, H., Das, A. C., Sridharan, R., Reinisch, B. W., and Khurshid Ahmed, 2012, "Effects of a magnetic cloud simultaneously observed on the equatorial ionosphere in midday and midnight sectors", *Earth Planets and Space*, v. 64, p. 353-360.
64. Reddy, B. S. K., Raghavendra Kumar, K., Balakrishnaiah, G., Rama Gopal, K., Reddy, R. R.,

- Sivakumar, V., Lingaswamy, A. P., Md. Arafath, S., Umadevi, K., Pavan Kumari, S., Nazeer Ahammed, Y., and Lal, S., 2012, "Analysis of Diurnal and Seasonal Behavior of Surface Ozone and Its Precursors (NO_x) at a Semi-Arid Rural Site in Southern India", *Aerosol and Air Quality Research*, v. 12, p. 1081-1094.
65. Reddy, K. K., Naja, M., Ojha, N., Mahesh, P., and Lal, S., 2012, "Influence of the boundary layer evolution on surface ozone variations at a tropical rural site in India", *J. Earth Sys. Sci.*, v. 121, p. 911-922.
66. Sahu, L. K., Sheel, V., Kajino, M., and Nedelec, P., 2013, "Variability in tropospheric carbon monoxide over an urban site in Southeast Asia", *Atmos. Environ.*, v. 68, p. 243-255.
67. Sahu, L. K., Kondo, Y., Moteki, N., Takegawa, N., Zhao, Y., Cubison, M. J., Jimenez, L. J., Vay, S., Diskin, G. S., Wisthaler, A., Mikoviny, T., Huey, L. G., Weinheimer, A. J. J., and Knapp, D., 2012, "Emission characteristics of black carbon in anthropogenic and biomass burning plumes over California during ARCTAS-CARB 2008", *J. Geophys. Res.*, v. 117, p. D16302, pp. 1-20.
68. Sahu, L. K., 2012, "Volatile organic compounds and their measurements in the troposphere", *Current Science*, v. 102, p. 1645-1649.
69. Samanta, G. K., Aadhi, A., and Ebrahim-zadeh, M., 2013, "Continuous-wave, two-crystal, singly-resonant optical parametric oscillator: Theory and experiment", *Optics Express*, v. 21, p. 1-21.
70. Sarkhel, S., Sekar, R., Chakrabarty, D., and Guharay, A., 2012, "Investigation on mesospheric gravity waves over Indian low latitude stations using sodium airglow observations and a few case studies based on thermal and wind structure", *J. Atmos. Sol. Terr. Phys.*, v. 86, p. 41-50.
71. Sharma, S., Sridharan, S., Chandra, H., Lal, S., and Acharya, Y. B., 2012, "Middle Atmospheric Thermal Structure over Sub-tropical and Tropical Indian Locations using Rayleigh Lidar", *Planetary and Space Science*, v. 63-64, p. 36-48.
72. Sheel, V., Haider, S. A., Withers, P., Kozarev, K., Jun, I., Kang, S., Gronoff, G., and Simon Wedlund, C., 2012, "Numerical simulation of the effects of a solar energetic particle event on the ionosphere of Mars", *J. Geophys. Res.*, v. 117, p. A05312, pp. 1-13.
73. Sheel, V. and Haider, S. A., 2012, "Calculated production and loss rates of ions due to impact of galactic cosmic rays in the lower atmosphere of Mars", *Planetary and Space Sc.*, v. 63-64, p. 94-104.
74. Sinha, H. S. S., Koh-Ichiro Oyama, and Watanabe, S., 2013, "Detection of long living neutral hydrated clusters in laboratory simulation of ionospheric D region plasma", *J. Geophys. Res.*, v. 118, p. 583-589.
75. Srivastava, S., Lal, S., Venkataramani, S., Guha, I., and Subrahmanyam, D. B., 2012, "Airborne measurements of O_3 , CO , CH_4 and NMHCs over the Bay of Bengal during winter", *Atmos. Environ.*, v. 59, p. 597-609.
76. Srivastava, R., and Ramachandran, S., 2013, "The mixing state of aerosols over the Indo-Gangetic Plain and its impact on radiative forcing", *Quart. J. Roy. Meteor. Soc.*, v. 139, p. 137-151.
77. Srivastava, S., and Varun Sheel, 2013, "Study of tropospheric CO and O_3 enhancement episode over Indonesia during Autumn 2006 using the Model of Ozone and Related chemical Tracers (MOZART-4)", *Atmos. Environ.*, v. 67, p. 53-62.
78. Sridharan, R., Bagiya, M. S., and Sunda, S., 2012, "A novel method based on GPS TEC to forecast L band scintillations over the equatorial region through a case study", *J. Atmos. Sol. Terr. Phys.*, v. 80, p. 230-238.
79. Sridharan, R., Das, T. P., Ahmed, S. M., Supriya, G., and Kamalakar, J. A., 2013, "Spatial heterogeneity in the radiogenic activity of the lunar interior: inferences from CHACE and LLRI on Chandrayaan 1", *Adv. Space Res.*, v. 51, p. 168-178.
80. Thampi, S. V., Tsunoda, R. T., Jose, L., and T. K. Pant, 2012, "Ionogram signatures of large-scale wave structure and their relation to equatorial spread F", *J. Geophys. Res.*, v. 117, p. A08314, pp. 1-14.
81. Thampi, S. V., and Yamamoto, Mamoru., 2012, "Evolution of plasma bubbles over Vietnam region observed using the CERTO beacon on board C/NOFS satellite", *Ind. J. Radio & Space Phys.*, v. 41, p. 233-239.
82. Vaity, P., and Singh, R. P., 2012, "Generation of quadrupoles through instability of dark rings in photorefractive media", *J. Optical Soc. America B*, v. 29, p. 2099-2102.
83. Vaity, P., and Singh, R. P., 2012, "Topological charge dependent propagation of optical vortices under quadratic phase transformation", *Optics Lett.*, v. 37, p. 1301-1303.
84. Vaity, P., Banerji, J., and Singh, R. P., 2013, "Measuring the topological charge of an optical vortex by using a tilted convex lens", *Phys. Lett. A*, v. 377, p. 1154-1156.
85. Vaity, P., Banerji, J., and Singh, R. P., 2013, "Manifestation of coherence decay of optical vortices on scattering through photorefractive SBN crystal", *J. Optics*, v. 15, p. 025711, pp. 1-5.

Geo Sciences

86. Achyuthan, H., Deshpande, R. D., Rao, M. S., Kumar, B., Nallathambi, T., Shashi Kumar, K., Ramesh, R., Ramachandran, P., Maurya, A. S., and Gupta, S. K., 2013, "Stable isotopes and salinity in the surface waters of the Bay of Bengal: Implications for water dynamics and palaeoclimate", *Mar. Chem.*, v. 149, p. 51-62.
87. Biswas, R. H., Williams, M. A. J., Raj, R., Juyal, N., and Singhvi, A. K., 2013, "Methodological Studies on Luminescence dating of volcanic ashes", *J. Quat. Geochronol.*, v. 17, p.14-25.
88. Chandraratne, W. M., Gaur, A. S., Rao, B. R., Bhushan, R., Muthucumarana, R., Manders, M., Khedakar, V. D. and Dayananda, A. M. A., 2012., "SEM-EDS analysis

- of copper, glass and iron recovered from the 1st century AD shipwreck site off Godawaya, Southern Sri Lanka", *Current Sci.*, v. 103, p. 482-485.
89. Chatterjee, J., and Singh, S. K., 2012, "⁸⁷Sr/⁸⁶Sr and major ion composition of rainwater of Ahmedabad, India: Sources of base cations", *Atmos. Environ.*, v. 63, p. 60-67.
 90. Deshpande, R. D., Maurya, A. S., Angasaria, R. C., Dave, M., Shukla, A. D., Bhandari, N., and Gupta, S. K., 2013, "Recent falls of Megacryometeors in Western India: Isotopic Investigations", *Current Sci.*, v. 104, p. 728-737.
 91. Deshpande, R. D., Maurya, A. S., Kumar, B., Sarkar, A., and Gupta, S. K., 2013, "Kinetic Fractionation of Water Isotopes during Liquid Condensation under Super-saturated Condition", *Geochim. Cosmochim. Acta*, v. 100, p. 60-72.
 92. Deshpande, R. D., and Gupta, S. K., 2013, "Groundwater helium: An indicator of active tectonic regions along Narmada River, central India", *Chem. Geol.*, v. 344, p. 42-49.
 93. Dutta, K., and Bhushan, R., 2012, "Radiocarbon in the Northern Indian Ocean two decades after GEOSECS", *Global Biogeochem. Cy.*, v. 26, p.1-14.
 94. Gandhi, N., Ramesh, R., Laskar, A. H., Sheshshayee, M. S., Shetye, S., Anilkumar, N., Patil, S. M. and Mohan, R., 2012, "Zonal variability in primary production and nitrogen uptake rates in the southwestern Indian Ocean and the Southern Ocean", *Deep Sea Res. Lett.*, v. 67, p. 32-43.
 95. Kanakidou, M., Duce, R. A., Prospero, J. M., Baker, A. R., Benitez-Nelson, C., Dentener, F. J., Hunter, K. J., Liss, P. S., Mahowald, N., Okin, G. S., Sarin, M. M., Tsigardis, K., Uematsu, M., Zamora, L. M., and Zhu, T., 2012, "Atmospheric fluxes of organic N and P to the global ocean", *Global Biogeochem. Cy.*, v. 26, p. GB3026, pp. 1-12.
 96. Kirpa, R., Sarin, M. M., Sudheer, A. K., and Rengarajan, R., 2012, "Carbonaceous and Secondary inorganic aerosols during wintertime fog and haze over urban sites in the Indo-Gangetic Plain", *Aerosol & Air Quality Res.*, v. 12, p. 359-370.
 97. Lagad, R. A., Alamelu, D., Laskar, A. H., Rai, V. K., Singh, S. K., and Aggarwal, S. K., 2013, "Isotope signature study of the tea samples produced at four different regions in India", *Anal. Methods*, v. 5, p.1604-1611.
 98. Laskar, A. H., Yadava, M. G., and Ramesh, R., 2012, "Radiocarbon and Stable Carbon Isotopes in two Soil Profiles from North-East India", *Radiocarbon*, v. 54, p. 81-89.
 99. Mamta, M., Thakkar, M. G., Bhushan, R., and Juyal, N., 2012, "Continental-marine interaction in the vicinity of the Nara River during the last 1400 years, Great Rann of Kachchh, Western India", *Current Sci.*, v. 103, p. 1339-1342.
 100. Mehta, N., Dinakaran, J., Patel, S., Laskar, A. H., Yadava, M. G., Ramesh, R., and Krishnaiyya, N. S. R., 2012, "Changes in litter decomposition and soil organic carbon in a reforested tropical decidual cover (India)", *Ecol. Res.*, v. 28, p. 239-248.
 101. Ngangom, N. J. M., Thakkar, M. G., and Bhushan, R., 2012, "Continental-Marine Interaction in the vicinity of the Nara River during the last 1400 years, Great Rann of Kachchh, Western India", *Current Sci.*, v. 103, p. 1339-1342.
 102. Pagonis, V., Morthekai, P., Singhvi, A. K., Thomas, J., Balaram, V., Kitis, G. and Chen, R., 2012 "Time-resolved infrared stimulated luminescence signals in feldspars: analysis based on exponential and stretched exponential functions", *J. of Luminescence*, v. 132, p. 2330-2340.
 103. Rahaman, W., Singh, S. K., and Shukla, A. D., 2012, "Rhenium in Indian rivers: Sources, fluxes and contribution to oceanic budget", *Geochem. Geophys. Geosyst. J.*, v. 13, p.1-21.
 104. Rajput, P., Sarin, M. M., and Kundu S. S., "Atmospheric particulate matter (PM_{2.5}), EC, OC, WSOC and PAHs from NE-Himalaya: Abundances and chemical characteristics", *Atmos. Pollution Res.*, v. 4, p. 214-221.
 105. Ramesh, R., 2012 "Predicting Extreme events", *Geography and You*, v.12, p. 16-19.
 106. Rana, N., Bhattacharya, F., Basavaiah, N., Pant, R.K., and Juyal, N., 2013, "Soft sediment deformation structures and their implications for the Late Quaternary seismicity around the South Tibetan Detachment System, Uttarakhand Himalaya, India", *Tectonophysics*, v. 592, p. 165-174.
 107. Rana, N., Sundriyal Y.P., and Juyal, N., 2012, "Recent cloudburst-induced landslides around Okhimath", *Current Sci.*, v. 130, p. 1389-1390.
 108. Ray, J. S., Kumar, A., Sudheer, A. K., Deshpande, R. D., Rao, D. K., Patil, D. J., Awasthi, N., Bhutani, R., Bhushan, R., and Dayal, A. M., 2013 "Origin of gases and water in mud volcanoes of Andaman accretionary prism: implications for fluid migration in forearcs", *Chem. Geol. J.*, v. 347, p. 102-113.
 109. Ray, J. S., Pande, K., and Awasthi, N., 2013, "A minimum age for the active Barren Island Volcano, Andaman Sea", *Current Sci.*, v. 104, p. 934-939.
 110. Schulz, M., Prospero, J. M., Baker, A. R., Dentener, F., Ickes, L., Liss, P. S., Mahowald, N. M., Nickovic, S., Garcia-Pondo, C. P., Rodriguez, S., Sarin, M. M., Ina Tegen., and Duce, R. A., 2012, "Atmospheric transport and deposition of mineral dust to the ocean: Implications for research needs", *Environ. Sci. Technol.*, v. 46, p. 10390-10404.
 111. Singh, S. P., Singh, S. K., Goswami, V., Bhushan, R., and Rai, V. K., 2012, "Spatial distribution of dissolved neodymium and ^σNd in the Bay of Bengal: Role of particulate matter and mixing of water masses", *Geochim. Cosmochim. Acta*, v. 94, p. 38-56.
 112. Sridhar, A., Chamyal, L. S., Bhattacharya, F. and Singhvi, A. K., 2013, "Early Holocene fluvial activity from the sedimentology and paleohydrology of gravel terraces in the semi arid Mahi river basin", *J. Asian Earth*, v. 66, p. 240-248.

113. Srinivas, B., and Sarin, M.M., 2012, "Atmospheric dry deposition of mineral dust and anthropogenic trace metals to the Bay of Bengal", Jour. Marine Systems, v. , pp.1-13.
114. Srinivas, B., and Sarin, M. M., 2012, "Atmospheric pathways of phosphorus to the Bay of Bengal: Contribution from anthropogenic sources and mineral dust", Tellus-B, v. 64, p. 17174, pp. 1-12.
115. Srinivas. B., and Sarin, M. M., 2013, "Atmospheric deposition of N, P and Fe to Arabian Sea and Bay of Bengal: Implications to C- and N-fixation", Sci. of Total Environ, v. 456-457, p. 104-114.
116. Srivastava, R., Ramesh, R., and Rao, T. N., 2012, "Relationship between stable isotopes and drop size distribution in tropical rainfall", Jour. Atm. Chem., v. 69, p. 23-31.
117. Sudheer, A. K. and Rengarajan, R., 2012, "Atmospheric Mineral Dust and Trace Metals over Urban Environment in Western India during Winter", Aerosol and Air Quality Res., v. 12, p. 923–933.
118. Thakkar. M. G., Ngangom, M., Thakker, P. S. and Juyal, N., 2012, "Terrain response to 1819 Allah Bund earthquake in Western Great Rann of Kachchh, Gujarat, India", Current Sci., v. 103, p. 208-212.

Theoretical and Computational Physics

119. Acharyya, S., and Amritkar, R. E., 2012, "Synchronization of coupled nonidentical dynamical systems", Europhys. Lett., v. 99, p. 40005, pp. 1-6.
120. Ananthanarayan, B., Lahiri, J., Patra, M. and Rindani, S. D., 2012, "Generalized top-spin analysis and new physics in e^+e^- collisions with beam polarization", Phys. Rev. D, v. 86, p. 114019, pp. 1-18.
121. Arora, B. and Sahoo, B. K., 2012, "State insensitive trapping of Rb atoms: linearly versus circularly polarized light", Phys. Rev. A, v. 86, p. 033416, pp. 1-12 .
122. Basak, T., and Mohanty, S., 2012, "Triplet-Singlet Extension of the MSSM with a 125 GeV Higgs and Dark Matter", Phys.Rev. D, v. 86, p. 075031, pp. 1-10.
123. Barger, V., Gandhi, R., Ghoshal, P., Goswami, S., Marfatia, D., Prakash, S., Raut, S. K., and Sankar, S. U., 2012, " Neutrino mass hierarchy and octant determination with atmospheric neutrinos", Phys. Rev. Lett., v. 109, p. 091801, pp.1-4.
124. Berera, A., and Rangarajan, R., 2013, "Quantum Phase of Inflation", Phys. Rev. D, v. 87, p. 043514, pp. 1-13.
125. Bhowmick, S. K., Amritkar, R. E., and Dana, S. K., 2012, "Experimental evidence of synchronization of time-varying dynamical network", Chaos, v. 22, p. 023105, pp. 1-9.
126. Chakrabarti, B., Biswas, A., Kota, V. K. B., Roy, K., and Haldar, S. K., 2012, "Energy level statistics of interacting trapped bosons", Phys. Rev. A, v. 86, p. 013637, pp. 1-11.
127. Chakraborty, J., Devi, H. Z., Goswami, S., and Patra, S., 2012 "Neutrinoless double- β decay in TeV scale Left-Right symmetric models", JHEP, v. 1208, p. 008, pp. 1-26.
128. Chakraborty, J., Das, M, and Mohanty, S., 2013, "Constraints on TeV scale Majorana neutrino phenomenology from the Vacuum Stability of the Higgs", Mod. Phys. Lett. A, v. 28, p. 1350032, pp. 1-13.
129. Chatterjee., B., Mishra, H., and Amruta, 2012, "Strong CP violation and chiral symmetry breaking in hot and dense quark matter", Phys. Rev. D, v. 85, p. 114008, pp. 1-9.
130. Chattopadhyay, S., Mani, B. K., and Angom, D., 2012 "Electric dipole polarizability from perturbed relativistic coupled-cluster theory: Application to neon", Phys. Rev. A, v. 86, p. 022522, pp. 1-6.
131. Chattopadhyay, S., Mani, B. K., and Angom, D., 2012, "Perturbed coupled-cluster theory to calculate dipole polarizabilities of closed-shell systems: Application to Ar, Kr, Xe, and Rn", Phys. Rev. A, v. 86, p. 062508, pp. 1-12.
132. Chavda, N. D., Kota, V. K. B., and Potbhare, V., 2012, "Thermalization in one- plus two-body ensembles for dense interacting boson systems", Phys. Lett. A, v. 376, p. 2972-2976.
133. Cowsik, R., Madziwa-Nussinov, T., Nussinov, S., and Sarkar, U., 2012, "Testing Violations of Lorentz Invariance with Cosmic-Rays", Phy.Rev. D, v. 86, p. 045024, pp. 1-13.
134. Das, M., Mohanty, S., and Prasanna, A. R., 2013, "Constraints on background torsion from birefringence of CMB polarization", Int. J. Mod. Phys. D, v. 22, p. 1350011, pp. 1-10.
135. Goswami, S., Dighe, A. and Ray, S., 2012, "Optimization of the baseline and the parent muon energy for a low energy neutrino factory", Phys. Rev. D, v. 86, p. 073001, pp. 1-16.
136. Gautam, S., Muruganandam, P., Angom, D., 2013, "Formation and stability of coreless vortex dipoles in phase-separated binary condensates", Phys. Lett. A, v. 377, p. 378-386.
137. Joshipura, A. S., and Ketan, M., 2012, "Yukawa coupling unification in $SO(10)$ with positive μ and a heavier gluino", Phys. Rev. D, v. 86, p. 035019, pp. 1-10.
138. Kishore, V., Santhanam, M. S., and Amritkar, R. E., 2012, "Extreme event-size fluctuations in biased random walks on networks", Phys. Rev. E, v. 85, p. 056120, pp. 1-7.
139. Lewty, N. C., Chuah, B. L., Cazan, R., Sahoo, B. K., and Barrett, M. D., 2012, "Spectroscopy on a single trapped $^{137}\text{Ba}^+$ ion for nuclear magnetic octupole moment determination", Optics express, v. 20, p. 21379-21384.
140. Mohanty, S., and Rao, S., 2012, "Neutrino processes with power law dispersion relations", Phys.Rev. D, v. 85, p. 102005, pp. 1-4.

141. Mohanty, S., Rao, S. and Roy, D. P., 2012, "Predictions of a Natural SUSY Dark Matter Model for Direct and Indirect Detection Experiments", JHEP, v. 1211, pp. 1-17.
142. Nandy, D. K., Singh, Y., Shah, B. P., and Sahoo, B. K., 2012, "Transition properties of a potassium atom", Phys. Rev. A, v. 86, p. 052517, pp. 1-12.
143. Resmi, V., Ambika, G., Amritkar, R. E., and Rangarajan G., 2012, "Amplitude death in complex networks induced by environment", Phys. Rev. E, v. 85, p. 046211, pp. 1-7.
144. Rindani, S. D., and Sharma, P., 2012, "CP violation in tbW couplings at the LHC", Phys. Lett. B, v. 712, p. pp. 413-18.
145. Roy, K., Chakrabarti, B., Biswas, A., Kota, V. K. B., and Haldar, S. K., 2012, "Spectral fluctuation and 1 noise in the energy level statistics of interacting trapped bosons", Phys. Rev. E, v. 85, p. 061119, pp. 1-8.
146. Sahoo, B. K., and Arora, B., 2013, "Magic wavelengths for trapping alkali-metal alkali atoms with circularly polarized light", Phys. Rev. A, v. 87, p. 023402, pp. 1-9.
147. Sahoo, B. K., and Das, B. P., 2012, " Ba^+ Quadrupole Polarizabilities: Theory versus Experiment", Phys. Rev. A, v. 86, p. 022506, pp. 1-5.
148. Singh, A., Sanjay, Puri., and Mishra, H., 2012, "Domain Growth and Ordering Kinetics in Dense Quark Matter", Phys. Atom. Nucl, v. 75, p. 689-692 .
149. Singh, A., Puri, S., Mishra, H., 2013, "Kinetics of phase transitions in quark matter", Europhys. Lett., v. 102, pp. 1-6.
150. Singh, A., Puri, S., Mishra, H., 2013, "Domain growth in chiral phase transitions: Role of inertial dynamics", Nucl. Phys. A, v. 908, p. 12-28.
151. Singh, A. K., Angom, D., and Natarajan, V., 2013, "Observation of the nuclear magnetic octupole moment of ^{173}Yb from precise measurements of the hyperfine structure in the 3P_2 state", Phys. Rev. A, v. 87, p. 012512, pp. 1-5.
152. Singh, N., and Paul, B., 2012, "Efficient Computational Approach to the Non-Markovian Second-Order Quantum Master Equation: Electronic Energy Transfer in Model Photosynthetic Systems", Mol. Phys., v. 110, p. 1815-1828.
153. Singh, Y. I, Nandy, D. K., and Sahoo, B. K., 2012, "Reexamining Nuclear Quadrupole Moments in $^{39-41}\text{K}$ Isotopes", Phys. Rev. A, v. 86, p. 032509, pp. 1-9.
154. Tiwari, S. K., Das, A., Angom, D., Patel, B. G., and Kaw, P., 2012, "Kelvin-Helmholtz instability in a strongly coupled dusty plasma medium", Physics of Plasmas, v. 19, p. 073703, pp. 1-7.
155. Varma, R. K., 2012, "Curl-free vector potential observation on the macro-scale for charged particle in a magnetic field as compared with that on the micro-scale: the Aharonov-Bohm effect", Phys. Scripta v. 86, p. 045009, pp. 1-10.
156. Varma, R. K., 2013, "A covering probability amplitude formalism for classical and quantum mechanics and possible new modes of non-classical behavior", arXiv:1301.5476v1 [quant-ph], pp. 1-26.
157. Vyas, Manan, Chavda, N.D., Kota, V.K.B., and Potbhare, V., 2012, "One plus two-body random matrix ensembles for boson systems with F-spin: Analysis using spectral variances", J. Phys. A: Math. Theor., v. 45, p. 265203, pp. 1-33.
158. Vyas, Manan,, and Kota, V. K. B., 2012, "Embedded Gaussian Unitary Ensembles with $U(\Omega) \otimes SU(r)$ Embedding generated by Random Two-body Interactions with $SU(r)$ Symmetry", J. Math. Phys., v. 53, p. 123303, pp. 1-18.
159. Wansbeek, L. W., Schlessler, S. S., Sahoo, B. K., Dieperink, A. E. L., Onderwater, C. J. G., and Timmermans, R. G. E., 2012, "Charge radii of radium isotopes", Phys. Rev. C, v. 86, p. 015503, pp. 1-9.

Library

160. Alam, Md. Nurul, Pandey, Pragya, 2012, "GeoTheses: development of union catalogue of Indian geoscience theses using GSDL", Electronic Library, The, v. 30, p.456 - 468.
161. Alam, Md. Nurul, Pandey, Pragya, and Dutta, Chaitali, 2012, "SpaceGL: An Indian Portal for Space Science Grey Literature", DESIDOC Journal of Library and Information Technology, v.32, p.335-338.

Publications in Proceedings of Conference/ Symposia/ Workshops

Astronomy and Astrophysics

1. Joshi, U. C., Ganesh, S., and Baliyan, K. S., 2012, "Optical polarization observations of R Aquarii during 1995-2008: What do they tell us?", AIP Proc. , v. 1429, p. 222-25.
2. Jain, Rajmal, 2012, "Remote Sensing of the Sun, Signatures, v. 23, Issue 4.
3. Jain, Rajmal, 2012, "Solar Signatures on the Earth's Climate, Proc. of Advances in Applied Mathematics and Computational Physics., pp. 1-34, World Education Publishers, Delhi, (eds: Kumar, Rakesh., Kumar, Anil., Khalil Ahmed and Kumar, Nagendra.,)
4. Naik, S., and Ashok, N. M., 2012, "Venus Transit: A rare astronomical event", Planex News, v. 2, pp. 23-26.
5. Singal, A. K., 2012, "Our large peculiar motion in the universe determined from the sky brightness anisotropy, Proc. of the national conference on Applied Mathematics and Computational Physics, World Education Publishers, Delhi, p. 111.
6. Vadawale, S. V., Shanmugam, M., Purohit, S., Acharya, Y. B., and Sudhakar, M., 2012, "Experimental measurements of charge carrier mobility: lifetime products for large sample of pixilated CZT detectors", SPIE Proceedings, v. 8453, p. 84532K-9.
7. Vadawale, S. V., Chattopadhyay, T., and Pendharkar, P., 2012, "A conceptual design of hard X-ray focal plane detector for simultaneous x-ray polarimetric,

spectroscopic, and timing measurements", SPIE Proceedings, v. 8443, p. 84434P-8.

Solar Physics

8. Ambastha, A. and Maurya R.A., 2012, "Spectral Line Profile Changes Associated with Energetic Solar Transients", A.S.I. Conf. Series, v. 6, pp 197-202.
9. S. F. Martin, O. Panasenco, M. Berger, O. Engvold, Y. Lin, A. Pevtsov, N. Srivastava, 2012, "The build-up to eruptive solar events viewed as the development of chiral systems, in Magnetic Fields from the Photosphere to the Corona. ASP Conf. Proc. v. 463., p.157.(Ed. T. Rimmele, et al)
10. N. Crosby, N., V. Astrid, E. Robbrecht, B. Vrsnak, S. Vennerstrom, O. Malandraki, S. Dalla, N. Srivastava, M. Hesse, D. Odstrcil, 2012, "Forecasting the space weather impact: the COMESEP project", AIP Conference Proceedings, v. 1500, pp. 159-164.

Planetary Sciences & PLANEX Program

11. Basu Sarbadhikari, A., Marhas, K. K., Sameer and Goswami, J. N., 2013, "Water content in melt inclusions and apatites in low-titanium lunar mare basalt, 15555, Lunar Planet. Sci. Conf., v. 44, pp. 5252.
12. Desai, A. J. and Murty, S. V. S., 2013, "Morphological investigations of Nicholson crater, mars: identification

- of aeolian processes*”, Lunar Planet. Sci. Conf., v. 44, pp. 1180.
13. Indhu, V., Srivastava, N., and Murty, S. V. S., 2013, “*Spectral reflectance studies of selected young basalts on the Moon using M3 datasets from Chandrayaan-1*”, Lunar Planet. Sci. Conf., v. 44, pp. 1185.
 14. Mahajan, R. R., and Murty, S. V. S., 2013, “*Noble gases and Nitrogen in the Martian meteorite Tissint*”, 12th ISMAS Triennial International Conference on Mass Spectrometry, p. 159-160.
 15. Misra, S., Arif, Md., Newsom, H., and Ray, D., 2013, “*Hydrothermal alteration of Lonar crater basalts, India-Impact related?*”, Lunar Planet. Sci. Conf., v. 44, pp.1030
 16. Misra, S., Panda, D., Ray, D., Newsom, H., Dube, A. and Sisodia, M.S., 2013, “*Geochemistry of glassy rocks from Ramgarh structure India*” Lunar Planet. Sci. Conf., v. 44, p.1020.
 17. Ranjith Kumar, P.M. and Murty, S.V.S., 2013, “*Solar Gases in Washington county Iron Meteorite*”, 12th ISMAS Triennial International Conference on Mass Spectrometry, p. 314-317.
 18. Ray, D., and Misra, S., 2012, “*Comparative study of lunar basalts and Lonar impact crater melts: an evaluation though modern trace element geochemistry*”, European Planetary Science Congress 2012, v. 7, EPSC2012-73-1 2012.
 19. Ray, D., Misra, S., and Arif, Md., 2013, “*Contrasting aerodynamic morphology and geochemistry of impact spherules from Lonar crater, India: Some insights into their cooling history*”, Lunar Planet. Sci. Conf., pp. 1031.
 20. Sinha, R. K., and Murty S. V. S., 2013, “*Nature and distribution of olivine in moreux crater in northern mid-latitude of mars*”, Lunar Planet. Sci. Conf., v. 44, pp. 1179.
 21. Srivastava, N., and Gupta, R. P., 2012, “*Compositional diversity inside Lowell crater, Orientale Basin: Evidences for extensive spinel rich deposits*”, 2nd Conf. on Lunar Highland Crust, pp. 9016.
 22. Srivastava, N., and Gupta, R. P., 2013, “*Spatial distribution of spinel in the Orientale Basin: New Insights from M3*”, Lunar Planet. Sci. Conf., v. 44, pp. 1509.
25. Kumar, A., Banerji, J., and Singh, R. P., 2012, “*HBT-Type Experiment with Optical Vortices*”, CLEO: QELS-Fundamental Science, OSA Technical Digest (Optical Society of America), paper JW4A.98 (1-2).
 26. Kumar, A., Vaity, P., Prabhakar, S., and Singh, R. P., 2012, “*Topological aberration of phase singular light beams*”, International Conference on Fibre Optics and Photonics, OSA Technical Digest (online) (Optical Society of America), paper M1C.2 (1-3).
 27. Prabhakar, S., Salla, G. R., Aadhi, A., Kumar, A., Samanta, G., and Singh, R. P., 2012, “*Spatial distribution of Spontaneous Parametric Down-Converted Photons*”, International Conference on Fibre Optics and Photonics, OSA Technical Digest (online) (Optical Society of America), paper T1C.2 (1-3).
 28. Prabhakar, S., Salla, G. R., Aadhi, A., Kumar, A., Samanta, G. K., and Singh, R. P., 2012, “*Spatial distribution of Spontaneous Parametric Down-Converted Photons*”, International Conference on Fibre Optics and Photonics, OSA Technical Digest (online) (Optical Society of America), paper T1C.2 (1-3).
 29. Salla, G. R., Prabhakar, S., Aadhi, A., Kumar, A., Shah, M., Singh, R. P., and Simon, R., 2012, “*Determination of Mueller matrix of an optical element with Simon-Mukunda gadget*”, International Conference on Fibre Optics and Photonics, OSA Technical Digest (online) (Optical Society of America), paper M1B.2 (1-3).
 30. Samanta G. K., and Ebrahim-Zadeh M., 2012, “*Theoretical and experimental study of two-crystal, continuous-wave, singly-resonant optical parametric oscillator*”, NLO50 International Symposium, Barcelona, Spain, 7-10 October, paper MO5.
 31. Vaity, P., Kumar, A., Salla, G. R., Aadhi, A., Chithrabhanu, P., and Singh, R. P., 2012, “*Determining orbital angular momentum of light using simple convex lens*”, in International Conference on Fibre Optics and Photonics, OSA Technical Digest (online) (Optical Society of America), paper MPo.4 (1-3).

Space, Atmospheric, Molecular And Laser Physics

23. Devi, K., Kumar, S. C., Samanta, G. K., Esteban-Martin, A., and Ebrahim-Zadeh M., 2012, “*Continuous-wave mode-locked optical parametric oscillator*”, Proceedings of SPIE, v. 8434, p. 84340D1-7.
 24. Jaiswal, V. K., Kandpal, H. C., Singh, R. P., and Sinha, R. K., 2012, “*Phase correlation study of coherent singular optical beam*”, International Conference on Fibre Optics and Photonics, OSA Technical Digest (online) (Optical Society of America), paper M1C.5 (1-3).
32. Achyuthan, H., Farooqui, A., Eastoe, C., Ramesh, R., Devi, M., and Ganesh, P.P., 2012, “*A five-century long limnological and environmental record from northeastern India*”, in: Holocene: Perspectives, Environmental Dynamics and Impact Events (ed. B. S. Kotlia) ISBN 978-1-62257-722-4 (hard cover) Chapter 11, pp. 129-144, Nova Publishers, New York.
 33. Kirpa, R., and Sarin, M. M., 2012, “*Carbonaceous aerosols over Northern India: Sources and spatio-temporal variability*”, Proc. Nat. Sci. Acad., v. 78, p. 523-533.
 34. Lekshmy, P.R., Midhun, M., Ramesh, R., and Jani R.A., 2013, “*Is the isotopic composition of rainfall of the south west coast India independent of local rainfall amount?*”, in: Proc. XII ISMAS Tricon Conference on mass Spectrometry (Eds. S. K. Aggarwal, P.J. Jaison, V. M. Telmore), ISBN 978-81-90442-5-5, pp.306-308.

35. Midhun, M., Lekshmy, P.R., Ramesh, R. and Jani R.A., 2013, "Stable isotopic composition of atmospheric vapour over the Bay of Bengal and its relation with ocean surface conditions", in: Proc. XII ISMAS Tricon Conference on mass Spectrometry (Eds.S. K. Aggarwal, P.J. Jaison, V. M. Telmore), ISBN 978-81-90442-5-5, pp.318-320.
36. Ramesh, R., Managave, S. R., and Yadava, M.G., 2013, "Paleoclimate of peninsular India", Climate change and Island and coastal vulnerability, (Eds.J. Sundaresan, S. Sreekesh, A.L. Ramanathan, L. Sonneschein, R. Boojh), Springer ISBN 978-94-007-6015-8(HB), pp.78-98.
37. Singh, S.P., and Singh, S.K., 2012, "Distribution of dissolved neodymium and ϵNd in the Bay of Bengal", Goldschmidt 2012, Montreal Canada, Mineralogical Magazine, v. 76, p. 2379.
38. Goswami, V., Singh, S.K., 2012, "Temporal variation in 187Os/188Os of the Arabian Seawater", Goldschmidt 2012, Montreal Canada, Mineralogical Magazine, v. 76, p. 1777.
39. Bhushan, R., "Accelerator Mass Spectrometer (AMS): A New Tool for Research in Geosciences", PRL News, May 2011.
40. Bhushan, R., Dutta, K., Agnihotri, R., Rengarajan, R., "Temporal Variation in the Oceanic Properties of the northern Indian Ocean since GEOSECS", In Proceedings of 21st International Radiocarbon Conference, Paris, France, July 2012.
41. Khonde, N., Maurya, D., Bhushan, R., Das, A., Joshi, P., Chamyal, L.S., "Late-Pleistocene-Holocene basin filling by Himalayan sediments in Great Rann of Kachchh: A palaeoclimatic perspective", In 4th Open Science Meeting of PAGES held in Goa, India, 13-16 February, 2013.
42. Sridhar, A., Bhushan, R., Band, S., and Chamyal, L.S., "Main stem- tributary sedimentation in response to flood events during last 1000 years in lower Narmada basin, India", In 4th Open Science Meeting of PAGES held in Goa, India, 13-16 February, 2013.
43. Bhushan, R., and Singh, S.K., "Synchronous variations in terrigenous flux to the Bay of Bengal and solar insolation: Implications to solar forcing on monsoon system", In 4th Open Science Meeting of PAGES held in Goa, India, 13-16 February, 2013
44. Goswami V., Singh, S.K., and Bhushan, R., "Reduced flow of North Atlantic Deep Water into the Arabian Sea during Last Glacial Maxima: Evidence from 187Os/188Os of the Arabian Seawater", In 4th Open Science Meeting of PAGES held in Goa, India, 13-16 February, 2013.

Theoretical and Computational Physics

45. Ananthanarayan, B., Patra, M., and Rindani, S.D., 2012, "Top-spin analysis of new scalar and tensor interactions in e^+e^- collisions with transverse beam polarization", Proceedings of the 25th International Symposium on Lepton Photon Interactions at High Energy (LP11), 22-27 August 2011, Mumbai, Pramana v.79 p. 1275-1279.
46. Barr A.J., Khoo T.J., Konar P., Kong K., Lester C.G., Matchev K.T., Park M., 2012, "A Storm in a 'T' Cup", AIP Conf. Proc., v. 1441, pp. 722 .
47. V.K.B. Kota, 2012, "Random Matrix Theory in Nuclear Structure: Past, Present and Future", Proceedings of the DAE Symposium on Nuclear Physics, Eds. Jain, S. R, Shukla, P., Chatterjee, A., and Datar V. M, v. 57, p.4-13.
48. Kota, V. K. B., 2012, "Wigner-Racah Algebra, Binary Correlations and Trace Propagation for Embedded Random Matrix Ensembles", Proceedings of International Conference on Horizons of Innovative Theories, Experiments, and Supercomputing in Nuclear Physics, Edited by K. D. Launey, M. A. Caprio, J. E. Escher, J. G. Hirsch and C. W. Johnson, J. Phys.: Conf. Ser, v. 403, 012006/1-7.
49. Srivastava, P. C., Hirsch, J. G., Ermamatov, M. J., and Kota, V. K. B., 2012, "Large-scale shell-model calculations for $^{32-39}\text{P}$ isotopes", in Beauty in Physics: Theory and Experiment, AIP Conf. Proc., v. 1488, p. 431- 435.

Books Edited/ Review Articles

Books Edited

1. Singhvi, A.K., and Banerjee, D.M., "*Glimpses of Geoscience Research In India: Indian Report to the IUGS*", Proceedings of the Indian National Science Academy (PINSAs), v. 78, Issue. 3, p. 239-614.

Review Articles

1. Banerjee, D. P. K., and Ashok, N. M., 2012, "*Near-infrared Properties of Classical Novae; A Perspective Gained from Mount Abu Infrared Observatory*", Bulletin of the Astronomical Society of India, v. 40, pp. 243.
2. Bhardwaj, A., Dhanya, M. B., Sridharan, R., Barabash, S., Futaana, Y., Wieser, M., Holmstr, M., Lue, C., Wurz, P., Schaufelberger, A., and Asamura, K., 2012, "*Interaction of solar wind with Moon: an overview on the results from the SARA experiment aboard Chandrayaan I* *Advances in Geosciences*, Planetary Science and Solar & Terrestrial Science (Ed. Anil Bhardwaj), v. 30, p. 35-55.
3. Chesneau, O., and Banerjee, D. P. K., 2012, "*Interferometric Studies of Novae in the Infrared*", Bulletin of the Astronomical Society of India, v. 40, pp. 267.
4. Dhir, R. P., and Singhvi, A. K., 2012, "*The Thar Desert and its antiquity 2012*", Current Science, v. 102, p. 1001-1008.
5. Ebrahim-Zadeh M., Kumar S. C., Esteban-Martin A., and Samanta G. K., 2013, "*Breakthroughs in optical parametric oscillators*", Photonics Journal (IEEE).
6. Sears, D. W. G., Ninagawa, K., and Singhvi, A. K., 2012, "*Luminescence studies of extraterrestrial materials: insights into their recent radiation and thermal histories and into their metamorphic history*", Chemie d' Erde, Invited Review.
7. Singhvi, A. K., Bhatt, N., Glennie, K. W., and Srivastava, P., 2013, "*Late Quaternary Climatic Change in India, Tibet, Arabia and the Middle East: the chronostratigraphic record*", In Environmental Change in Humid Tropics (D. Nash and S. Metcalfe eds), Blackwell Publications, Oxford pp. 151-235.

Promotion of Basic Sciences and Official Language

Activities on the promotion of Basic Sciences

PRL has been coordinating several programs jointly with the Institutions and learned societies in the region to promote science and create a better scientific environment. Some of the programs include popular lectures by eminent scientists, interactions of scientists with school, college and university students, one day seminars and workshops for students, teachers and researchers, and publication of scientific booklets. In this series following two seminars were supported during the last year.



Figure 88: PRL scientist interacting with young student's during a three days seminar at Rajasthan Hindi higher secondary school, Ahmedabad.

- i. Three-Days Seminar on Current Trends in Science, held at Rajasthan Hindi Higher Secondary School, Ahmedabad, during December 21 to 23, 2012.
- ii. National Seminar on High Potential Research Areas in Physics, held at St. Xavier's college, Ahmedabad, on 31st January, 2013.



Figure 89: Eminent Scientists and faculty members at the National Seminar on High Potential Research Areas in Physics, St. Xavier's College, Ahmedabad.

Eminent scientist from PRL and outside PRL delivered talks in these seminars and interacted with young students about excitement in scientific research. Special sessions on career opportunities in sciences were also organized during the above seminars and in addition to students, teachers and

parents had also participated in these discussions.

- iii. Witnessing the rare event "Venus Transit" from Physical Research Laboratory, Ahmedabad.

The historic transit of the planet Venus across the disc of the Sun unfolded on 6th June 2012. The spectacular event was visible from sunrise up to 10:23 hrs across India. Arrangements were made for public viewing of this event at Thaltej Campus of Physical Research Laboratory, Ahmedabad. A couple of telescopes and required support systems were installed in the campus. Several posters explaining the facts behind the scientific event and related explanations were displayed for the public. A large number of enthusiastic visitors, beginning from the kids of a few years of age who barely understand our solar system to senior people who do not want to miss the opportunity to see the event kept on coming till the event got over. Astronomers and volunteers tried to explain the various queries on Venus transit and the long periodicity associated with it.



Figure 90: A young child curiously viewing the Venus transit through a telescope at Thaltej Campus of Physical Research laboratory, Ahmedabad

- iv. PRL exhibit at Vibrant Gujarat Global Trade Show 2013.



Figure 91: PRL exhibit at VIBRANT GUJARAT GLOBAL TRADE SHOW 2013

PRL was invited to participate in a state level exhibition called "VIBRANT GUJARAT GLOBAL TRADE SHOW 2013", held during 08-13 January, 2013 at Gandhinagar, Gujarat. For the very first time, in such summit, an Education Pavilion was introduced to showcase the Education Sector. PRL

exhibited its research activities and academic programmes through posters, models and video presentations. Students and Scientist from PRL had actively participated in this exhibition and interacted with students from schools, colleges, government officials and general public who visited the exhibit. The responses from school students were overwhelming as they were curious to know about the excitement in space, planetary, solar sciences. The exhibit was visited by few thousands of visitors during the span of 06 days.

2. Science Day Celebration and PRL Scholarship

As has been the practice for several years, a day-long celebration was held on 02 March, 2013 at the Physical Research Laboratory, Ahmedabad to mark the National Science Day (In India National Science Day is celebrated on 28 February every year to commemorate the discovery of Raman effect which was announced by Nobel laureate Sir C. V. Raman on this day). The celebrations aim to attract young minds and motivate them to take up science as one of their career options. National Science Day is also observed to spread the message of importance of science and its application among the people and to accelerate the pace of development among them.



Figure 92: Glimpses of various activities during National Science Day Celebration, March 2013.

PRL Scholarships from the Aruna Lal Endowment Fund, established by late Prof. Devendra Lal, former Director, were awarded to five students on this occasion. The selection was done on the basis of their performances in the state level screening test, poster competition and oral interview. All the five students are to receive Rs. 10,000/- per year for two consecutive years and for the third year provided the students continue to study in science stream with high academic record.

In addition to the Aruna Lal scholarship, other prizes were awarded like top five students in the state level screening test held in February 2013, poster competition and quiz competitions (03). Most students were accompanied by their teachers. Teachers and students had close interaction with PRL scientists and the judges of the poster and experiment

competitions throughout the day.

3. 8th Space and Atmospheric Science Course (August 2012-April 2013)

PRL conducts a Post-Graduate Course in Space Science every alternate year. This course is conducted under the auspices of Center for Space Science and Technology Education in Asia and the Pacific (CSSTEAP). CSSTEAP has headquarters in Dehradun and is affiliated to the United Nations. About 50 students from the Asia-Pacific region have participated in this course since 1998. In suitable cases this course leads to an M.Tech. Degree on fulfilment of the requirements of the Andhra University. Recently, 8th Space and Atmospheric Science course was concluded. This course was attended by 14 participants from 07 countries of the Asia Pacific region including Mongolia.



Figure 93: Participants of 8th Space and Atmospheric Science Course at the Inaugural function at PRL, Ahmedabad.

4. Respond Program

RESPOND Programme for Space Sciences, sponsored by ISRO, is being administered by PRL since 1976. At the beginning of the financial year 2012-13, there were around 30 proposals of which seven were completed during this period. Around twelve new proposals were submitted and they are at different stages of reviewing and recommendation processes. About 45 publications resulted out in peer reviewed journals during this period and around 17 theses were resulted out during last three years.

Annual RESPOND (Space Science) review meeting was held on 8-9 February 2013 at the Physical Research Laboratory to monitor the progress of ongoing projects and also to evaluate a few projects which are in pipeline for funding. Reports on 22 projects were presented by investigators

(PIs/Co-PIs/research students of PIs) working in different fields in space sciences and hailing from universities spanning from different part of our country. The subjects of the proposals encompass Astronomy and Astrophysics, Physics of the Earth atmosphere/ionosphere, Solar Physics, Space Weather, and the Space Plasma Physics.

5. Activities on the promotion of Official Language

As a part of implementation and progressive use of Hindi in PRL, the Hindi Pakhwada was celebrated at PRL from September 14 – 28, 2012. The highlights of the celebrations included word quiz, essay, elocution, Hamara Karya, self written poetry competition.



Figure 94: Glimpses of Activities for the promotion of Rajbhasha at PRL.

Vishwa Hindi Divas was organized in PRL on 10.1.2013 and an essay competition was held on Prospects of Use of Hindi in Scientific Work.

A Technical Seminar in Hindi on "Societal Perspectives of scientific activities in PRL" was held at PRL on 22 March, 2013. Sixteen members presented their papers in this Seminar.

Shri R.S. Gupta, Hindi Officer-II & OSD delivered lectures in Hindi at workshops held by various Departments like Space Applications Centre, Airport Authority, Food Corporation of India, Income Tax, Doordarshan, ONGC on different topics including Various applications of computers in Hindi.

Hindi Workshops are being organized regularly in PRL. Lectures based on the works of different fields in administration in the office are organized in the workshops.

The newly appointed employees are being given in-house training of Hindi Typing.

Facilities and Services

Computer Centre

To cater to the High Performance Computing needs of our scientists, Computer Centre is equipped with High Performance Compute Cluster having 20 compute nodes, 1 master node with 64GB RAM on each node, 20TB storage capacity and 3.2 TF peak computing performance and 2.2 TF sustained computing performance. The HPC cluster has a Backup node, I/O node, Management node, Storage node, and a Visualization node. The HPC facility is homed in a special chamber that is maintained at controlled temperature and humidity and has a dual UPS system for round the clock operation. The primary network of HPC is with Infiniband and secondary network is Gigabit. Computer Center has SGI server having 16 Intel Xeon processors, 24GB RAM, with 25TB disk capacity. Computer Center also has Dell server having 16 AMD processors, 64GB RAM with 4TB disk capacity, four HP servers, each having four AMD processors, 4 GB RAM, 1.5 TB disk space providing computing power with large disk storage. Computer centre has also IBM Power7 4 CPU based server providing additional computing power. The Internet connectivity is upgraded to 30Mbps through BSNL Optical Fiber Cable. All these computing machines are connected to our high-speed (1Gbps) local area network (LAN) to provide easy, fast and reliable access to more than 300 PC's and a few workstations distributed throughout all the campuses of our laboratory. PRL dispensary in the colony campus opposite IIM is now connected to the Main Campus over an 1Gbps Optical Fiber link. Through this link, the PRL Medical Officers access the Dispensary database housed in the CoWAA cell in computer center. Through the same Optical Fiber link, the students and PDFs have a round the

clock access to PRL LAN/Internet from their rooms via a few Wi-Fi devices installed in the buildings. Students from Thaltej Hostel also can access Internet through a Wi-Fi device installed in the common room in the hostel. The connectivity between Udaipur Solar Observatory (USO), and PRL Main Campus is upgraded to 6 Mbps through BSNL Optical Fiber Cable. Mt.Abu is also connected to PRL main campus over 2 Mbps MLLN link provided by BSNL. Our Thaltej Campus is connected over a Optical Fiber 34 Mbps through BSNL-MLLN link. Thus, round the clock connectivity has been provided to users all the time from Thaltej, USO, and Mt. Abu. Our main campus is also connected to Thaltej via BSNLs 2 Mbps MLLN for voice communication providing intercom telephone facility between the campuses. The Centre provides centralized virus free E-mails by automatically scanning all incoming E-mails. Anti-Spam filter has been centrally installed to fight the Spam mails. The center also provides web enabled email service. Internet authorizations, monitoring and reporting functions have been added to have optimal usage of Internet bandwidth.

To cater to the High end computing needs, PRL has become resource partner of C-DAC's Grid Garuda Project. The Grid Garuda network is integrated to PRL LAN providing seamless access of Garuda resources to PRL scientists.

PRL SPACENET connectivity for Data, Intranet, and video conferencing has been established at Main Campus, Thaltej Campus, USO and IR Observatory over IP to interact with ISRO centers.

Mathematical, numerical and visualization application software like IMSL, IDL, Mathematica, SigmaPlot, MATLAB, Lahey FORTARN 95, and Statistica etc. have also been installed to cater the needs of the scientific community.



Figure 2: Optical element coupling unit of an imaging polarimeter for 1.2 m telescope at Mt Abu Observatory. The fully assembled coupling unit is shown in the left and the gear box on the right.

Solar Telescope work at Thaltej

Thaltej Solar-flare Telescope (TSFT) is a CCD based telescope for routine survey of solar flares, installed on the terrace of Astronomy & Astrophysics Division. An optical bench using aluminium rail section was designed and fabricated in PRL Workshop. The precision lens and CCD holders were designed and fabricated. A precision X-Y-Z linear drive was fabricated and installed on optical bench. A stand for telescope having 1.5 meter height was fabricated to mount the Telescope. Counter-weight was provided for balancing of Telescope. The mechanical setup of the telescope is made in the PRL workshop. The mechanical setup of the telescope includes optical bench, telescope stand, objective lens, CCD and H α filter holders and X-Y position movement setup. The optical bench is made of aluminium and the size is ~ 2.3 m. The telescope stand is made for the celestron german equatorial mount to affirm the telescope setup. The objective lens holder is made of brass and similar 5 holders have been made for other lenses viz. reducer lens etc. For CCD holding and alignment with the objective lens, an robust holder is made and put together with the X-Y position movement flexibility. The X-Y movement facility is designed and developed in-house for all the lens holders too. A collimating tube of $4\sim 3.5$ cm diameter is designed and coupled with the filter for removing unnecessary background light. Further, for telescope balancing, few weights have also been designed.

Turntable mount for assembling Compton scattering experiment for the threshold estimation for solar X-ray polarimetry in plastic detector

Compton scattering depends on the scattering angle and the photon energy. The experiment is to determine the scattering angle, at which scattered photon energy is the threshold

energy for the CdTe detector, where plastic scintillator is being used. A photomultiplier mount is provided just behind the plastic scintillator, and the CdTe detector was mounted on an arm, which is rotatable with respect an axis through the sample holder. Both CdTe detector and the plastic are housed in Al blocks. The detector block can slide along the arm and its position can be locked at any distance from the plastic scintillator. To keep a radioactive source in front of the plastic detector, a source holder, made of Al was fabricated.

The entire assembly was designed and was fabricated in PRL Workshop and it is performing well.

Airglow Photometer



Figure 3: The fully assembled airglow photometers, fabricated in PRL workshop.

A new airglow photometer was fabricated in PRL Workshop. It consists of front-end optics to collect the light from the sky and have narrow field of view like three degree field of view which is controlled through small aperture. Then

the beam is made parallel and then pass through a narrow band temperature controlled filter to select the wavelength of interest. The emerging light is focused on the detector like PM tube or CCD detector with the help of focusing lens. A filter-wheel assembly also was made to choose different wavelengths in the experiment. The components of airglow photometer are lens holders with locking rings,

filter holders with locking rings, housings, flanges, adaptors, stands, mounting platform/brackets. These components were fabricated with high accuracy and surface finish in workshop. Workshop also helped in the critical assembly of the system at laboratory testing as well as on site. The components were made from graded aluminium alloy material and brass material. The instrument is working satisfactorily.

Honorary Fellows

J. E. Blamont

P. Crutzen

A. Hewish

K. Kasturirangan

D. Lal*

M. G. K. Menon

U. R. Rao

*Deceased, December 2012

Honorary Faculty

R. K. Varma
FNA, FASc, FNASc., NASI Senior Scientist

S. Krishnaswami
FNA, FASc, FNASc, FTWAS, INSA Senior Scientist

R. G. Rastogi
FNA, FASc, FNASc

S. K. Gupta
FNASc

A. C. Das

N. Bhandari
FNA, FASc, FNASc, INSA Honorary Scientist

D. P. Dewnagan
FNASc

B. G. Anand Rao

S. P. Gupta

Harish Chandra

H. S. S. Sinha

U. C. Joshi

R. Sridharan
FASc, FNASc, CSIR Emeritus Scientist

Honorary Technical Faculty

R. N. Mishra

H. O. Vats

Academic Faculty

Name	Designation	Specialization	Academic Qualification
Goswami J. N. <i>FNA, FASc, FNASc, FTWAS</i>	Director	Solar System Studies (Pre-Solar Processes)	Ph.D., PRL, Gujarat. Univ. (1978)
Ambastha A. K.	Professor	Solar Plasma Physics	Ph.D., PRL, Gujarat. Univ. (1981)
Amritkar R. E. <i>FASc, FNASc</i>	Senior Professor	Nonlinear Dynamics & Chaos	Ph.D., IISc, Bangalore (1978)
Ashok N. M.	Senior Professor	Close Binary Stars, Novae/IR spectroscopy	Ph.D., PRL, Gujarat Univ. (1983)
Baliyan K. S.	Professor	AGNs, Comets, Atomic Physics, Milky Way	Ph.D., Roorkee Univ. (1986)
Banerjee D.	Associate Professor	Thermoluminescence & Planetary Physics	Ph.D., PRL, Gujarat Univ. (1997)
Banerjee D. P. K.	Professor	Novae, Be Stars, Planetary Nebulae, IR and Optical Studies	Ph.D., PRL, Gujarat Univ. (1990)
Banerji J.	Professor	Classical Optics, Quantum Physics	Ph.D., City Univ.(New York) (1982)
Bapat B.	Associate Professor	Atomic & Molecular Processes	Ph.D., T.I.F.R, Bombay Univ. (1997)

Name	Designation	Specialization	Academic Qualification
Bhatt J. R.	Associate Professor	Astrophysics	Ph.D., IPR, M.S. Univ.(1992)
Bhattacharyya R.	Reader	Plasma Physics	Ph.D., Jadavpur Univ., (2006)
Bhushan Ravi	Scientist-SF	Oceanography and Paleoclimatology	Ph.D., PRL, M.S. Univ. (2009)
Chakrabarty A.	Associate Professor	Extra-solar planets, Star Formation & Instrumentation	Ph.D., PRL, Gujarat Univ. (1999)
Chakrabarty D.	Reader	Upper Atmosphere and Geomagnetic storm	Ph.D., PRL, M.L.S Univ.(2008)
Chandrasekhar T.	Professor	High Angular Resolution Studies, Late type stars Solar Coronal, Studies Comets	Ph.D., PRL, Gujarat Univ.(1982)
Deshpande R. D.	Scientist-SF	Application of Environmental Tracers in Hydrology	Ph.D., PRL, M.S. Univ. (2007)
Gosain S.	Scientist-SD	Solar Physics and Instrumentation	Ph.D., PRL, M.L.S Univ. (2007)
Goswami S.	Professor	High Energy Physics	Ph.D., Calcutta Univ. (1998)
Haider S. A. <i>FASc, FNA</i>	Professor	Planetary and Cometary Atmospheres	Ph.D., Banaras Univ. (1984)
Jain R.	Professor	Solar Physics	Ph.D., PRL, Gujarat Univ. (1983)
Janardhan P.	Professor	Solar Radio Astronomy & Space Weather	Ph.D., PRL, Gujarat Univ. (1991)
Joshi B.	Reader	Solar Physics, Astronomy	Ph.D., ARIES, Kumaun Univ.(2007)
Joshi A. S. <i>FNA, FASc, FNASc</i>	Outstanding Scientist	Particle physics	Ph.D., TIFR, Bombay Univ.(1979)
Juyal N.	Scientist-SF	Quaternary Geology & Paleoclimate	Ph.D., PRL, M.S. Univ.(2004)
Konar, Partha	Reader	Particle Physics	Ph.D., HRI, Allahabad Univ.(2005)
Kota V. K. B.	Senior Professor-H	Nuclear Physics	Ph.D., Andhra Univ.(1977)
Kumar B.	Scientist-SE	Solar Physics	Ph.D., PRL, M.L.S Univ.(2007)
Kumar S.	Reader	Aquatic and Terrestrial Biogeochemistry	Ph.D., PRL, M.S. Univ., (2004)
Lal S. <i>FNA, FASc, FNASc</i>	Senior Professor	Atmospheric Chemistry and Trace Gases	Ph.D., PRL, Gujarat Univ.(1982)
Mahajan N.	Reader	Particle Physics	Ph.D., Delhi Univ.(2004)

Name	Designation	Specialization	Academic Qualification
Marhas K. K.	Reader	Solar System studies	Ph.D., PRL, D.A.V.V Indore (2001)
Mathew S. K.	Associate Professor	Solar Magnetic & Velocity Fields	Ph.D., PRL, Gujarat Univ. (1999)
Mishra H.	Professor	Strong Interaction Physics & Nuclear Astrophysics	Ph.D., IOP, Utkal Univ. (1994)
Mohanty S.	Senior Professor	Astroparticle Physics	Ph.D., Wisconsin Univ. (1989)
Murty S. V. S. <i>FASc</i>	Senior Professor	Isotope Cosmochemistry	Ph.D., IIT, Kanpur (1981)
Naik S.	Reader	High Energy Astro- physics, X-ray Binaries	Ph.D., T.I.F.R, Bombay Univ.(2003)
Navinder Singh	Reader	Theoretical condensed matter and Statistical physics	Ph.D., RRI, Bangalore (2006)
Pallam Raju D.	Associate Professor	Space Weather and Atmospheric coupling processes	Ph.D., PRL, D.A.V.V Indore(1997)
Rai V.	Reader	Stable Isotope Cosmochemistry	Ph.D., PRL, M.S Univ. (2001)
Ramachandran S.	Associate Professor	Atmospheric AerosolsRadiative & Climate Impacts	Ph.D., PRL, M.S Univ. (1996)
Ramesh R. <i>FNA, FASc, FNASc, FTWAS</i>	Senior Professor	Paleoclimatology, Oceanography & Modelling	Ph.D., PRL, Gujarat Univ. (1984)
Rangarajan R.	Associate Professor	Particle Physics & Cosmology	Ph.D., Univ. of California, Santa Barbara (1994)
Ray J. S.	Associate Professor	Isotope Geochemistry	Ph.D., PRL, M.S Univ. (1998)
Ray Dwijesh	Scientist-SD	Marine Geology & Igneous Petrology	Ph.D., Jadavpur Univ. (2009)
Rengarajan R.	Scientist-SE	Atmospheric aerosols & aqueous geochemistry	Ph.D., PRL, M.L.S Univ.(2004)
Rindani S. D. <i>FNA, FASc, FNASc</i>	Senior Professor-H	Particle Physics	Ph.D., IIT, Bombay (1976)
Sahoo B. K.	Reader	Atomic Physics	Ph.D., Mangalore Univ.(2006)
Sahu L. K.	Reader	Atmospheric Science, Trace gases	Ph.D., PRL, M.L.S.Univ., (2005)
Samanta G. K.	Reader	Laser and Nonlinear optics	Ph.D., Universitat Politecnica de Catalunya University, Barcelona, (2009)
Sarbadhikari Amit Basu	Scientist-SD	Petrology & Geochemistry	Ph.D., IIT, Kanpur (2009)

Name	Designation	Specialization	Academic Qualification
Sarin M. M. <i>FNA, FASc, FNASc</i>	Senior Professor	Geochemistry and Oceanography	Ph.D., PRL, Gujarat Univ.(1986)
Sarkar U. <i>FNA, FASc, FNASc</i>	Senior Professor	Particle Physics	Ph.D., Culcutta Univ.(1984)
Sekar R.	Professor	Upper Atmospheric & Ionospheric Physics	Ph.D., PRL, Gujarat Univ.(1991)
Sharma Som K.	Reader	Middle Atmosphere & Long Term Atmospheric Changes	Ph.D., PRL, Gujarat Univ.(2010)
S. Ganesh	Scientist-SE	Milky Way, Comets, AGN, Astronomical polarimetry	Ph.D., PRL, Gujarat Univ.(2010))
Sheel V.	Associate Professor	Modelling of Lower Atmosphere	Ph.D., PRL, Gujarat Univ.(1996)
Shukla A. D.	Scientist-SE	Geochemistry & Cosmochemistry	Ph.D., PRL, M.S. Univ. (2012)
Singal A. K.	Associate Professor	Radio Astronomy & Astrophysics	Ph.D., TIFR, Bombay Univ. (1986)
Singh A. D.	Associate Professor	Atomic Physics	Ph.D., IIA, Bangalore Univ.(1998)
Singh R. P.	Scientist-SF	Laser Physics	Ph.D., J.N.U., New Delhi.(1994)
Singh S. K.	Associate Professor	Isotope Geochemistry	Ph.D., PRL, M.S. Univ.(1999)
Singhvi A. K. <i>FNA, FASc, FNASc, FTWAS</i>	Outstanding Scientist	Palaeoclimatology and Geochronology	Ph.D., IIT, Kanpur (1975)
Srivastava N.	Associate Professor	Solar Physics	Ph.D., PRL, Ravi Shankar Shukla Univ.(1994)
Subramanian K. P.	Associate Professor	Experimental Atomic and Molecular Physics	Ph.D., PRL, Gujarat Univ.(1987)
Thampi S.	Reader	Atmospheric Physics	Ph.D., V.S.S.C, Kerala Univ, (2007)
Vadawale S. V.	Reader	High Energy Astrophysics and X-Ray Spectroscopy	Ph.D., T.I.F.R, Bombay Univ. (2003)
Venkatakrishnan P.	Senior Professor-H	Solar Physics	Ph.D., IIA, Bangalore Univ.(1984)
Yadava M. G.	Scientist-SF	Palaeoclimate, Radiocarbon dating and stable isotopes	Ph.D., PRL, D.A.V.V., Indore (2003)

Technical Faculty

Name	Designation
Acharya Y. B.	Engineer-G
Adhiyaru P. R.	Engineer-SE
Narayanan R.	Scientist-SF
Rao D. K.	Scientist-SE
Shah A. B.	Engineer-SF
Shah K. J.	Computer-Scientist-SE
Shah R. R.	Engineer-SF
Singh Mahendra	Sci./Eng.-SF
Ubale G. P.	Engineer-SF
Venkataramani S.	Scientist-SF



पी.आर.एल. में गतिविधियां Event at PRL





पी.आर.एल. में गतिविधियां Event at PRL





पी.आर.एल. में गतिविधियां Event at PRL



प्राथमिक प्रयोगशाला, अहमदाबाद पर अंतरराष्ट्रीय संशोधन
International Symposium on
Atmospheres of Terrestrial Planets: Observations & Modeling
23-24 July, 2012
भौतिक अनुसंधान प्रयोगशाला, अहमदाबाद, भारत
Physical Research Laboratory, Ahmedabad, India



